Proceedings of the Workshop on Possibilities and Limitations of Accelerators and Detectors held at Fermi National Accelerator Laboratory October 15 – 21, 1978

April, 1979

Fermi National Accelerator Laboratory
Batavia, Illinois

Sponsored by the International Committee for Future Accelerators (ICFA) and Fermi National Accelerator Laboratory

PREFACE

A Workshop on Possibilities and Limitations of Accelerators and Detectors was held at Fermilab on October 15 through 21. This was the first workshop sponsored by the International Committee for Future Accelerators (ICFA), which is a committee of the International Union of Pure and Applied Physics and is presently chaired by John Adams (CERN). ICFA is the successor to and outgrowth of the series of informal Very Big Accelerator (VBA) meetings held over the last few years.

The workshop was hosted by Fermilab and organized by a U. S. Committee consisting of Burton Richter (SLAC), Jack Sandweiss (Yale), James Sanford (BNL), and William Willis (BNL), with Lee Teng (Fermilab) as chairman. Approximately 45 people from many different countries participated, including 3 from the People's Republic of China.

Since this meeting was the first of its kind, we had essentially a free hand at setting the style. As organized, this workshop differs from the previous VBA meetings in several essential respects. First, its purpose was taken to be purely technical; no attempt was made to tackle the complex socio-political problems of international collaboration and World Laboratory. Second, this workshop was aimed at investigating the general accelerator and experimental technology and techniques available for super-high energies instead of the design of specific accelerators and experiments. Third, it was run as a true workshop; participants were expected to work on identifying, studying, and solving problems that may be encountered at super-high energies. To accomplish these goals, for example, we invited

only general interest talks on superconducting and beam-cooling technologies and minimized reports on the status and plans of national or regional projects.

The effort of the week was organized in seven working groups. The groups and the group leaders are: Electron Accelerators and Storage Rings (John Rees, SLAC); Proton Accelerators (Victor Yarba, IHEP); Colliding Beams pp, $\bar{p}p$, and ep (Eberhard Keil, CERN); Particle Detectors (George Charpak, CERN); Neutrino Experiments (Ugo Amaldi, CERN); Hadron Experiments (Robert Diebold, ANL); Lepton and Photon Experiments (Barry Barish, Caltech). The energies of interest for the workshop were defined in the ground rules to be greater than 5 TeV for protons and greater than 100 GeV for electrons. It is assumed that smaller accelerators will be constructed on regional bases with less broad sponsorship.

The enthusiasm of the participants, the flexible program, and the informal atmosphere all contributed to making a successful workshop. Many problems were identified, some were resolved, others serve to point out the direction where future efforts should be devoted. Whether or not it takes us a step closer to the World Accelerator and World Laboratory, the findings of the workshop, a part of which is contained in these Proceedings, edited by D. A. Edwards, are in themselves a major contribution to science and technology.

ICFA met on October 20 and decided to hold a follow-up workshop of approximately the same character and format in approximately a year. This workshop will be hosted by CERN. Beyond that, a workshop is planned for the spring of 1980 on high-field superconducting magnets and superconducting rf cavities.

L. C. Teng

TABLE OF CONTENTS

Editor: D. A. Edwards

Proton Synchrotrons

Page

Summary of the Proton Accelerator Group 1
V. Yarba, V. I. Gridasov, L. Lederman, D. Möhl,
K. P. Myznikov, W. B. Sampson, R. Stiening, L. Teng,
V. A. Titov, R. R. Wilson, Y. Yamaguchi and Others

Some Thoughts About a 20-TeV Proton Synchrotron 3
R. Stiening

Synchrotron Radiation in the 20-TeV Proton Synchrotron 11
R. R. Wilson

The IHEP Accelerator - Storage Complex Status Report 13

The Problem of Forming Precision Magnetic Fields in
Superconducting Dipoles of UNK 35
V. I. Balbekov, V. I. Gridasov, K. P. Myznikov,
I. A. Mosalevski, N. A. Monoszan, and V. A. Titov

Protection Measures for Superconducting Magnet Units of the UNK
Against Radiation 49
V. I. Balbekov, S. L. Kuchinin, V. N. Lebedev,
N. V. Mokhov, K. P. Myznikov, Yu. S. Fedotov, and
V. N. Chepegin

The Pentevac: A Site-Filling Accelerator at Fermilab 67
R. R. Wilson

RF Superconductivity for Accelerators--Is It a Hollow Promise? . . . 81
M. Tigner

Colliding Beams

Limitations on Performance of e^+e^- Storage Rings and Linear
Colliding Beam Systems at High Energy 87
J.-E. Augustin, N. Dikanski, Ya. Derbenev, J. Rees,
B. Richter, A. Skrinski, M. Tigner, and H. Wiedemann

Summary Report of the Working Group on Colliding Beams 107
S. Y. Chen, E. D. Courant, E. Keil, N. M. King,
P. McIntyre, T. Nishikawa, and M. Vivargent

Page

Coasting p-p Colliding Beam Machines 117
E. Keil and N. Marshall King

Bunched-Beam p-$\bar{p}$ and p-p Collisions 135
E. D. Courant and E. Keil

Stochastic Cooling 145
D. Möhl

Note on ep Collisions 177
T. Nishikawa and E. Keil

Experiments and Detectors

Neutrino Experiments at a 10-20 TeV Proton Synchrotron 187
U. Amaldi, A. Diddens, C. Fisher, and N. Samios

Report of the Hadron Experiments Group 199
R. Diebold

Features of Experiments at Energies Above 1 TeV 221
V. I. Kryshkin, Yu. D. Prokoshkin, A. S. Vovenko,
V. A. Yarba, and A. M. Zaitsev

Particle Detectors and Their Limitations 237
G. Charpak

Some Limits in the Localization of Charged Particles 239
G. Charpak

Particle Identification and Energy Measurement at High Energies . . 245
W. Willis

High Accuracy Vertex Detectors for the Measurement
of Short Living States 257
K. Lanius

Vertex Detectors for Ultra High Energy Hadron Spectrometers . . . 265
C. Fisher and J. Sandweiss

ICFA Workshop Attendees 277

Proton Synchrotrons

Colliding Beams

Experiments and Detectors

Proton Synchrotrons

SUMMARY OF THE PROTON ACCELERATOR GROUP

V. Yarba, Chairman
V. I. Gridasov
L. Lederman
D. Möhl
K. P. Myznikov
W. B. Sampson
R. Stiening
L. Teng
V. A. Titov
R. R. Wilson
Y. Yamaguchi
and others

After a general discussion the group agreed to consider a definite energy of 20 TeV. The problems specific to the design of a proton synchrotron of that energy were expected to clarify the limiting energy. It is anticipated that in ten or fifteen years superconducting magnets will attain fields of 10 T and will be available for the construction of the accelerator. This technology will considerably reduce the cost of construction and operation. The design intensity was chosen arbitrarily to be 10^{13} protons/second with a cycle which would include 20 seconds of filling, 40 seconds of acceleration and 40 seconds of magnet recovery.

The discussion led to a magnet ring of average radius about 12 km The cells with dipoles would occupy 65 km, the cells without dipoles (total straight section) would occupy 9 km. With the 100 second cycle the protons per pulse would be 10^{15} which corresponds to a frightening energy of 3000 MJ stored in the beam at 20 TeV.

An 8 cm diameter beam pipe implies that the total stored energy in the magnetic field would be about 8000 MJ. It is anticipated that the average static load due to radiative and conductive heat loss in the superconducting magnets would be about 75 kW. The load loss in the leads would be about 10 kW and the loss due to ramping the magnetic field would be about 200 kW.

The total average power requirement of the accelerator might be about 300 MW of which the rf system would take about 100 MW.

Exclusive of the injector system (which might correspond to the equivalent of a Tevatron) and of the experimental areas, the cost might be one or two billion dollars depending on the conditions of construction.

No serious problem of beam dynamics were encountered for the 20 GeV example. Very serious problems were anticipated associated with beam losses. Although the use of normal iron-copper dipole magnets placed downstream of regions were beam losses will occur will be helpful, this problem was not resolved and must be further investigated for it will be the most important limitation of the intensity.

The conclusion of the group is that there does not appear to be a fundamental obstacle in the construction of a 20 - TeV proton accelerator, although there might be trouble in reaching an average intensity of 10^{13} protons per second. It would be useful to examine a 30 TeV or even higher energy machine in order to better determine if a limiting energy exists, or if the physics interest should require such an energy.

SOME THOUGHTS ABOUT A 20-TEV PROTON SYNCHROTRON

R. Stiening
Fermi National Accelerator Laboratory, Batavia, Illinois 60510

This proposal will discuss a 20-TeV proton synchrotron with an average beam intensity of 10^{13} protons/second. The design cycle would include 20 seconds of filling, 40 seconds of acceleration and 40 seconds of magnet recovery. Since it is anticipated that 10T superconducting magnets will be available at the start of construction, full advantage will be taken of the reduction in cost that the magnet technology offers. The design intensity corresponds to an average power output of the synchrotron in the form of beam of 50 mW. Since superconducting magnets do generate heat at helium temperature when they are pulsed, a large fraction of the refrigerator capacity is devoted to absorbing this load. If the average intensity could be reduced by a factor of two by lengthening the cycle time to 200 seconds, the cost of the refrigerator and rf system would be greatly reduced. The cost of the machine would be reduced by 25% by such a strategy. It is, however, of interest to consider a maximum performance machine at this time.

The machine as it is described here does not include an injector, or any provision for experimental use. These factors must be added to the cost. Long straight sections are provided with the normal quadrupole lattice for transporting the beam. Special magnets must be installed for experimental use of these areas.

A number of features unique to a large superconducting synchrotron require departures from the usual scaling laws for such machines. A high tune is chosen to minimize the effect of gradient errors in the magnets. Since the size of the magnet is directly linked with the field accuracy that can be achieved, this consideration is of great economic importance. Regions of normal iron-copper dipole magnets will be placed downstream of regions where there are to be extraction devices or beam scrapers to protect the superconducting magnets from the beam. An automatic, dynamic, orbit correction scheme will be incorporated to cancel the effects of surveying errors, foundation movement, and magnet errors. Since such systems have been demonstrated (at least in principle) on existing machines, it can be assumed that the requirements on the choice of site can be eased and that construction costs can be reduced.

Lattice

Present experience with the two 400-GeV synchrotrons shows that large machines are very sensitive to magnetic field imperfections even if the magnets are made very carefully. Since it appears at present that the quality of superconducting magnets may be inferior to that of iron-copper magnets, the design of the 20-TeV machine must be such that the influence of the field imperfections is minimized. This is accomplished by making the momentum dispersion and β-functions as small as possible by increasing the fraction of the circumference occupied by quadrupoles, from the 10% value characteristic of present machines to about 25%. The benefit of such a choice of quadrupole strength has already been demonstrated. The CERN 400-GeV machine with a tune of 27 is considerably less sensitive to dispersion

related errors than is the Fermilab machine which operates at a tune of 19. The extreme sensitivity of betatron oscillation instability to the amplitude of the oscillations in the presence of field imperfections requires that the magnification of the transverse dimensions of the beam in the transfer from the injection be minimized. This is accomplished by choosing a small β value in the lattice.

The usual FODO lattice has been chosen for the usual reasons. This lattice is characterized by a cell length 2L and a quadrupole focal length F. The ratio $L/F = \sqrt{2}$ is chosen to give a 90° phase advance in the cell. The maximum value of the betatron function is then $\beta = (2 + \sqrt{2})\ L = \sqrt{2}(2+\sqrt{2})F$. A beam-pipe diameter of 8 cm is assumed and the quadrupole gradient is $(dB/d_x) = (B_d/a)$ where B_d is the dipole field and a is the pipe radius. At the peak energy $(dB/dx) = 250$ T/M. The size of the beam pipe is determined by a consideration of the manner in which conductor placement errors distort the guide field. The 8 cm value at this moment is something of a guess.

A 10 meter long quadrupole will have a focal length of 27 meters. From the above consideration the cell length 2L = 76.4 meters. In this cell 50 meters will be occupied by dipole and 6.4 meters will be free space for correction elements and magnet connections. At 20 TeV, $B\rho = 6.67 \times 10^4$ Tm. Therefore 41900 meters of 10T bending magnet length is required. Thus 840 cells with dipoles are needed. In addition the machine will have 120 cells without bending magnets. The Q value will therefore be 240. Although this value is 10 times larger than that of present machines, there should be no difficulty in achieving the required power supply accuracy at a reasonable

cost. Table I summarizes the geometrical specifications.

Table I.

Quadrupole length/cell	20.0 meters
Dipole length/cell	50.0 meters
Free space/cell	6.4 meters
Total cell length	76.4 meters
Cells with dipoles	840 (65.17 km)
Cells without dipoles	120 (9.17 km)
Total number of cells	960 (73.34 km)

Beam Intensity

It is assumed that the 20-TeV ring will be "box car" loaded from a smaller injector. Existing 400-GeV machines (with $\beta_{max} \simeq 120$ m) demonstrated that a particle density of 5×10^{12} protons/km can be achieved. Since the β-max value of the lattice described above is only 130 meters there will be only a very small beam since magnification in the transfer from an injector like the Tevatron will be negligible and there should be no difficulty in accepting the particle density given above. The total intensity is then $5 \times 10^{12} \times 73.3 = 3.6 \times 10^{14}$ protons. We shall adopt 10^{15} as the peak intensity in anticipation of improvements that will be incorporated in the design of the injector. It is interesting to note that the stored energy in this beam at 20 TeV will be 3.2×10^{9} joules.

Cycles

To achieve 10^{13} protons/second on the average, a cycle time of 100 seconds is required. It will be assumed that this cycle will be 20 seconds

of filling time, 40 seconds of acceleration, and 40 seconds of flat-top and magnet de-excitation.

RF Requirements

A 40 second acceleration time with 10^{15} particles in the beam implies a power input to the beam of 80 MW. Taking into account the losses in copper cavities, the final rf power requirement is 160 MW during acceleration. If superconducting cavities are developed, an 80 MW saving can be achieved. Since the revolution frequency is 4090 Hz, the required rf voltage (assuming a synchronous phase angle of 60°) is 141 MV. An rf frequency of 300 MHz has been chosen so that efficient klystrons can be used as the power source. The harmonic number at this frequency will be 73,340. The synchrotron frequency corresponding to the above parameters is 2.85 Hz at the peak energy.

Magnet Power Supply

The magnetic field volume is approximately 211 m^3. At 10T the energy density in magnetic field is 39.8 MJ/m^3 so the total stored energy will be 8.4×10^9 joules. The peak power flow during a cycle with a constant acceleration of 500 GeV/second will be 420 MW. This could be reduced to 300 MW without greatly increasing the cycle time by reducing the rate of acceleration near the top energy. This pulsed power requirement is within the capabilities of existing power grids.

Refrigeration

The two main sources of heat load at low temperature are the static radiation load, and the losses in the superconductor when the magnets are excited in a pulsed mode. In a high-field machine with a short cycle the

latter load will dominate. A static radiation load of 1W/meter is assumed. The pulsed load is more difficult to predict because it is dependent on superconductor technology. A guess at this number is 400 J/machine cycle-meter. For the proposed machine the static heat load will be 73 kW at low temperature. In addition another 10 kW must be reserved for power leads and cold-warm transitions. The pulsed load will be 22 MJ/cycle at low temperature or 220 kW on the average. These results are summarized in Table II.

Table II. Average Heat Load at Helium Temperature

Static (radiation)	73 kW
Power leads	10 kW
AC loss	220 kW
Total	303 kW

To estimate the room temperature power consumption of the refrigerator a multiplication factor of 600 is assumed. With that conversion the power grid average load will be 182 MW.

Table III. Power Requirements

	Peak	Average
RF System[a]	246 MW	98 MW
Magnet Power	± 420 MW	10 MW
Refrigerator	300 MW	180 MW
Total	946 MW	288 MW

[a] 65 % efficiency is assumed for the klystrons.

Cost

A summary of the basic machine cost is summarized in the following table:

Table IV. Cost of the Basic Machine

Tunnel at $1000/m	73×10^6	$
RF at $1/watt input	246×10^6	$
Magnets at $2000/foot	332×10^6	$
Refrigerator	200×10^6	$
Controls and corrections	10×10^6	$
Magnet power supply	25×10^6	$
Total	$\$ 886 \times 10^6$	$

Conclusion

There does not appear to be any fundamental technical obstacle to the construction of a 20-TeV machine. Energy costs and availability may limit the repetition rate to a value lower than that given in this proposal.

SYNCHROTRON RADIATION IN THE 20 TEV PROTON ACCELERATOR

R. R. Wilson

Because of their mass, protons radiate less than electrons of the same energy by a factor of about 10^{13}. The synchrotron radiation per turn by a proton E_r is given by

$$E_r = 7.8 \cdot 10^{-12} E^4/R$$

where the proton energy E is measured in TeV and the radius of curvature is in kilometers. For the 20 TeV proton synchrotron used as an example in the ICFA study at Fermilab, the radius of curvature is 10.5 km which leads to about 120 KeV of radiative energy per turn at 20 TeV. For a circulating beam of 10^{15} protons, this means a total energy radiation of 100 KW which is comparable to the normal heat losses at 4°K. The characteristic wave length is about 0.5μ, so there should be considerable visible light which should help with beam diagnostics. The coherent radiation, calculated by Shiff, is not important.

The damping of vertical betatron oscillations is given approximately by $E_r/2E$, which for this case implies that the vertical size of the beam will be reduced by half in about 24 hours. Although not significant during the acceleration period, such damping will limit the growth of a beam due to multiple scattering to a small size, depending of course on the pressure.

THE IHEP ACCELERATOR - STORAGE COMPLEX STATUS REPORT

1. Introduction

The IHEP Accelerator - Storage Complex (UNK) is being developed as a basis for further deepening and advancement of high-energy physics research.[1-4] A 3-TeV superconducting proton synchrotron with a prospect for colliding beams in the future has been chosen as a basis of the UNK.[4] Presently the design study of the UNK has been completed.

The basic parameters of the accelerator are listed in Table I.

Table I. The Main Parameters of the UNK.

Name	Unit of measurement	1st stage	2nd stage
1. Total length	m	19288	19288
2. Injection energy	GeV	70	400
3. Maximum energy	GeV	400	3000
4. Injection field	T	0.117	0.670
5. Maximum magnetic field	T	0.670	5.0
6. Cycle duration	sec	78	78
7. Pulse intensity	p /cycle	6×10^{14}	6×10^{14}

It is a two-stage accelerator. The first stage is a proton synchrotron with conventional magnets and is designed to stack and preaccelerate protons up to 400 GeV. Acceleration up to the maximum energy is to be achieved in the second stage, where superconducting magnets are to be utilized. Both

accelerators are located in a common tunnel. The presently existing IHEP 70-GeV accelerator (U-70), whose intensity is planned to be increased up to 5×10^{13} ppp, is to be used as an injector into the UNK.

The two-stage system enables us to facilitate the superconducting accelerator operating mode substantially. Beam preacceleration in the first stage makes it possible to reduce the effects of residual fields. Due to the decrease in the beam dimensions, the requirements imposed on the field quality of the superconducting magnets are made less severe. Single-turn beam injection onto the central orbit of the second stage is employed for the same reason. Beam stacking is performed in the first stage; this also offers the opportunity to free the superconducting accelerator from inevitable particle losses.

There are other advantages of the two-stage system. It allows the maximum use of the injector intensity, and therefore achieves the maximum mean intensity of the accelerated beam. The two rings available in the same tunnel provide an option for a 0.4 TeV and 3-TeV proton-proton colliding-beam facility, with 2.2-TeV energy in the c. m. s. The ring of the first stage can also be used to stack beams of electrons, antiprotons, etc.

Figure 1 shows the layout of the UNK. The location of the UNK tunnel is chosen taking into account a preliminary study of geologic conditions. The ring center is within 6.5 km of the U-70 accelerator center. The UNK tunnel dimensions are chosen to allow the future possibility of installing a superconducting storage ring. This will enable us to stack a 3-TeV proton beam and to collide it with a beam of the same energy accelerated in the pulsed

superconducting ring. As a result, the pp-collision energy can be increased up to 6 TeV in the c. m. s.

The UNK project is designed with a view for its future development. Six straight sections, each 485 m long, are introduced into the structure of both stages (Fig. 1). The U-70 beam is injected into section 1, in which the beam transfer system into the second stage is also located. The accelerated particles are extracted from Section V. The accelerating systems are placed in Section II, and the beam abort systems in Section IV. Sections III and VI are reserved for colliding beams. The layout of the accelerator and storage rings in the tunnel and the construction of the straight sections are chosen so that the intersections of the maximum energy beam would be subsequently obtained more easily. In designing the long straight sections, all measures eliminating the influence of ring intersections on the ψ-function and the momentum compaction factor were taken. Figure 2 presents a schematic view of the UNK tunnel cross section and the position of the magnets therein.

2. The Characteristics of the UNK

The scheme of the UNK operation is shown in Fig. 3. A 5×10^{13} proton/cycle beam is recaptured in the U-70 accelerator by an rf field with a frequency of 200 MHz, equal to the UNK accelerating voltage frequency. Stacking of 6×10^{14} ppp during 71.5 sec is achieved by successive injection of 12 pulses from the U-70. The UNK circumference is exactly 13 times that of the U-70, therefore a part of the first stage circumference is not filled with a beam. This makes it possible to arrange "time slots" between the beam pulses, necessary to facilitate the operation of injection and extraction

devices and thus to reduce particle losses. On completion of stacking, the beam is accelerated in the first stage up to 400 GeV and single-turn transferred into the second stage of the UNK. The cycle of the second stage comprises a 20-sec acceleration, a 38-sec beam extraction, and a 20-sec field decay time.

The basic parameters of the UNK magnetic structure are given in Table II.

Table II. The Basic Parameters of the Magnetic Structure of the First and the Second Stages of the UNK.

Parameter	Unit of Measurement	Value
1. Number of superperiods		6
2. Total number of periods		180
3. Length of a period	m	91
4. Length of a matched straight section	m	484.67
5. Total number of dipoles		2160
6. Total number of quadrupoles including matched straight sections		402
7. Dipole length	m	5.8
8. Length of a standard quadrupole	m	4
9. Magnetic bending radius	m	1993.89
10. Ratio of the quadrupole gradient to the dipole field	m^{-1}	14.75
11. Betatron frequencies		40.75
12. Momentum compaction factor		5.83×10^{-4}
13. Transition energy	GeV	38.8

The lattices of the magnetic structure of the first and the second stages are identical. They comprise 180 periods of the FODO type with

separated functions, each having 12 dipoles and 2 quadrupoles. The requirements on the magnetic characteristic spread and on the accuracy of the dipole and quadrupole positioning are listed in Table III.

Table III.

1.	r. m. s. spread of dipole fields (horizontal and vertical components)	5×10^{-4}
2.	r. m. s. accuracy of horizontal and vertical survey of the optic axes of quadrupoles to the geodetic survey marks.	0.1 mm
3.	r. m. s. misalignment of adjacent lenses (vertical and horizontal)	0.05 mm

Since the dipoles are to be installed after taking into account the magnetic measurement results, the tolerance stated in the first line of the table signified the uncertainty due to magnetic measurement errors and field variation in the cycle and from cycle to cycle. An orbit correction is envisaged in either oscillation plane. With use made of 180 correctors in each plane and with 0.5 mm r. m. s. orbit measurement resolution, the design correction accuracy is ± 2 mm. Considering all the factors above, the maximum beam dimensions at injection into the first stage are 50 mm in the vertical direction and 70 mm in the horizontal plane. During injection into the second stage, the corresponding dimensions are 42 mm and 50 mm. The dimensions of the vacuum chamber of the first stage are of two types, 47×87 mm^2 and 65×65 mm^2; the chamber of the second stage has an elliptical cross section of 60×70 mm^2.

The vacuum requirements in the chambers of the UNK two stages are determined by proton losses due to the residual gas. The mean pressure of

the residual gas in the first stage should not exceed 3×10^{-7} Torr in nitrogen equivalent and 2×10^{-8} Torr in the second stage. Preliminary calculations show that with the 20 - 40 °K temperature of the chamber walls of the superconducting ring a 2×10^{-11} Torr vacuum can be obtained for hydrogen and $\sim 10^{-13}$ Torr for the other gases.

The UNK accelerating system should provide a 12 MV total amplitude at 20 MHz for the first stage and 17 MV for the superconducting ring. The maximum powers consumed by the beam are 6.6 MW and 18 MW, respectively. At present, scientists of IHEP, MEPI, and MRTI are doing theoretical and experimental research aimed at choosing waveguides or cavities for the UNK accelerating systems. Synchronization of rf fields of the U-70 accelerator and the first stage of the UNK may be difficult due to the large length of the injection line, which is about 6 km. Therefore, fast rf phase correction by the information on bunch phase position is presumed on completion of each injection pulse. The rf field of the UNK second stage will be synchronized similarly.

The injection line is a strong focusing channel of the FODO type with lenses installed within every 50 m. The maximum beam dimension in the channel does not exceed 35 mm. Over the whole length of the channel, within every 1 km there are correction stations of the beam trajectory in either plane. They consist of beam position pick-ups and three correction magnets. With the 0.2 mm r. m. s. tolerance for lens misalignment with respect to the channel axis, the beam trajectory distortion should not exceed 5 mm over the whole length. The final correction station should provide matching of the channel axis and the UNK orbit to within 1 mm. The beam is injected into the first stage and transferred into the second in the vertical plane.

Three extraction modes are foreseen: single-turn extraction, ~ 30 sec slow resonance extraction, and fast resonance extraction of 10 pulses spaced at 3 second intervals with each pulse yielding 6×10^{13} protons in ~ 1 msec. For single-turn extraction, a kicker magnet 30 m in length with a rise time of 1.5 μsec to 0.9 kG is intended to be used. For slow and fast resonance extractions, the $3\ Q_r = 122$ resonance will be employed. To gain maximum extraction efficiency, the structure of a matched straight section is arranged in such a fashion that the maximum of the horizontal amplitude function can be obtained in its center. With the maximum value of the amplitude functions in the straight section approximately a factor of 10 larger than that in the accelerator lattice, one can obtain a 20 mm step-size at the ES septum for a maximum excursion in the normal cell-dipoles of 2 cm. The tolerance for relative values of the magnetic field nonlinearities at the chamber edge should be 10^{-4} and ~ 10^{-3} for odd and even components, respectively. With these requirements, the value of the extraction efficiency will be 99%. To achieve a good duty factor of the beam with a 30-sec extraction duration, the tolerance for the relative value of current ripple in the sextupoles is to be 10^{-6} and about 10^{-9} in the magnets of the superconducting ring.

The average electric power consumed by all the UNK systems is about 100 MW. The maximum peak power does not exceed 300 MW. Such loadings are acceptable for the 220-kV mains available. To reduce oscillations of the mains voltage due to UNK pulsed components to acceptable levels, regulators of reactive power are foreseen.

3. Field Quality Requirements

The superconducting dipole field has relatively large nonlinearities due to real and ideal coil differences. This results in Q-shifts dependent on oscillation amplitudes and particle momenta. To ensure a lossless beam acceleration in the superconducting ring, the working point in the frequency lattice of betatron oscillations was chosen in the area most free from strong resonance lines ($Q_r \approx Q_z \approx 40.7$), and tolerances for systematic field nonlinearity in the dipoles are established so that betatron frequency spread in the beam would not exceed 0.02 within the whole acceleration cycle. This permits us to avoid intersections of low-order resonances lines. The requirements for fabrication of the dipoles are such that the neighboring strong resonances would cause beam dimension modulation not greater than 10 %.

Since the values of nonlinear field components are minimal in the aperture center of the dipoles, measures are taken to hold the beam close to the central orbit during the whole acceleration period in the UNK. This is facilitated by a decrease in the beam dimensions with the help of pre-acceleration in the first stage, single-turn injection into the central orbit of the superconducting accelerator, and a precise correction of the orbit within the whole acceleration cycle.

The question of residual field effects of the dipoles, which is closely related to a choice of the injection energy into the second stage, is very important. Figure 4 shows the calculated dependence of residual field nonlinearities on the field level in the center of the UNK dipoles. Relative

2nd, 4th and 6th order nonlinearities at a distance of 35 mm from the chamber axis are shown. Quadratic nonlinearity, which is supposed to be corrected by the sextupoles, is the most influential one. The total spread of betatron frequencies is a function of the dipole nonlinearity and of the number of the correction system sextupoles and their positioning. The magnitude of the dipole nonlinearity and the strength of the correction element make it necessary to take into account terms in $(\Delta H_z/H)_2^2$. With 360 sextupoles used, the permissible value of quadratic nonlinearity of the dipole is 1.5×10^{-3}, corresponding to the field of 4 kG in the dipole center as indicated by Fig. 4. Considering the poor data on spread of residual fields and their reproducibility, the value of the injection field into the second stage was chosen to be 6.7 kG. This corresponds to an energy of 400 GeV. With a $\pm 1 \times 10^{-3}$ relative momentum spread of the beam injected into the second stage, it is necessary to correct chromaticity in order to satisfy the requirements for betatron frequency spread. This will be done with the help of the same sextupoles.

Systematic nonlinearities of low even orders can be suppressed by an appropriate choice of the dipole construction. Analysis showed that a dipole with a two-shell coil meets the imposed requirements quite well. Choosing the angles of the shells, one can suppress 2nd and 4th order nonlinearities. The remaining higher order ones have a weaker effect, and tolerances for tune spread are satisfied in the region filled with the beam. The value of higher order harmonics can be decreased, if necessary, by calibrated spacer positioned in the first shell of a coil. Therefore,

correction systems for systematic nonlinearities higher than the 2nd order are not foreseen in the UNK second stage.

Inaccuracies in the superconducting dipole fabrication lead to a random spread of even nonlinearities and appearance of odd ones. The requirements for the dipole fabrication precision stem from tolerances for r. m. s. spreads of nonlinearities exciting resonances near the working point. The admissible value of r. m. s. spreads for quadratic nonlinearity is 3×10^{-4}, 6×10^{-4} for cubic nonlinearity, and 10^{-3} for the 6th order one. The precision of dipole fabrication and assembly needed to ensure such an accuracy is about 0.1 mm and seems to be attainable. That is why correction of nonlinear resonances is not foreseen in the UNK second stage.

With the stated fabrication precision, the relative value of the constant components of cubic nonlinearity and the skew gradient may turn out to be inadmissibly large. Therefore, provision is made for the relevant correction stations to be installed in the long matched straight sections. To adjust betatron frequencies, chromaticity, and the equilibrium orbit, the universal superconducting correctors placed near the main quadrupoles are to be used. These universal correctors contain dipole, quadrupole, and sextupole coils.

4. Space-Charge Effects

Each successive injection into the UNK second stage of 5×10^{13} protons is followed by nonchoherent Q-shifts, $\Delta Q_r = 0.017$ and $\Delta Q_z = -0.013$ (Fig. 5), which are practically identical for all particles. Therefore applying magnetic field gradient correction, one can maintain noncoherent betatron frequencies within the given position with an accuracy better than 0.01, though the total noncoherent Q-shifts at the 6×10^{14} proton cycle intensity

can reach large values, $\Delta Q_r^{noncoh.} = 0.21$ and $\Delta Q_z^{noncoh.} = -0.15$. The field nonlinearity from space charge will result in ~ 0.01 betatron frequency spread, which is not a serious limitation.

At this intensity, coherent betatron frequencies of protons will differ from noncoherent ones: $\Delta Q_r^{coh.} = -0.3$ and $\Delta Q_z^{coh.} = -0.26$. The limiting intensity, determined by an intersection of one of the coherent frequencies with the integral resonance, is 1 to 2×10^{15} protons/cycle.

The foregoing effects and related beam losses are important in the UNK first stage only. In the second stage, noncoherent Coulomb shifts are negligibly small and coherent ones, at the 400-GeV energy and 6×10^{14} ppp intensity, are about -0.02.

To suppress transverse coherent beam instabilities, dampers with feedback from ~ 1 MHz band position pick-ups will be used. A peculiar feature of the UNK is an extremely fast development of wall instability. At the 6×10^{14} ppp intensity, the time interval for instability to develop is 60 μsec in the first stage; i. e., it approximately coincides with the revolution time. This difficulty seems to be overcome, though it may lead to making the damping system more complicated. In the second stage this time is about 5 times larger and instability suppression is made easier.

A study of longitudinal instabilities arising during beam interaction with the resonant elements of the vacuum chamber merits serious consideration. Design of elements of the vacuum chamber (pick-up electrodes, vacuum branch pipes, flange fittings, etc.) calls for a thorough control of their resonance frequencies and impedances.

5. Irradiation Problems of the Superconducting Ring

Estimates of high-energy radiation effects due to beam losses on the UNK superconducting coils showed that radiation heating can become a factor limiting the beam intensity.[5] Instantaneous beam losses lead to coil temperature increase and may initiate a quench. Heat energy flow, loading the cryogenic system, is a limiting factor for time-distributed losses. The admissible value for it should not exceed 1 W per 1 m of the superconducting magnet. Instantaneous beam losses are a most severe limitation under these conditions. The value of admissible losses is dependent on the particle energy and the nature of their time and space distribution. At the initial period of acceleration in the UNK second stage, the bound for admissible beam losses is 10^{10} ppp in order of magnitude.

With a 6×10^{14} ppp accelerated beam, this level of irradiation of the superconducting magnets can be ensured only when taking special measures. The UNK project attaches a great importance to developing such measures; 70-GeV beam stacking and beam preacceleration take place in the first stage. This will afford an opportunity to decrease substantially the space-charge effects in the second stage. Besides, various methods of beam halo scraping and introduction of gaps in the beam azimuthal distribution will be employed in the first stage. This will enable an effective, close to 100%, beam transfer into the second stage. To localize possible beam losses during acceleration, in both UNK stages beam scraping stations are arranged in the long straight sections. Their large length makes it possible to put a sufficient number of collimators after these stations to suppress particle fluences to the level suitable for the normal operation of the superconducting

magnets. In case of inadmissibly large beam losses, the accelerated beam will be extracted from the accelerator during one turn with the help of beam-abort systems into the outer stoppers.

There arise serious extraction problems since the radiation fluences due to the extraction septum losses cause intolerable energy releases in the superconducting magnets located downstream. A beam deflection at an angle of a few mrad with respect to the central orbit before the extraction septum is a most effective protection technique against these fluences. Due to the large length of the straight sections this allows a substantial decrease of superconducting element irradiation. The residual fluences can be suppressed to the required level by protection collimators.

Observation of the whole variety of measures makes the UNK superconducting magnet irradiation problems solvable.

6. Stages of the UNK Developments

For economic reasons, the first step of the UNK construction intends to achieve an operating mode with the field rise and fall time increased to 40 sec in the superconducting stage. At the price of decreasing the mean intensity, this will allow a substantial cut in the cost for the cryogenic system, rf accelerating system, the power supply system of the magnets, and of the whole complex. However, the complex of the engineering facilities is being designed keeping in mind the further development of the above-mentioned systems and increase of the mean intensity of the accelerator up to the maximum value.

Subsequent stages of the complex development intend to realize in the superconducting ring the storage mode of the maximum energy proton beam.

Collision of this beam with another proton beam accelerated in the opposite direction in the first stage of the UNK will permit an energy in the c. m. s. up to 2.2 TeV at a luminosity value of 10^{32} cm^{-2} sec^{-1}.

A further energy step in p-p collisions up to 6 TeV in the c. m. s. can be obtained by construction in the tunnel of a 5 T constant field superconducting storage ring. At a 6×10^{14} ppp intensity in each beam the luminosity value will be about $10^{32} cm^{-2}$ sec^{-1}. The length chosen for the straight section enables us to meet all the experimental requirements.

A possibility to achieve a 6-TeV energy in the c. m. s. without an additional superconducting storage ring is also under study. It is related to realization of proton - antiproton colliding beams in the UNK and application of the electron-cooling method. A preliminary study[6] showed that with a reasonable antiproton storage time one can achieve a luminosity of 10^{30} - 10^{31} cm^{-2} sec^{-1}. Yet, a number of technical problems does not permit, at the moment, a firm conclusion on the advisability of undertaking the project. The UNK scheme is, however, such that additional elements necessary to produce, store, and preaccelerate antiprotons can be introduced into it in the future.

7. The UNK Status

Creation of the UNK superconducting dipole prototypes is one of the main problems. Presently, the Institute for Electrophysical Apparatus, CEN (Saclay) and IHEP are carrying out a joint program on development and production of 1-m long dipole models. Their efforts are aimed at the determination of superconducting cable requirements, and the choice of basic design and technological solutions for construction of magnets. IHEP

has manufactured and put into operation a machine for cabling and built the equipment to test short samples. Preparation of the test equipment for 1-m long dipoles in a vertical dewar and in horizontal force-circulating ones is being completed. It is furnished with the necessary devices for critical parameter measurements, cryogenic and magnetic measurements, etc. To shorten test time, a system of data handling with an EC-1010 computer is being developed. The devices are manufactured by joint efforts of IHEP, Saclay, MRTI, and JINR.

The IHEP will produce equipment for magnetic, vacuum, and cryogenic tests of the UNK dipole prototypes. Model work on the UNK cryogenic system is envisaged. For these purposes a refrigerator with 400 W capacity at 4.5 °K will be employed. Joint work on cryogenic test equipment automatization is underway in collaboration with Saclay.

Other systems of the UNK are being developed and prototype work is underway. Equipment is being prepared to test rf accelerating systems, injection and extraction devices, devices for magnetic field correction, magnet power supply systems, etc. The development of the beam recapture station at 200 MHz has been initiated in common with JINR.

In the area of the planned location of the UNK, geologic work is being continued. Studies of the ground long-term stability are in progress.

The purpose of the research being carried out is to choose the most economic and rational solution for the UNK project.

References

[1]Yu. M. Ado et al., Proc. III All-Union Meeting on Charged Particle Accelerators, "Nauka," Moscow, 1973, v. II, p. 275.

[2]Yu. M. Ado et al., Proc. IV All-Union Meeting on Charged Particle Accelerators, "Nauka," Moscow, 1975, v. I, p. 44.

[3]A. A. Vasiliev and A. A. Logunov, Proc. V All-Union Meeting on Charged Particle Accelerators, "Nauka," Moscow, 1977, v. I, p. 18.

[4]V. I. Balbekov et al., Proc. X International Conf. on High Energy Accelerators, Serpukhov, 1977, v.I, p. 127.

[5]A. G. Dajkovski et al., Preprint IHEP 77-139, Serpukhov, 1977.

[6]G. I. Budker et al., Proc. V All-Union Meeting on Charged Particle Accelerators, "Nauka," Moscow, 1977, v. II, p. 299.

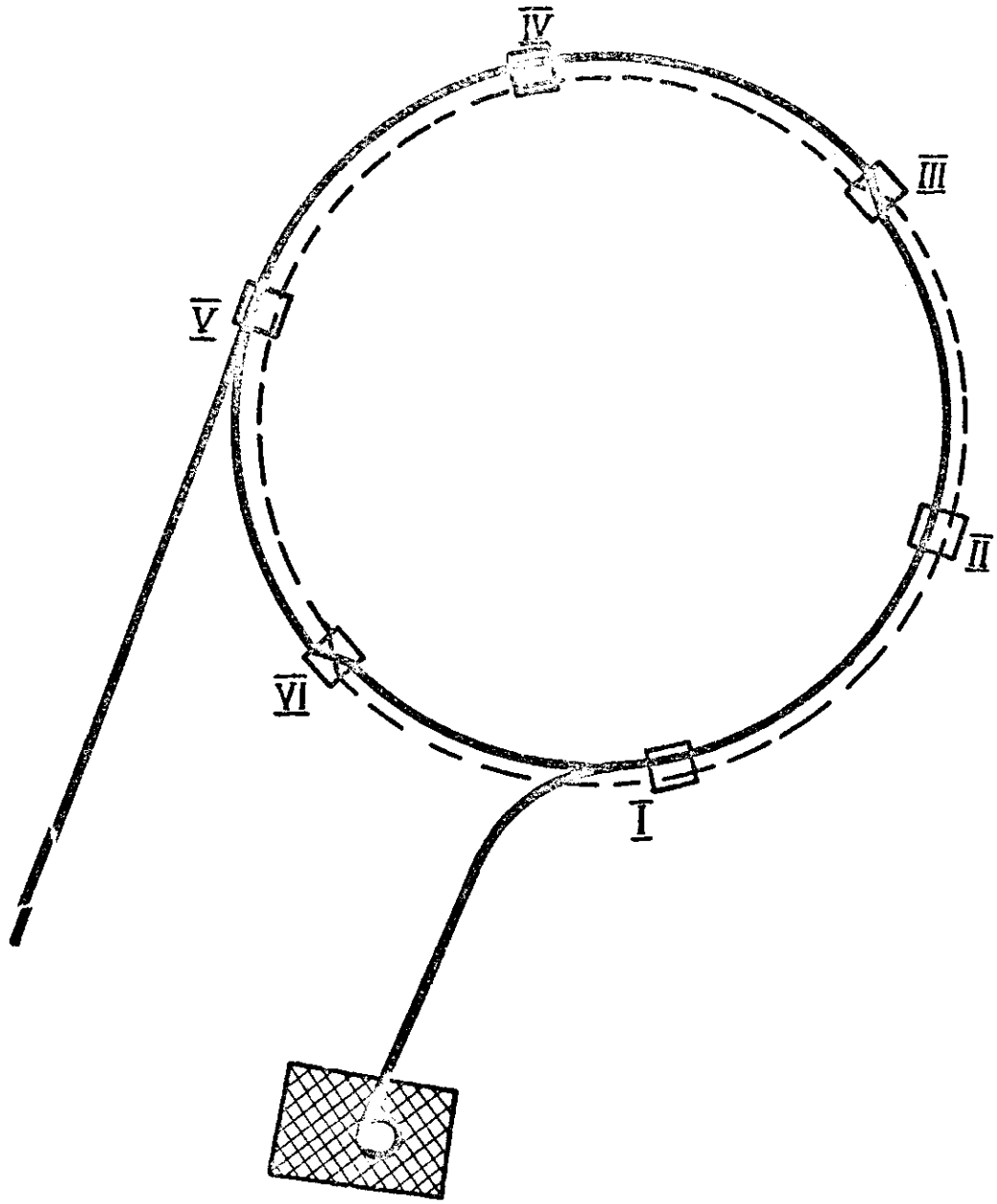

Fig. 1. The layout of the IHEP Accelerating and Storage Complex; the dashed line shows the superconducting storage ring.

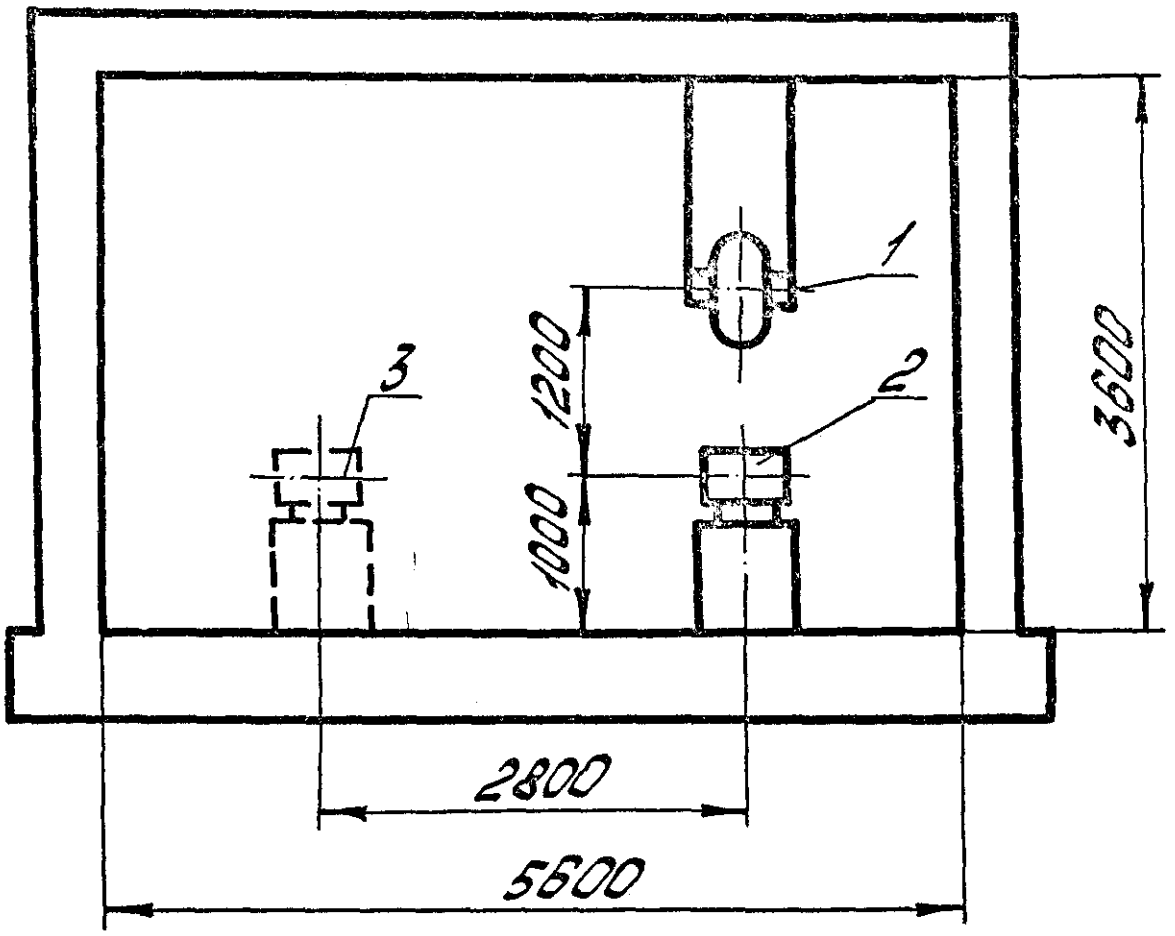

Fig. 2. The view of the UNK tunnel cross section: 1 denotes the first stage of the UNK; 2 denotes the second stage of the UNK; 3 is the storage ring.

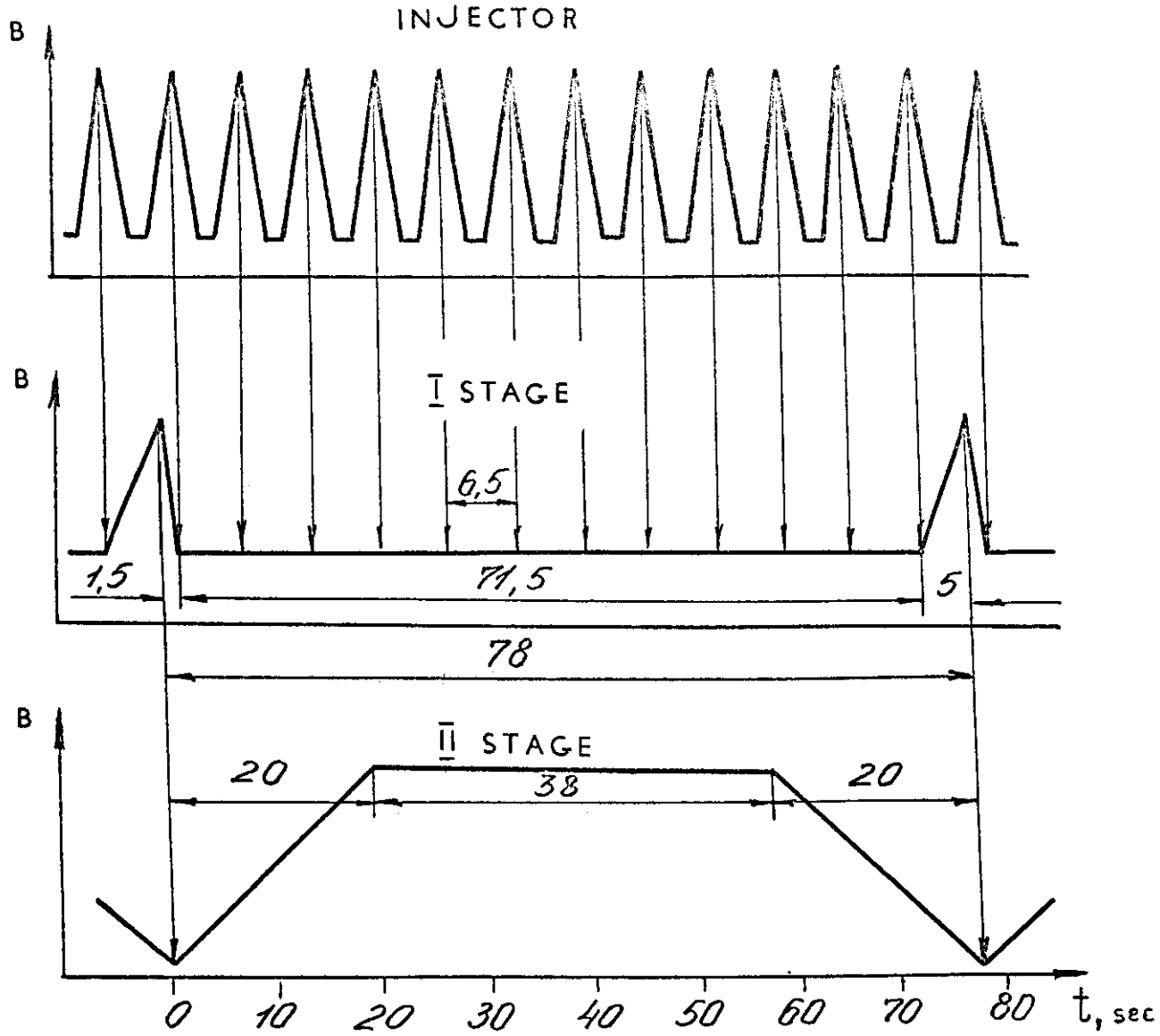

Fig. 3. The magnetic cycle of the U-70 injector and of the UNK first and second stages.

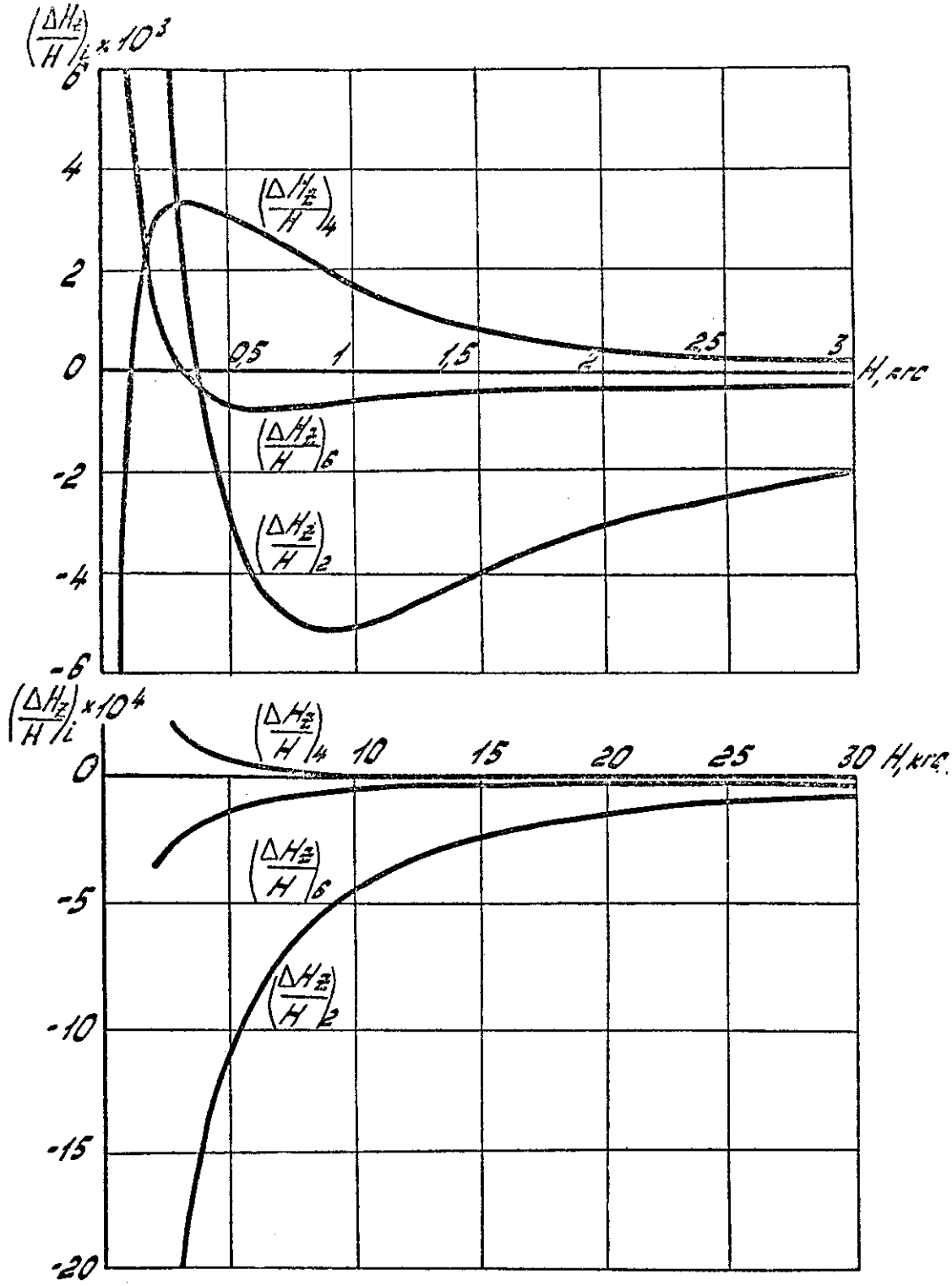

Fig. 4. The residual field nonlinearities as a function of the field value in the superconducting dipole center.

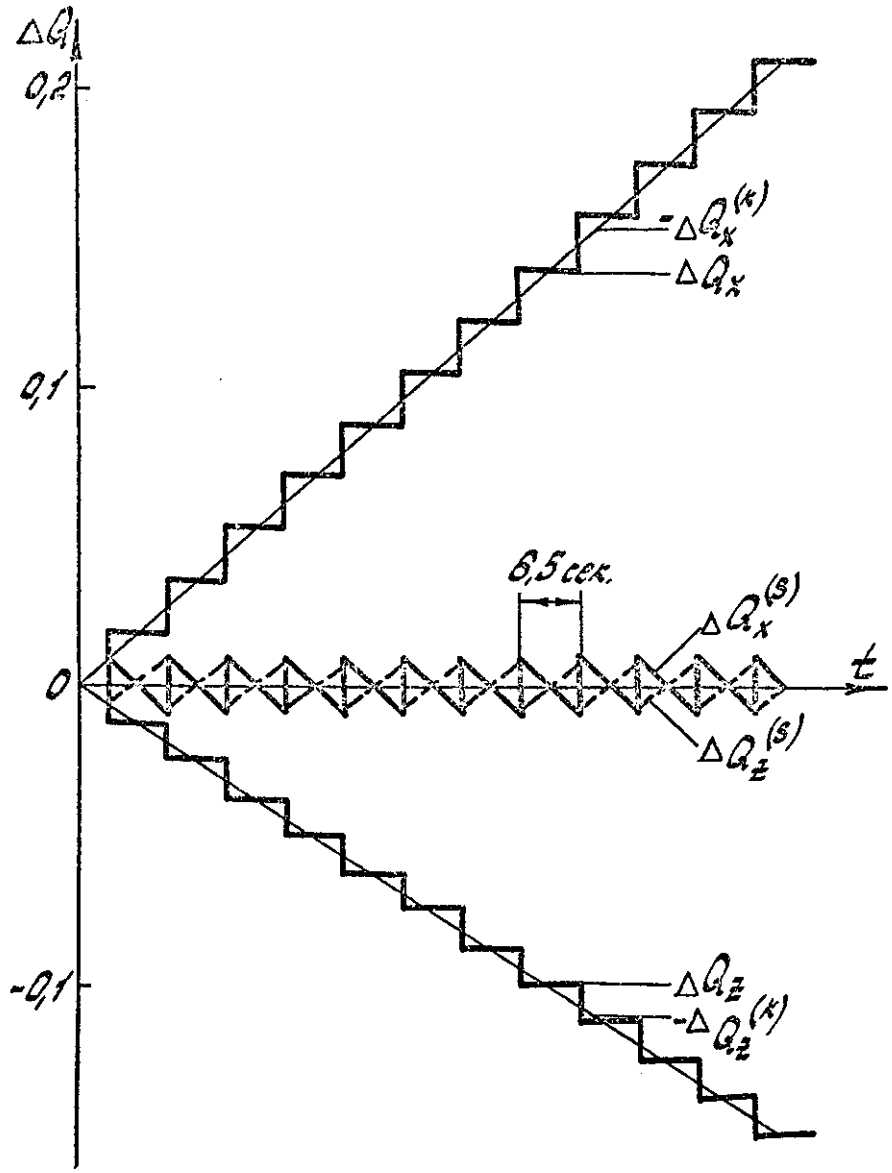

Fig. 5. The change of noncoherent betatron frequencies during beam stacking in the UNK first stage:

ΔQ_r, z - noncoherent Coulomb shifts per injection pulse;

$\Delta Q_r^{(c)}$, z - betatron frequency correction;

$\Delta Q_r^{(s)}$, z - the total Q-shifts.

THE PROBLEM OF FORMING PRECISION MAGNETIC FIELDS IN SUPERCONDUCTING DIPOLES OF UNK

V. I. Balbekov, V. I. Gridasov, K. P. Myznikov,
I. A. Mosalevski, N. A. Monoszon, and V. A. Titov
Institute for High Energy Physics, Serpukhov, USSR

The problems arising in the course of construction of superconducting magnetic dipoles are mainly connected with achieving precise magnetic characteristics, reliability, and manufacture of the dipoles in a quite short period of time. From our analysis carried out for the 3-TeV proton synchrotron (UNK),[1] it became clear that these problems can be solved. As a basic scheme for designing the UNK dipoles, we have chosen a two-layer dipole of the shell type.

Requirements for Magnetic Characteristics of the UNK Dipoles

The calculated beam dimensions in the UNK superconducting stage are 40×50 mm^2. A vacuum chamber of somewhat larger dimensions (60×70 mm) has been chosen since we foresee some trouble with irradiation of the superconducting magnets. The design values for betatron oscillations are $Q_x = 40.69$; $Q_z = 40.73$ (Fig. 1). When designing the superconducting ring and magnetic field correction system, we proceeded from the requirement that no traverse of dangerous stop-bands $3Q_x = 122$, $4Q_z = 163$, and $Q_x - Q_z = 0$ should take place during acceleration. This puts limitations on the Q-spread in the beam: $\delta Q_{x,z} \lesssim 0.02$ at the betatron oscillation amplitudes $A_z \leq 20$ mm and $A_x \leq 25$ mm. The admissible values for nonlinearities are listed in Table I, where $(\Delta B_z/B)_n$ is the multipole coefficient of the nth order at a distance of 35 mm from the chamber center.

Table I.

n	2	3	4	5	6	7	8	9	10
$(\Delta B_z/B)_n \times 10^4$	15	0.5	3	2	10	7	40	30	100

The tolerance for the sextupole component (n = 2) as indicated carries with it the presumption of a sextupole correction system, which is needed in any case for the tuning of the accelerator chromaticity. A large value for the dipole nonlinearities and correcting ones leads to the necessity of taking into account the contributions $\sim (\Delta B_z/B)_2^2$, which are dependent on the number of the correctors. The tolerance 1.5×10^{-3} is acceptable with 360 correctors connected in two sets, each containing 180 elements and located near the main quadrupoles. The limitations may be less strict if we locate the correcting sextupole windings on each dipole; however, such a complication of the dipole design seems to be unjustified.

Even nonlinearities of 4th or higher orders influence mainly the motion of particles with displaced equilibrium orbits, creating additions to the chromaticity dependent on the betatron oscillation amplitude. They are most dangerous during injection when beam dimensions are maximum and the momentum spread may be almost $\pm 1 \times 10^{-3}$.

At the chosen position of the working point, one should consider the influence of the adjacent resonances of the 2nd-4th orders, as well as the possibility of traversing the resonances of the 7th order with center at the point $Q_x = Q_z = 40.714$ (Fig. 1). The corresponding tolerance for the average value for the skew quadrupole component $(\Delta B_x/B)_1$ is 5×10^{-6}. The tolerances for the r. m. s. spreads of the nonlinear components $\langle(\Delta B_z/B)_2\rangle$,

$<(\Delta B_z/B)_3>$, and $<(\Delta B_{x,z}/B)_6>$ are 3×10^{-4}, 6×10^{-4}, and 1×10^{-3} respectively. Then the amplitude growth during a cycle does not exceed 10%.

Attainment of Required Magnetic Characteristics

There are five main sources for magnetic field disturbances: superconductor residual field, deviation of the cross-section shape of the winding from the perfect one, fabrication errors, deformation of the windings caused by ponderomotive forces, and magnetic shielding saturation.

Disturbances caused by magnetization of the superconductor are mainly determined by the diameter of the superconducting filaments, critical current density of the superconductor and its quality.[2] Figure 2 presents the calculated nonlinearities of the 2nd, 4th, and 6th orders for the UNK dipole with the filament diameter of 10 μm, whose critical current density is

$$j\left(\frac{A}{cm^2}\right) = \frac{1\times10^6}{0.8 + B(T)}.$$

Tolerances indicated in Table I are satisfied in fields higher than 0.4 T. Bearing in mind that we do not complete data on the superconductor properties, we have chosen the injection field of 0.67 T for the UNK superconducting stage, which corresponds to an injection energy of 0.4 TeV.

The calculated magnetic field contains only systematic even nonlinearities. The nonlinearities of the lowest order have greatest influence on the particle motion, thus when designing a dipole we seek to reduce them. The compensation of the nonlinearities of the lower orders is realized by proper choice of the angular dimensions of the layers. As an example, we list in Table II calculated nonlinearities in two- and three-layer dipoles with the

Table II.

n	Type	2	4	6	8	10	12
$\left(\frac{\Delta B_z}{B}\right)_n \cdot 10^4$	2-layer	0	0	15.6	-31.3	15.2	-4.3
	3-layer	0	0	0	-8.8	8.3	-5.7

windings uniformly filled with conductors. The inner radius of the winding is 45 mm.

Proceeding from these data, we have derived the dependence of chromaticity on betatron oscillation amplitudes (Fig. 3). From the figure, it follows that in a two-layer dipole chromaticity satisfies the tolerance $|\xi_{x,z}| \lesssim 10$, corresponding to the Q-spread of 0.02, within the limits of the region occupied by the beam. In a three-layer dipole this tolerance is satisfied practically in the whole aperture of the vacuum chamber. In design of the UNK dipoles, a two-layer dipole was chosen since it is easier to fabricate. If necessary, the quality of a two-layer dipole may be improved by introducing one or two calibrated spacers in the first shell of the coil.

Disturbances caused by deformation of the winding cross section under the influence of the ponderomotive forces may conditionally be classified as deformations of the bands and deformation of the winding itself with respect to the bands. The bands made of laminated stainless-steel rings and half rings with radial dimensions ~25 mm are deformed not more than 50 μm at the field of 5 T.

Most dangerous are distortions caused by deformation of the winding itself. The winding, consisting of conductors, insulators and spacers with the cooling channels acquires an elasticity modulus of $\sim 10^5$ kG/cm^2 when

a pre - load of 100 to 150 kG/cm^2 is created. The quantity of epoxy compound must be small. Thus pre-stresses in the winding are quite necessary not only to avoid microcracks but to reduce deformations of the winding.

We are now studying some versions of the bands, consisting of rings and half-rings, from the standpoint of their rigidity, creation of pre-stresses in the winding, precise fixing of the winding position in the bands, as well as examining ways to simplify the winding units for large-scale fabrication. Figures 4 and 5 present the construction of bands made from rings and half-rings for lateral shrinkage of the winding. The left and right rings and half rings are assembled with the help of a tongue-and-groove arrangement. Further glueing of the rings and half rings makes fixation more reliable.

A laminated inner support tube with centering lugs to fix the winding in the azimuthal direction will be used to improve the conditions for winding and to increase rigidity.

Figure 6 presents a design of a winding unit with laminated bands that after being warmed up to 200° C, is mounted on the winding cooled in liquid nitrogen.

The position of a shell-type winding may be fixed with the help of rigid bands with a quite satisfactory accuracy only with respect to the inner radius of the bands and at the edges of layers in the azimuthal direction. The azimuthal position of separate conductors is determined both by the deviations in the conductor dimensions and insulation, and the rigidity of separate sections of the winding along the azimuth. We are now investigating technological means that would allow us to fix (or at least to control) the position of

a set of conductors in azimuthal position. It is of particular importance to make the position of the boundary between the upper and lower coils very precise. It seems possible for us to provide an accuracy in fixing the layer edges in the azimuthal direction of ±50 μm, and a precision of conductor azimuthal position with rms deviation of 50 μm, and that of layer radial position of ±100 μm, deformations due to ponderomotive forces included.[3] *In this all the systematic distortions of the field are within admissible limits* with exception of the octupole and skew quadrupole components; these may be corrected with the help of rather simple correction systems.

With the aforementioned accuracies in conductor position, the requirements for the sextupole component and, moreover, for nonlinearities of higher order will also be fulfilled. It is quite necessary that the critical current density spread in separate sets of superconductors should not exceed ±30% so that the spread of nonlinearities due to residual fields in the superconductors would not go beyond the admissible limits. This requirement can be satisfied. Therefore, at the present state of designing the UNK, correction for nonlinear resonances has not been planned. This question will finally be resolved as soon as we obtain experimental data.

Field disturbances due to saturation of the iron shield for the chosen geometry of the dipole are within admissible limits.

One may expect that at the quoted accuracy in fabrication of the magnets a relative spread of the dipole components would be 1×10^{-3}. Using the data from measurement of the magnetic fields, we may arrange the dipoles in such a sequence that dangerous harmonics of the magnetic field distortion

would be suppressed. Then the value of the orbit distortions would be determined by the precision of magnetic measurements and by variations of the field in the dipole during one cycle and from cycle to cycle.

For these reasons, the effective spread of the dipole fields will be 5×10^{-4}; that is quite acceptable if a closed orbit correction system is available.

The program of manufacturing the prototypes of superconducting dipoles is now being carried out at NIIEFA and IHEP. The main goal of the program is to work out engineering and technological solutions that would provide the aforementioned accuracies in fabrication of magnets. In the superconducting UNK ring, 360 universal correctors are planned for magnetic field corrections. In each universal corrector there will be a dipole winding with vertical or horizontal fields for orbit corrections, and quadrupole and sextupole windings for chromaticity and Q-corrections. A few lenses located in the long straight sections will be used to correct average constituents of the octupole components and of the skew quadrupole term. The decision on the number, power, and location of these lenses will be made when we get experimental data on the UNK magnet characteristics.

References

[1] V. I. Balbekov et al., The IHEP Accelerator and Storage Complex, Proc. VI All-Union Conf. on High Energy Accelerators, Dubna, 1978.

[2] P. F. Smith and T. D. Lewin, Nucl. Instrum. Methods 52, 298 (1967).

[3] The Energy Saver, A Design Report for the Energy Saver Project, Batavia, Illinois, 1978.

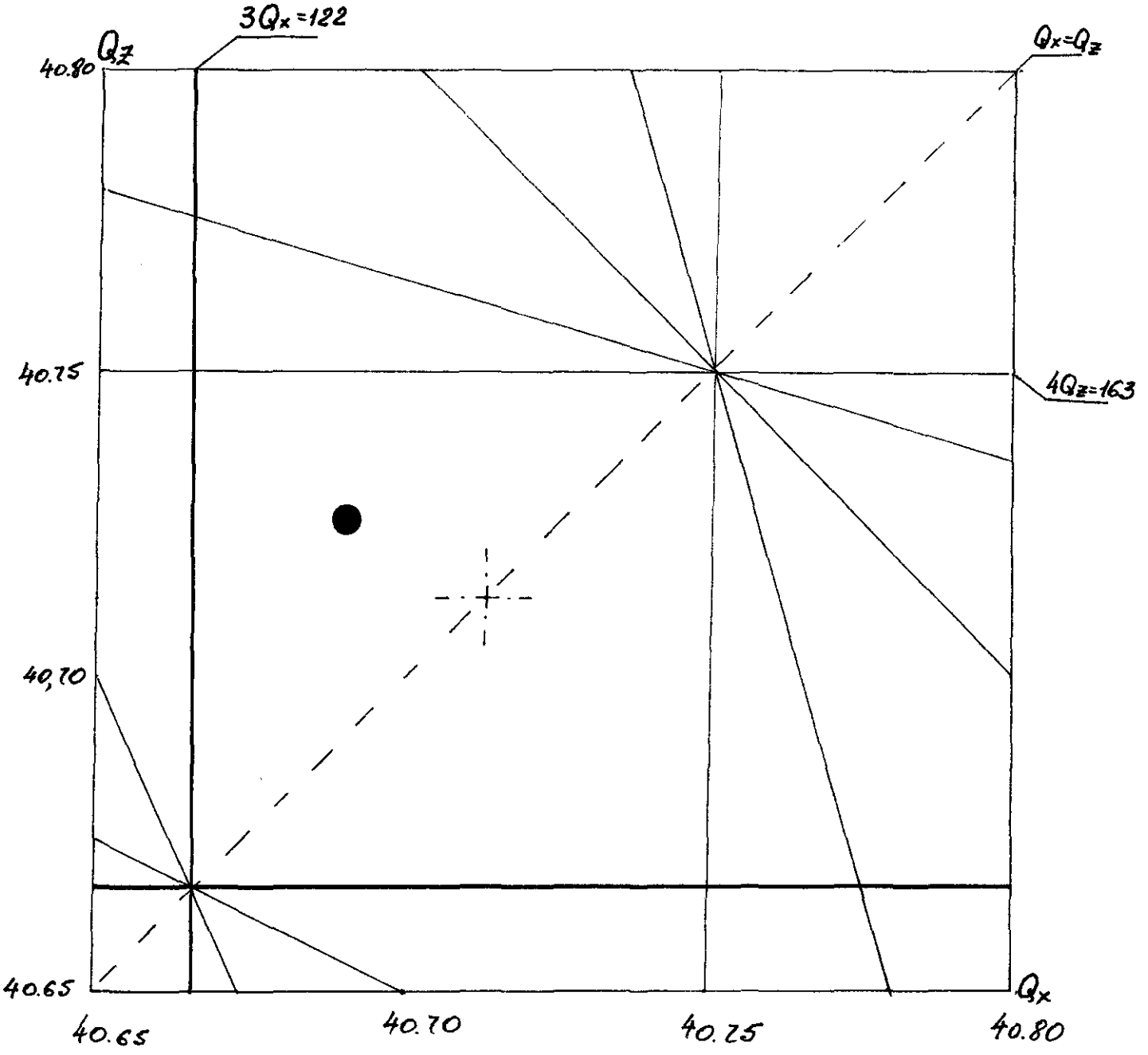

Fig. 1. Position of the working point in the diamond of betatron oscillations.

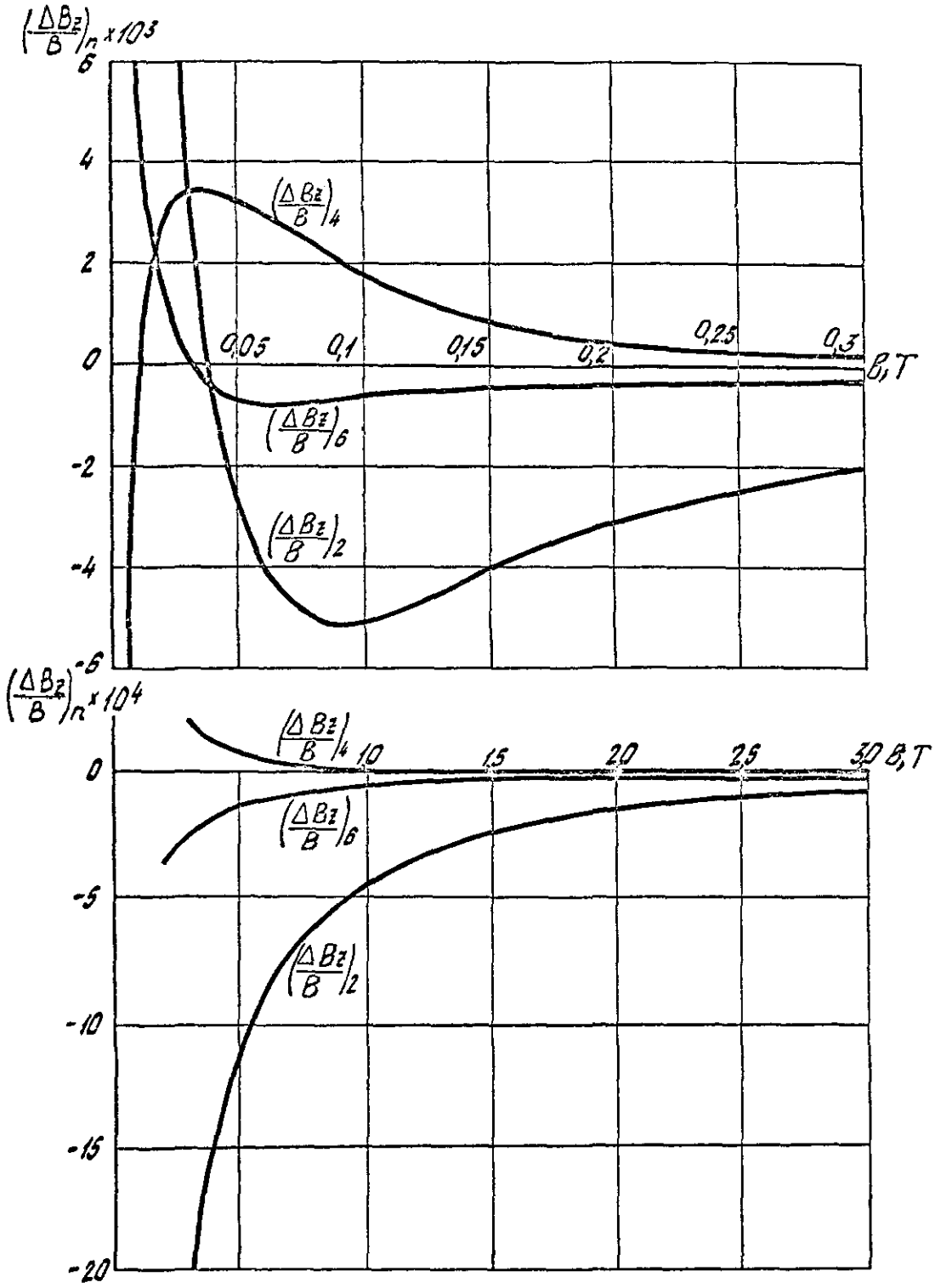

Fig. 2. Nonlinearities of residual fields relative to the field in the vacuum chamber center.

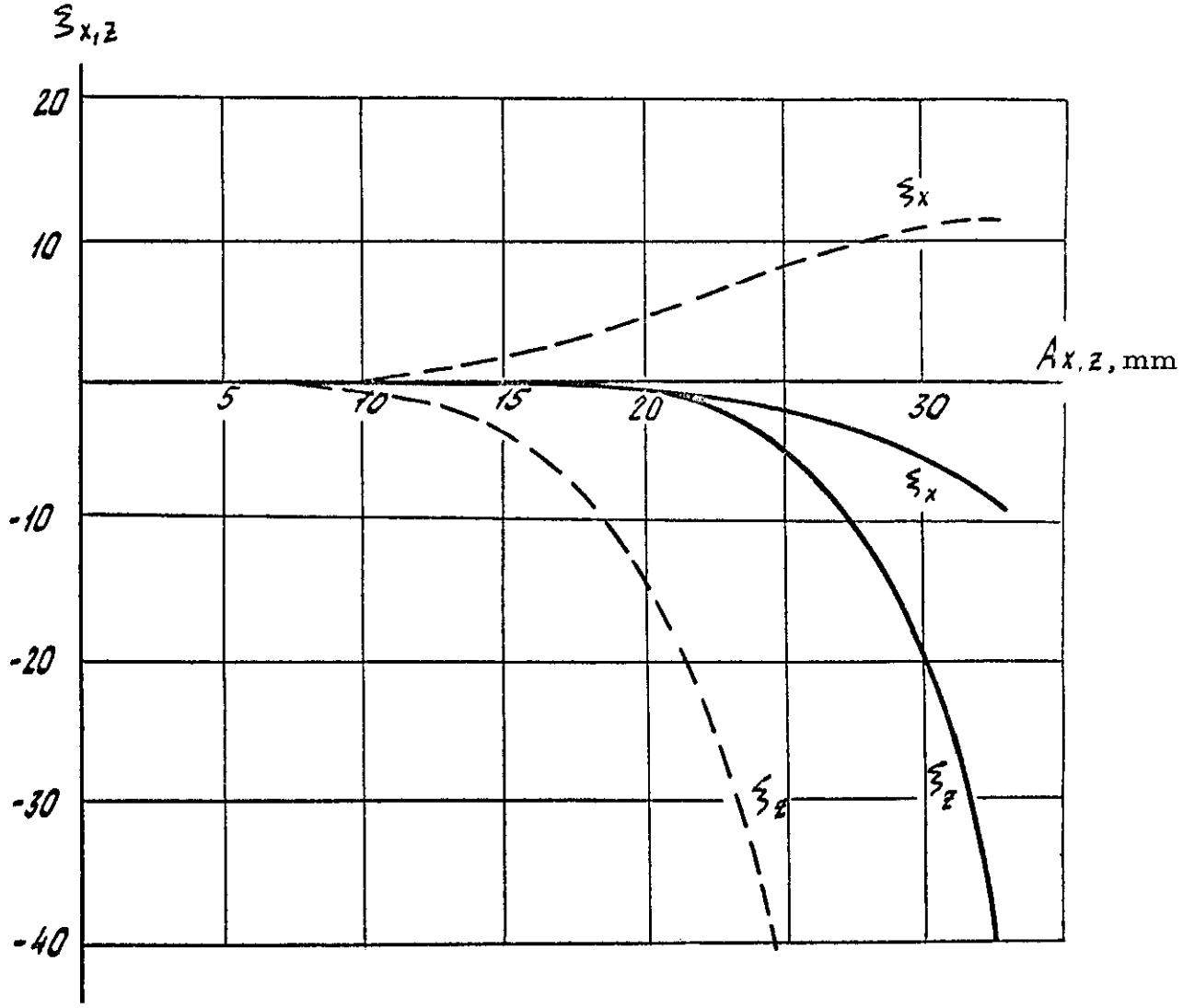

Fig. 3. Chromaticity dependence on the betatron oscillation amplitude.

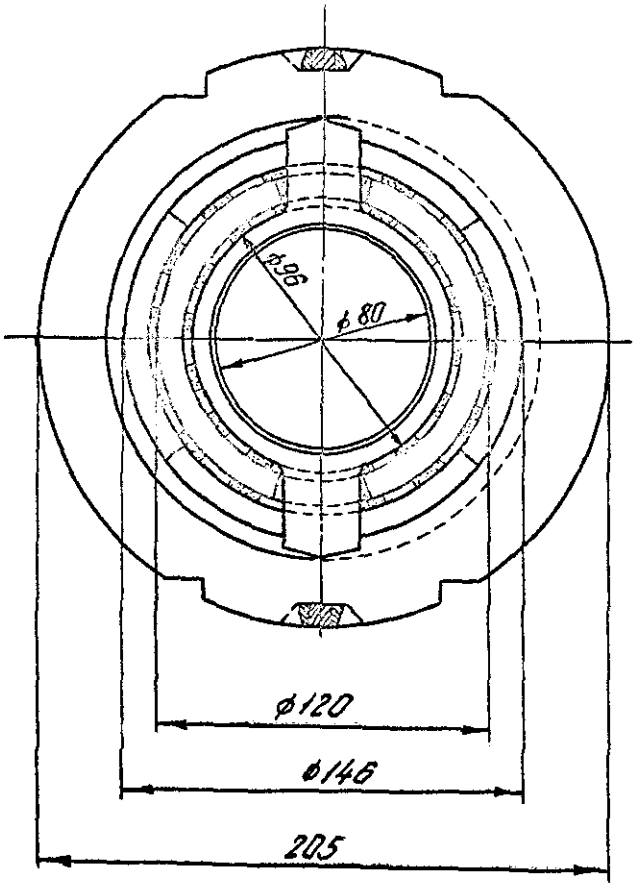

Fig. 4. A design for mechanical shrinkage using bands.

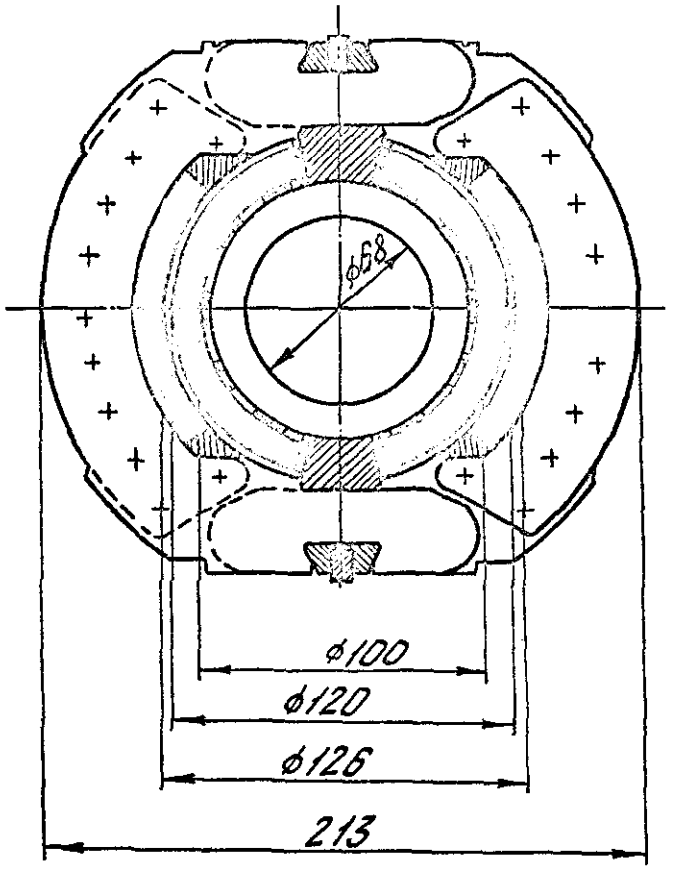

Fig. 5. A design for mechanical shrinkage using half rings.

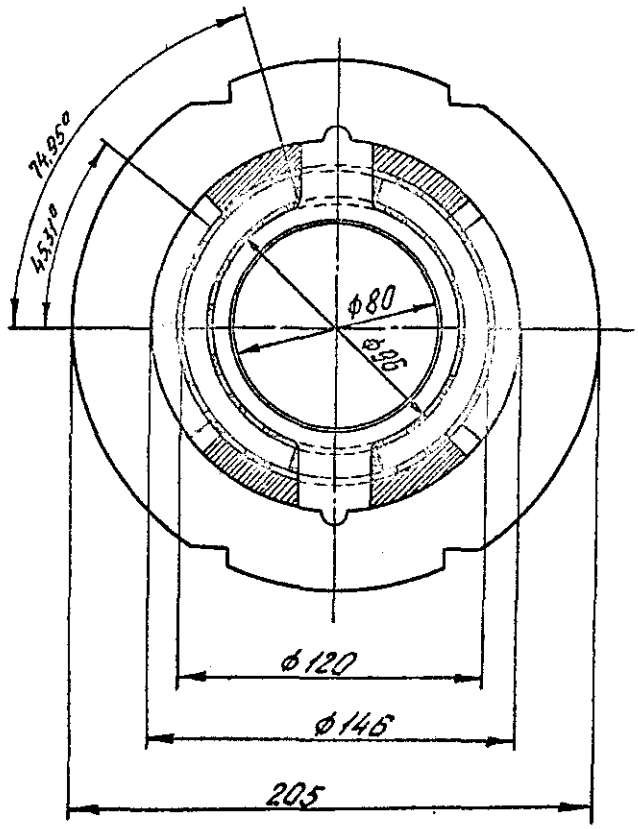

Fig. 6. A design for thermal shrinkage using circular bands.

PROTECTION MEASURES FOR SUPERCONDUCTING MAGNET UNITS OF THE UNK AGAINST RADIATION

V. I. Balbekov, S. L. Kuchinin, V. N. Lebedev, N. V. Mokhov,
K. P. Myznikov, Yu. S. Fedotov, and V. N. Chepegin
Institute for High Energy Physics, Serpukhov, USSR

Further progress in high-energy physics is closely connected with the creation of accelerators incorporating superconducting magnets (SM).[1] Even the very first experiments and calculations devoted to the estimates of the effects of high-energy radiation on the operation of the SM[3-8] made it clear that radiation-heating effects on the superconducting windings caused by beam losses might turn out to be a decisive factor that would impose limitations to the beam intensity. In the present work possible protection measures have been treated by the example of the accelerating-storage complex of IHEP.

The UNK project foresees the construction of a two-stage proton accelerator. The first stage is a 400-GeV accelerator with conventional magnets. Acceleration up to the ultimate 3 TeV energy is realized in the second stage with superconducting magnet units. The U-70 accelerator, whose intensity will be raised up to 5×10^{13} ppc, will be used as an injector for the first stage. During injection, 10-12 proton pulses from the U-70 are stacked in the first stage so that the UNK intensity should be $(5\text{-}6)\,10^{14}$ ppc.

If we take into account the SM cooling dynamics,[7] beam losses on the UNK elements during injection, stacking, acceleration, and extraction may conditionally be classified as instantaneous ($\tau \lesssim 1$ msec) and continuous ones ($\tau \gtrsim 100$ msec). Instantaneous losses may occur during injection, the first revolution, and fast extraction as well as during the development of fast

instabilities in the beam during acceleration. As for the continuous losses, they may take place during scattering on the residual gas, gradual hitting of the vacuum chamber walls by the fraction of protons not captured into the acceleration mode, and at slow beam extraction. Beam losses may also be classified as distributed ones when protons hit the vacuum chamber walls (at angles from 0.1 to 1 mrad) along $\ell > 10$ m and concentrated ones for which ℓ is less than 3 m.

Particles interacting with the matter initiate internuclear cascades in the elements of the system. Energy emission during the cascade development provokes heating of the superconducting winding which may thus undergo a quench. A Monte-Carlo method was used to calculate the internuclear cascade in the UNK magnets with the help of the MARS-4 program.[9] In this we used a model[7] presented in Fig. 1.

For distributed losses, a divergent proton beam strikes the walls of a circular vacuum chamber with uniform intensity along the length of the chamber and at a fixed angle of incidence in the transverse plane; i. e., each element of surface area receives the same flux at the same angle of incidence. To simulate a concentrated loss, the divergent beam strikes the vacuum chamber at a single position along its length but still with a uniform distribution transversely. Figure 2 illustrates radial distributions at the cascade maximum for concentrated losses. Here, the effect of the magnetic field on the internuclear cascade development was not taken into account, and the results were averaged azimuthally over the magnet cross section. According to our estimates the effect of the magnetic field may increase several-fold

the maximum energy density. In contrast to Ref. 7, the results were extrapolated to the inner radius of the coil winding.

Transformation from the calculated values for energy density to the admissible values for beam losses depends on the choice of the value for admissible heating of the superconducting winding as a function of the current density in it. The temperature increment ΔT due to radiation heating should be lower than the maximum increment, determined by that permitted by the critical temperature.[8] There are no reliable data for the quantity ΔT. In the calculations quoted below the following values for the quantity ΔT due to radiation heating are assumed: $\Delta T = 2.0°$ at the injection energy and at the beginning of the acceleration cycle and $\Delta T = 0.2°$ at the maximum beam energy. Knowing ΔT and the maximum energy density (Fig. 2) allows us to estimate the value for the admissible instantaneous losses of the beam ΔI. This value depends on the radiation conditions, initial temperature of the winding T_0 and the state of the SM at the instant of time considered, characterized by the beam energy E_0 and ΔT. The dependence of the admissible instantaneous distributed beam losses on proton energy at fixed ΔT and T_0 is given in Fig. 3. The longer the duration of the losses, the higher values for ΔI are needed for the SM to quench, i.e., the value for the admissible losses increases as compared with those in the figure. As follows from Fig. 3, for homogeneously distributed instantaneous losses at $\theta \simeq 1$ mrad and $T_0 = 4.55°$ K the value for the admissible beam losses will be

$$\Delta I = 2.6 \times 10^8 \, p \, m^{-1} \tag{1a}$$

during injection and the beginning of acceleration (E_0 = 400 GeV), and

$$\Delta I = 5.7 \times 10^{6}\ \mathrm{p\,m}^{-1} \tag{1b}$$

at the end of acceleration (E_0 = 3000 GeV).

From comparison of these values with the design beam intensity it becomes clear that the admissible level of SM irradiation may be achieved only if we take special measures as considered below.

While tracking the beam around the first turn in initial operation, the beam may be lost practically anywhere. Assuming that the minimal length of the section where losses occur will comprise six magnet units azimuthally, then the admissible value is 10^{10} protons. Thus this value is the maximum intensity of the injected beam while tuning up.

When the complex was designed as a whole we considered the necessity of reducing the losses and protecting the elements of the UNK. In the approved two-stage acceleration version the losses are mainly concentrated in the iron circular magnet of the first stage. The beam is recaptured at the accelerating frequency of 200 MHz in the U-70 accelerator. Here, before injection into the first stage of the UNK, sharp edges of the beam are formed so that less than 0.1% of intensity occurs outside of the emittance of 2 mm mrad. High intensity is stacked at 70 GeV in the first stage. In the first stage we foresee forming sharp edges to the beam before its transfer to the second stage. There are gaps in the longitudinal beam distribution during the stacking process to allow for the rise time of the current pulses of the kickers in the transfer and extraction systems. The aperture of the transfer channel is chosen equal to that of the first stage. All these measures allow a transfer efficiency better than 99%. Strict tolerances are imposed on the

stability of the magnet currents in the transfer system, so that the coherent oscillations caused by instabilities in the injection would not result in beam losses. Straight sections (485 m long) in the UNK permit the installation of a beam scraper in both stages to localize the losses. The beam scraper consists of a scatterer and an absorber after it. The local orbit is distorted near the absorber in such a way that protons with large oscillations hit the scatterer. Due to the multiple coulomb scattering in it the particles then come to the absorber. With our choice of the target thickness, the density distribution of the scattered protons at the edges of the absorber is shown in Fig. 4. Here at 400 GeV up to 2% of particles inelastically interact with the scatterer. As for the particles that hit the absorber, they initiate an inter-nuclear cascade in it. A fraction of the particles produced in the cascade goes through the vacuum-chamber aperture and irradiates the SM elements installed behind the absorber. The beam scraper efficiency is defined as the fraction of the beam energy striking the scatterer that is absorbed in the absorber itself. When the steel absorber is 6 m long the value for the efficiency obtained from the calculation is 97% at 200-400 GeV taking into account the radial density distribution of the incident beam (Fig. 4) and inelastic interactions on the scatterer.

In the acceleration mode in the second stage the most dangerous moment from the standpoint of heating is injection into the second stage and beginning of acceleration. The admissible value for the losses localized in the beam scraper during injection will be defined from the conditions of admissible radiation heating of the superconducting winding in the nearest

lens, located at a distance of 150 m from the beam scraper. Secondary hadrons generated in the absorber produce an almost homogeneous (along the lens length) distribution with the density per meter 10^{-4} hadrons/m, normalized for one proton incident on the absorber. Taking into account relations (1) this corresponds to the capturing during injection of a few per cent from the design intensity. When it is necessary to capture the largest fraction of the beam during injection we plan to solve the problem of protecting the SM in the straight section in the same way as it is done in the case of beam extraction.

Three extraction modes have been planned for the UNK, i. e., one turn fast extraction, slow resonance extraction (38 sec) and fast resonance extraction of 1 msec duration almost 10 times per accelerator cycle, i. e., 6×10^{13} protons per burst in 3 seconds at the magnetic field flattop. Figure 5 presents the scheme of the matched straight section of the UNK where the ejection system units are located. A kicker magnet (KM 1) guides the beam into the septum magnet during fast extraction. In resonance fast and slow extraction the beam is steered into the ES septum through resonance excitation of betatron oscillations. Since we do not plan to extract the whole intensity during one-turn fast extraction, the most dangerous from the standpoint of SM irradiation would be the mode of fast resonance extraction. The fraction of beam hitting the 0.1 mm septum is one per cent of the extracted intensity. At 3 TeV 10-15% of the particles will leave the septum avoiding nuclear interactions due to the multiple coulomb scattering. The remaining part of the beam (5×10^{11}) experiences inelastic nuclear interactions with the septum matter.

Secondaries produced in inelastic interactions in the ES septum irradiate the superconducting elements installed downstream. Hadrons initiate internuclear cascades; γ-quanta from pion decay generate electron-photon showers. Figure 6 illustrates the dependence of energy emission density in the lens superconducting winding installed at a distance of 170 m from the ES (lens Q_5 in Fig. 5) on the thickness of the iron shielding layer covering the vacuum chamber. As is seen the shielding layer of some mm reduces energy emission in the winding due to a reduction of the contribution from the electron-photon shower from photons produced in the ES. When the thickness of the shielding is more than 3 mm this contribution is almost completely suppressed. In practice this can be achieved by a proper chamber thickness. A steel shielding ~ 1 cm thick surrounding the vacuum chamber inside the SM may protect quite reliably the superconducting windings. This measure also allows one to reduce 2-3 times the value for energy emission density from any hadrons hitting the chamber at the angle $\theta \lesssim 1$ mrad in the windings.

Figure 7 gives the value for the coefficient K_0 that characterizes over-irradiation of the SM, depending on the distance between the SM and ES when the number of interactions on it is 5×10^{11}. At $K_0 = 1$, energy emission density is equal to the adopted admissible value at which the overheating does not exceed $\Delta T = 0.2^\circ$. The calculated dependence of the coefficient K_0 on the distance L for different energies of protons on the ES and aperture of the irradiated SM are presented. The angle between the beam hitting the septum and the vacuum chamber axis in the straight section is taken as a parameter.

As is clear from Fig. 7 at 3 TeV and $\theta = 0$ the value for the coefficient K_0 may be almost 40. The increase of the diameter of the SM aperture does not result in any significant reduction of the coefficient K_0. At energies above 1 TeV an effective measure would be an increase of the angle θ. For the geometry of the considered straight section at 1.5-3 TeV and the angle $\theta = 2$ mrad one manages to reduce the irradiation of the superconducting elements located in the straight section almost down to the admissible value. As follows from Fig. 7 irradiation of the SM in the ring magnet becomes considerably lower as well. The angle needed in practice may be created if the beam is deflected before hitting the septum with the help of bending magnet (BM3). Magnets BM3, BM2, and BM1 may compensate for the disturbances of the circulating beam.

It should be noted that the influence of the magnetic elements, located downstream from the ES, would re-distribute the particle flux, which would result in the change of the value for the coefficient K_0. This effect should be taken into account when choosing the construction of the straight sections and installing the equipment in them.

Application of special collimators is another protection measure for the SM. The aperture sizes of separate collimators are determined proceeding from a condition of complete shielding of the vacuum chamber surface of the protected element against secondaries generated in the ES. The coefficient when protection is realized with a collimator whose length is 6 m is practically constant and equal ~ 4 at hadron energy 0.2-3 TeV. In order to increase the coefficient we may propose to use several collimators at a

certain distance from each other. Under proper shielding conditions for a sequence of collimators the value for the coefficient may be 100. However, the fulfillment of this condition results in a noticeable decrease of the accelerator acceptance. This fact puts quite considerable limitations on application of this type of protection.

To avoid destruction and overheating of the SM, in emergency cases a beam-abort system with an efficiency better than 99% is foreseen in both stages of the UNK.

The results quoted in the report are quite preliminary. This important problem is still being studied. However, the results obtained give us hope that the measures on minimizing the losses and protecting the SM worked out in the frame of the UNK project would provide possibilities for operating the complex at the design beam intensity.

R E F E R E N C E S

1. The Energy Doubler, FNAL, Batavia, 1976.
2. В.И.Балбеков и др. Труды X Международной конферкнции по ускорителям заряженных частиц высоких энергий. Протвино, 1977, т. I, стр. 127.
3. C.Restat et al. Preprint CERN ISR-MA/75-20, 1975.
4. Н.В.Мохов и др. Препринт ИТЭФ-114, Москва, 1975.
5. A.Van Ginneken. Preprint FNAL, TM-685, Batavia, 1976.
6. Л.Н.Зайцев. Сообщение ЛИЯИ Р16-10480, Дубна, 1977.
7. А.И.Дайковский и др. Препринт ИФВЭ 77-139, Серпухов, 1977.
8. Г.Брехна. Сверхпроводящие магнитные системы. М., "Мир",1976.
9. И.С.Байшев и др. Препринт ИФВЭ .78-2, Серпухов, 1978.

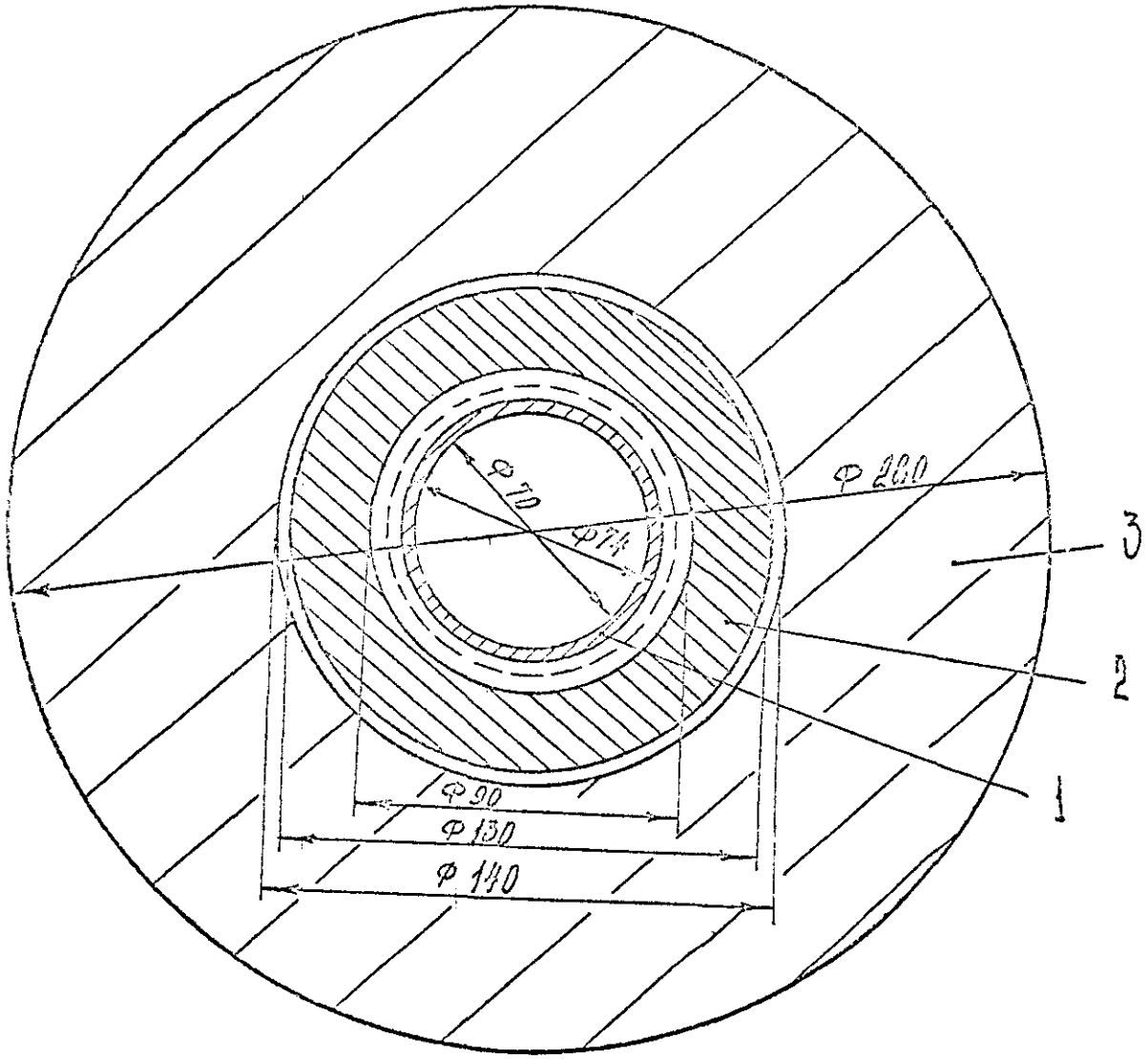

Fig. 1. The cross section of the magnet model used in calculations of internuclear cascades for distributed and concentrated losses. 1: vacuum chamber; 2: superconducting winding; 3: iron yoke.

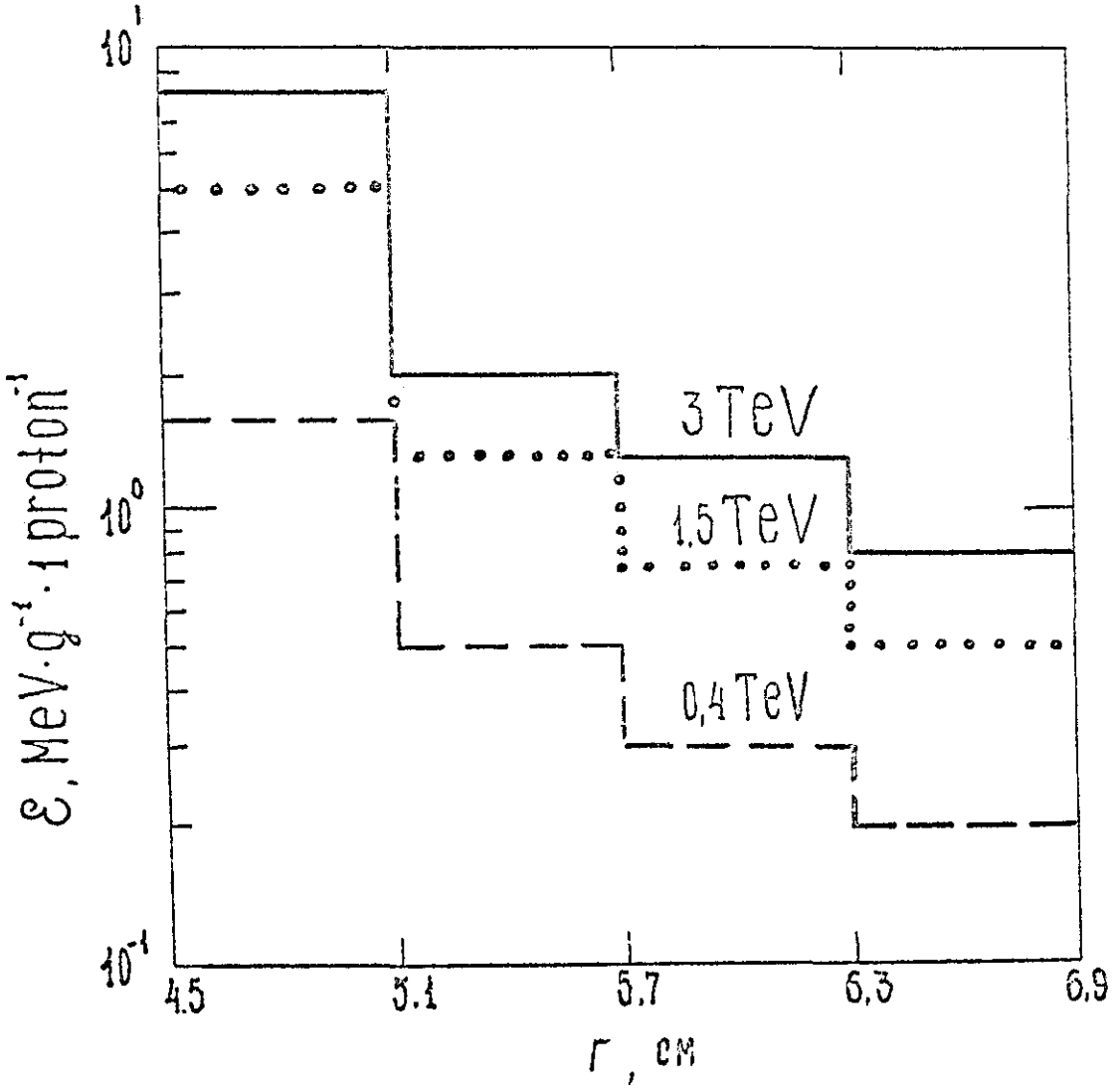

Fig. 2. Radial distributions of energy emission density in the magnet windings at the maximum of the cascade for concentrated losses of protons with different energies. The vacuum chamber wall thickness is 0.5 mm.

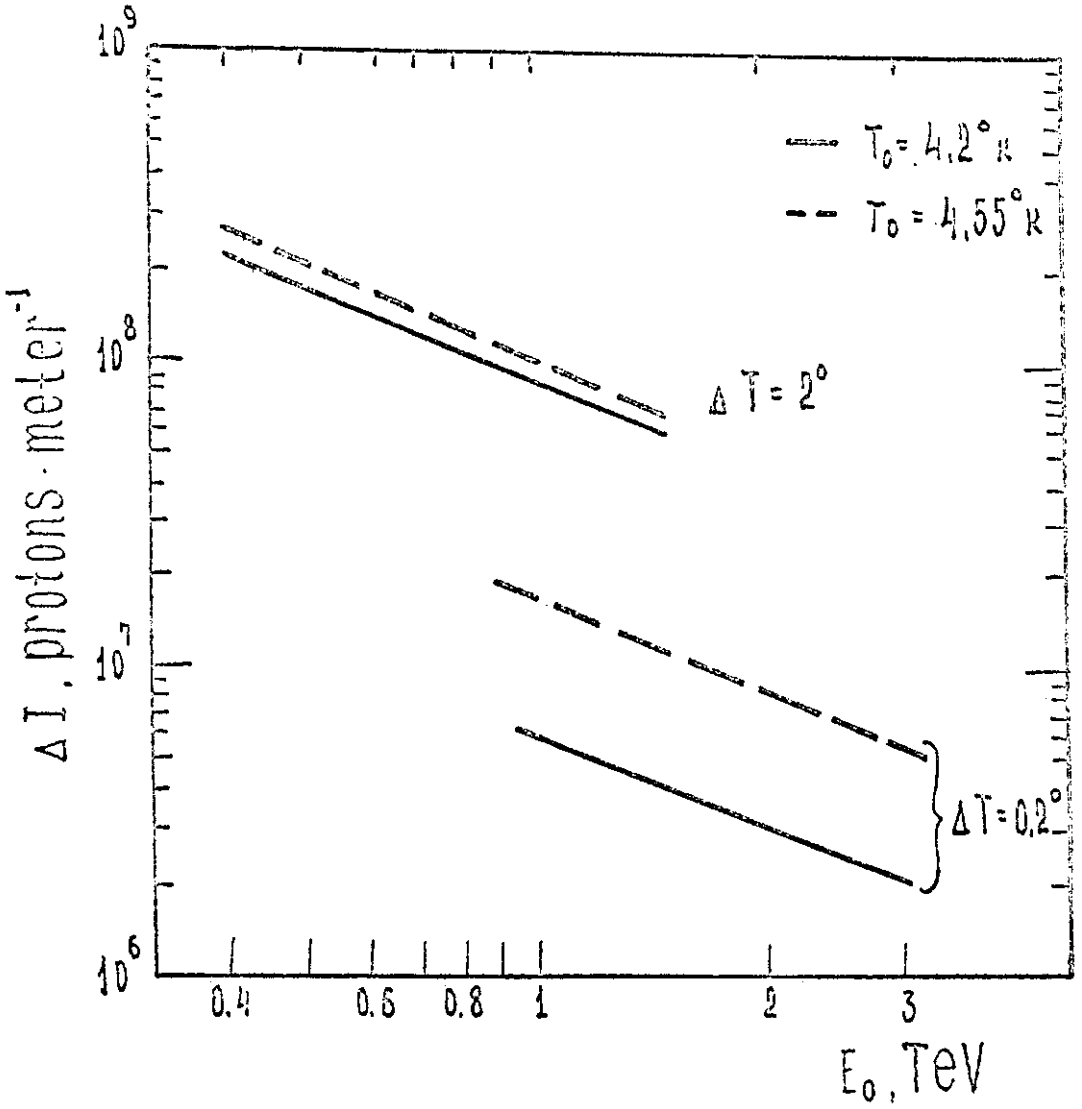

Fig. 3. Dependence of admissible values for instantaneous distributed losses of protons on their energy. T is the initial temperature of the winding before irradiation.

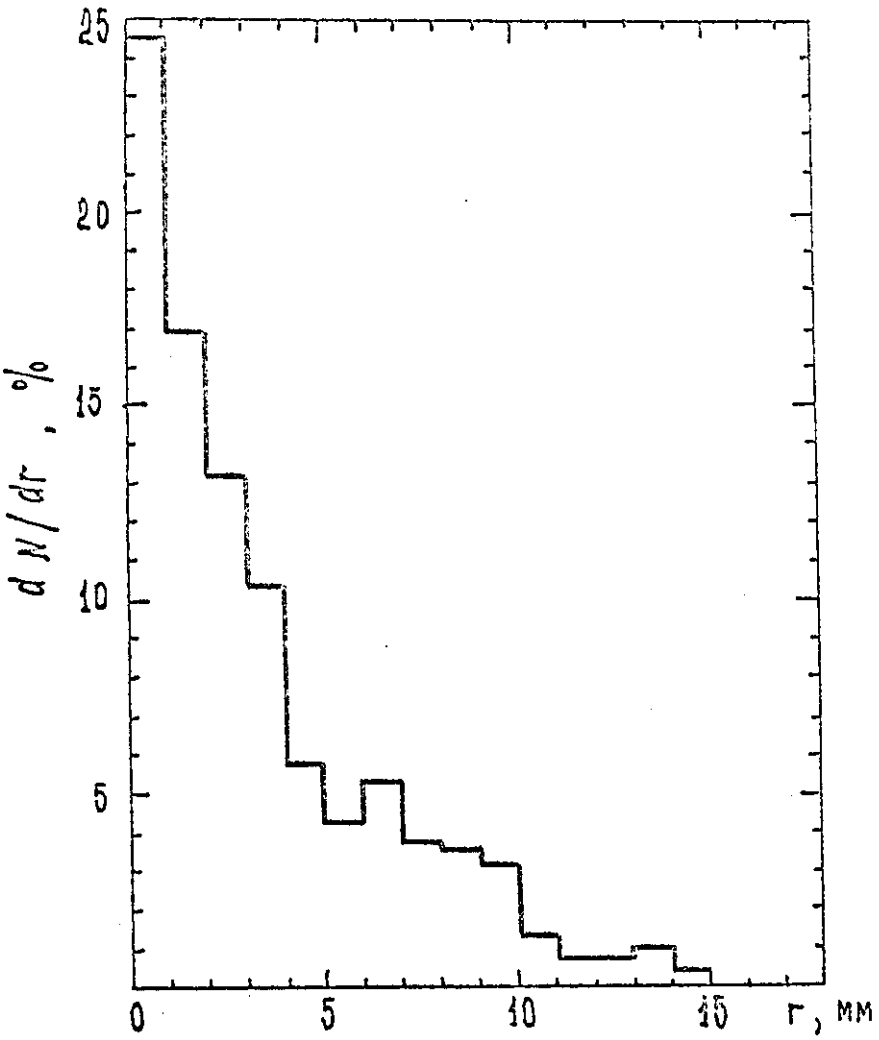

Fig. 4. Radial distribution of proton beam density at the edge of the aperture of the absorber in the scraper during injection.

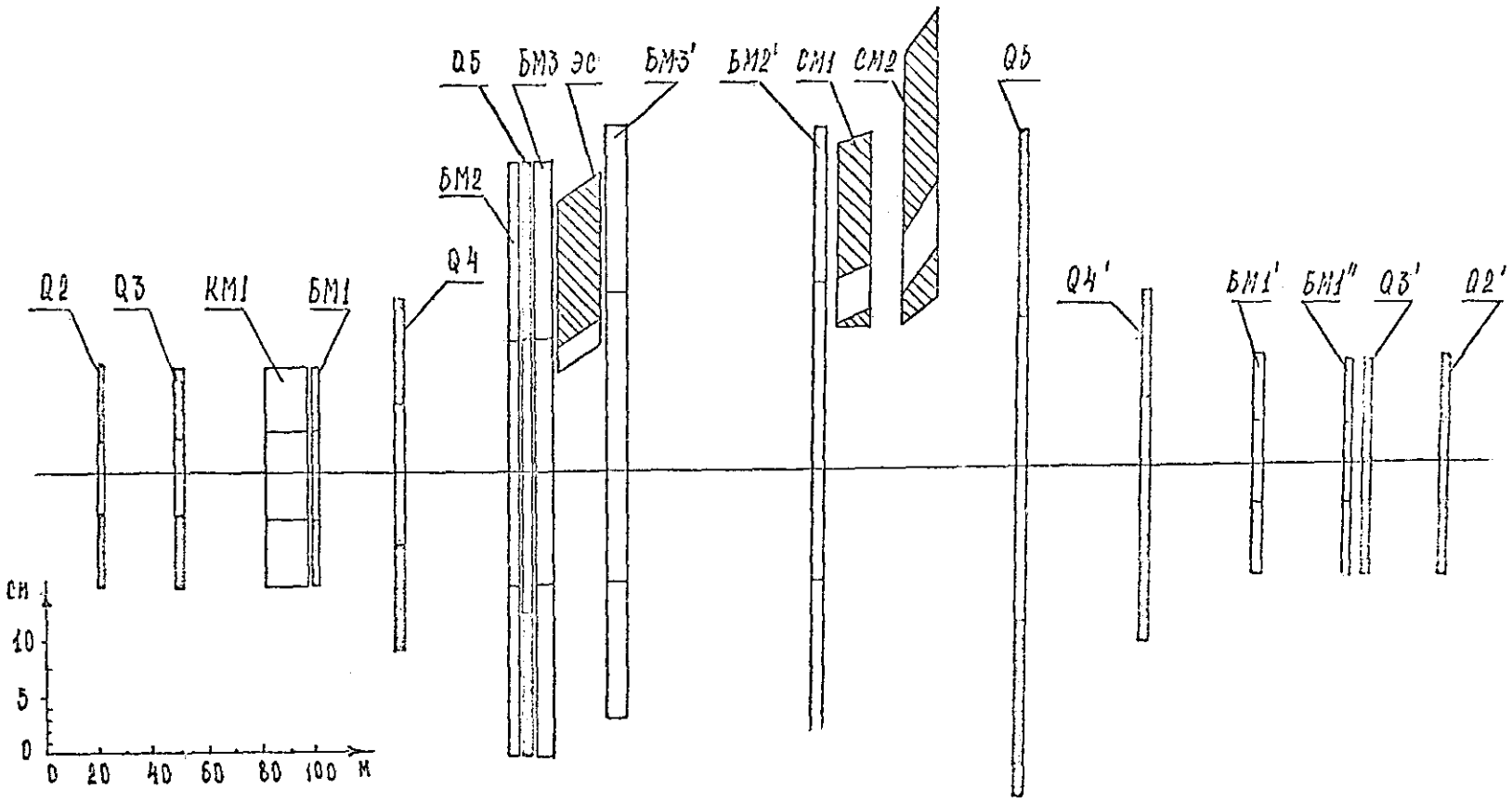

Fig. 5. The layout of the extraction straight section of the UNK. Q2-Q4: quadrupole matching lenses; KM1: kicker magnet of fast extraction system; ES: electrostatic septum; SM1-SM2: extraction magnets with a current septum; BM1-BM3: auxiliary bending magnets.

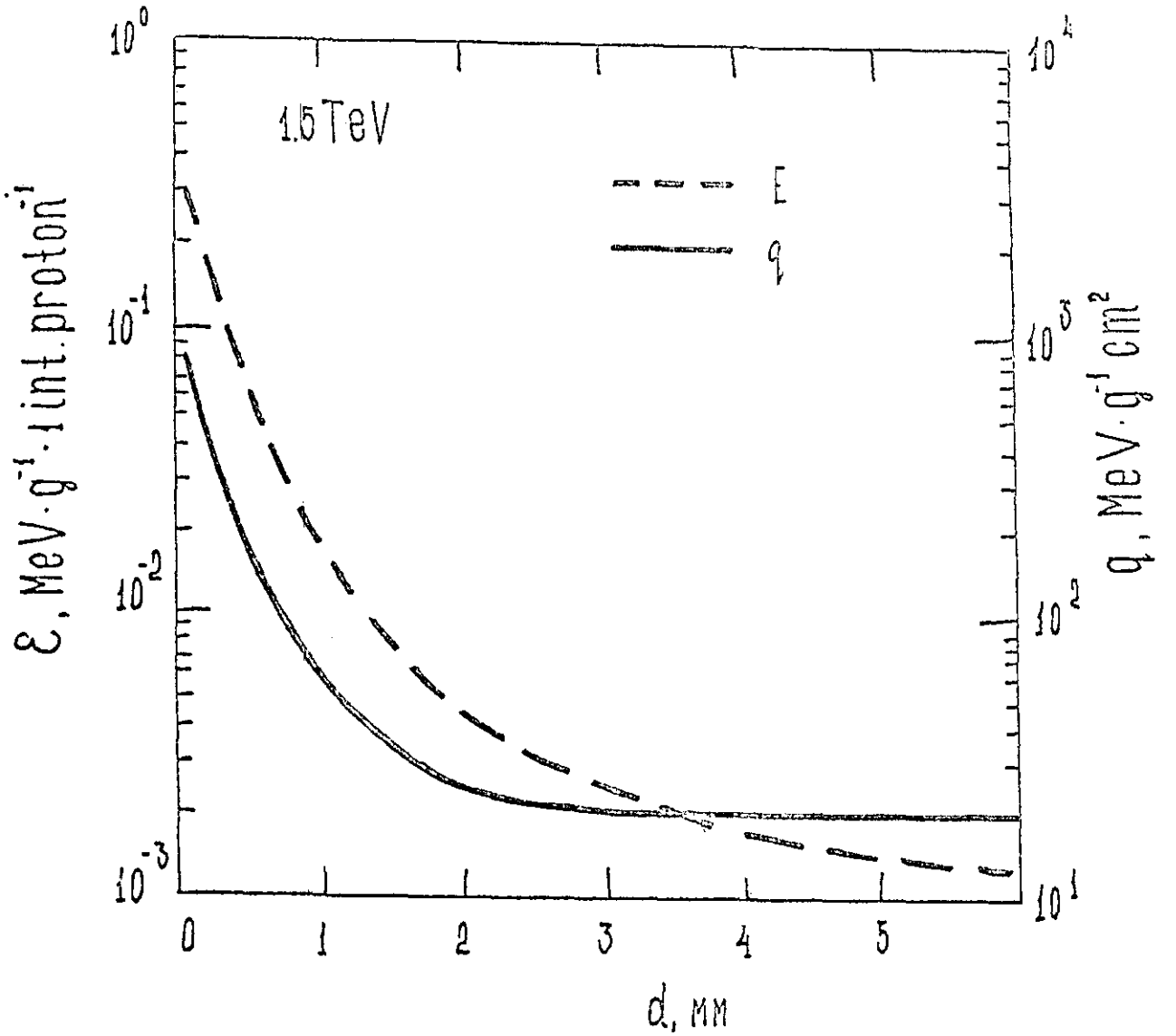

Fig. 6. Typical dependence of the maximum density of energy emission ϵ in the superconducting winding on the thickness of the vacuum chamber when irradiated by secondaries from the ES septum; q: transformation coefficient of hadronic fluence in the winding to the energy emission density.

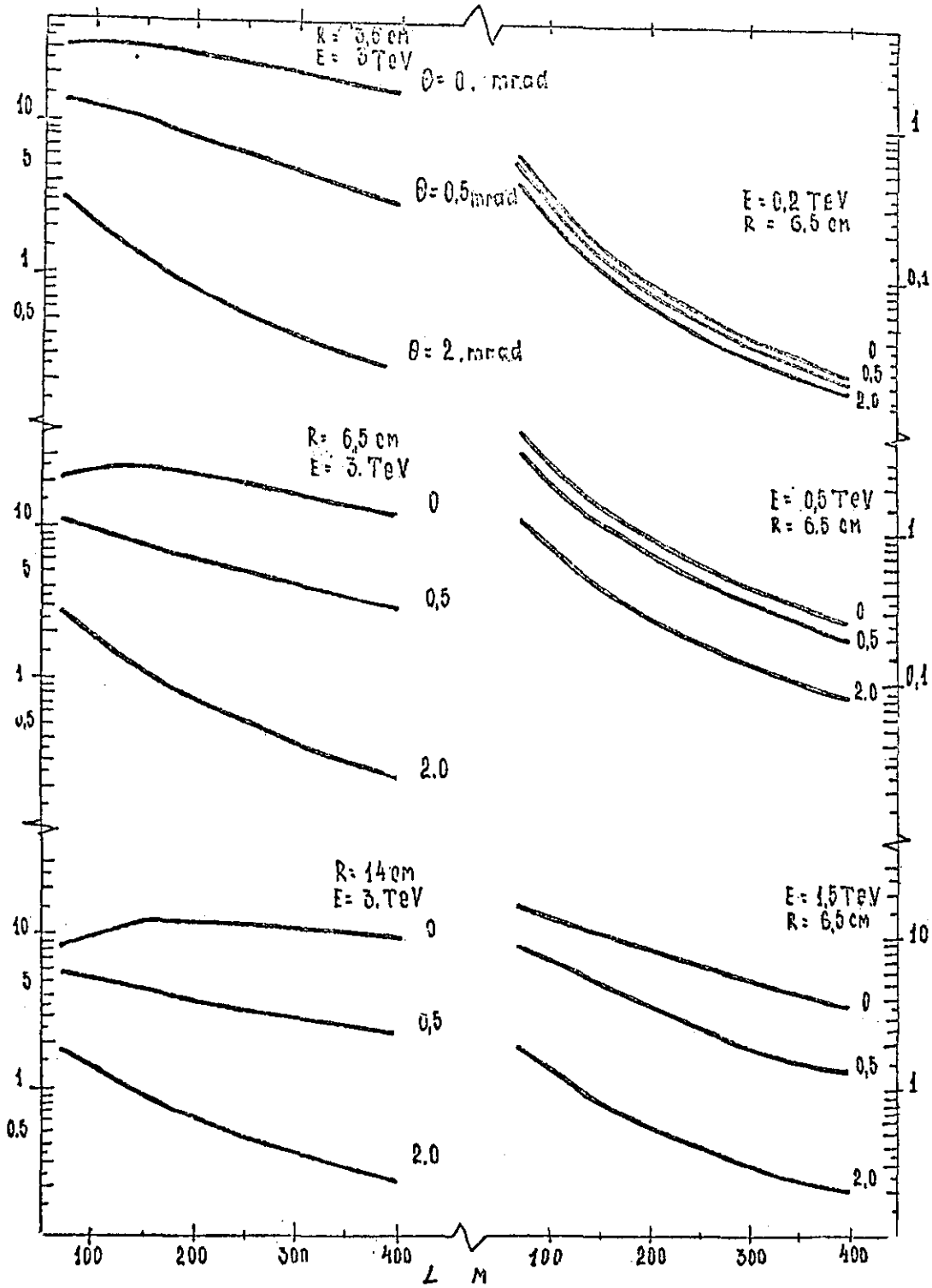

Fig. 7. The dependence of the coefficient K_0 on the distance L between the E_s septum and irradiated superconducting element. R: element aperture radius; E: beam energy, TeV; θ: the angle between beam direction on the septum and the vacuum chamber axis in the straight section.

THE PENTEVAC: A SITE-FILLING ACCELERATOR AT FERMILAB

R. R. Wilson

The Fermilab site is large and one might ask, "What is the largest accelerator that can be built within its confines?". The ring shown in Figure 1 has a radius of 2.5 km, and, although a slightly larger circle would also fit, it is well to stay some distance away from the site boundaries. The rigid off-site radiation limitation, whether it be due to muons or neutrons presents a serious problem. Starting with a tunnel 2.5 km in radius, we can ask what might go into the tunnel. Rather than putting three magnet rings in the tunnel so we could attempt every possibility at once, we might instead imagine a scenario in which we would install only one or two rings at a time, ringing the changes in a manner most likely to develop the information about particles that we most want, and thereby drawing out a view of nature as a novelist draws out his story, for the maximum satisfaction of his reader - or in this case, for a maximum amount of insights about the physical world within the limitation of available funding.

(a) 5 TeV Protons on Fixed Targets

Let us consider first the accelerator as a source of protons to be incident on fixed targets. Because it will not be built in the immediate future, we must ask what magnetic field that we can anticipate might be attainable in

the magnets at the time, say ten years from now, when such a large accelerator might be started. Although by the use of new materials there is no obvious reason not eventually to reach fields of the order of hundreds of kilogauss, I suggest that a factor of two, beyond the field of 42.5 kG which obtains in the Tevatron, i.e., to 85 kG is nearly within the state of the art right now. In that case 5 TeV protons could be produced, hence the name Pentevac.

The present limitation of the field in the Tevatron magnets is imposed primarily by three factors; (a) the current density that can be reached using the present superconductor, NbTi; (b) the mechanical distortion caused by the tremendous magnetic force on the conductors; and (c) the removal of the large amount of magnetic energy intrinsically stored in each magnet without melting the conductor. Doubling the magnetic field in the present Tevatron magnets by simply doubling the current density, were that possible, would quadruple the forces and the stored energy.

Fig. 2 shows in cross section a suggested design of a dipole supermagnet for the Pentevac which might reach 85 kG; it is based on the present Tevatron magnet design. Instead of NbTi, Nb_3Sn would be used as superconductor, for it will reach the required current density at the required field strength. The present difficulty with Nb_3Sn is that practical conductors made of it are not ductile enough so that sharp bends in the coils can be made without destroying the superconducting property of the wire. Although this problem may be solved, for example, by

making the filaments of the superconductor much finer than at present, there is even at present a technique for fabricating the coil. Bronze is used as the matrix material in which fine filaments of pure Nb have been imbedded. This material is ductile so that coils made of it can be wound in the appropriate shape. Then if the temperature of the material is raised to about 750°C, the tin component of the bronze will migrate and interact with the Nb to form Nb_3Sn. The coils must then be insulated after having been formed and heat-treated and then installed within the stainless steel collars. The present coil structure of NbTi and insulator tends to be "squishy," and might not withstand a quadrupoling of the force without collapsing. However, loading the epoxy heavily with alumina makes a much stiffer material than the present epoxy-fiberglass (B-stage) material now in use, and there is some empirical evidence that the alumina-loaded material is satisfactory. Sprayed-on glass might also be a good insulator for use with Nb_3Sn, and one which might withstand the heat conditioning. The cable is shown to be much larger than in the Tevatron magnets, in order to reduce the number of turns and thereby also reduce the voltage on the coil during ramping and quenching, and also reduce the work of insulating the turns.

The free opening in the coil shown in the design is roughly elliptical in shape, 2-1/2" wide by 2" high; it is smaller than the opening of the Tevatron magnets, which is circular in shape and 3" in diameter. The smaller opening should reduce the stored energy for a given value of the magnetic field by nearly a factor of two and the total force on the conductors should also be

reduced accordingly. The "good" magnetic field aperture as indicated by the calculations of S. Snowdon is about 0.75 inches wide instead of being about 1 inch wide as in the Tevatron magnets. The reduction in aperture should be possible because the size of the injected beam of 300-1000 GeV protons would be somewhat smaller and stiffer than the beam of about 100 GeV protons which are to be injected into the Tevatron. A stronger lattice might also be used to reduce the size of the beam.

The energy stored in the magnetic field, about 1 megajoule per magnet assuming the same length as for Tevatron magnets,* must be rapidly disposed of in the event of an accidental quench in order to prevent the superconducting cable from melting. The stored energy in the present Tevatron magnets, 0.5 MJ per magnet, is absorbed in the coil when it goes normal. It is important that the whole coil be driven normal by means of a heater once a quench is detected. This method can still be expected to work even for the high field design because the coil is still capable of absorbing about twice as much energy without melting or burning the insulation.

As shown in Fig. 1 protons can be transferred from the Main Ring or the Tevatron to the Pentevac through an intermediate ring of average radius 0.5 km. A different possibility not shown, would be to build an external bypass on the Main Ring so as to

---

* It is suggested that the magnets be made about 25 M in length rather than the 7M of the present Doubler magnets.

be tangent to the Pentevac ring at one of its straight sections.

A typical cycle might require 60 seconds: it would be comprised of a 10 second dwell-time at low field while three pulses of 300 GeV protons from the Main Ring were successively injected to fill the Pentevac ring head-to-tail fashion, then a 15 second ramping-period to full field, then a flattop of any length but let's say 20 seconds, after which the cycle ends with a 15 second ramp back to injection field. By using tricks such as stacking multiple turns in the Tevatron and then transferring these to the Pentevac, the injection time could be reduced to a few milliseconds, and then by using a faster rise time for the magnets, the total pulse time of the Pentevac, apart from the flattop, might be reduced to about twenty seconds, i.e., comparable to the present pulse time for Main Ring operation at 400 GeV. If we assume that each injected pulse from the Main Ring would contain 3×10^{13} protons, the total pulse intensity of the Pentevac would be about 10^{14} protons. When these have been accelerated to 5 TeV, the total beam energy would be a frightening 100 megajoules per pulse. Clearly should a pulse get out of control it could destroy many of the supermagnets. The experience with the present one megajoule level of beam energy is that seldom does the beam get out of control, and, although what is now called "out of control" would correspond in the 5 TeV case to an inadvertent loss of only about one percent of the beam, my judgment is that the beam abort system could be tightened up enough to abort the beam reliably before a dangerous beam loss could occur. Even a smaller loss, as little

as about 10^{-6} in one magnet, may be enough to quench the supermagnet. This does not mean that the problem of containing a large beam of protons is impossible, but it does mean that new techniques of sensing a small abnormal growth of the beam would be necessary. Tuning the machine would necessarily become a much more sophisticated exercise than it now is - but not an impossible one.

Beam extraction and targeting are the really serious problems. One solution it to limit the intensity of the beam to levels for which solutions have already been found, and then, as new techniques are developed, slowly to raise the beam intensity. For short flattops, this would mean reducing the envisaged intensity by a factor of about 100. For longer flattops, the rate of energy deposition would be reduced, and thermal cooling could then occur, however, radiation damage and induced radioactivity would still be important. The solution to the problem of extraction lies in increasing the efficiency of extraction. One measure to help increase the efficiency of the extraction process would be to make an insertion of large-aperture magnets in the vicinity of the extractor. These could be arranged in a lattice insertion that would locally increase the betatron oscillation amplitude which would help the extraction process. The large aperture would also decrease the interception by local magnets of the beam lost in the extraction process and thereby allow the radiation to be intercepted by an inert shield,or at lower density in the following magnet structure. The downstream magnets in which the greatest loss can be expected to occur could be of conventional design, and hence capable of absorbing much

greater radiation. They would constitute a form of magnetic beam scrapers and apertures.

Increasing the targeting capability is difficult but more straightforward. Both the thermal energy and the radioactivity deposited would be ten times greater per proton than is presently the case, but present techniques can very likely be extended by that factor - although with considerable difficulty.

Without having to confront problems of beam extraction, an internal target area could be built in the Pentevac so that the kinds of experiments which have been done in the Main-Ring internal-target area could be extended to the new energies - but a less-dense gaseous target would have to be used to minimize beam loss in the magnets just downstream from the target.

Assuming that the extraction and targeting problems can be solved, what about the external proton beam and its experimental areas. There are numerous possibilities. Several tangents can be drawn to the ring having lengths to the site boundary of between 2 and 3 km, as can be seen in Fig. 1. For comparison, the present distance from the Main-Ring extraction point to the 15' bubble chamber is about 2 km. By extracting the proton beam inward instead of outward and by bending it as shown in Fig. 1 with a 20% stronger magnetic field than exists in the bending magnets of the Pentevac, then a 4 km-long straight beam line can be drawn to the site boundary. The proton beam would be pointed downward at a slight angle so as to direct muons into the earth. Alternatively, by bending the beam radially inward with a short radius, about 2/3 of that in the Pentevac,

the 5 TeV protons could be brought into the present switchyard where, with stronger magnets, the protons might be led to the present experimental areas where some of the present experiments could be repeated at a higher energy, but probably not at the fuel energy. It appears that the distances available on the site are large enough to do almost any experiment presently envisaged for 5 TeV protons or their secondary particles. It is interesting to note that a 5 TeV muon has an average range in earth of 2-3 km. At these energies the stopping power is dominated by the radiation of photons and electron pair production rather than by ionization loss, and the range is given by $R = \log (E + 1)$, where R is measured in muon interaction lengths and E, the muon energy, is measured in critical energy units given by $E_{TeV}/35$. The tunnel must be placed at a low enough level so that the muons produced by an inadvertent loss of protons will remain well below the deepest inhabited level. This requirement suggests that the plane of the tunnel should not be absolutely level, but rather should tilt slightly to correspond to the average tilt of the ground around the site. There may be some economic advantage to be gained by having the accelerator follow the average contour of the surface so that it is not in a plane at all. There are small chromatic effects introduced by this procedure but these might be compensated by a careful choice of the contour.

It appears from the above discussion that eventually 5 TeV protons might be produced in copious amounts at Fermilab and that the site is large enough for the fixed target experiments

which can presently be envisaged. With regard to the experimental areas and the experiments that could be made in them, almost everything that was said about the Tevatron in extrapolating from 0.4 to 1 TeV could be further extrapolated in the same way to 5 TeV. The nature of the physics, of course, cannot be foreseen or there would be small reason to build the Pentevac.

A rough estimate of the cost, assuming one pulse per minute and an intensity of 10^{14} protons per pulse, might be about $500 million in 1980 dollars. Of this, $100 million might be identified for conventional facilities connected with the accelerator, $200 million might be identified for the accelerator components, i.e., magnets, extraction, etc., and $200 million might be identified for the experimental areas. For a rough comparison, the Main Ring in 1970 cost about $75 million and the present experimental areas cost about $50 million. Multiplying the Main Ring cost by 2.5 and adding $100 million to provide for roughly the same amount of experimental areas gives $287 million in 1970 dollars. When a factor of 1.8 is allowed for inflation, this comes to about $500 million. My expectation is that the superconducting magnets might be less costly and that the conventional facilities might be constructed at somewhat less cost because of the magnitude of the job. In summary, it should be possible to construct the Pentevac to firm beam in about three years after it is funded and for a cost of less than $500 million - and with the creative imagination of younger designers, for considerably less.

(b) 5 TeV Antiprotons on 5 TeV Protons

By the time the Pentevac in constructed, we can assume that techniques for cooling antiprotons will have been developed and will have been used for colliding beam experiments in the Tevatron. These beams could be transferred directly to the Pentevac ring for slow acceleration to 5 TeV each. Thus we can contemplate the exciting prospect of reaching a center-of-mass energy of 10 TeV in colliding beam experiments in the Pentevac. There would be space galore about the 15 km peripheral length of the Pentevac tunnel in which to design and install colliding beam experimental areas. It is too soon to estimate the luminosity, but presumably it will be somewhat greater than values presently projected for $\bar{p}p$ collisions in the Tevatron, i.e., $\sim 10^{32}$ cm^{-2} sec^{-1}.

The Pentevac magnet ring becomes ready for beam collision studies as its first phase of operation, because at that stage, just as with the Tevatron, it is not necessary to solve the problems of extraction, of beam targeting, and of fast acceleration. Thus studying $\bar{p}p$ collisions in the Pentevac becomes a particularly attractive possibility, particularly if such studies have already been feasible in the Tevatron, because the problems of antiproton production would have been solved, and because there would be little interference with the Tevatron or the Inner-Ring experimental programs.

If it should turn out for some unexpected reason that the cooling of antiprotons is more difficult than is now anticipated and we have not realized high luminosity beams of antiprotons in the Tevatron, then a fall-back position would be to consider

collision studies between the 5 TeV protons of the Pentevac with the 1 TeV protons of the Tevatron in an external bypass which might have been built to load the Pentevac in any case. Alternatively, the transfer ring shown in Fig. 3, could be used as a storage ring for 1 TeV protons (85 kG) which could be collided against the 5 TeV protons - both schemes giving about 4 GeV in the center of mass.

Whether to go on and build a second proton storage ring in the Pentevac tunnel should depend on the experimental results forthcoming from one of the above programs, a factor of about two in c.m. energy would result from having 5 TeV upon 5 TeV in collisions rather than 5 TeV upon 1 TeV.

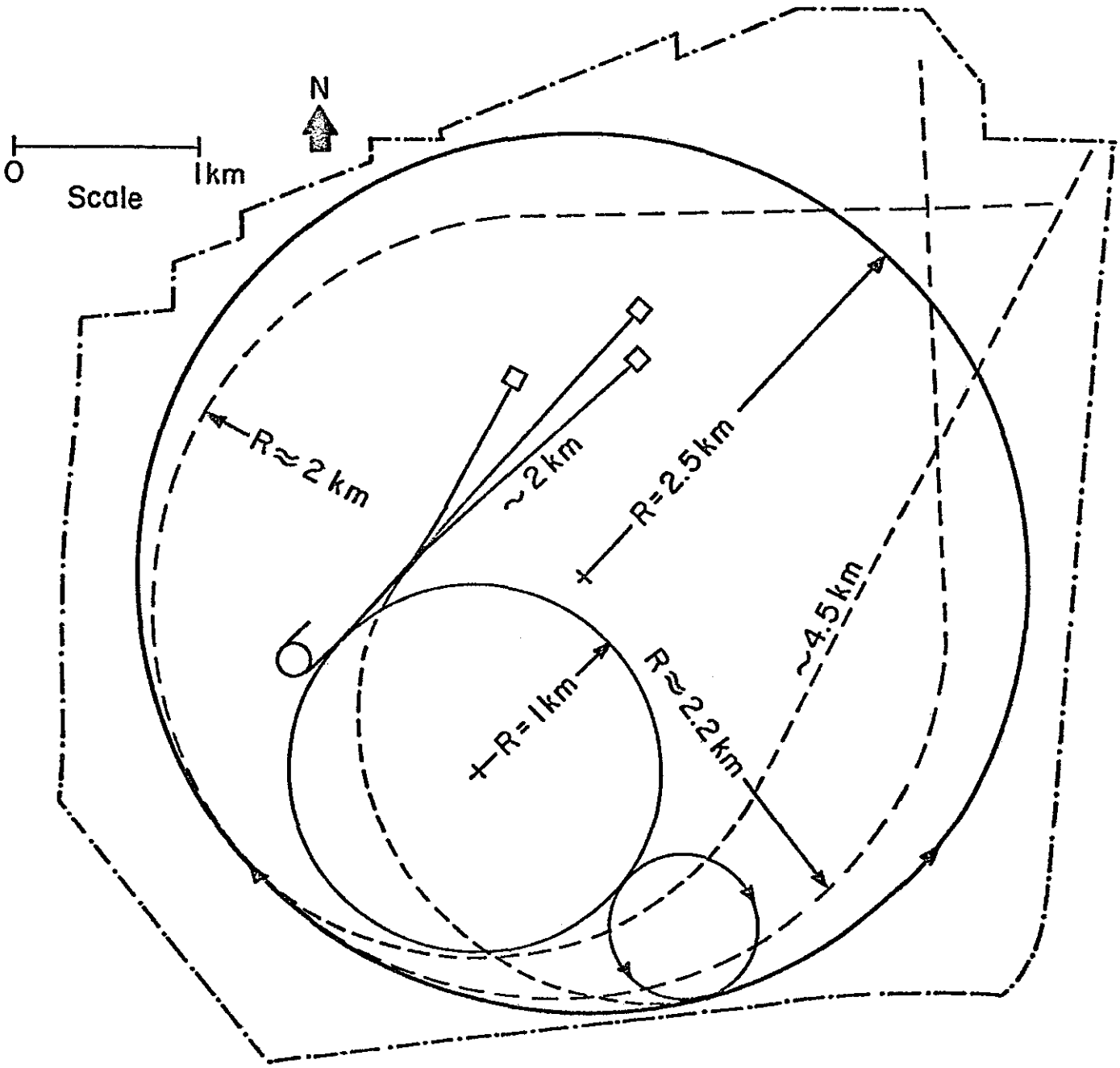

Fig. 1. The Fermilab site with a ring 2.5 Km in radius inscribed and with possible external beam lines indicated.

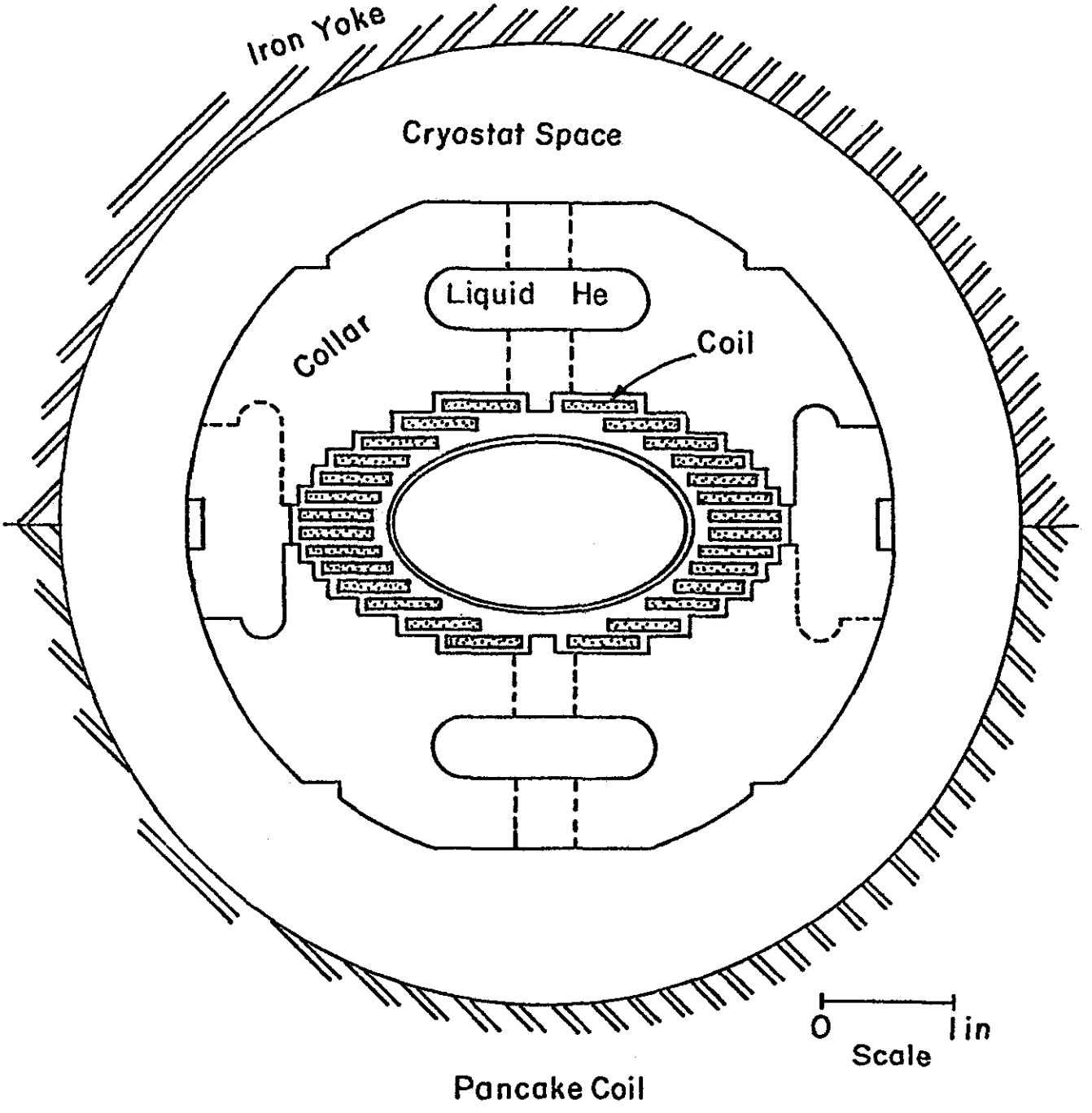

Fig 2. A possible design for an 85 kG magnet for the Pentevac.

RF SUPERCONDUCTIVITY FOR ACCELERATORS -- IS IT A HOLLOW PROMISE?

M. Tigner*

SUMMARY

This review will attempt to offer a realistic and coherent overview of the failures and partial successes in harnessing rf superconductivity of niobium to particle acceleration. Work in materials, preparation processes, heat transfer, cavity structures and vacuum electronic phenomena are discussed and put in perspective. An attempt is made to draw lessons from these observations and to outline the tasks and opportunities for the future.

INTRODUCTION

Since the early 60's and the measurements of Banford and Stafford[1] and of Wilson et al[2], we have known that it is possible to sustain rf electric fields of many millions of volts per meter in large volumes by the expenditure of a few watts of rf power. Since those early days of inflated hopes and expectations, almost twenty years ago now, we have become considerably sadder and, I hope, a little wiser.

It is my intention here to evaluate, critically, the accomplishments of this period in practical terms and to try and draw from this evaluation indications about profitable future approaches and applications and about needs for research and development. I will argue that before we can expect a realization of the full potential of rf superconductivity for accelerators a two pronged approach will be necessary. On the one hand we need to select a very few accelerator applications where the existing state of the art is competitively advantageous with respect to alternative existing technologies. Having selected these applications and accepted the limitations of the existing state of the art, the construction and putting into useful, continuous operation of the devices must be aggressively pursued. Success in this will provide the motivational and economic support necessary to continue on the second front, namely, the discovery and invention of the new ideas, techniques and materials that will be required to make devices approaching the ideal in performance. To some extent these two avenues are already being travelled.

GENERAL BACKGROUND

The theory of rf superconductivity and expermental progress up to a year ago are dealt with in a number of readily available review articles.[3,4,5,6,7]

Below the superconducting transition temperature, the condensed Cooper pairs of electrons can carry current without dissipation. They do, however, have inertia so that fields must be present inside the conductor to make the pairs carry an alternating current. These fields will drive the other charges present and thereby engender dissipation, even in the ideal case. The phenomena are described by the approximate rule

$$R_s \sim \frac{\text{const. } f^2}{T} \exp\left(-\text{const. } T_{c/T}\right) + R_{residual}, \quad T < T_c/2 \qquad (1)$$

The first term, the BCS part of the resistance, takes into account the processes in an ideal material. The R_{res} term represents all of the non-idealities of the surface and is, in general, a composite of terms depending on f, the operating frequency, T the operating temperature of the surface, and many other physical and chemical parameters of the surface.[7,9,10] It cannot be calculated from first principles. Once the material parameters are known, the first term can be computed from basic principles.[8] The residual effects, coming from a wide variety of sources, are less well understood although some progress has been made. As we shall see, these residual resistances do not limit the performance of devices now being constructed.

In addition to the surface losses, the maximum supportable field is also important. If only the ideal superconductor properties were involved, one would expect to be able to reach a surface magnetic field of about the thermodynamic critical field at least. In macroscopic samples of several type I superconductors, rf fields in excess of B_c are possible[11]. In accelerating type cavities of Nb[12,13] and Nb_3Sn[14,15], the first flux penetration critical field, B_{c1}, has been exceeded. The achievement of these fields in extended accelerating devices would correspond to 10's of MV/m. Thus, as is the case with the surface losses, very good performance is within the fundamental capability of rf superconductivity.

PRESENT LEVEL OF ACHIEVEMENT

By now a bewildering array of superconducting accelerating devices have been made from various materials, utilizing a wide range of forming, polishing, cleaning and final preparation procedures. The mainstream of activity has focussed on structure made from niobium and to some extent lead plated copper. Since it is my purpose to emphasize the practical and the search for near term payoffs, I will emphasize Nb based devices. They have received the most attention, have given the best performance, and have the most well elaborated lore for successful preparation.

A. Technology Base

Before discussing levels of performance presently achieved in devices, a brief review of the scientific and technological base upon which these devices rest is in order. In this I include, besides the basic superconductivity phenomenon itself, provenance of material, construction and processing procedures, rf structures, trouble shooting procedures and instrumentation, knowledge of the basic surface physics and chemistry of Nb and knowledge about vacuum electronic phenomena which affect device performance.

a) Provenance of Material

Virtually all of the work done so far is with so called reactor grade Nb. Several companies* provide the material in ingot, bar, plate, sheet, and tube form. As far as is known, the materials from the various suppliers perform equally well. Impurities of the common elements range from a few ppm to a few hundred ppm. Since significantly purer material

Manuscript received September 28, 1978.

Work supported by the National Science Foundation

*Laboratory of Nuclear Studies, Cornell University, Ithaca, New York 14853.

*Wah-Chang, Kaweki-Berylco, Aremco

is not readily available, it is not known whether substantial device performance gains might be had in that direction. As some devices have achieved very high levels of performance, it is likely that present purities are sufficient.

b) Construction Procedures

Cavities have been fabricated by machining from solid material[5] without any joints, by combinations of hydroforming, machining and welding,[21] by deep drawing and welding,[16] and by rolling and welding Nb explosion bonded to copper.[19] All of these methods have been successful to a degree and show that Nb is a flexible material. Welding has been largely carried out by the electron beam method but has also been done successfully by the TIG process in a glove box that can be evacuated and filled with Argon. While successful current carrying joints have been made by welding, operating them at high fields requires UHV firing at above 1800°C. Demountable joints have been developed[22,23,19] which can carry some rf current and are suitable for specialized use.

c) Processing Procedures

Crucial to what success has been achieved are the currently used surface treatment procedures. While mechanical polishing finds some use in finishing welds[16,17] machined surfaces or commercial plate finishes are normally good enough to start with. After fabrication the structures are degreased thoroughly. Ultrasonic agitation of the bath has proved useful. The final preparation sequence varies from laboratory to laboratory but some combination of electropolishing[24], chemical polishing[21], oxypolishing[25] and UHV firing are commonly used[16,17,21,26] depending upon the type of device.

d) RF Structures

The exploitation of rf superconductivity for accelerators has inspired the development of rf structures peculiarly adapted to the task as well as the adaptation of conventional structures for cooling in helium. For low frequencies, heavily loaded structures, such as the helix, an old time favorite, and a new invention, the elegant split ring structure[31] have been used. At UHF both the alvarez[45] and re-entrant, klystron, type of cavity have been built.[32] At microwave frequencies special versions in the iris loaded waveguide with both circular[33] and rectangular[16] symmetry have been designed to make use of sheetmetal techniques. A bar loaded waveguide has also been made for S-band.[46] All of these structures have been made to work at respectable levels, at least in single cell versions, and are still under active development. The helix has proven to be very difficult, although possible to control, because of its mechanical weakness and so will probably have a limited future.

e) Basic Surface Physics and Metallurgy

A large amount of work of a more or less basic nature has been carried out to date in an effort to understand the behavior of rf superconducting surfaces on a microscopic level. It has heightened the sensitivity of device builders to surface cleanliness and homogeniety and the important role of the oxides. An appreciation of that work would require a review in itself. Access to the extensive literature can be had through refs[43] and [44] concerning the role of oxygen enrichment in surface layers.

f) Trouble Shooting Methods

One of the most important developments of recent years has been the realization that most breakdowns, i.e., transitions to the normal state while the rf field is on, occur at well localized spots. Instrumentation for locating these spots easily has been indispensible in elucidating breakdown mechanisms[16,27] and in repairing defective structures.[23] The principle is simple. A network of low mass resistors is placed on or near the device body and temperature rises due to electronic heating or to breakdown are seen directly or by second sound propagation with pulse timing used to locate the fault. Also very useful have been the methods for detecting electronic activity directly by collecting electrons on probes and by measuring X-rays with counters or photographic methods.[28]

g) Vacuum Electronic Phenomena

For some time it has been known that free electrons are caught up in the fields inside the cavities and can cause wall heating[7,28] and surface damage where they strike, as well as more subtle problems such as the excitation of other modes of the structure.[27] The source of the electrons can be field emission or secondary electron multiplication, that is, multipactoring, and perhaps bremsstrahlung followed by photo emission. It is not always clear which mechanism is at work in any given instance. By means of theoretical calculations[7,27,29] and measurements[30] it has been found that one point multipactoring due to transverse electric fields, in concert with the rf magnetic field near the outside cavity walls, is an important source of wall heating in L and S-band cavities operating at or near their maximum fields. This is an important discovery, the exploitation of which has just started.

B. Device Performance

Figure 1 displays, in practical terms, our present capabilities for building large scale devices. The points plotted show the maximum accelerating fields achieved under cw conditions versus the wall power per meter required to support an accelerating field of 1 MV per meter, the surface resistance used being that appropriate to the maximum operating field. Thus, the actual rf power per meter for a given device at its maximum field operating point is found by multiplying the number given in the figure by $(E_a \text{ in MV/m})^2$. The operating frequency of the device is indicated by the band designation, X, S, etc. Squares indicate a multi-cell accelerating device, circles a single cell and triangles the low field losses for a selection of single cell accelerating devices. Sources of the data are indicated by superscript numerals adjacent the points. Each point represents a real accelerating device with beam holes and pertains to its operation in the fundamental accelerating mode.*

*Points plotted are representative rather than comprehensive. Separator devices are not included.

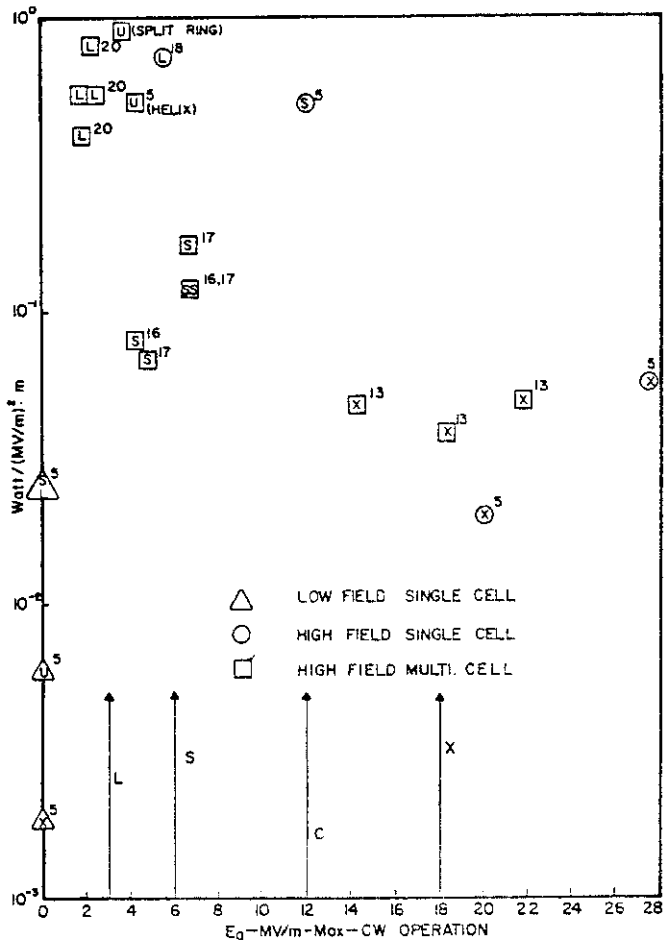

Fig. 1 Wall losses per meter per $(MV/m)^2$ v.s. max. accelerating fields at various frequencies for Nb structures of various designs.

EVALUATION OF CURRENT Nb DEVICE PERFORMANCE

The absolute values of the parameters and the trends evident in the data can be explained only partially in more fundamental terms. A more complete and quantitative understanding is still in the future.

The low field losses are very good. Despite the almost two orders of magnitude ratio of operating frequencies represented in the plot, the actual surface resistances implied are all in the nanoohm range. Thus, the achieved losses in real devices reflect the low residual resistance rather than the BCS resistance. At high fields the losses are at least an order of magnitude higher than at low fields. It is generally believed that high field effects on the residual resistance play no important role in this behavior but that, because of its exponential dependence on surface temperature, it is the BCS component that is responsible. The BCS resistance has a dependence on the surface magnetic field as well as on the temperature.[34] Perhaps this effect manifests itself at the highest frequencies where we are getting close to bulk critical fields.[26] Heating is probably still the dominant effect at present levels of performance. Putting the BCS temperature and field dependences in the rf dissipation together with the heat transfer which is governed by the thermal conductivity, wall thickness and kapitza resistance between wall and bath,, one can find, ad hoc, semi-quantitative agreement with some data at X-band.[26] For example, under certain circumstances, a decrease in wall thickness can increase the achievable field level by the predicted amount and the achieved field level is consistent with the calculation. The parameters which describe these circumstances are not clear. At S-band, assemblages of cavities having a factor of two different wall thicknesses[16,17], achieve about the same maximum fields. There are complicating factors which prevent the emergence of a clear picture at our present state of knowledge: the sources of heat vary in different frequency and geometry regimes, thermal conductivities vary over the surfaces, e.g., at welds, the kapitza resistance may play a role in some circumstances and not in others, the T_c varies over the surface,[43,44] local heating rather than general heating governs the breakdown, local breakdown of the superfluid heat transport may play a role.[35]

Likewise the general tendency to lower breakdown fields at lower frequencies can be explained only in vague terms at the moment. There are several factors which probably play a role here: the field at which a given order of multipactoring will occur is proportional to frequency, lower frequenty structures have larger surface areas and are harder to handle and process, so that the probability of having defective or poorly processed areas is larger.[47] The lower frequency structures tend to have deeper and longer welds, also increasing the probability of defects. In discussing the higher field for higher frequency trend,.one important caveat must be observed: at X-band, the multi-cell structure data plotted are for two cell structures. The only true multi-cell data are from an X- band separator model[36] where a field of 74mT was recorded, and a 32 cell accelerator unit just being put into operation,[37] no data being available at the moment. The separator field is roughly equivalent to the lowest multi-cell X-band point plotted.

The difference in performance between single cell and multi-cell structures of the same design and frequency are believed to be due in large part to the less severe multipactoring encountered in single cells, owing to the slightly different field patterns, and in part to the relative ease of cleaning and treating the smaller units.

Finally, can we explain the rather large scatter in performance among different examples of the same design and frequency? Nothing more dramatically demonstrates that there are still parameters which are not under our control and are therefore not understood. Even the behavior of a single unit repeatedly subjected to an "identical" processing cycle can show factors of 2 or 3 in loss and peak field, not necessarily correlated, from cycle to cycle. These cycles remove small amounts of material. Are we revealing different bad spots in the material as we process? Do the processing solutions have inhomogeneous composition or internal temperature gradients, are physical or chemical inhomogenieties on the surface responsible for nucleating bad oxide growth in a stochastic fashion? Are residues of the processing fluids clinging to the surface more or less with each cycle? Are there physical and chemical effects we don't know about?

Despite this rather negative recital we should not lose signt of the fact that we've done rather well at X-band. I take this as a strong indication that we now understand many of the important parameters. Clearly the first order of business is to understand why structures scaled down from X-band to lower frequencies do not operate up to X-band standards. The understanding of the difference between current X-band performance and the ideal and, to

some extent, of the fluctuations in individual unit performance belong to the future.

FUTURE DIRECTIONS IN Nb DEVICE DEVELOPMENT

The evidence gathered to date indicate strongly that multipactoring and limitations in heat transfer are responsible for the relatively poor performance of the lower frequency structures. This has been suspected for some time but we were unable to see how the secondary electron multiplication process could operate at the high fields achieved, even though we could see the electrons. The new element is the understanding of the one point multipactoring which depends on the interplay of the rather small transverse electric field with the large rf magnetic field at the outer wall.[27,30,7] To test these ideas the technology base needs to be expanded to include methods for suppressing multipactoring and for increasing, materially, the heat transfer ability of the structures. Methods for suppressing multipactoring by surface coatings such as TiN, Ti and Rh[38] and NbN[40] have been investigated for some time without great success. The utility of helium processing for getting through high order multipactor barriers suggests that adsorbed or frozen-on gas layers are significant contributors to the secondary emission coefficient so that such coatings may be irrelevant. Recent work shows that[29] the coatings tried so far have secondary emission coefficients greater than one if they are exposed to air. Successful application of coatings would appear to require some sort of in situ deposition and cleaning of the surfaces. The appreciation of the importance of one point multiplication gives us another handle by suggesting that cavity shaping may allow us to alleviate the problem.[27] One should not be too optimistic, given the past history of this business. The problems seem to have an onion like structure: no sooner is one layer of difficulty overcome than one sees another right behind it. If we are able to overcome the 2nd order multipactoring barrier we all now seem to be up against, we may find thermal breakdown due to defects or field emission problems right behind.

With regard to thermal transport, simultaneous increase of surface area and decrease in wall thickness need development. Some success along these lines has already been reported.[26,39] Considerable work will be necessary to learn how to build full structures with very thin walls of sufficient rigidity and enhanced surface area, should this step turn out to be crucial.

The behavior of existing devices gives other indications of areas of potential profit in structure work. The prevalence of fluctuations from unit to unit and the fact that breakdown occurs in well localized places, suggests that large accelerating units should be built up from smaller subunits which can be individually tested on a semi-automatic basis. In this way high performance units can be selected for assembly into the final unit while substandard units can be repaired by recycle or rework of the bad spot. Units that cannot be improved can be scrapped. Location and repair of bad spots has been effective at low frequencies[23] but has been less so at microwave frequencies. This clearly is an area where some emphasis should be put. Another area for potential profit is in the elimination of welds. Fabrication of multi-cell units solely by drawing or hydroforming would save on cost and reduce the probability of defects.

Finally, we should not fail to take another lesson that the accumulated experience has taught: the best structure is the simplest structure. The more complex a structure is the more costly it is to fabricate and the more difficult it is to process. It is hard to over emphasize this point.

An important aspect of the application of rf superconductivity to accelerators often left out is that there is considerably more to an accelerator than a low loss, high field cavity. The experience with the recyclotron[41] and the microtron[42] show the central role played by modes of the structure other than the fundamental which can be beam or multipactor excited. A rather large number of ad hoc damping probes with all their attendant constructional and cryogenic complexity are absolutely necessary. Heavy damping of higher modes will also be necessary for other applications. Thus, in addition to the features listed above, the structures of the future will have to accommodate the higher mode damping ab initio.

ARE PRESENT CAPABILITIES USEFUL AND COMPETITIVE

The vertical arrows in Fig. 1 indicate performance levels we can expect today at the frequencies marked. Are there uses for the art at this present state in which the advantages offered by superconducting devices are so compelling as to justify the obvious risks? There are ongoing projects for the construction of heavy ion accelerators operating at UHF.[23,48] Some of the progress will be reported at this conference. Electron accelerators for low and intermediate energy physics have been under construction for some time.[41,49,50] For a relatively small accelerator, especially of the recirculating type, in which the facilities cost will be substantial compared to the accelerator, it is not clear that conventional technology wouldn't be very competitive. Using well shaped cavities at S-band, one might obtain 75 MΩ/m shunt impedance and so achieve an accelerating field of 2 MV/m for an expenditure of 53 KW/m. The rf power for a 50 meter linac giving 100 MeV would be 2-2/3 MW which can be supplied by two klystrons. Such a system will be very reliable and, given the relatively low Q for the higher modes, rather less liable to beam breakup problems.

If one were to opt for a superconducting solution, one would certainly use the highestpossible frequency. As will be discussed momentarily, perhaps C-band would be most appropriate.

For a separator one would certainly choose superconductivity if the device were to be used with a long pulse accelerator, just on power grounds, since the shunt impedance of the separator structure is rather low. The CERN separator[51] works. A second version would surely work better and with higher performance levels.

The most natural applications are those in which the cw field level required must be high compared to conventional standards and the total power must be kept low. Such an application is at hand. The success of electron-positron colliding beams in revealing new aspects of sub nuclear behavior has inspired many to contemplate an instrument capable of producing the neutral intermediate boson. This is desired both for studying the nature of the weak interaction itself and as a copious source of other elementary particles. Such a machine will require electron beam energies of 50-100 GeV. At present it appears that the most practical form for such a machine would be a storage ring. The copious synchrotron radiation from such an instrument will require accelerating cavity voltages in the range from 1.7 to 3.7 GV[52,53]. The nature of the beam dynamics in such a machine requires that the operating frequency be in the UHF or L bands. The high peak currents in the beams requires a large stored energy in the cavity and thus high fields. The sheer size of the acceleration requires the minimum possible power for establishing the fields if such a

device is to be practical. The application of rf superconductivity to these machines have been examined by several groups.[53,54] One group concluded[53] that a factor of two overall savings in the cost of the instrument could be had by the use of superconducting rf. To produce several GV, a cavity length of the order of a km or two is needed. Clearly one would not launch such a project without a large scale test in an existing storage ring. The beginning of such tests are being planned actively in Europe.[55] It will be surprsing if studies along that line are not soon begun in the U.S. It should be noted that a central feature of cavities developed for this application must be a well engineered mechanism for the damping of the beam excited modes. The extracted power must be removed to a room temperature sink to prevent excessive refrigeration requirements and beam instabilities. For one case studied,[53] the beam excited losses to higher modes is about 2 MW total or about 2 kW per meter of structure. This represents a substantial engineering challenge.

As an exercise to expose the economic potential of the present state of the art, one might ask for the cost of a very large linac built using existing technology. Figure 2 shows the cost for a 100 GeV electron linac built using the technology developed at Cornell for S and X-bands, projected to frequencies between L and X-band. The costs of the structures and non-refrigeration items are based on current experience. The refrigeration costs are based on a compilation of recent refrigerator costs.[56] In addition, Fig. 2 contains the costs for possible advance states of superconducting technology.

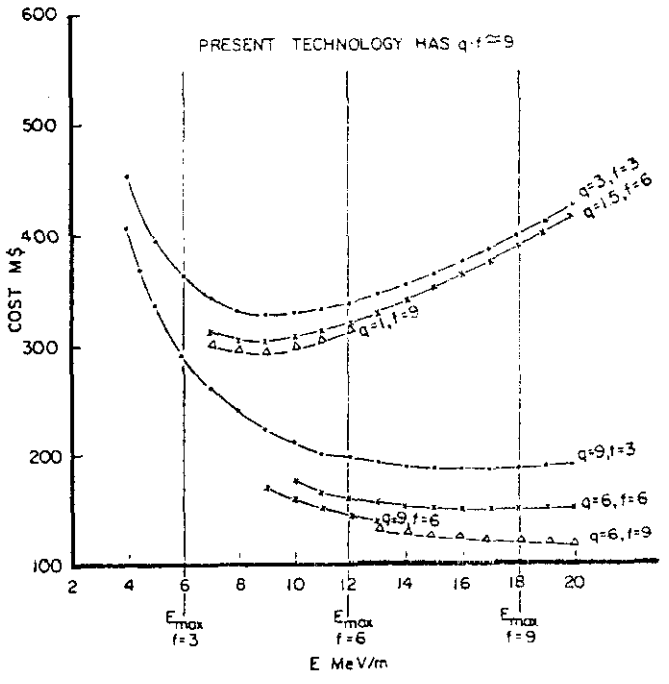

Fig. 2 Cost estimate for a 100 GeV cw linac vs. operating field with ($Qx10^{-9}$) x frequency as a parameter.

The approximate empirical formula for the costs, is based upon costs for small structure units:

$$C_{tot} \sim \left[9000 + \left(\frac{9450}{f} + 650 \right) + \left(\frac{3000}{f} + 1000 \right) + \left(\frac{\mathcal{E}^2}{.8qf} + .5 \right) \times 1.26\times10^3 \right] \times \frac{E}{\mathcal{E}} \left[\$\text{-}1978 \right] \quad (2)$$

Proceeding from l. to r. inside the large brackets on the r.h.s., we have the terms representing (1) the standard components, e.g., vacuum, instruments and controls, tunnel, piping, rf distribution, supports and alignment, quadrupoles, etc., (2) the accelerating structure, (3) the cryostat, (4) the refrigerator. f is the operating frequency in GHz, q is the Q of the structure in units of 10^9, E is the total beam energy in GeV and $\mathcal{E}$ is the operating accelerating field in MV/m. The crucial parameter turns out to be q.f., q because that governs losses at a fixed frequency and f because the r/Q for a constant geometry scales with f. For the particular type of hardware picked,[16,13] q.f. = 9. On the low field side the costs rise because the structure length becomes excessive. On the high field side the costs rise because the refrigerator cost becomes excessive. The top three curves show the present status of this particular technique. In these cases we believe the operating Q to be limited not by the superconductivity but by the structure tolerances achieved, coupled with the presence of joints, coupling ports, probes, etc.. C-band is favored because of its relatively high operating field and relative ease of meeting construction tolerances as compared with X-band. If we could increase q.f. by a factor of 4, the cost would be halved and C-band would probably still be the choice.

One might ask why we have not built small and very compact accelerators for industrial and medical uses using this technology. Perhaps a natural skepticism regarding the reliability is partially to blame. However, the biggest stumbling block is the lack of closed 2-4°k refrigeration devices with the reliability and ease of operation of home and industrial units for higher temperatures. The existence of such units would open a host of new applications.

OTHER MATERIALS

Only passing reference has been made to materials other than niobium. Great strides have been made in the use of lead plated copper structures.[57] The performance of lead is inherently worse than Nb and Nb has turned out to be quite easy to work with. Thus, lead will probably be confined to specialized applications. A large number of other materials have been discussed in the literature, especially the A-15 compounds. The technology of their use is at present so involved that evaluating their utility must await future developments.

CONCLUSIONS

Despite its rather long history, rf superconductivity still has a long way to go to prove its worth for a wide range of applications. It appears that there are applications for scientific instruments where it can make a significant impact. It will have utility for common industrial devices only in the future, if ever. To bend the phenomenon to our needs now and in the future, considerable advance in the engineering aspects of its use and in its basic development are necessary. The engineering advances will only come through the aggressive application of the art at its present level to instruments requiring

its peculiar advantages. In advancing the engineering aspects through building large numbers of identical devices for an acceleration application, some more basic advances will emerge: in coping with the epidimology of a large number of supposedly identical units, some of the important parameters of the materials and preparation methods, parameters now only dimly perceived, will reveal themselves. Thus, both extensive engineering work on devices having immediate payoffs and basic development of the art and science of superconductivity will be needed for realization of the full potential of the phenomenon. Those of us, the faithful, who are striving to make rf superconductivity our servant, have a long, hard road ahead of us before we have shown that the promise is real.

ACKNOWLEDGEMENTS

I am greatly indebted to H. Padamsee for his instruction and correction in the course of preparing this review. Absolutely indispensable also were extensive information and thoughtfully written comments from representatives of many of the principal institutions engaged in the field: A. Citron, J. Halbritter, W. Bauer, P. Kneisel of the Kernforschungszentrum, Karlsruhe; J. Turneaure of Stanford HEPL; Lowell Bollinger of Argonne; A. O. Hanson of U. of Illinois; G. J. Dick of Cal. Tech.; H. Hahn of Brookhaven; H. Pfister, Siemens AG; and H. Piel, Gesamthochschule Wuppertal.

REFERENCES

1. A. P. Banford, H. G. Stafford, J. Nucl. Energy, Part C3, 287 (1961).
2. P. B. Wilson, Nucl. Instr. Methods 20, 336 (1963).
3. J. M. Pierce in Methods of Experimental Physics, Ed. L. Marton, Voll. 11, 541-594, AP (1974).
4. W. H. Hartwig, C. Passow in Applied Superconductivity, Ed. V. Newhouse, V.II, 541-640 AP (1975).
5. H. Pfister, Cryogenics, Jan. 1976, p. 17 ff.
6. H. Lengeler, Cryogenics, Aug. 1978, p. 465 ff.
7. J. Halbritter, Internal Report 304/78, Kernforschungszentrum, Karlsruhe.
8. See, for example, J. Halbritter, Ext. Report 3/69-2, Kernforschungszentrum, Karlsruhe. P. B. Wilson, SLAC TN-70-35, Stanford Linear Accelerator Center, Dec. 1970.
9. J. Halbritter, IEEE Trans. Mag-11, 427 (1975).
10. P. Kneisel, O. Stoltz, J. Halbritter, Measts. of Nb_3Sn Cavities, this conference.
11. T. Yogi, Thesis, Cal. Tech. (1976).
12. K. Schnitzke et al., Phys. Lett. 45A, 3, p. 241 Sept. 1973.
13. H. Padamsee, et al., Muffin-Tin Cavities at X-band, this conference.
14. B. Hillenbrand, et al., IEEE Trans. Mag-13; 1, p. 491, Jan. 1977.
15. R. Shaw, et al., IEEE Trans. Mag-13, 1; p. 811, Jan. 1977.
16. H. Padamsee, et al., IEEE Mag-13, 1; p. 346 ff, Jan. 1977.
17. P. Kneisel, et al., IEEE NS-22, 3, p. 1197 ff, June 1975.
18. J. P. Turneaure, HEPL 672, Stanford Univ., May 1972.
19. K. Shepard, this conference.
20. J. Calarco et al., (1977 Part. Accel. Conf.).
21. J. P. Turneaure, IEEE NS-18, 3; p. 166 (1971).
22. W. Bauer, et al., IEEE NS-22, 3; p. 1144 (1975).
23. ATLAS, A Proposal for a Heavy Ion Accelerator at Argonne Nat'l. Lab, Bollinger, 1978.
24. H. Diepers, et al., Phys. Letts. 37A, 2, p. 139 Nov. 1971
25. H. Martens, et al., Phys. Lett. 44A, p. 213 1973.
26. B. Hillenbrand, et al., IXth Int'. Conf. on High Energy Particle Accelerators, p. 143, Stanford, 1974.
27. C. Lyneis et al., Appl. Phys. Lett. 31, 5, p. 541, Oct. 1977.
28. I. Ben-Zvi et al., IEEE NS-20; 3, p. 54, 1973.
29. H. Padamsee and A. Joshi, CLNS-388, Cornell University, 1978.
30. H. Padamsee, et al., CLNS-387, Cornell University 1978.
31. K. Shepard et al., IEEE NS-22; 3, p. 1179, June 1975.
32. P. Ceperly, et al., IEEE 22; 3, p. 1153, June 1975.
33. J. P. Turneaure, et al., Appl. Phys. Lett. 25, 247 (1974).
34. J. Halbritter, Karlsruhe, External Report 3/69-6 Mar. 1969.
35. H. A. Schwettman, IEEE NS-22; 3, p. 1118, June 1975.
36. J. Aggus et al., App. Phys. Lett. 24; 3, p. 144, Feb. 1974.
37. H. Piel, Gesamthochschule, Wuppertal, private communication.
38. H. Padamsee, et al., IEEE NS-24; 3, 1101, 1977.
39. S. Isagawa, S.C. Cavity with cooling fins, Nat. Lab for H.E.P., Oho-machi, Tsukuba-gun, Ibaraki 300-32, Japan, 1978.
40. S. Isagawa, et al., IX Int'l. Conf. on High Energy Accelerators, p. 147, Stanford, 1974.
41. M. S. Brittan et al., X Int'l. Conf. on Part. Accel., p. 283, 1977.
42. A. O. Hanson, et al., Technote 78-43, U. of Illinois, March 1978.
43. S. Giordano et al., J. Appl. Phys. 44, 9, p. 4185, Sept. 1973.
44. W. Schwarz, H. Halbritter, J. Appl. Phys. 48, 11, p. 4618, Nov. 1977.
45. K. Mittag, IEEE NS-24, 3 (1977).
46. H. Padamsee, et al., Bar Loaded Waveguide, this conference.
47. P. B. Wilson, SLAC, PUB 1134, 1972 Proton Linac Conf., Los Alamos.
48. J. W. Noe' et al., IEEE NS-24, 3, p. 1144, 1977.
49. P. Axel et al., IEEE NS-22, 3, p. 133 (1975).
50. P. Axel, et al., X Int'l. Conf. on High Energy Accel., p. 235, 1977.
51. A. Citron et al., First Operation of an S.C. Separator, Kernforschungszentrum, Karlsruhe, Feb. 1978.
52. J. Bennett et al., CERN 77-14, Aug. 1977.
53. D. Ritson, M. Tigner, CLNS-406, Cornell Univ., July 1978.
54. A. Citron, X Int'l. Conf. on H. E. Accelerators, p. 202, 1977.
55. W. Bauer, et al., Kfk-Ext. 3/78-2, Kernforschungszentrum, Karlsruhe, March 1978.
56. Strobridge, et al., IEEE NS-24, 3, p. 1224, 1977.
57. G. J. Dick, et al., IEEE NS-24, 3, p. 1130, 1977.

Colliding Beams

LIMITATIONS ON PERFORMANCE OF e^+e^- STORAGE RINGS AND LINEAR COLLIDING BEAM SYSTEMS AT HIGH ENERGY

J.-E. Augustin*, N. Dikanski†, Ya. Derbenev†, J. Rees‡,
B. Richter‡, A. Skrinski†, M. Tigner**, and H. Wiedemann‡

Introduction

This note is the report of working Group I (J. Rees - Group Leader). We were assisted at times by U. Amaldi and E. Keil of CERN. We concerned ourselves primarily with the technical limitations which might present themselves to those planning a new and higher-energy electron-positron colliding-beam facility in a future era in which, it was presumed, a 70-GeV to 100-GeV LEP-like facility would already exist. In such an era, we reasoned, designers would be striving for center-of-mass energies of at least 700-GeV to 1-TeV. Two different approaches to this goal immediately came to the fore: one, a storage ring based on the principles of PEP, PETRA, and LEP and the other, a system in which a pair of linear accelerators are aimed at one another so that their beams will collide. We realized early in the study that a phenomenon which has been negligible in electron-positron systems designed to date would become important at these higher energies - synchrotron radiation from a particle being deflected by the collective electromagnetic field of the opposing bunch - and we dubbed this phenomenon "beam-strahlung." During the rest of the week we investigated the scaling laws for these two colliding-beam systems taking beam-strahlung into consideration.

* Orsay
† Institute of Nuclear Physics, Novosibirsk
‡ SLAC
** Cornell

We concluded that it would be necessary to depart from some of the common design features of PEP, PETRA, and LEP in order to push electron storage rings into the energy regime of interest. Either the stored bunches would have to be markedly longer, presumably requiring a radio-frequency well below the 350-500 MHz range, or the number of bunches in each beam would have to be increased as it could, for example, by providing separate storage rings for the two beams or by arranging discrete beam separations in a single ring. By taking such measures, however, it does appear possible to make electron-positron storage rings work in this energy regime.

Colliding linac beams are less sensitive to the effects of beam-strahlung. The feasibility of this technique appears to rest more on the achievable density of the beams in phase space. If the necessary densities are attained, we suggest that, for sufficiently high energies, the cost of the linac system will fall below that of an equivalent storage ring system.

In the following sections, we shall first review briefly the formulae relevant to beam-strahlung; then we shall apply them to storage rings to obtain scaling laws; and finally we shall derive some scaling laws for the system of colliding linac beams. Before embarking on that program, however, we wish to put the reader on notice that our intent throughout will be <u>to estimate</u>, not to calculate in detail. Our results are therefore approximate and should be taken in that spirit.

Beam-strahlung

As a particle of either beam passes through a bunch of the opposing beam at an interaction region, it is deflected by the collective electro-

magnetic field of that bunch to a degree and in a manner which is determined by the particle's coordinates entering the interaction region and by the spatial distribution of charge in the bunch. The net angular deflection itself, being a non-linear function of the particle's coordinates, is the source of the familiar incoherent beam-beam limit (Amman, 1973; Amman and Ritson, 1961) which has been regarded as a fundamental limitation on performance in the design of all single-ring electron-positron systems. (It should be remarked here that efforts are being made at Orsay, France, to circumvent this limitation by means of a multiple-beam scheme called DCI which, if successful, will vitiate the incoherent limit and the beam-strahlung effects about to be described.) As the particle is being deflected it emits synchrotron radiation, the properties of which are strongly dependent on particle energy. The radiated energy and the critical energy of the spectrum both increase rapidly with particle energy even though the beam-beam tune shift is being held constant, and at sufficiently high energy, the beam-strahlung process imposes its own limitations.

Figure 1 shows a typical particle incident on an opposing bunch. The particle density distributions are taken as tri-Gaussian with horizontal, vertical and longitudinal standard deviations of σ_x^*, σ_y^*, and σ_z, respectively. The typical incident particle's vertical position is taken as σ_y^* and its horizontal position is taken as zero. The deflection of the trajectory is characterized by the focal length F, considered to be large compared to the bunch length $2\sigma_z$. The bending radius during deflection is designated ρ_b.

$$\frac{1}{\rho_b} = \frac{1}{F}\frac{\sigma_y^*}{\sigma_z} \tag{1}$$

The distance over which the bending takes place is only σ_z because the relative velocity between particle and bunch i. 2c.

The total energy radiated by the particle in one such collision is

$$\Delta U = \frac{2}{3} mc^2 \gamma^4 \frac{r_e \sigma_z}{\rho_b^2}$$

$$= (14 \times 10^{-6}) \frac{E^4 \sigma_z}{\rho_b^2} \quad , \tag{2}$$

where lengths are measured in meters and energies in GeV. The symbol r_e refers to the classical radius of the electron and mc^2 is the electron's rest energy. The critical energy of the beam-strahlung is

$$\varepsilon_c = \frac{3}{2} \hbar c \frac{\gamma^3}{\rho_b}$$

$$= (2.2 \times 10^{-6}) \frac{E^3}{\rho_b} \quad . \tag{3}$$

The mean number of photons emitted in the collision is (Sands, 1971)

$$n_\gamma = \frac{5}{2\sqrt{3}} \alpha\gamma \frac{\sigma_z}{\rho_b}$$

$$= 20 \frac{E\sigma_z}{\rho_b} \quad . \tag{4}$$

where α is the fine-structure constant.

Effects of Beam-strahlung in Storage Rings

Whether the effects of beam-strahlung are important in any particular storage-ring design or not depends, of course, on the value of ρ_b. Re-

turning to Eq. (1) we first relate the focal length to the beam-beam tune shift, the touchstone of the incoherent limit. A thin lens located at the interaction point where the vertical betatron function is β_y^* produces a tune shift

$$\Delta\nu = \frac{\beta_y^*}{4\pi}\,\frac{1}{F} \quad ,$$

approximately if the storage-ring tune, unperturbed by the lens, is not too close to an integer, so we can write

$$\frac{1}{\rho_b} = \frac{4\pi\Delta\nu}{\beta_y^*}\cdot\frac{\sigma_y^*}{\sigma_z} \tag{5}$$

Note that we would have got the same value for ρ_b if we had chosen for our typical trajectory $y = 0$, $x = \sigma_x^*$; because storage rings such as PEP, PETRA, and LEP have been designed to operate simultaneously at the vertical and horizontal incoherent limit where $(\sigma_y^*/\beta_y^*) = (\sigma_x^*/\beta_x^*)$.

The values of ρ_b computed from Eq. (5) for PEP, PETRA, and LEP are not very different. LEP parameters are taken from CERN/ISR-LEP/78-17. The values are of the order of 10^2m, being about 200 m for LEP at peak performance ($E = 70$ GeV). This is not surprising since all of these machines have been designed to use their full apertures which themselves are similar, have similar β_y^*-values and have similar bunch lengths. In other words, the design practices currently in favor for large electron-positron storage rings tend to hold ρ_b roughly constant independent of energy. This fact leads us to observe that the energy loss ΔU and the critical energy ε_c will be rapidly increasing functions of energy as the machines are pushed to higher and higher energies.

Next let us note that the mean number of photons emitted per collision is small. In LEP at 70 GeV, $n_\gamma = 0.25$. Even at five or ten times that energy, the number is of the order of one, so we conclude that the beam-strahlung process will always involve strong fluctuations from collision to collision.

Evaluating Eqs. (2) and (3) for LEP at 70 GeV we get

$$\Delta U = 0.24 \text{ MeV}$$

$$\varepsilon_c = 3.5 \text{ MeV}$$

(See also Hofmann and Keil, LEP-70/85, Dec. 1978.) Inasmuch as the synchrotron radiation loss-per-turn in the bending magnets is 906 MeV compared to a total loss to beam-strahlung at all eight interaction regions of 2 MeV, we can neglect any contributions to radiation damping due to beam-strahlung. Thus beam-strahlung introduces an important source of energy fluctuations over and above those already present without bringing any new damping with it. The result will be an increased energy spread in the stored beams.

The total fractional energy spread (σ_e/E) can probably not be allowed to increase much above 10^{-3}, the approximate value it has in PEP, PETRA, and LEP, because the correction of chromatic effects has already, at that level of energy spread, become very difficult. This assertion is, of course, somewhat arbitrary and argumentative. Work is in progress in several centers on improved methods of chromaticity correction in large storage rings and accelerators. If this work bears fruit it may allow the accommodation of significantly larger energy spreads in these machines, and in that event, our findings here may simply serve to emphasize the importance of this work. Nevertheless,

for our purposes we take the following as principles: (1) The equilibrium fractional energy spread due to the synchrotron radiation in the magnets (σ_{eo}/E) cannot be allowed to be greater than that allowed in LEP at 70 GeV, and (2) the additional energy spread created by beam-strahlung (σ_{eb}/E), which adds in quadrature, cannot itself be greater than (σ_{eo}/E).

$$\left(\frac{\sigma_{eb}}{E}\right)^2 \leq \left(\frac{\sigma_{eo}}{E}\right)^2 \leq \left(\frac{\sigma_e}{E}\right)^2_{LEP} \tag{6}$$

To apply these criteria we need to collect formulae relating these quantities to the storage-ring parameters (Sands, 1971).

$$\left(\frac{\sigma_{eo}}{E}\right)^2 = \frac{55}{32\sqrt{3}} \frac{\hbar}{mc} \frac{\gamma^2}{J_\varepsilon \rho_o} \quad , \tag{7}$$

where J_ε is the longitudinal damping partition number and ρ_o is the radius of curvature in the bending magnets, considered to be constant. We shall assume $J_\varepsilon = 2$ as it is in a separated-function lattice so that

$$\left(\frac{\sigma_{eo}}{E}\right)^2 = (0.7 \times 10^{-6}) \frac{E^2}{\rho_o} \quad . \tag{8}$$

The contribution due to the beam-strahlung is estimated as follows. Let n_d be the number of orbital periods in a longitudinal damping time.

$$n_d = \frac{E}{U_o} = \frac{3}{4\pi} \frac{\rho_o}{\gamma^3 r_e}$$

$$= (1.13 \times 10^4) \frac{\rho_o}{E^3} \tag{9}$$

The equilibrium energy spread due to beam-strahlung alone then would be

$$\sigma_{eb}^2 = \frac{1}{4} n_d n_{ir} n_\gamma \langle u^2 \rangle$$

where n_{ir} is the number of interaction regions where beam-strahlung is emitted and $\langle u^2 \rangle$ is the mean-square energy (Sands, 1971).

$$\langle u^2 \rangle = \frac{11}{27} \varepsilon_c^{\,2} .$$

$$\left(\frac{\sigma_{eb}}{E}\right)^2 = (1.1 \times 10^{-7}) \frac{E^2 n_{ir} \rho_o \sigma_z}{\rho_b^{\,3}} \tag{10}$$

Now we are prepared to apply the criteria of Eq. (6) which, combined with Eq. (8), gives

$$(0.7 \times 10^{-6}) \frac{E^2}{\rho_o} \leq \left(\frac{\sigma_e}{E}\right)^2_{LEP} = (1.2 \times 10^{-3})^2$$

We conclude that

$$\rho_o \geq 0.5 E^2 \tag{11}$$

The bending radius must scale as the square of the beam energy. Next we combine Eqs. (6), (10), and (11) to obtain

$$\frac{E^4 n_{ir} \sigma_z}{\rho_b^3} \leq 26 \tag{12}$$

We have chosen the equality in Eq. (11) in order to permit the smallest value of ρ_b. Now we could express this result in terms of the tune shift via Eq. (5), but our goal is to determine the limitation on luminosity as a function of energy imposed by the restriction we have adopted on beam energy spread, so we shall employ the usual luminosity and tune-shift formulae

$$\mathscr{L} = \frac{f_o N^2}{4\pi \; n_b \; \sigma_x^* \; \sigma_y^*} \tag{13}$$

and

$$\Delta\nu = \frac{N \; \beta_y^* \; r_e}{2\pi \; \gamma \; n_b \; \sigma_x^* \; \sigma_y^*} \; , \qquad (\sigma_y^* << \sigma_x^*) \tag{14}$$

where N is the number of particles per beam and n_b is the number of bunches per beam. These two expressions, taken together with Eq. (5) yield

$$\frac{1}{\rho_b} = 4\sqrt{\pi} \; r_e \; \frac{\mathscr{L}^{\frac{1}{2}} \; \sigma_y^{*\frac{1}{2}}}{\gamma \; n_b^{\frac{1}{2}} \; f_o^{\frac{1}{2}} \; \sigma_y^{*\frac{1}{2}} \; \sigma_z}$$

$$= (10^{-17}) \; \frac{\mathscr{L}^{\frac{1}{2}} \; \sigma_y^{*\frac{1}{2}}}{E \; n_b^{\frac{1}{2}} \; f_o^{\frac{1}{2}} \; \sigma_x^{*\frac{1}{2}} \; \sigma_z} \; , \tag{15}$$

which, together with Eq. (12) gives finally

$$(4 \times 10^{-53}) \; \frac{\mathscr{L}^{3/2} \; E \; n_{ir}}{f_o^{3/2} \; \sigma_z^2 \; n_b^{3/2}} \left(\frac{\sigma_y^*}{\sigma_x^*}\right)^{3/2} \leq 1 \; . \tag{16}$$

Now f_o is just $(c/2\pi R)$, where R is the gross radius of the ring which must be larger than ρ_o but not greatly larger. Its actual value will depend on requirements for free space along the orbit for experimental areas, radiofrequency systems, etc. We estimate

$$R = 1.5 \; \rho_o$$

which implies, according to Eq. (11), that

$$R = 0.75 \; E^2$$

and

$$f_o = 64 \times 10^6 \; E^{-2} \tag{17}$$

As noted above the beam dimensions σ_x^* and σ_y^* at the interaction regions do not vary greatly among PEP, PETRA, and LEP. Equation (16) argues that the ratio (σ_y^*/σ_x^*) should be made as small as possible to maximize luminosity, but we do not believe it is feasible to reduce this ratio much below its value in LEP of 0.06. The reason for this belief is that, in a practical machine, the minimum attainable orbit distortions together with the sextupole systems necessary to correct chromaticity produce non-zero vertical dispersion in the bending magnets where quantum excitation drives vertical oscillations. Hence we take

$$\frac{\sigma_y^*}{\sigma_x^*} = 0.06$$

as in the LEP design. With this choice, and using Eq. (17) we get the approximate scaling law,

$$(10^{-66}) \; \frac{\mathscr{L}^{3/2} \; E^4 \; n_{ir}}{\sigma_z^2 \; n_b^{3/2}} \leq 1 \tag{18}$$

The reader is reminded that energies are in GeV, distances are in meters and $10^{32} cm^{-2} s^{-1} = 10^{36} \; m^{-2} s^{-1}$.

Choosing LEP-like parameters

$$n_b = \frac{n_{ir}}{2} = 4$$

$$\sigma_z = 3 \times 10^{-2} \; m$$

$$\mathscr{L} = 10^{36} \; m^{-2} \; s^{-1}$$

we find the energy restricted to

$$E \lesssim 200 \text{ GeV}$$

In order to push machines of this type to higher energies, either the bunch length or the number of bunches stored would have to be increased dramatically.

At constant luminosity E varies as $\sigma_z^{1/2}$. To increase the maximum energy by a factor of two, the bunch length, and with it presumably the rf wavelength, would have to be increased by a factor of four. The corresponding radiofrequency is about 90 MHz.

To accomplish the same result by increasing the number of bunches, which could be done either by building two separate rings or by providing many special beam-separation sections in a single ring, the number of bunches would have to be increased by a factor of $2^{8/3}$ to about 24 with collisions taking place in only eight interaction regions.

Finally, we add a remark on costs. The peak luminosity of a storage ring is given by

$$\mathscr{L} = \frac{3}{8\pi\, r_e^2\, mc^2} \frac{P\, \rho_o}{\gamma^3\, \beta_y^*} \tag{19}$$

where P is the power delivered to each beam. According to Eq. (11) $\rho_o \sim \gamma^2$, so for constant luminosity, the power must vary as γ and the circumference as γ^2. The rf cavity length also varies as γ^2 because the voltage gradient is limited and the total voltage varies as γ^2. Consequently, we expect the cost of a storage ring to increase almost in proportion to the square of the energy, and this expectation is borne out by recent cost optimizations of large e^+-e^- storage-ring designs (Richter, 1976).

Colliding Linac Beams

In an electron storage ring with the customary distribution of radiation damping among the oscillation modes, the longitudinal damping time may be interpreted as the time in which each particle would radiate away all of its kinetic energy if it were to continue radiating at the same rate. It follows that the rf system re-supplies to each beam its entire kinetic energy each damping time (n_d/f_o). In LEP this damping time is 5.8 milliseconds and, following the dictates of Eq. (11), it scales as γ to higher-energy storage rings, so the damping time for a 350-GeV storage ring would be about 30 milliseconds.

Now consider two linacs aimed at one another so that their output beams collide. Suppose, for comparison, that their energies are the same as that of a given storage ring and that they accelerate, in each pulse, the same number of particles as is stored in each beam of the storage ring. Then if their pulse repetition period is equal to a damping time of the storage ring, they will have to deliver no more average power to the beams than does the rf system of the storage ring. In terms of rf power, the linacs are at no disadvantage relative to the storage ring provided the efficiency of rf power usage is equivalent. In order to produce the same luminosity, however, the lateral area of the linac bunches at the interaction point must be much smaller than it is in the storage ring. For example, if we compare the linac system with all its particles in one bunch -- that is an rf bunch, not a pulse train -- with a storage ring having n_b stored bunches in each beam, the interaciton areas must stand in the ratio

$$\frac{A_L}{A_s} = \frac{n_b}{n_d} \tag{20}$$

to obtain the same luminosity, where A_L is the interaction area of the linac bunch and A_s is the interaction area of the storage ring bunches. This relation follows from the relation

$$\mathscr{L} = \frac{f_r N^2}{A_L} = \frac{f_o N^2}{n_d A_L} = \frac{f_o N^2}{n_b A_s} \tag{21}$$

in which f_r is the repetition frequency of the linacs and $A_s = 4\pi \sigma_x^* \sigma_y^*$. What Eq. (20) tells us is that (A_L/A_s) is a small number. For orientation we may compare LEP with a pair of 70-GeV linacs. In this case $n_b = 4$ and $n_d = 70$, so $(A_L/A_s) = 0.05$.

We conclude from these comparisons that colliding linac beams may compete favorably with storage rings at the energies of interest if sufficiently high phase-space densities can be attained in them. Our next goal will be to determine the phase-space densities required in the general case, to assess how severe the beam-beam disruption will be and to estimate the effects of beam-strahlung.

We begin by restating Eq. (21) in the form

$$\mathscr{L} = \frac{f_r N^2}{4\pi \sigma_y^{*2} R}, \tag{22}$$

where $R = (\sigma_x^*/\sigma_y^*)$ the aspect ratio of the beam cross section at the interaction point. We are still considering a single linac bunch in each pulse. The average beam power of each linac is

$$P = f_r N \gamma mc^2 \tag{23}$$

Next we define a "disruption parameter",

$$D = \frac{\sigma_z}{F} = \frac{2r_e \sigma_z N}{\gamma \sigma_y^{*2} (1+R)} \tag{24}$$

This parameter may be understood through Fig. 1. If the focal length F is long compared to the bunch length, D << 1 and the trajectories of incident particles are little affected by the beam-beam interaction. If, on the other hand, F is short compared to σ_z, disruption is severe and the focal length is meaningless.

We also define the beam-strahlung energy loss δ in units of the beam energy.

$$\delta = \frac{\Delta U}{E} = \frac{2r_e}{3} \cdot \frac{\gamma^3 D^2 \sigma_y^{*2}}{\sigma_z^3} \tag{25}$$

From Eqs. (22), (23), and (24) we find immediately that

$$\mathscr{L} = \frac{DP}{8\pi\, mc^2\, r_e\, \sigma_z} \left(\frac{1+R}{R}\right) \tag{26}$$

independent of γ and independent of δ! However, we must also obey the following laws at the same time:

$$f_r = \frac{4r_e^2}{3mc^2} \frac{\gamma\, DP}{\delta\, \sigma_z^2\, (1+R)} \tag{27}$$

$$N = \frac{3}{4r_e^2} \frac{\delta\, \sigma_z^2\, (1+R)}{\gamma^2\, D} \tag{28}$$

$$\sigma_y^{*2} = \frac{3}{2r_e} \frac{\delta\, \sigma_z^3}{\gamma^3\, D^2} . \tag{29}$$

We must pick our way among these relations to find a satisfactory set of parameters. For example, having chosen D, P, σ_z, and R to give the desired luminosity, we must choose δ, probably on experimental grounds.

The smaller we choose it, the higher is the repetition frequency and the smaller are N and σ_y^*. Furthermore, the energy dependencies of the last three equations dictate that

$$f_r \sim \gamma$$

$$N \sim \gamma^{-2}$$

$$\sigma_y^{*2} \sim \gamma^{-3}$$

The beam cross section becomes very small at very high energy.

Figure 2 shows Eq. (27) and Eq. (28) plotted as functions of energy for both a flat beam and a round beam. Also plotted is the normalized emittance of the beam

$$\phi = \gamma \, \sigma_y^{*2} / \beta_y^*$$

We have assumed $\beta_y^* = \sigma_z$, approximately the optimum value it can take. The normalized emittance of a machine is independent of beam energy. For the SLAC linac the values measured as averages over many S-band bunches are $\phi^- = 6.4 \times 10^{-4}$ mc-m for electrons and $\phi^+ = 6 \times 10^{-3}$ mc-m for positrons. For single bunches the values may be smaller.

We close by putting forth the following example of colliding linac beams followed by some remarks on this technique. We choose

D	=	1	(upper limit?)
σ_z	=	5×10^{-3} m	(S-band)
R	=	1	(round beams)
δ	=	10^{-2}	
$\mathscr{L}$	=	$10^{36}\ m^{-2}\ s^{-1}$	$(= 10^{32}\ cm^{-2}\ s^{-1})$

with these choices

$$P = 14 \times 10^6 \text{ W} \quad \text{(each beam)}$$
$$f_r = 3.7 \times 10^{-3} \gamma \text{ s}^{-1}$$
$$N = 4.7 \times 10^{22} \gamma^{-2}$$
$$\sigma^{*2} = 6.6 \times 10^5 \gamma^{-3} \text{ m}^2$$

For E = 350 GeV, $\gamma = 6.8 \times 10^5$

$$f_r = 2500 \text{ s}^{-1}$$
$$N = 1.0 \times 10^{11}$$
$$\sigma^{*2} = 2 \times 10^{-12} \text{ m}^2 = 2 \ \mu\text{m}^2$$

For this example the average beam current from each linac would be 40 microamperes.

These parameters appear quite challenging in the light of current linac technology. For comparison the SLAC linac can now produce an electron beam with more than 10^9 electrons in one S-band bunch. Nevertheless, suggestions have been made to get around some of the difficulties. At CERN (Amaldi, 1976) and at Novosibirsk (Balakin, Budker and Skrinski, 1978) studies have been made to regenerate positrons from the spent beams and to "cool" them in intermediate storage rings to decrease the spot size. Amaldi also suggested recovering energy from the spent beam.

The cost of a colliding-linac-beam system may be expected to increase approximately linearly with energy, because the length of the machines will increase in that way. Since, as we have remarked above, the costs of storage rings will vary approximately as the square of the energy, linac systems, should they prove feasible, may become economically quite attractive at sufficiently high energies.

REFERENCES

Amaldi, U., 1976, Phys. Lett. B61, 313.

Amman, F., 1973, IEEE Trans. Nucl. Sci. NS-20, p. 858.

Amman, F. and D. Ritson, Proceedings of the International Conference on High-Energy Accelerators (Brookhaven, 1961), p. 262.

Balakin, V.E., G.I. Budker and A.N. Skrinski, 1978, Institute of Nuclear Physics, Novosibirsk, to be published.

Richter, B., 1976, Nucl. Inst. and Meth. 136, 47.

Sands, M., 1971, Physics with Intersecting Storage Rings, Proceedings of the International School of Physics "Enrico Fermi," (Academic Press, N.Y.), p. 257.

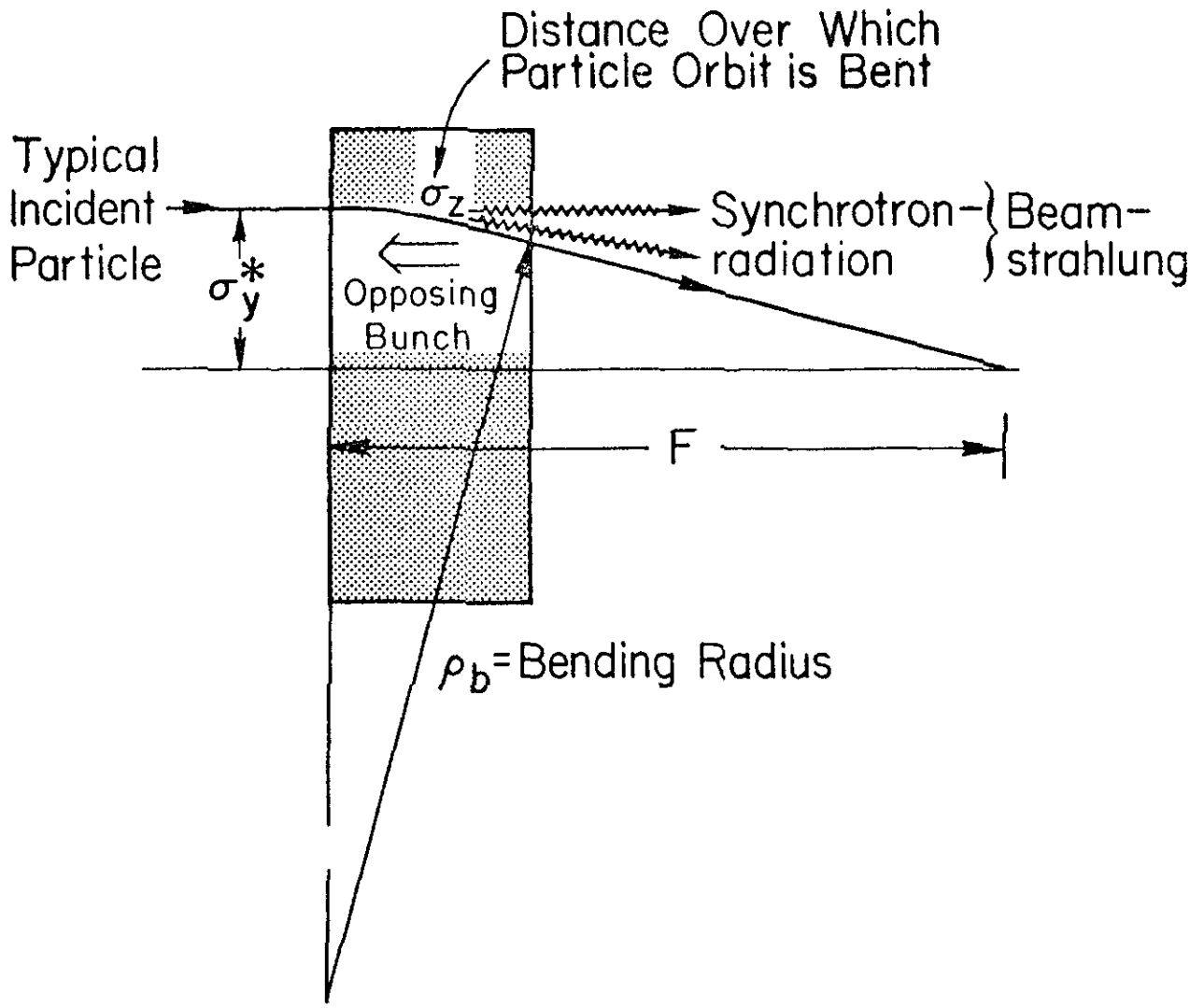

Fig. 1. Typical particle incident on an opposing bunch.

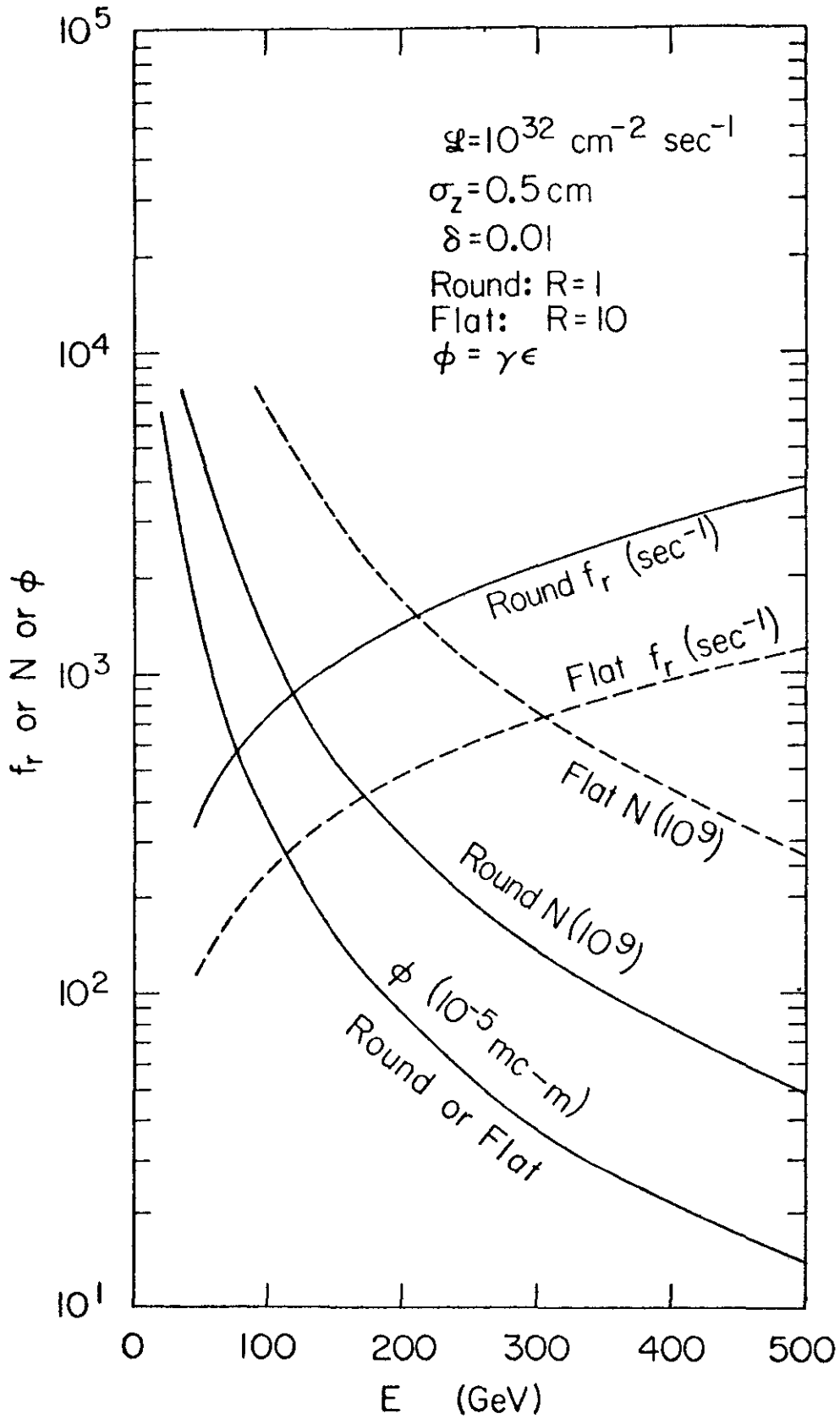

Fig. 2. Colliding linac beams. Parameters for constant luminosity.

SUMMARY REPORT OF THE WORKING GROUP ON COLLIDING BEAMS

S.Y. Chen, E.D. Courant, E. Keil, N.M. King,

P. McIntyre, T. Nishikawa, M. Vivargent

15th-21st October 1978

Fermilab, Batavia, Illinois, USA

1. Introduction

The working group considered the possibilities of p-$\bar{p}$, p-p and e-p colliding beams associated with a large proton synchrotron.

2. Assumptions

Our considerations are based on the performance parameters of the proton synchrotron shown in Table I.

Table I. Proton synchrotron performance parameters

Maximum energy	E	20	TeV
Proton flux	$\dot{N}_p$	10^{13}	s^{-1}
Repetition frequency	f_{rep}	1	min^{-1}
Normalized emittance	E_t	30π	μm
Peak magnetic field	B_M	10	T
Circulating current	I	0.5	A

The performance estimates of the p-$\bar{p}$ colliding beams are based on the parameters of the $\bar{p}$ factory shown in Table II.

Table II. Antiproton factory performance parameters

$\bar{p}$ flux	$\dot{N}_{\bar{p}}$	10^{12}	day^{-1}
Filling time	T_{fill}	1	day
Emittance	}	suitable	
Momentum spread	}		

These figures are close to the design values of the CERN p-$\bar{p}$ facility[1]. They might be improved by optimizing the energy and flux of the protons which are used in the $\bar{p}$ production.

In order to avoid lengthy discussions on the maximum proton current which can be stored in a storage ring, due to heating of superconducting magnets by continuous beam losses, beam abort systems, collective phenomena etc., we have assumed that the currents in the synchrotron and

the storage ring are identical.

3. Results

The results of our discussions on p-$\bar{p}$, p-p and e-p colliding beams are summarized in Table V which has been compiled from the following more detailed documents:

i) Bunched p-$\bar{p}$ and p-p colliding beams, E.D. Courant and E. Keil

ii) Coasting p-p colliding beams, E. Keil and N.M. King

iii) e-p colliding beams, T. Nishikawa and E. Keil

iv) A bypass for p-$\bar{p}$ colliding beams, P. McIntyre.

3.1 p-$\bar{p}$ colliding beams

The performance is limited by the p and $\bar{p}$ currents and by the design of the low-β insertion. The stored currents are 10^{12} particles in each beam. The design of the low-β insertions is governed by the field at the edge of the aperture of the quadrupoles nearest to the crossing points and the possibility of correcting chromatic effects. The beam sizes and apertures are smaller than in machines like the FNAL and SPS synchrotrons. We did not study the tolerances associated with the small apertures and large machine size. At a total cross section of 100 mb, the event rate per collision is about 7, which may be uncomfortable for event analysis.

The scaling laws for the most important machine parameters with the machine energy γ are summarized in Table III.

Table III. Scaling laws for bunched p-$\bar{p}$ colliding beams

Assumed independent of γ :	
Number of p and $\bar{p}$	N
Beam-beam tune shift	$\Delta\nu$
Number of bunches	k_b
Quadrupole field at aperture limit	B_Q
Ratio of amplitude functions at crossing	β_y^*/β_x^*
Found proportional to $\gamma^{1/3}$:	
Vertical amplitude function	β_y^*
Horizontal amplitude function	β_x^*
Length of interaction region quadrupole	ℓ_Q
Free space around crossings	$\pm\ell_{int}$
Found independent of γ :	
Normalized emittances	E_x, E_y
Found proportional to $\gamma^{-1/3}$	
Luminosity	L
Quadrupole aperture	A_x

The interference between p-$\bar{p}$ colliding-beam and fixed-target operation can be reduced by bypassing the p-$\bar{p}$ interaction region for proton acceleration in the synchrotron. This may be particularly advantageous if the number of bypasses and their length are small, because of the large circumference of the synchrotron.

3.2 Bunched p-p colliding beams

If a proton storage ring is added to the synchrotron with roughly the same radius as the synchrotron, but exactly the same bunch spacing, bunched p-p collisions can be obtained.

If the current per bunch is kept the same as in the p-$\bar{p}$ colliding beams, the results of the p-$\bar{p}$ calculations on the machine parameters apply. However, in this case the number of bunches becomes $k_b = 2400$ in each beam, and the bunch spacing 25 m. This might give rise to multi-bunch instabilities and long-range tune shifts[2].

In contrast to the p-$\bar{p}$ collisions where the beams always collide in the crossing regions in the absence of transverse electric fields, the p-p scheme requires careful beam alignment in order to ensure collisions. In the calculation, we have assumed head-on collisions although the beams must collide at a small angle in order to avoid the long-range tune shifts.

The main parameters are summarized in Table V. The event rate per collision, 7, is the same as for the p-$\bar{p}$ scheme.

3.3 Coasting p-p colliding beams

We have followed the standard procedure[3] for designing coasting-beam p-p storage rings, and assumed the same total current as in the bunched p-p scheme above. This results in closed expressions for the luminosity L, optimum amplitude function β^* and crossing angle α (r_p is the classical proton radius, σ^* the rms beam radius at the crossing):

$$L \approx \frac{4}{3} \gamma \left(\frac{\pi I^3 \Delta\nu}{E_t \ell_{int} r_p e^2 c} \right)^{\frac{1}{2}} , \tag{1}$$

$$\beta^* \approx \left(\frac{\Delta\nu \; E_t \ell_{int} ec}{8 \pi I r_p} \right)^{\frac{1}{2}} , \tag{2}$$

$$\alpha \approx \left(\frac{2}{\pi} \right)^{\frac{1}{2}} \frac{I r_p \beta^*}{\Delta\nu \; \gamma \; \sigma^* ec} \tag{3}$$

The scaling laws for the main parameters are summarized in Table IV and the parameters themselves in Table V. It should be noted that the luminosity in the coasting-beam mode is only a factor of about three lower than in the bunched-beam mode. At a total cross section of 100 mb, the event rate is 46 MHz. A sketch of half an interaction region is shown in Fig. 1.

Table IV. Scaling laws for coasting p-p colliding beams

Assumed independent of γ :	
Number of protons	N
Normalized emittance	E_t
Free space $\pm\ell_{int}$	$\sim \gamma^*$
Amplitude function β^*	
Luminosity	$L \sim \gamma^{-1}$
Crossing angle	$\alpha \sim \gamma^{-1}$

* imposed by chromaticity correction

By accumulating a few synchrotron pulses, using e.g. RF stacking, the luminosity can be increased in proportion to $I^{3/2}$ according to (1). Collective phenomena such as the longitudinal stability of the injected beam, the single-beam tune shift and the resistive-wall instability limit the performance well above the luminosity arrived at in Table V.

3.4 Bunched e-p colliding beams

The electron energy is assumed to be 140 GeV, obtained by rough scaling from LEP[4]. In order to simplify the estimate, we have assumed that the beam sizes at the crossing points are the same for electrons and protons, i.e.

$$\sigma_{xe} = \sigma_{xp} \qquad \sigma_{ye} = \sigma_{yp} \tag{4}$$

We further assume that the proton beam has the same bunch population as in the p-p and p-$\bar{p}$ schemes, that the electron beam has 'a' times that population and that there are k_b bunches in each beam. Then the total numbers are

$$N_p = \frac{1}{4} \cdot 10^{12}\, k_b \qquad N_e = \frac{1}{4} \cdot 10^{12}\, k_b\, a \tag{5}$$

The differences in energy and in the permissible beam-beam tune shifts ($\Delta\nu_p = 0.005$, $\Delta\nu_e = 0.06$) require that the following condition should hold for the amplitude functions at the crossing points in both planes:

$$\beta_e = 0.084 \text{ a } \beta_p \tag{6}$$

This condition looks feasible. The luminosity then becomes

$$L = 0.65 \cdot 10^{30} \, k_b \quad cm^{-2}s^{-1} \tag{7}$$

In order to reach the canonical luminosity $L = 10^{32}$ $cm^{-2}s^{-1}$, k_b must be about 150. The synchrotron radiation power is about 110 MW.

The performance of a coasting proton beam colliding with an electron beam was also estimated. For about the same luminosity and synchrotron radiation power, the proton current is much higher.

4. Conclusions

The estimates show that adequate luminosities can be obtained for p-p and p-$\bar{p}$ colliding beams at 20 TeV, even with relatively conservative assumptions about the circulating p and $\bar{p}$ currents. The bunched p-p scheme has a slightly larger luminosity, but the coasting p-p scheme is much simpler and avoids the problem of several events per collision. Colliding e-p beams are also possible with good luminosity for electron energies above 100 GeV.

5. References

1) CERN Report, SPS/SI/PP/Int. Note/77-9.

2) E. Keil, C. Pellegrini and A.M. Sessler, Nucl. Instr. Methods 118, 165 (1974).

3) E. Keil, Proc. 8th Internat. Conf. on High Energy Accelerators, Stanford 1974, 660 (1974).

4) CERN/ISR-LEP/78-17.

Table V. Parameter list for p-$\bar{p}$, p-p and e-p colliding beams

	p-$\bar{p}$	p-p bunched	p-p coasting	e-p* bunched
Energy/TeV	20	20	20	0.14/20
Bending magnet field/T	10	10	10	0.07/10
Number of particles	10^{12}	$6\cdot10^{14}$	$6\cdot10^{14}$	$4\cdot10^{13}$
Number of bunches	4	2400	-	160
Beam-beam tune shift	0.005	0.005	0.005	0.06/0.005
Hor. ampl. function β_x^*/m	25	25	-	2.1/25
Ver. ampl. function β_y^*/m	6.25	6.25	18.6	0.5/6.25
Crossing angle/μrad	0	0	47	small
Free space around crossing/m	±124	±124	±170	±20
Hor. norm. emittance/μm	48π	48π	30π	560/48π
Ver. norm. emittance/μm	12π	12π	30π	140/12π
Low-β quadrupole field/T	1	1	1	1
Low-β quadrupole half aperture/mm	23	23	65	35/23
Hor. rms beam radius at crossing/μm	120	120	-	120
Ver. rms beam radius at crossing/μm	31	31	84	31
Stored energy in beam/MJ	3.2	1900	1900	0.9/130
Synchrotron radiation power/MW	-	-	-	110/-
Luminosity/$cm^{-2}s^{-1}$	$2.6\cdot10^{30}$	$1.6\cdot10^{33}$	$4.6\cdot10^{32}$	10^{32}

* First number applies to electrons, second to protons.

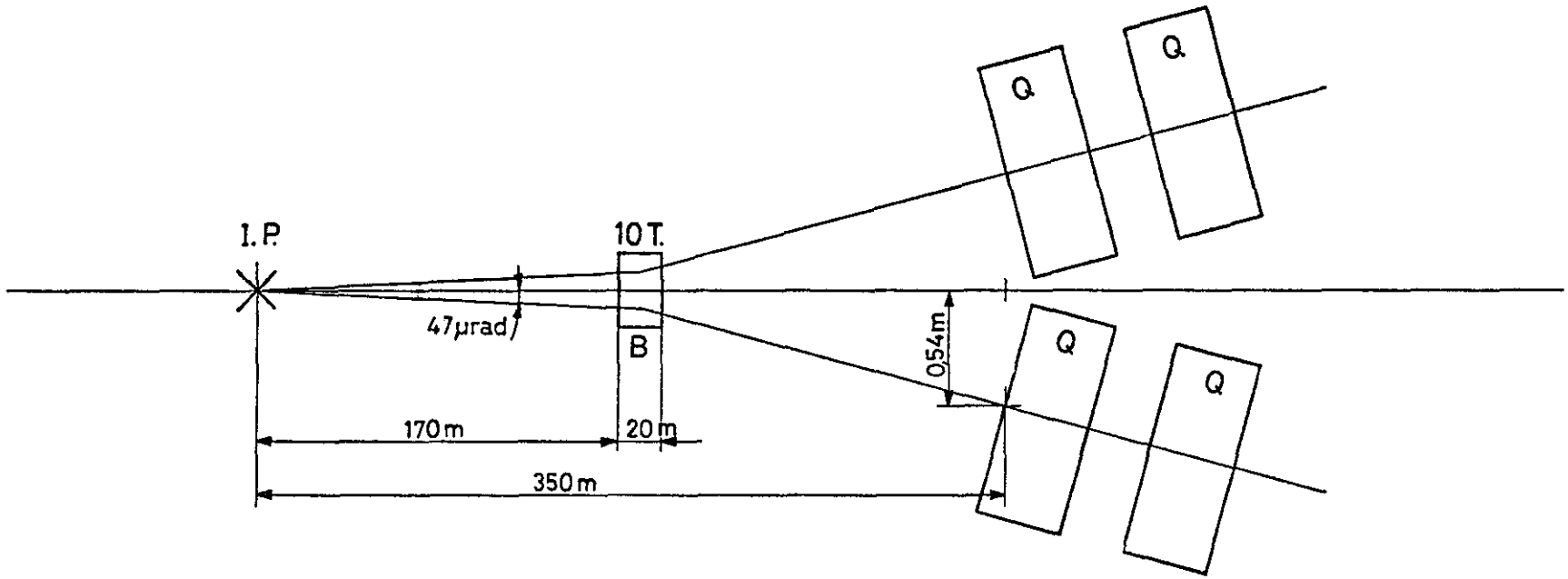

Fig. 1. Rough layout of half a coasting-beam p-p interaction region.

COASTING p-p COLLIDING BEAM MACHINES

E Keil & N Marshall King

SUMMARY

The designs considered cover the energy range 20 TeV to 100 TeV per proton beam, with collisions taking place at small crossing angle. The crossing angle and luminosity are optimized at each energy. With single-turn filling of the storage rings, luminosities per intersection of order 10^{32} cm^{-2} sec^{-1} can be achieved throughout most of the energy range, provided that the incoming momentum spread from the injector synchrotron is blown up for storage. The ring lattices follow closely on design principles for lower energy machines, but invoke the use of 10 T superconducting dipoles and correspondingly high-gradient quadrupoles.

1. NORMAL CELL LATTICE

To arrive at design parameters for the normal cell lattices, the following strategy is adopted:

i) Fields and Gradients

Assuming niobium-tin superconductor to be a well-established choice by the time these large machines would be constructed, the dipole field is taken to be B = 10 T throughout. We envisage that this value of field will correspond to a few centimetres coil radius in a practical magnet design. The resulting bending radius, ρ, and total length of dipole in the ring, $(\ell_B)_{tot}$, are then given by:

$$\rho = \frac{10}{c_o} \cdot \frac{P}{B} = \frac{P}{c_o} \quad , \qquad .....(1)$$

$$(\ell_B)_{tot} = 2\pi\rho \quad , \qquad .....(1a)$$

for ρ and $(\ell_B)_{tot}$ in km, P in TeV/c, B in Tesla, and where $c_o = 2.997925 = c/10^8$ m/s.

To quote a maximum quadrupole gradient k_{max}, the difficulty is that some practical inner coil radius r_Q has to be estimated at which some field B_Q may be achieved, where $B_Q < 10$ T. Provisionally, we take:

$$k \leq k_{max} = 250 \text{ T/m} , \qquad .....(2)$$

corresponding to, say,

$$B_Q = 6.25 \text{ T at } r_Q = 2.5 \text{ cm} . \qquad .....(2a)$$

However, since we lack practical magnet design information for niobium-tin superconducting quadrupoles at present, we shall consider a wide range of k values.

The usual lattice gradient parameter K is given by:

$$K = c_o \times 10^{-4} \, k/P , \qquad .....(2b)$$

where K is in m^{-2}, k in T/m and P in TeV/c.

ii) Phase Advance, Lattice Functions

Choosing a simple FODO cell structure, as sketched in Fig 1, we take $\pi/2$ phase advance per cell. A thin lens analysis, with $K_F = K_D$, then leads to the approximate relations:

$$\mu_{np} \approx \pi/2 , \quad Q_{np} \approx N_p/4 , \qquad .....(3)$$

$$\ell_Q \ell_p \approx 2\sqrt{2}/K , \qquad .....(3a)$$

$$\beta_{F,D} \approx (1 \pm \tfrac{1}{2}\sqrt{2}).\ell_p , \qquad .....(3b)$$

$$\eta_{F,D} \approx \tfrac{1}{2}(1 \pm 0.25\sqrt{2}) \, \ell_p \theta , \; \theta = 2\pi/N_p . \qquad .....(3c)$$

Here, the subscript 'np' refers to normal periods: contributions from the insertions are neglected for the moment. The number of normal cells is N_p, their length is ℓ_p, and the length of each quadrupole is ℓ_Q.

iii) Geometry of Normal Cells

Following lower-energy lattice designs, the ratio of mean radius to bending radius in the normal cell part of the ring is taken to be 1.6 :

$$R_{np}/\rho = 1.6 = \ell_p/\ell_B \ , \quad \text{giving : } \ell_B = 0.625\ \ell_p \ . \qquad .....(4)$$

Similarly, the ratio of space in a period occupied by quadrupoles to the space left unoccupied by dipoles is taken to be 0.6 :

$$2\ell_Q/(\ell_p - \ell_B) = 0.6 \ , \text{ giving : } \ \ell_Q = 0.1125\ \ell_p \ . \qquad .....(4a)$$

The remaining free space for correction elements, diagnostic equipment, bellows, flanges, etc, is given by:

$$\ell_s = 0.15\ \ell_p \ . \qquad .....(4b)$$

Combining the thin lens result (3a) with equs. (4a) and (2b), a lower limit for the period length ℓ_p is obtained :

$$\ell_p \geqslant (2.8959/k_{max}^{\frac{1}{2}}) .\ P^{\frac{1}{2}} = c_1 .\ P^{\frac{1}{2}} \ , \qquad .....(5)$$

where ℓ_p is in m, P in TeV/c, and k_{max} in T/m. For the equ.(2) value of k_{max}, 250 T/m, this corresponds to :

$$\ell_p \geqslant 18.3154\ .\ P^{\frac{1}{2}} \ . \qquad .....(5a)$$

Using equs.(1), (4) and (5), the corresponding upper limit for the number of normal cells is given by :

$$N_p \leqslant (3.2\pi \times 10^3/c_o\ c_1)\ .\ P^{\frac{1}{2}} \ , \qquad .....(5b)$$

$$= 183.1 \times P^{\frac{1}{2}} \ , \text{ for } k_{max} = 250 \text{ T/m} \ . \qquad .....(5c)$$

iv) <u>Superperiod Considerations</u>

Assuming that these large machines should have at least 8 interaction regions, we choose superperiodicity S = 8, and take N_p to be the largest integer divisible by 8, consistent with equ.(5c). The resulting normal cell lattice parameters are given in Table I, where the bracketed values are the result of subsequent accurate matching in the 'AGS' computer program.

TABLE I

NORMAL CELL LATTICE PARAMETERS

P(TeV/c)	20	40	60	80	100
ρ(km)	6.671	13.34	20.01	26.685	33.35
C_{np}(km)	67.06	134.1	201.2	268.3	335.3
N_p	816	1152	1408	1632	1824
ℓ_p(m)	82.19	116.4	142.9	164.4	183.85
$\frac{1}{2}\ell_B$(m)	25.68	36.39	44.66	51.37	57.45
$\frac{1}{2}\theta$(mrad)	3.85	2.73	2.23	1.925	1.72
ℓ_Q(m)	9.25 (10.0)	13.10 (14.15)	16.08 (17.36)	18.49 (20.0)	20.68 (22.34)
K(m^{-2})	3.75×10^{-3} (3.77×10^{-3})	1.87×10^{-3} (1.88×10^{-3})	1.25×10^{-3} (1.25×10^{-3})	0.937×10^{-3} (0.941×10^{-3})	0.750×10^{-3} (0.753×10^{-3})
$\frac{1}{4}\ell_s$(m)	3.08 (2.71)	4.37 (3.84)	5.36 (4.72)	6.16 (5.41)	6.89 (6.07)
Q_{np}	204.25	288.25	352.25	408.25	456.25
β_F(m)	136.2	193.0	236.9	272.4	304.7
β_D(m)	24.7	35.0	43.0	49.4	55.3
η_F(m)	0.424	0.426	0.428	0.425	0.425
γ_T	189.1	266.8	326.1	377.9	422.4

The chief result of the accurate matching calculation, compared with the thin lens approximation, is that the quadrupole lengths ℓ_Q have had to be augmented at the expense of ℓ_s. Accordingly, equs.(4a) and (4b) should be replaced by:

$$2\ell_Q/(\ell_p - \ell_B) = 0.648 \; ; \; \ell_Q = 0.1215\ell_p \; ; \; \ell_s = 0.132 \; \ell_p \; . \qquad .....(6)$$

These are the values used when calculating the luminosity and associated parameters at the crossing points.

2. INJECTION CONSIDERATIONS

We envisage injection from a chain of synchrotrons, the final one having much the same lattice geometry as the storage rings, - in particular, having the same 10 T peak field. Its minimum field should be in the region of 0.25 T if non-linear field effects in the superconducting dipoles at injection are to be kept to a safe level: hence, the final synchrotron would accelerate over a factor of about 40 in energy. Consequently, the penultimate synchrotron of the chain for the 20 TeV case would be a machine of about 0.5 TeV.

This brings us on to familar ground, and we may assume that such a machine has properties not unlike the existing CERN SPS and FNAL synchrotrons.

For instance, its mean radius could be about 1 km, (or less if it uses superconducting magnets), so that about 10 of its pulses could be used to fill one turn of the 20 TeV synchrotron, in box car fashion. Allowing for some future improvements in circulating flux and in fast ejection technique, we envisage 6×10^{13} ejected protons per pulse, so that the number of protons in the 20 TeV ring for single-turn filling would be:

$$N \simeq 6 \times 10^{14} \qquad .....(7)$$

Since, at these high energies, stored energy in the beam begins to loom large as a problem in emergency conditions - eg. 1.92 GJ at 20 TeV - we shall assume that no further stacking is contemplated in the storage ring. We shall retain this value of the total number of protons in all the designs from 20 TeV to 100 TeV, so that the consequent line density decreases linearly with energy.

Next, the presence of an SPS-type synchrotron in the chain allows us to propose a value for invarient normalized transverse emittances, ε_t. We assume that ε_t does not become diluted significantly during subsequent transfers from one ring to another, and persists at the following value all the way through to the storage ring:

$$\varepsilon_t \approx 30\pi \times 10^{-6} \text{ m x rad} . \qquad .....(8)$$

In the storage ring, this emittance may be defined in terms of the rms beam radius σ^* and the betatron function β^*, at the crossing point:

$$\varepsilon_t = 4\pi.(\beta\gamma).\sigma^{*2}/\beta^* . \qquad .....(8a)$$

This last relation will be used later to evaluate the rôle of σ^* in the scaling of interaction point parameters with energy.

Finally, a similar identification of an SPS-type machine with one of the injector synchrotrons serves to define a normalized longitudinal emittance. Scaling to the 20 TeV machine, the SPS momentum spread of about 2×10^{-3} corresponds to a debunched $\Delta(\beta\gamma)$ value given by:

$$\Delta(\beta\gamma)_{20\text{ TeV}} = 1.3 \times 10^{-2} . \qquad .....(9)$$

This provides a scale for normalized longitudinal emittance ε_ℓ in the coasting beam of the storage ring:

$$\varepsilon_\ell = \Delta(\beta\gamma).\ 2\pi R \ , \qquad .....(9a)$$

where R is the mean radius of the complete machine, including the insertions. Allotting 12 km to the insertion regions in the 20 TeV machine:

$$\varepsilon_\ell \approx 1.0 \times 10^3 \text{ m} \qquad .....(9b)$$

is the invariant value of longitudinal emittance.

On the assumption that the beam is not allowed to debunch in the chain of synchrotrons, the injection parameter $\Delta(\beta\gamma)_{inj} = \beta\gamma.\Delta P/P$ corresponding to a bunched beam, is allowed to vary as $P^{\frac{1}{2}}$ for the higher energy storage rings. As will be remarked in Section 5, this assumption does not affect our argument, since the debunched value $\Delta(\beta\gamma)_{st}$ required for coasting beam storage turns out to be much larger.

3. LUMINOSITY, ASSOCIATED PARAMETERS, AND SCALING LAWS

A procedure for determining optimum luminosity, crossing angle and β-value at the crossing point in coasting beam p-p storage rings has been described by one of the present authors.[1] The significant formulae are:-

$$L \simeq \frac{4}{3}\gamma \left[\frac{\pi \cdot \Delta\nu \cdot I^3}{e^3 c r_p \varepsilon_t . \ell_{int}}\right]^{\frac{1}{2}} , \qquad \ldots (10)$$

$$\beta^* \simeq \left[\frac{ec \cdot \Delta\nu . \varepsilon_t . \ell_{int}}{8\pi r_p I}\right]^{\frac{1}{2}} , \qquad \ldots (11)$$

$$\alpha \simeq \left(\frac{2}{\pi}\right)^{\frac{1}{2}} \frac{r_p I \beta^*}{ec . \Delta\nu . \gamma\sigma^*} . \qquad \ldots (12)$$

In these expressions, the notation is:

L = Luminosity per intersection, $(m^{-2}s^{-1})$,

$\Delta\nu$ = Limiting beam-beam tune shift, taken to be 0.005.

I = Proton current, (amp) = $Nec/2\pi R$, with $N = 6 \times 10^{14}$, (equ. 7).

r_p = Classical proton radius = 1.5347×10^{-18}m.

ε_t = Normalized transverse emittance = $4\pi(\beta\gamma)\sigma^{*2}/\beta^*$, (equ. 8a).
= $30\pi \times 10^{-6}$m, (equ. 8),

ℓ_{int} = Free space each side of the crossing point, (m). (cf. Fig 2).

β^* = Value of betatron function at the crossing point, (m).

α = Crossing angle, (rad).

σ^* = RMS beam radius at crossing point, (m), (equs. 8 and 8a).

γ = E/Eo; $c=2.997925 \times 10^8$ ms^{-1}; $e = 1.602 \times 10^{-19}$ coul.

In considering how the interaction point parameters scale with energy, the length ℓ_{int} plays an important part. Leaving its rôle unspecified for the moment, equs. (8a), (10), (11), and (12) show that:-

$$L \sim (\gamma\ell_{int})^{-\frac{1}{2}}$$

$$\beta^* \sim (\gamma\ell_{int})^{\frac{1}{2}}$$

$$\sigma^* \sim (\ell_{int}/\gamma)^{\frac{1}{4}} \qquad \ldots (13)$$
$$\alpha \sim (\ell_{int}/\gamma^5)^{\frac{1}{4}} ,$$

since ε_t, $\Delta\nu$ are constant, and since $I \sim \gamma^{-1}$ for constant N.

Referring to Fig 2, $(\alpha\ell_{int})$ is seen to determine the separation of beam centres, d_1, at the first magnetic element they encounter each side of the interaction point. Equs. (10)-(12) are valid only when the beams are sufficiently well-separated: we shall express d_1 in terms of some multiple 'm' of the local rms beam radius σ, and shall later interpret m=4 to mean 'sufficient separation':

$$d_1 \simeq \alpha\ell_{int} \sim (\ell_{int}/\gamma)^{5/4} , \qquad \ldots (14)$$
$$\alpha\ell_{int} \geqslant m\,\sigma , \qquad \ldots (14a)$$
$$\sigma^2 = \sigma^{*2} + (\varepsilon_t\ell_{int}/4\pi\gamma\sigma^*)^2 . \qquad \ldots (14b)$$

Using equs. (12),(11), (14b) and (8a) in equ. (14a), a lower limit is obtained for ℓ_{int}:

$$\ell_{int} \geqslant \frac{m^2 C.\Delta\nu.\varepsilon_t}{8Nr_p} \left[1 + \{ 1 + \frac{2}{m^2\pi} \}^{\frac{1}{2}}\right] ,$$

or, ignoring the last small factor on the right hand side,

$$\ell_{int} \geqslant \frac{m^2 C.\Delta\nu.\varepsilon_t}{4Nr_p} \sim \gamma, \qquad \ldots (15)$$

where $C = 2\pi R$ is the total circumference of the ring.

With m = 4 at 20 TeV, allowing a total 12 km for the 8 insertions, the resulting minimum value for ℓ_{int} would be 162 m. We shall use the scale:

$$\ell_{int} = 8.75P, \qquad \ldots (15a)$$

where ℓ_{int} is in m for P in TeV/c.

Returning to equ. (13), the scaling laws are now seen to be:

$$\left.\begin{aligned} L &\sim \gamma^{-1} , \\ \beta^* &\sim \gamma , \\ \sigma^* &\sim \gamma^{o} , \\ \alpha &\sim \gamma^{-1} . \end{aligned}\right\} \qquad \ldots (16)$$

Recalling that the proton current I is defined by Nec/C, all the significant parameters at the crossing point may now be computed once the total circumference C has been defined. This requires further examination of the insertions.

4. THE INSERTIONS

Fig 2 illustrates schematically our present notion of a half-insertion. At the end of the free space ℓ_{int}, a dipole of length ℓ_1 and field B_1 diverts the opposing beams : after a further distance ℓ_2, they are separated by an amount $2d_2$, sufficient for locating the first sets of quadrupoles. Neglecting the small initial separation d_1 occasioned by crossing angle, d_2 is given by:

$$d_2 = c_o \times 10^{-4} . \quad \ell_1 \ell_2 B_1 / P \geqslant 0.5\text{m, say.} \qquad \ldots (17)$$

Taking B_1 = 10T and ℓ_1 = 20m, then at P = 20 TeV/c this condition is met by $\ell_2 \geqslant 167$m. We shall adopt these values for B_1 and ℓ_1 throughout; and, since the minimum value of ℓ_2 is close to ℓ_{int}, we shall equate these two lengths:

$$\left.\begin{aligned} B_1 &= 10\text{T} \\ \ell_1 &= 20\text{m} \\ \ell_2 &= \ell_{int} = 8.75\text{P, (m, TeV/c)} \\ d_2 &= 0.525\text{m} \end{aligned}\right\} \qquad \ldots (17a)$$

It may prove possible to reduce ℓ_2 in a more detailed design, (eg. using greater values of ℓ_1 at the higher energies), but at present we take the view that allowing ℓ_2 to vary as γ will permit easier matching conditions for the high-β quadrupoles, and will also be consistent with the experimental physics requirements.

Similarly, considering the remainder of the insertion - length ℓ_3 in Fig 2 - rough scaling arguments based on insertion matching and on chromaticity correction lead us to propose, as a conservative choice:

$$\ell_3 \simeq (\ell_{int} + \ell_2) \sim \gamma. \qquad \ldots (17b)$$

Detailed consideration may allow this length to be reduced in a final design. However, using equ (17b), the length of a half-insertion is given by $4\,\ell_{int}$, and we define:

$$\ell_{ins} = 8\,\ell_{int} = 70P, \text{ (m, TeV/c)}, \qquad \ldots (18)$$

$$(\ell_{ins})_{tot} = 8\,\ell_{ins} = 0.560P, \text{ (km, TeV/c)}, \qquad \ldots (18a)$$

$$C = C_{np} + (\ell_{ins})_{tot} = (3.3534+0.560).\ P = 3.913.P, \text{(km, TeV/c)}.. \qquad (18b)$$

With constant proton flux of 6×10^{14}, the coasting beam current is then given by:

$$I = Nec/C = 7.364.P^{-1}, \text{ (amp, TeV/c)}, \qquad \ldots (19)$$

and the proton line density λ by:

$$\lambda = N/C = 1.533 \times 10^{14}.\ P^{-1}, \text{ (km}^{-1}\text{, TeV/c)}. \qquad \ldots (19a)$$

The stored energy in the beam is:

$$W = NeE \simeq 0.0961.P, \text{ (GJ, TeV/c)}. \qquad \ldots (20)$$

Each insertion will contribute a phase shift π to the total machine tune, so that:

$$Q = Q_{np} + 4. \qquad \ldots (21)$$

5. CALCULATED STORAGE RING PARAMETERS

The equations quoted in Sections 2,3 and 4 allow most of the important storage ring parameters to be calculated, and Table I may now be complemented by the quantities listed in Table II. The interaction point parameters L, β^*, α and ℓ_{int} are also plotted in Figs. 3-6.

TABLE II

STORAGE RING PARAMETERS

ADDITIONAL TO TABLE I

P (TeV/c)	20	40	60	80	100
C (km)	78.26	156.5	234.8	313.0	391.3
R (km)	12.46	24.91	37.37	49.82	62.28
ℓ_{int} (km)	0.175	0.350	0.525	0.700	0.875
ℓ_{ins} (km)	1.4	2.8	4.2	5.6	7.0
I (amp)	0.364	0.182	0.121	0.091	0.073
W (GJ)	1.92	3.84	5.76	7.68	9.60
Q	208.25	292.25	356.25	412.25	460.25
L ($cm^{-2}s^{-1}$)	4.06×10^{32}	2.03×10^{32}	1.35×10^{32}	1.02×10^{32}	0.813×10^{32}
β^* (m)	16.79	33.57	50.38	67.16	83.92
σ^* (μm)	79.32	79.29	79.34	79.32	79.29
α (μrad)	30.95	15.48	10.31	7.737	6.191
$\Delta(\beta\gamma)_{inj}$	0.013	0.0184	0.0225	0.0260	0.0291
$\Delta(\beta\gamma)_{st}$	4.00	6.73	9.12	11.32	13.38

These results have been checked using the CERN program STORPA2. Besides calculating the above parameters, this code incorporates all the single beam limiting phenomena discussed in Ref. (1) - incoherent tune shift, transverse and longitudinal resistive wall instabilities, as well as the "stored energy limited current" defined by:

$$I_w = WB/2\pi \ (m_p c/e)^2 \ (R/\rho)\gamma^2 \qquad \ldots (22)$$

In accord with the Ref. (1) discussion, the following parameters were specified to cover these additional features:

Incoherent tune shift limit,	$\Delta Q \leq 0.025$	
Transverse resistive wall tune spread	$\delta Q \geq 0.02$	
Resistive wall mode number,	$(n-Q)=0.75$	... (23)
Conductivity of vacuum chamber wall,	$\sigma_c = 10^6$ A/Vm	

Further, the computations covered a range of different aperture radii 'b' for different values of maximum quadrupole field B_Q at the inner coil radius:

$$2\text{cm} \leq b \leq 6\text{cm} \ , \ 4\text{T} \leq B_Q \leq 10\text{T} \qquad \ldots (24)$$

In no case did any of the single beam limits affect the argument: the corresponding limiting currents were always greater than those quoted in Table II: the luminosity and crossing point parameters of Table II were always attainable for single-turn filling of 6×10^{14} protons into the storage rings.

One significant outcome of this wide survey concerned the momentum spread required in the stored beam. As seen in the last row of Table II (for k = 250T/m) the $\Delta(\beta\gamma)_{st}$ spread is many times that present in the injected beam from the synchrotron, (cf. penultimate row of Table II). This effect is very dependent upon the parameters of the normal cell part of the lattice. Figs 7 and 8 show how the Q_{np} and $\Delta(\beta\gamma)_{st}$ vary for different values of k_{max}, (corresponding to any relevant choice of 'b' and B_Q within the equ (24) range). The factor of blow-up required is reduced for lower Q-values, as suggested by the η-variation of equ (3c).

This effect places demands on the RF system, examined briefly in the next Section.

6. RF VOLTAGES REQUIRED

The RF voltage required for stationary buckets of half height $\Delta(\beta\gamma)$ is given by:

$$V_{RF} = \left[\frac{\Delta(\beta\gamma)}{Q}\right]^2 . \frac{R}{\gamma} . (\pi^2 . f_{RF} . m_p c/e). \qquad \ldots (25)$$

Choosing f_{RF} = 200 MHz, as in the SPS, this formula reduces to:

$$V_{RF} = 6.178 \times 10^6 . \frac{R}{\gamma} . \left[\frac{\Delta(\beta\gamma)}{Q}\right]^2 \qquad \ldots (25a)$$

where V_{RF} is given in MV for R in km.

The quantity $\Delta(\beta\gamma)_{st}$ in Table II and Fig 8 is the full width of the distribution at half-height. Making the approximation that this is roughly equal to the half-width at the base of the distribution, $\Delta(\beta\gamma)_{st}$ may be used directly in equ (25a). The resulting voltages for the worst case, (k_{max} = 250 T/m), are listed in Table III.

TABLE III

RF VOLTAGE , k = 250T/m.

P (TeV/c)	20	40	60	80	100
R (km)	12.46	24.91	37.37	49.82	62.28
Q	208.25	292.25	356.25	412.25	460.25
$\Delta(\beta\gamma)_{st}$	4.00	6.73	9.12	11.32	13.38
V_{RF} (MV)	1.42	2.04	2.52	2.90	3.25

Even allowing for the approximations involved in this calculation, the voltage requirements seem to be very reasonable.

7. CONCLUSIONS

Based on existing lattice design techniques but using niobium-tin superconductor, these high energy coasting-beam p-p storage rings appear to present no insuperable technical difficulties. Luminosities of order 10^{32} $cm^{-2}s^{-1}$ per crossing seem possible, even though only single-turn filling has been contemplated: greater values could be achieved by stacking further turns, if the resulting currents and stored energies could be controlled.

Stored energy in the beams reaches very high levels by present-day standards - for instance 1.92 GJ per beam at 20 TeV. However, this beam has a revolution time of about 260 μs, so that dumping procedures which deal with sections of a few kilometres may be contemplated and could reduce the problem considerably.

We have studied designs in which the vacuum chamber bore is several centimetres radius, even though the beam itself should occupy only a fraction of a millimetre. This approach may be necessary from vacuum considerations, as well as from the point of view of practical magnet design. One outcome is that there should be space to spare for closed orbit correction; and that once the correction has been achieved, the beam should occupy an excellent 'good-field' region, with consequent relative freedom from non-linear effects. However, these features of the design have to be examined in greater detail to verify such arguments.

Siting and cost are problems which we have not considered seriously as yet. No doubt both are formidable, but do not seem to constitute technical limitations.

The provision of electrical power for the entire accelerator and storage ring complex presents a severe practical problem. One suggestion we offer for future consideration: namely, to power the complex with an accelerator-driven heavy ion fusion plant.

ACKNOWLEDGEMENTS

The authors wish to thank M Hanney and Y Marti of the CERN ISR Division for their assistance in using the programs AGS and STORPA2.

REFERENCE

(1) E Keil. Perspectives on Colliding Beams. Proc. 8th Inter. Conf. on High Energy Accels., Stanford, p660, (1974).

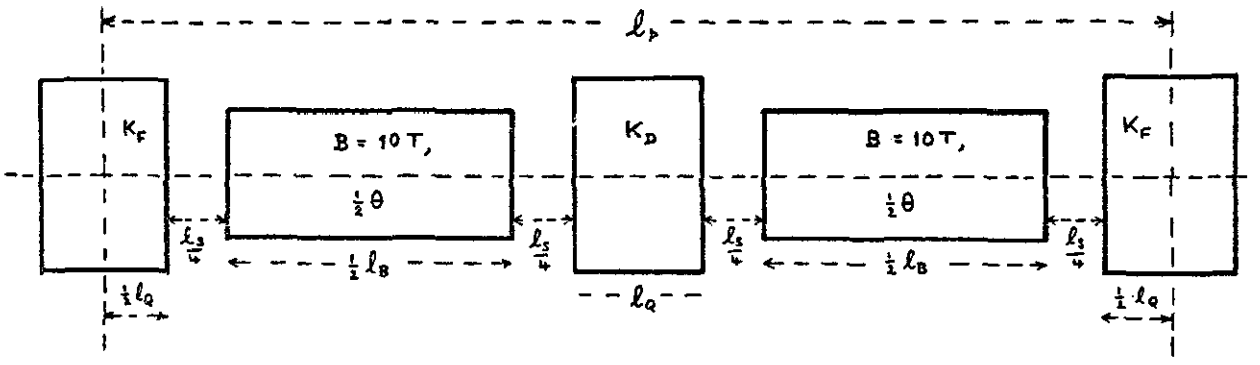

FIG. 1 SCHEMATIC NORMAL CELL

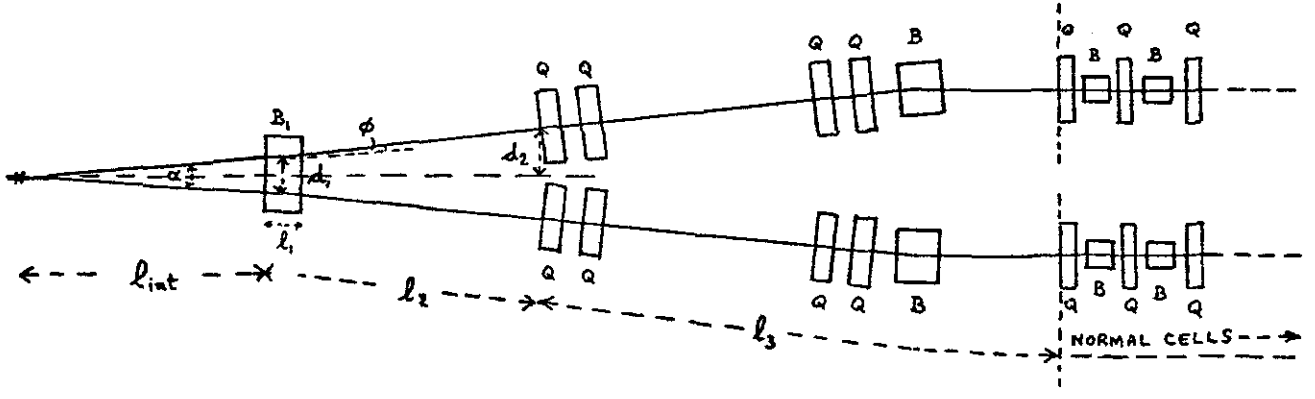

FIG. 2 SCHEMATIC HALF-INSERTION

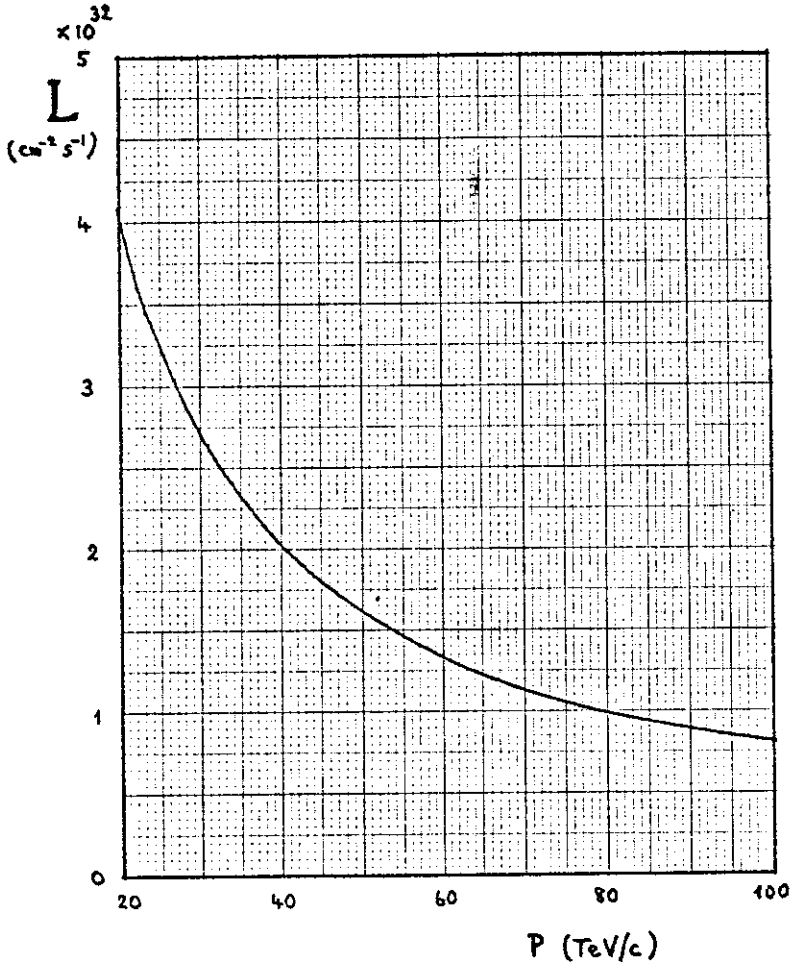

FIG. 3 LUMINOSITY

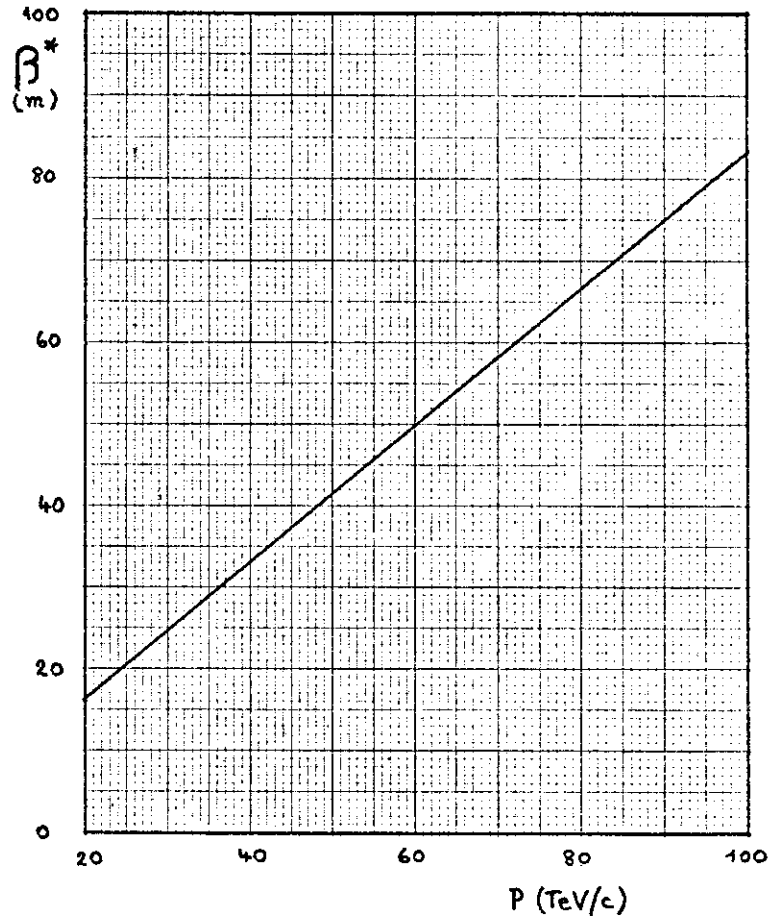

FIG. 4 β^*

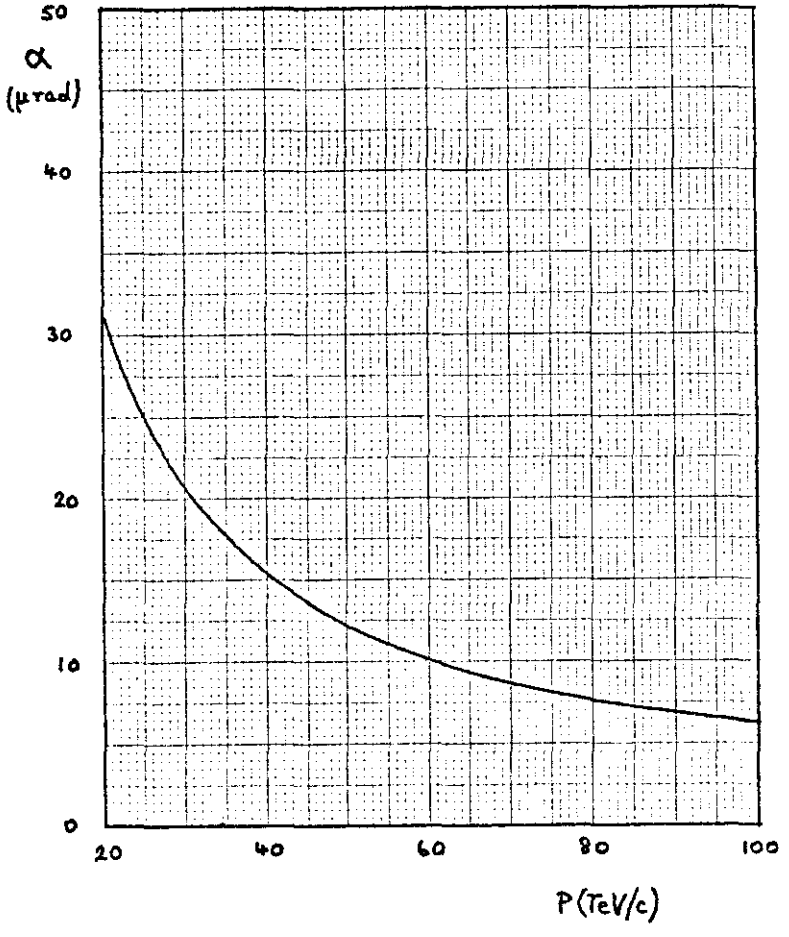

FIG.5 CROSSING ANGLE

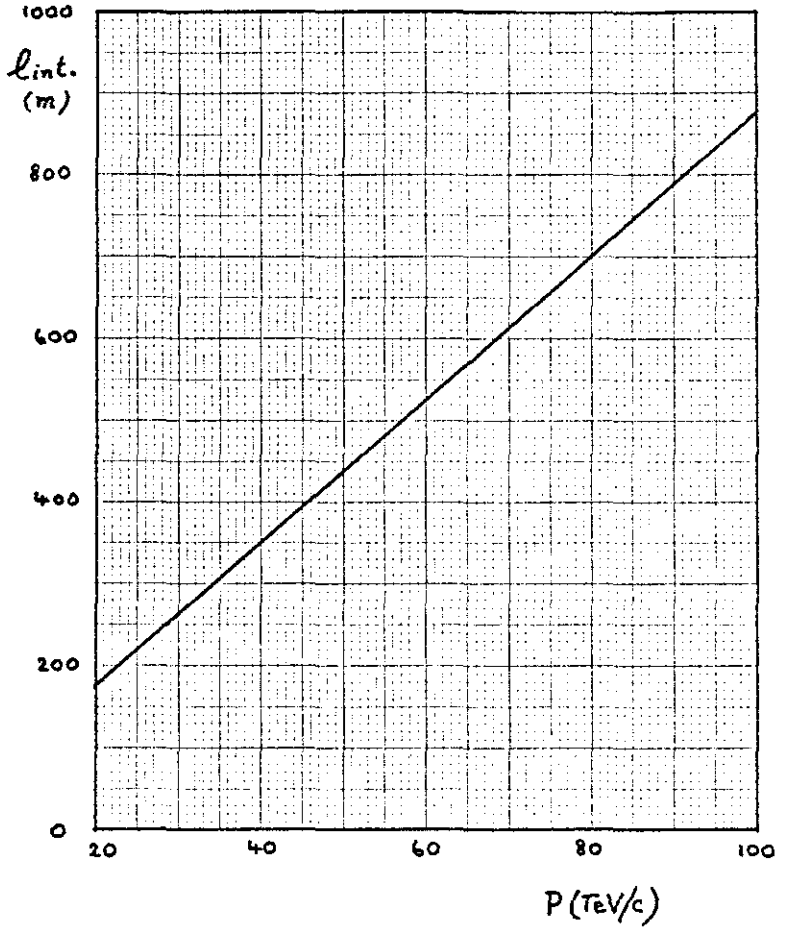

FIG.6 FREE SPACE ℓ_{int}

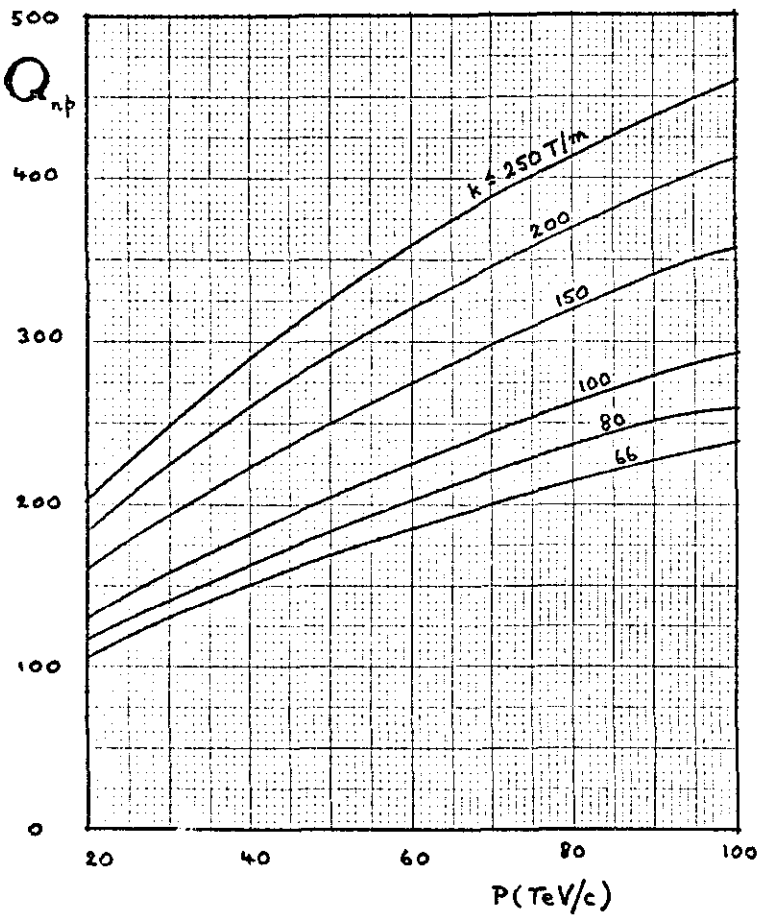

FIG. 7 . VALUES DIFFERENT k_{max}

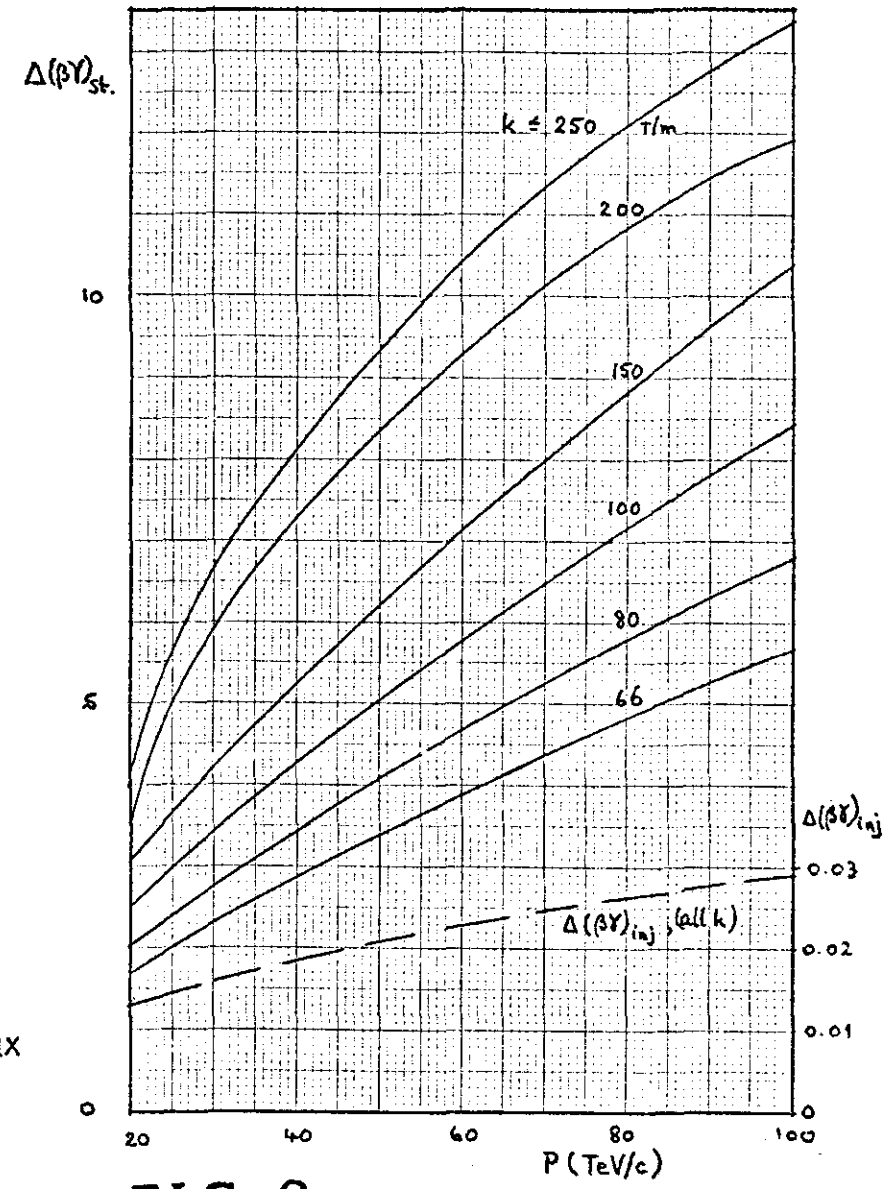

FIG. 8 $\Delta(\beta\gamma)$ SPREAD

BUNCHED-BEAM p-$\bar{p}$ AND p-p COLLISIONS

E.D. Courant and E. Keil

1. Introduction

In the following, we study collisions between bunched beams of protons and/or antiprotons. We assume, for simplicity, that the bunches collide head-on, and that the two beams have the same number of particles N and rms beam radii σ_x and σ_y at the crossing point.

2. Basic luminosity formulae

The luminosity L and beam-beam tune shifts $\Delta\nu$ are given by the standard formulae for e^+e^- storage rings[1]:

$$L = \frac{N^2 f}{4\pi k_b \sigma_x \sigma_y} \tag{1}$$

$$\Delta\nu_x = \frac{N r_o \beta_x}{2\pi k_b \gamma (\sigma_x + \sigma_y)\sigma_x} \tag{2}$$

$$\Delta\nu_y = \frac{N r_o \beta_y}{2\pi k_b \gamma (\sigma_x + \sigma_y)\sigma_y} \tag{3}$$

Here f is the revolution frequency, k_b the number of bunches in each beam, β_x and β_y the amplitude functions at the crossing point, r_o the classical proton radius and γ the usual relativistic factor.

If we make

$$\sigma_x/\sigma_y = \beta_x/\beta_y \tag{4}$$

as we shall assume in the following, the beam-beam tune shifts $\Delta\nu_x$ and $\Delta\nu_y$ become the same. Using (3) to eliminate one power of N in (1) yields, assuming that $\sigma_y \ll \sigma_x$:

$$L \approx \frac{N f \gamma \Delta\nu}{2 r_o \beta_y} \tag{5}$$

There is no reason not to build p-p colliding-beam machines with the highest possible magnetic fields in the dipoles B_M at all energies. Hence, the product $f\gamma$ is independent of the energy. We conclude that the luminosity does not depend explicitly on the energy of the machine, but only on the number of particles, the field in the dipoles and the value of β_y.

3. Stored beam intensity

The number of particles necessary for obtaining a given luminosity is obtained by solving (5) for N:

$$N = \frac{2Lr_o\beta_y}{f\gamma\Delta\nu} \tag{6}$$

The invariant emittances of the beams E_x and E_y are obtained from (2) and (3), again assuming $\sigma_y << \sigma_x$:

$$E_x = \frac{4\pi\gamma\sigma_x{}^2}{\beta_x} = \frac{2Nr_o}{k_b\Delta\nu} = \frac{4Lr_o{}^2\beta_y}{k_b f\gamma(\Delta\nu)^2} \tag{7}$$

$$E_y = \frac{4\pi\gamma\sigma_y^2}{\beta_y} = \frac{\beta_y}{\beta_x}\frac{2Nr_o}{k_b\Delta\nu} = \frac{4Lr_o{}^2\beta_y{}^2}{k_b f\gamma\beta_x(\Delta\nu)^2} \tag{8}$$

Because of the factor $f\gamma$, the invariant emittances do not depend on the design energy. In deriving (7) and (8) we have assumed that the crossings occur in regions without dispersion.

4. Limits on interaction region design

It is clear from (5) that the amplitude function β_y should be small in order to obtain a high luminosity. Lower limits on β_y are imposed by

(i) the bunch length

(ii) chromaticity correction

(iii) the strength of the nearest quadrupole.

The value of β_y should be large compared to σ_z, in order to avoid a reduction of the luminosity by the β_y-variation in the interaction region. The difficulty of chromaticity correction is proportional to ℓ_{int}/β_y where ℓ_{int} is the distance from the crossing point to the nearest quadrupole. In e^+e^- storage rings, ℓ_{int}/β_y must be less than about 50 to 100 in order to correct chromatic effects over a momentum range of about ±1%.

The effect of the quadrupole strength on β_y is obtained by calculating the horizontal aperture of the first quadrupole A_x which must be a factor F_a larger than the rms beam size at the quadrupole entrance.

$$A_x = F_a \sigma_{xQ} \quad . \tag{9}$$

The beam size σ_{xQ} is given by:

$$\sigma_{xQ} = \sigma_x \left(\frac{\beta_{xQ}}{\beta_x}\right)^{\frac{1}{2}} \approx \frac{\sigma_x \ell_{int}}{\beta_x} \quad . \tag{10}$$

Substituting from (7) yields for the necessary quadrupole aperture:

$$A_x = F_a \ell_{int} \left(\frac{Nr_o}{2\pi\beta_x k_b \gamma\Delta\nu}\right)^{\frac{1}{2}} = \frac{F_a \ell_{int} r_o}{\gamma\Delta\nu} \left(\frac{L\beta_y}{\pi k_b f \beta_x}\right)^{\frac{1}{2}} \quad . \tag{11}$$

The quadrupole must have a focal length of about $\frac{1}{2}\ell_{int}$. Hence, its length ℓ_Q, magnetic field B_Q at a distance A_x from the centre ("poletip field") and the proton rigidity $B\rho$ are related by

$$A_x = \frac{B_Q \ell_{int} \ell_Q}{2B\rho} \tag{12}$$

Equating (11) and (12) yields an equation for ℓ_Q:

$$\ell_Q = \frac{e Z_o F_a}{2\pi B_Q \Delta\nu} \left(\frac{L \beta_y}{\pi k_b f \beta_x}\right)^{\frac{1}{2}} = \frac{e Z_o F_a}{2\pi B_Q} \left(\frac{N\gamma}{2\pi\beta_x k_b \Delta\nu r_o}\right)^{\frac{1}{2}} \quad . \tag{13}$$

Here e is the elementary charge and Z_o is the impedance of free space. Experience with the design of e^+e^- interaction regions indicates that there is a relation between ℓ_Q and ℓ_{int}, of the form

$$\ell_{int} = G_e \ell_Q \tag{14}$$

where the coefficient G_ℓ is of the order of 2 or more. In addition, chromaticity correction imposes a relation of the form

$$\ell_{int} = G_c \beta_y \tag{15}$$

By combining (13) to (15) we finally arrive at equations for β_y:

$$\beta_y = \frac{G_\ell F_a}{G_c} \frac{e\, Z_o}{2\pi B_Q \Delta\nu} \left(\frac{L\beta_y}{k_b f \beta_x} \right)^{\frac{1}{2}} \tag{16}$$

$$\beta_y^{3/2} = \frac{G_\ell F_a}{G_c} \frac{e\, Z_o}{2\pi B_Q} \left(\frac{N\gamma\beta_y}{2\pi k_b \Delta\nu r_o \beta_x} \right)^{\frac{1}{2}} \tag{17}$$

These equations include all the limitations on the interaction region design imposed by the poletip field B_Q, optical constraints (G_ℓ) and chromaticity (G_c); they contain only the ratio β_y/β_x on the right-hand side.

5. Application to p-$\bar{p}$ collisions

For p-$\bar{p}$ collisions we make the assumptions and obtain the scaling laws shown in Table 1.

Table 1. Assumptions and scaling laws for p-$\bar{p}$ collisions

Assumed independent of γ:	N, $\Delta\nu$, k_b, F_a, G_ℓ, G_c, B_Q, β_y/β_x, B_M
Proportional to γ^o:	E_x, E_y
Proportional to $\gamma^{1/3}$:	β_x, β_y, ℓ_Q, ℓ_{int}
Proportional to $\gamma^{-1/3}$:	L, A_x

A few comments are in order on the fixed parameters used in the detailed examples. The aperture allowance F_a includes the extra space required at the injection energy which is about twenty times smaller than the design energy. The chromaticity factor G_c is smaller than in e^+e^- storage rings because the tolerances on the chromaticity correction may be tighter in p-$\bar{p}$ schemes. The limit $\Delta\nu$ on the beam-beam tune shift is the conventional value for coasting proton beams. There are strong doubts whether it also applies to bunched proton beams.

The number of particles corresponds to that of the CERN p-$\bar{p}$ project[2]. It is used here as a lower limit of what might be achieved in an optimized $\bar{p}$-factory fed from a 20 GeV proton synchrotron with a flux of 10^{13} protons/s, or from one of its injectors with even higher fluxes.

When actual numbers are inserted into the equations above, it turns out that the apertures of the interaction region quadrupoles are rather small by comparison

with present values. The physical reason for this is the constant invariant emittance which results in decreasing beam size with energy. In order not to deviate too much from present practice in quadrupole construction, we have assumed rather a low value of the poletip field B_Q.

The number of bunches is 4 in each beam, because we assume that the machine has 8 equidistant interaction regions. This choice avoids the complications of a higher number of bunches where the beams have to be separated in the unwanted crossings while they are in collision at the interaction regions. As a consequence of this choice, the total number of events in each collision between bunches increases as $\gamma^{2/3}$.

Table 2 shows the main machine parameters for three different different energies, namely about 200 GeV, 2 and 20 TeV. The 200 GeV machine has parameters which are fairly close to those of the CERN p-$\bar{p}$ project[2]. It is included here as a useful check of the interaction region design procedure. There is fairly good agreement between the actual and the computed parameters.

As the design energy increases, the quadrupole aperture and beam size decrease, and the quadrupole length increases. The mechanical tolerances of the quadrupole must be roughly proportional to the aperture. Avoiding the field errors associated with the tolerances is the essential reason for the choice of B_Q. At the low value chosen, the windings of a superconducting quadrupole could be far away from the beam, thus relaxing considerably the tolerances on the coil position.

So far, we have tacitly assumed that the synchrotron can be modified to include p-$\bar{p}$ interaction regions with the properties described above. This must also hold during synchrotron operation, with injected beam sizes which are larger than those at the design energy. This problem can be alleviated by increasing the amplitude functions at the crossing points during synchrotron operation, or circumvented by taking the synchrotron beam through a by-pass around the interaction region[3].

Table 2. Parameters for p-$\bar{p}$ collisions at various energies

$N = 10^{12}$	$F_a = 40$	$B_Q = 1T$
$\Delta\nu = 0.005$	$G_\ell = 5$	$\beta_x/\beta_y = 4$
$k_b = 4$	$G_c = 20$	$C/2\pi\rho = 1.5$

γ	200	2×10^3	2×10^4	
β_y	1.33	2.9	6.2	m
β_x	5.3	11.4	25	m
ℓ_{int}	27	57	124	m
ℓ_Q	5.3	11.4	25	m
E_x	48π	48π	48π	μm
E_y	12π	12π	12π	μm
B_M	1	10	10	T
f	48	48	4.8	kHz
L	1.2×10^{30}	5.5×10^{30}	2.6×10^{30}	$cm^{-2}s^{-1}$
A_x	107	49	23	mm
σ_x	0.56	0.26	0.12	mm
σ_y	141	65	31	μm
W	0.032	0.32	3.2	MJ

We studied neither the RF system required for keeping the beams bunched, nor the magnet lattice outside the interaction regions and space-charge phenomena. We do not expect particular difficulties with the RF system. The magnet lattice is similar to that of the coasting-beam p-p collisions[4].

A luminosity well above 10^{30} $cm^{-2}s^{-1}$ is within reach over the whole energy range. As the energy increases, the number of events in a single collision between bunches increases. It reaches about 7 at 20 TeV, assuming a total cross-section of about 100 mbarn. If this turns out to be

too inconvenient for event analysis, th. our concept of colliding a few bunches breaks down somewhere in the TeV range.

The only two alternatives are increasing the number of bunches and changing to coasting beams. Increasing the number of bunches implies beam separation at the unwanted crossing points at the same time as beam collisions in the interaction regions, and all the difficult tolerances associated with separation. Coasting beams imply a reduction of the luminosity to about $\mathcal{L} = 10^{28}\ cm^{-2}s^{-1}$ at $N = 10^{12}$. Hence, in order to obtain a luminosity of about $\mathcal{L} = 10^{30}\ cm^{-2}s^{-1}$, approximately 10^{13} protons and antiprotons must be stored.

6. Application to p-p collisions

If a storage ring is added to the synchrotron, p-p collisions can be obtained. We assume that the circumference and the number of bunches in the synchrotron and in the storage ring are chosen to be such that the bunch spacings in the two machines are identical.

For the time being, we also assume that no proton accumulation takes place in the storage ring, but that the available protons are arranged in a suitable number of bunches. It then seems natural to make the number of protons in a bunch the same as in the p-$\bar{p}$ scheme. In this case the beam sizes at the crossing points are the same as in the p-$\bar{p}$ scheme, and the conclusions on the interaction region design also apply to p-p collisions.

The number of protons is the same as in the synchrotron; we take $N = 6\times10^{14}$. The technical problems associated with the stored energy in the beam are all the same as in the synchrotron, provided that the beam transfer between the machines is clean enough, and can be considered solved. With 0.25×10^{12} protons in a bunch we thus arrive at 2400 bunches and a bunch spacing of about 25 m. The performance which might thus be achieved is summarized in Table 3.

Table 3. Parameters for p-p collisions at 20 TeV

$N = 6\times10^{14}$	$F_a = 40$	$\beta_Q = 1T$
$\Delta\nu = 0.05$	$G_\ell = 5$	$\beta_x/\beta_y = 4$
$k_b = 2400$	$G_c = 20$	$C/2\pi\rho = 1.5$
$\beta_y = 6.2$ m	$\ell_{int} = 124$ m	$E_x = 48\pi$ μm
$\beta_x = 25$ m	$\ell_Q = 5$ m	$E_y = 12\pi$ μm
$B_M = 10T$	$f = 4.8$ kHz	$L = 1.6\times10^{33}$ cm^{-2}s^{-1}
$A_x = 23$ mm	$\sigma_x = 0.12$ mm	$\sigma_y = 31$ μm
$W = 1900$ MJ		

Since head-on collisions are assumed, and the close bunch spacing is neglected, the luminosity figures must be considered optimistic.

Since the bunch population is the same as in the p-$\bar{p}$ scheme, the number of events for a single collision is again about 7. Hence the remarks made above also apply.

7. Conclusions

We have studied schemes for p-$\bar{p}$ and p-p collisions between bunched beams. With rather conservative assumptions about available $\bar{p}$ fluxes we obtain a luminosity in the 10^{30} cm^{-2}s^{-1} range which has rather a weak variation with the energy. The most natural scheme where the number of bunched beams is half the number of interaction regions, has the difficulty that the number of events in a single collision increases with the energy.

For p-p collisions, we make use of the full current available from the synchrotron. We find luminosities in the 10^{33} cm^{-2}s^{-1} range, and the same difficulties with the number of events in a single collision as in the p-$\bar{p}$ scheme. Since the luminosities are not much larger than for coasting p-p collisions[4)], there does not seem to be a good reason for bunched p-p collisions.

References

1) M. Sands, SLAC-121 (1970).

2) CERN Report, SPS/SI/PP/Int. Note/77-9.

3) P. McIntyre, contribution to this workshop.

4) E. Keil and N.M. King, contribution to this workshop.

CERN/PS/DL 78-25
October, 1978

STOCHASTIC COOLING

reported by
D. Möhl

Invited talk given at the Workshop on
Accelerator and Detector Possibilities and
Limitations, FERMILAB, October 15-21, 1978

TABLE OF CONTENTS

0. Introduction
1. The principle
2. Historical notes
3. Limitations
4. Recent refinements of the theory
5. Practical systems
   5.1 Betatron cooling (ICE results)
   5.2 Momentum cooling, Palmers method (AA Design)
   5.3 Momentum cooling, filter method (ICE results, AA precooling)
6. Future applications
7. Acknowledgements

---

0. Introduction

This is an attempt to give a "self-contained summary of recent theoretical and experimental work done at CERN on stochastic cooling". I hope that the names of those who contributed to this venture are adequately covered in the historical notes and in the list of references given below. My role here is that of a rapporteur.

The participants of this workshop on the future "world accelerator" (and the reader of this report) should like, I assume, to appreciate the beauty and to learn about the possibilities and limits of stochastic cooling, in order to understand the promises which phase-space cooling of "rare" particles may hold at the highest and lowest accelerator energies. I will try to satisfy this curiosity.

1. The principle

Stochastic cooling is in principle simple: a sensor measures the error in some property of each successive sample of beam particles (say, the error in transverse position <x>). The sample length is determined by the resolution i.e. by the rise time T_s - or if you prefer by the bandwidth $W = \frac{1}{2T_s}$ of the system.

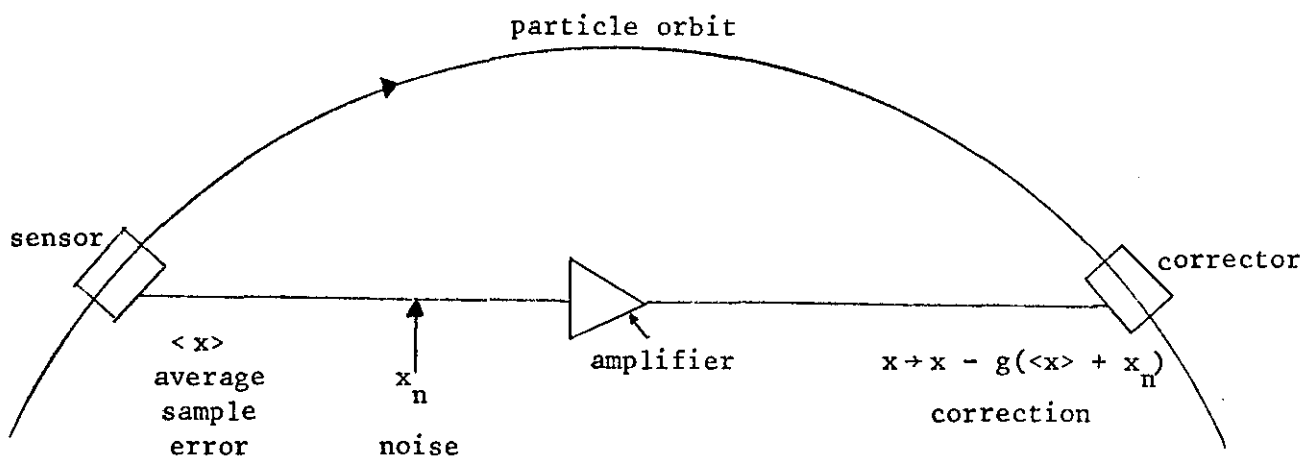

Figure 1

A correction signal is derived and applied on a corrector (transverse kicker). The system can only detect and correct the average error of the samples (centre of gravity <x >). The corresponding beam signals are called Schottky noise.

For zero energy spread cooling would stop once the average sample errors are corrected. However, due to the dispersion in revolution frequencies, particles will migrate between samples (mixing), the error will reappear and correction continues until ideally all particles have zero error.

A few equations may illustrate the principle. At the corrector each sample member gets its error changed by

$$x_c = x - \underbrace{g\,(\langle x\rangle}_{\text{correction}} + \underbrace{x_n}_{\text{noise}}) \qquad (1.1)$$

x — error of i-th sample member before passage of corrector

x_c — error after passage of corrector

Here $\langle x \rangle$ is the average sample error, x_n the system noise and $g \leq 1$ the fractional correction per passage; g depends on the amplification, the number of particles and other system parameters.

As a very rough approximation, assume that each particle interacts only with itself whereas the mutual influence "averages out". Then, with a sample population of $N_s = N\,T_s / T_{rev}$

$$\langle x \rangle = \frac{1}{N_s}\left(x_{test} + \sum_{\substack{\text{all}\\ \text{others}}} x\right) \approx \frac{1}{N_s}\, x_{test}$$

In this approximation the change at the corrector $\Delta x = x_c - x$ becomes for any sample member

$$\Delta x \approx -\frac{g}{N_s}\, x$$

and the cooling rate for f_{rev} passages per second

$$\frac{1}{\tau} = \frac{1}{x}\frac{dx}{dt} \approx f_{rev}\frac{\Delta x}{x} \approx \frac{f_{rev}\, g}{N_s} = \frac{2Wg}{N} \qquad (1.2)$$

This simple result overestimates $1/\tau$ at most by a factor 2. However, it does not show up the heating due to noise and other particles.

To include these effects a slightly more elaborate evaluation of (1.1) is needed. The approach (due to Hereward) is summarized in Table 1. The result for the cooling of the rms beam error x_{rms} is

$$\frac{1}{\tau} = \frac{f_{rev}}{N_s}\left[g - \frac{g^2}{2}\left(1 + \frac{x^2_{n\,rms}}{x^2_{rms}}\right)\right] \qquad (1.3)$$

heating by noise

heating by other particles

coherent effect (cooling) eq.(1.3)

sample population, given by bandwidth and beam population N because $N_s = N\,T_s / T_{rev} = N f_{rev} / 2W$

Note that the derivation assumes perfect mixing between consecutive turns and no mixing between sensor and corrector.

TABLE 1 : EVALUATION OF COOLING RATE

Change at corrector for one passage (eq.(1.1))

$$x_c = x - g\,(\langle x\rangle + x_n)$$

Work out $\Delta x^2 = x_c^2 - x^2$:

$$\Delta x^2 = -\,2\,g\,x\,(\langle x\rangle + x_n) + g^2\,(\langle x\rangle + x_n)^2$$

Take the sample average

$$\langle\Delta x^2\rangle = -\,2\,g\,\langle x\rangle^2 - 2\,g\,\langle x\rangle\,x_n + g^2\,(\langle x\rangle^2 + 2\langle x\rangle\,x_n + x_n^{\,2})$$

For many passages, replace these quantities by their expectation values for random samples (mixing) of the beam. For $N_s \gg 1$

$$E\,(\Delta\langle x^2\rangle) = x^2_{rms.c} - x^2_{rms} = \Delta x^2_{rms}$$

$$E\,(\langle x\rangle^2) = \frac{1}{N_s}\,x^2_{rms}$$

$$E\,(x_n\langle x\rangle) = 0 \quad \text{(no correlation between noise and correction)}$$

$$E\,(x_n^{\,2}) = \frac{1}{N_s}\,x^2_{n\,rms}$$

where all rms are the beam rms values.

Hence

$$\frac{\Delta x_{rms}}{x_{rms}} \approx \frac{1}{2}\,\frac{\Delta x^2_{rms}}{x^2_{rms}} = \frac{-g}{N_s}\left[1 - \frac{g}{2}\left(1 + \frac{x^2_{n.rms}}{x^2_{rms}}\right)\right]$$

TABLE 2 : HISTORY (with emphasis on work at CERN)

Prehistory

Liouville	ca 1850	Invariance of phase space
Schottky	1918	Noise in DC electron beams

History

van der Meer	1968	Idea of stochastic cooling
ISR staff (Borer, Bramham, Hereward, Hübner, Schnell, Thorndahl)	1972	Observation of proton beam Schottky noise
van der Meer	1972	Theory of emittance cooling
Schnell	1972	Engineering studies
Hereward	1972-74	Refined theory, low intensity cooling
Bramham, Carron, Hereward, Hübner, Schnell, Thorndahl	1975	First experimental demonstration of emittance cooling
Palmer (BNL) Thorndahl	1975	Idea of low intensity momentum cooling
Strolin Thorndahl	1975	$\bar{p}$ accumulation, schemes for ISR using stochastic cooling
Rubbia	1975	$\bar{p}$ accumulation, schemes for SPS
Thorndahl	1976	Experimental demonstration of p cooling
Thorndahl	1977	Filter method of p cooling
Sacherer, Thorndahl van der Meer	1977-78	Refinement of theory; imperfect mixing, Fokker-Planck equations
ICE Team	1978	Detailed experimental verification
Herr	1978	Demonstration of bunched beam cooling.

2. History

For long the idea of stochastic cooling was regarded as too far fetched to be practical. A first experimental demonstration was tried and succeeded only 7 years after the invention (3 years after the first publication).

The inventor and the early workers had (mainly?) emittance cooling of high intensity beams in mind in order to improve the luminosity in the ISR. A new era began in 1975 when Strolin (coming back from a visit to Novosibirsk) and Thorndahl realized the interest of stochastic cooling, both in emittance and momentum, of low intensity $\bar{p}$ beams for the purpose of stacking. Stochastic cooling at low intensity is different from the original van der Meer cooling and the extension of the theory (to $g < 1$ in eq. 1.1) first done by Hereward and Thorndahl as well as the design of the momentum cooling hardware (Thorndahl, Carron) are perhaps as fundamental as the original invention and the earlier feasibility studies (van der Meer, Schnell, ...).

Following this broadening of the scope, Strolin and Thorndahl worked out in 1975 $\bar{p}$ collection schemes for the ISR using stacking in momentum space and Rubbia et al. made first proposals of the $\bar{p}$-p scheme for the SPS using similar techniques of stochastic cooling and accumulation. This work has given new life to the idea at a time when the ISR was routinely stacking such high proton currents that proton beam cooling became unnecessary or even impossible. Further mile stones since 1975 are the invention of the filter method of momentum cooling, the refinement of the theory and of the stacking schemes, the CERN $\bar{p}$-p proposal which has now become a project and the encouragement from the results of the cooling experiment ICE including the discovery of bunched beam cooling.

Table 3 : Experimental results

Year	Machine	Type of cooling	No. of Particles	Cooling Time
1975	ISR	vertical	$\approx 10^{13}$	100 h
1976/77	ISR	vertical	$\approx 10^{8}$	2 h
1978	ICE	vertical	3×10^{8}	4 min
		longitudinal	10^{7}	15 s
1980	AA	longitudinal	$2{,}5 \times 10^{7}$	1 s
		longitudinal	6×10^{11}	$\sim$ 1 h
		vert./horiz.	6×10^{11}	$\sim$0,5 h

3. Some limitations

A few fundamental limits are obvious from eq. (1.3)

a) Bandwidth limit

In the best of all cases g = 1 and

$$\frac{1}{\tau} = \frac{W}{N} \tag{3.1}$$

Let for technical reasons $W < 1$ GHz. Then, particles can be cooled at best at a rate

$$\frac{dN}{dt} \approx \frac{N}{\tau} = W < 10^9/s \qquad (\simeq 8 \times 10^{13}/\text{day})$$

b) Noise limit

It follows from (1.3) that with noise fastest initial cooling is for $g = g_o$ given by

$$g_o = \frac{1}{1 + x_n^2/x^2} \tag{3.2}$$

and the cooling rate (3.1) is reduced by 1 + signal power/noise power.

Further since the heating term contains the instantaneous rms beam error (x), cooling for any g will stop once x is small. In fact, $1/\tau \to 0$ for

$$x^2_{final} = \frac{x_n^2}{2/g - 1}$$

and for $g = g_o$

$$x^2_{final} = \frac{x_n{}^2}{1 + 2x_n^2/x^2_{initial}} = \begin{cases} x_n^2 \ , \ x_{initial} \gg x_n \\ \dfrac{x^2_{initial}}{2} \ ; \ x_{initial} \ll x_n \end{cases}$$

Hence the larger g (the faster the initial rate), the smaller the final reduction of the error. For the fastest initial cooling, the asymtotic reduction in the presence of large noise is only $\sqrt{2}$. A remedy is of course dynamic gain, decreasing g (and $1/\tau$) as the error gets smaller.

c) Mixing limit

Interpreting g as the fractional correction per turn, we may intuitively require mixing (rms migration by one sample length $T_s = \frac{1}{2W}$) in at least 1/g turns

$$\Delta T_{rev} \frac{1}{g} \geq \frac{1}{2W} \tag{3.3}$$

As an example (AA precooling) take

$$\Delta T_{rev} = \eta\, T_{rev} \frac{\Delta p}{p} \approx 0.1 \times 550 \text{ ns} \times 5 \times 10^{-3}$$

$$W = 500 \text{ MHz to find } g \lesssim 0.25$$

$$\frac{N}{\tau} \leq 0.25\, W = 1.2\ 10^{8}/\text{s} \quad (10^{13}/\text{day})$$

[In fact, the mixing limit (3.3) is approximate. A rigorous calculation leads to a modification of the "heating by other particles" term (the "1" in the inner bracket in (1.3)) by a sum over the Schottky bands involded (see ref. 10, 11, 12), which for momentum cooling with constant g is written as

$$1 \to \Gamma = \frac{1}{\ell} \sum \frac{f_{rev}}{\Delta f_n} \geq 1 \tag{3.4}$$

where ℓ is the number of Schottky lines in the pass-band f_{min} to $f_{min} + W$ and Δf_n the width of the nth line due spread in the beam. Hence "optimum" $g = g_o = \frac{1}{\Gamma + x_n^2/x^2}$; $g_o = 1/\Gamma$ for negligible noise.

For ideal momentum cooling and non overlapping bands

$$\Gamma \approx \frac{1}{W\Delta T_{rev}} \ln (f_{max}/f_{min})$$

For betatron cooling with two Schottky bands per revolution harmonic, the appropriate modification is ½ of (3.4) as long as adjacent bands do not overlap. For overlapping bands ($\Delta f_n > f_{rev}$), the corresponding terms in (3.4) have to be *replaced by 1 both for p and betatron cooling.*]

d) Power limit

The larger the gain, the higher the power consumption of the amplifier. Thus the available broadband power may further *restrict the cooling rate by requiring* $g << g_o$.

[For (Palmer) momentum cooling, the damping rate may in this case be expressed [6,19] as

$$\frac{1}{\tau} \lesssim \frac{4ef_{rev}W}{(\Delta p\ c/e)_{rms}} \sqrt{n_{PU}\ R_{PU}\ n_g\ R_g} \sqrt{\frac{P}{P_n}}$$

This holds provided, one is limited by amplifier noise as is the case at low intensity. Here $P_n = 10^{v/10}\ kT_nW$ ($\approx 10^{-20}$ Watt/Hz x W at $T_n = 290^oK$ room temperature) is the preamplifier noise power, n_{PU} *(200) the number of pick-ups,* R_{PU} *(50 Ω) their impedance,* n_g (200) and R_g (50 Ω) are the corresponding characteristics of the correction gaps. The assumption is that the signal from the n_{PU} pick-ups is added, sent through the same amplifier and then split and distributed onto the n_g gaps; Δp (in eV/c) is the rms momentum spread of the beam.

Taking W = 0.5 GHz, P = 10 kW, $\Delta p = 10^{-2}$ x 3.5 GeV/c and f_{rev} = 2 MHz (figures corresponding roughly to the AA precooling), we find

$$\frac{1}{\tau} \leq 1\ s$$

In a similar way the transverse cooling rate [6] may be limited to

$$\frac{1}{\tau} \lesssim \frac{2}{3} \; \frac{e\, f_{rev}\, W}{(p\, c/e)\; \frac{\varepsilon}{\pi}} \; \sqrt{n_{PU}\, R_{PU}\, n_k\, R_k\, L_k^2} \; \sqrt{\frac{P}{P_n}}$$

Here L_k is the length, R_k the impedance and n_k the number of correction kickers, ε is the beam emittance.

Note that for constant $\Delta p/p$ and for constant emittance ε, these power limited cooling rates decrease linearly with increasing momentum, P.]

As a result of the different limitations discussed above, we may conclude that it is hard to cool more than, say, 10^{13} particles per day.

4. Refinements of the theory

4.1 Bad mixing

The appropriate generalization of the basic equation (1.3) has been obtained in ref. 23. Assuming a rectangular distribution dN/df of particles revolution frequencies of total width Δf, the modification mentioned above and generalized to include frequency dependent g is to replace "1" in the inner bracket of (1.3) by

$$\Gamma = \frac{1}{\ell\,\bar{g}^2} \sum_n \frac{g^2(f)\, f_{rev}}{\Delta f_n} \geq 1 \qquad (3.4\,a)$$

$$(\Delta f_n < f_{rev}\,, \text{ else replace } f_{rev}/\Delta f_n \to 1)$$

This modification has been explained in ref. 26 by the fact that the noise density in the nth Schottky band is larger by $f_{rev}/\Delta f_n$ as compared to white noise (for non overlapping betatron bands, reduce (3.4) by 2). The consequence of (3.4) is stronger heating by the presence of the other particles.

4.2 Fokker-Planck equations

All cooling equations discussed so far were concerned with the rms - width (second moment) of the particle distribution. To obtain more detailed information about the evaluation of the distribution (tails, stacking etc.) a Fokker-Planck type of equation can be derived by working out higher order moment equations from the single particle dynamics in the presence of feedback and noise.

$$\text{Let} \quad \psi\,(x,t) = \frac{dN}{dx}$$

be the distribtion function. The Fokker-Planck equation used by Thorndahl, van der Meer and Sacherer was written in the form:

$$(4.1) \qquad \frac{\partial\psi}{\partial t} = \frac{-\partial}{\partial x}\left\{\frac{\Delta x_c}{T_{rev}}\;\psi\right\} + \frac{1}{2}\;\frac{\partial}{\partial x}\left\{\frac{\Delta x^2{}_{ic}}{T_{rev}}\;\frac{\partial\psi}{\partial x}\right\}$$

where $\Delta x_c/T_{rev}$ is the coherent correction per unit time for a single particle and $\frac{\Delta x_{ic}^2}{T_{rev}}$ is the mean square blow up due to noise (the diffusion term if you like). Both quantities are in general functions of the error x.

Note that usually the Fokker Planck equation is derived in the form

$$\frac{\partial\psi}{\partial t} = \frac{\partial}{\partial x}\left(\alpha_1\psi\right) + \frac{1}{2}\frac{\partial^2}{\partial x2}\left(\alpha_2\psi\right) \tag{4.2}$$

It seems that for cooling problems the relation between $\alpha_1 = \langle\delta x\rangle/T_{rev}$ and $\alpha_2 = \langle(\delta x)^2\rangle/T_{rev}$ the average of the change and of the square of the change expected per time interval, permits to write (4.2) in the "diffusion form" (4.1). Equation (4.1) can be used to work out the detailed evolution of the stack including x dependent gain. It can be amended to include walls (losses) and particle influx (stacking).

4.3 Feedback via the beam

If mixing is imperfect a coherent modulation imposed on the beam by the corrector will remain to some extent. The effect is a reduction of the heating terms by the modulus $|T|$ of some complex transfer function T and of the cooling term by Re(T). The function T depends on the frequency spread within the beam. The corresponding reduction of Schottky noise has been observed both on the ISR and on ICE.(Fig. 2). On first sight the effect is beneficial since the heating is stronger reduced than the cooling. For more details we have to refer to the work of Sacherer [26].

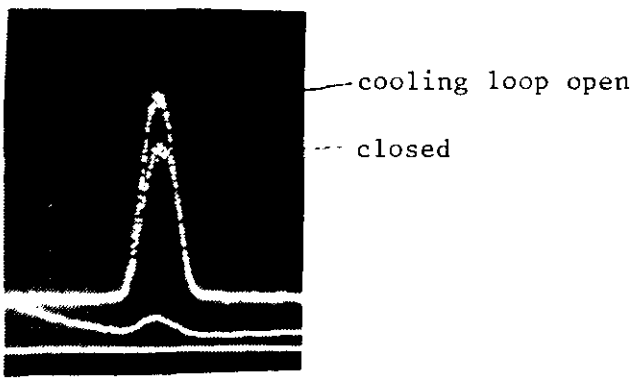

Fig. 2 : Reduction of Schottky noise in ICE

5. Practical systems

Systems proposed and tested are summarized in Table 4.

Table 4 : Different cooling systems

Type	Sensor	Corrector	Optimum Spacing	Tested on
Betatron cooling horizontal or vertical	Difference pick-up	Transverse kicker	$(2k+1)\lambda_\beta/4$	ISR ICE
Momentum cooling Palmer type	Horizontal difference pick-up	RF gap (acceleration/ deceleration)	$(2k+1)\lambda_\beta/2$ for simultaneous horizontal betatron cooling	ISR
Momentum cooling filter type	Longitudinal (sum) pick-up + comb filter	RF gap	$(2k+1)\lambda_\beta/2$ between 1st and 2nd corrector	ICE

We shall discuss the three systems and some results in more detail.

5.1 Betatron Cooling

Let the betatron oscillation of a particle be described by

$$y_i = a_i \sin\left(Q_i \; S/R + \varphi_i\right)$$

$$\tilde{y}_i = y_i' \; R/Q = a_i \cos\left(Q_i \; S/R + \varphi_i\right)$$

The kicker located at a phase advance $Q_i \; S/R = \theta_i$ downbeam of the pick-up (pu) corrects the angle

$$\tilde{y}' \rightarrow \tilde{y}' + g \; \langle Y \rangle_s$$

where $\langle Y \rangle_s$ is the sample average of the position error at the PU. Referred back to the PU the correction is

$$y \to y - g(\langle y\rangle + y_n) \sin\theta$$

$$\tilde{y}' \to \tilde{y}' + g(\langle y\rangle + y_n) \cos\theta$$

Repeating for both of these equations Hereward's analysis leading from (1.1) to (1.3) one obtains the cooling rate for the rms amplitude $A = \sqrt{y^2_{rms} + \tilde{y}'^2_{rms}}$

$$-\frac{1}{A}\frac{dA}{dt} = \frac{W}{N} g \left[\sin\theta - \frac{g}{2}\left(1 + \frac{A^2 n}{A^2}\right) \right] \qquad (5.1)$$

Optimum conditions are for $\sin\theta = \pm 1$ (-1 with phase inversion such that $g < 1$) i.e. if the betatron advance between PU and kicker is an odd multiple of a quater wavelength. Note also the factor 2 difference between (5.1) and (1.3) which is due to the fact that the kicker corrects only angle i.e. on average half the amplitude error of a particle.

As an example of a practical design we analyse the vertical cooling system in ICE (Fig. 3). The approach (due to Thorndhal) is to start from the beam Schottky current (I_{PU}) induced on the difference PU, to compare it to the preamplifier noise current I_n to determine the optimum

$$g = g_o = \left(\Gamma + I_n^2/I_{PU}^2\right)^{-1} \qquad (5.2)$$

which determines the "optimum" cooling rate.

To work out the amplifier power one determines: the rms sample displacement σ_s = rms beam height / N_s ; the correction per turn $g_o\,\sigma_s$. Details are summarized in table 5.

The actual system in ICE consists of 2 pick-ups and 2 kickers[20] with signal addition in front of the amplifier and splitting at the exit. Assuming ideal signal combination one expects twice the optimum cooling rate. Hence one calculates:

Cooling rate	$1/\tau_o = (4.3\ \text{min})^{-1}$
Amplifier power	$P \approx 0.5$ Watts

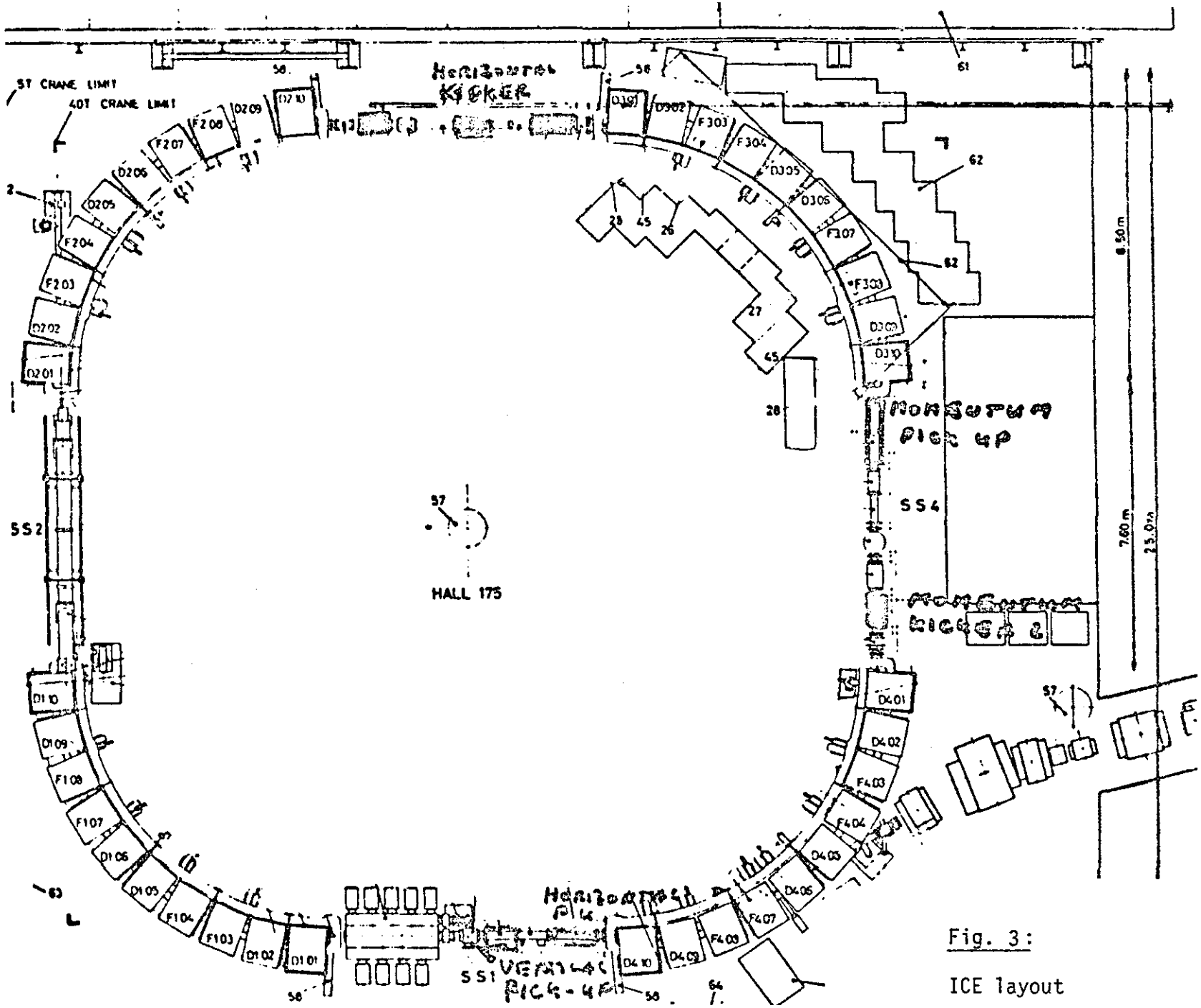

Fig. 3:

ICE layout

TABLE 5

VERTICAL COOLING IN ICE

PARTICLE MOMENTUM	1.7 GeV/c
REVOLUTION FREQUENCY	$f_{rev} = 3.5$ MHz
NUMBER OF PARTICLES	$N = 3.5 \times 10^8$
CIRCULATING CURRENT	$I_0 = Nef_0 = 196\ \mu A$
MOMENTUM SPREAD	$\Delta p/p \simeq \pm 2 \times 10^{-3}$
BANDWIDTH	$W = 250$ MHz (250 - 500 MHz)
SAMPLE LENGTH	$T_s = \frac{1}{2W} = 2$ ns
NUMBER OF PARTICLES/SAMPLE	$N_s = NT_s/T_{rev} = 2.4 \times 10^6$
LONGITUDINAL SCHOTTKY NOISE	$I_{SC} = \sqrt{2e\ I_0\ W} = 125$ nA
RMS BETATRON AMPLITUDE	$a_v = 7$ mm
EFFECTIVE BEAM HEIGHT	$h \simeq 2\ a_v = \pm 14$ mm
RMS DIPOLE MOMENT	$D_{rms} = a_v\ I_{SC}/\ 2 = 620$ nA mm
SPACING OF PU PLATES	± 30 mm
PU SENSITIVITY (60% AT EDGE)	$S = 0.6$
PICK-UP CURRENT	$I_{PU} = S\ D_{rms}/h = 12.5$ nA
PHASE SHIFT PU KICKER	$1.5\ \pi$
NOISE CURRENT ($v = 1.5$ dB NOISE FIGURE AT 300^0 K AND $R = 50\ \Omega$)	$I_n = \sqrt{10^{v/10}\ kTW/R} \simeq 170$ nA
MIXING PARAMETER	$\Gamma = \frac{\ln f_{max}/f_{min}}{2W\ \Delta T_{rev}} \simeq 1.8$
OPTIMUM $g = g_0$ ($\Gamma \ll 1/g_0$)	$g_0 \approx I_{PU}^2/I_n^2 = 0.0054$
OPTIMUM COOLING RATE	$\frac{1}{\tau_0} = \frac{g_0 W}{2N} = (8.5\ \text{min})^{-1}$
RMS CENTRE OF GRAVITY DISPLACEMENT OF SAMPLE	$\sigma_s = \frac{a_v/\sqrt{2}}{\sqrt{N_s}} = 3.2 \times 10^{-3}$ mm
CORRESPONDING ANGLE AT $\beta \simeq R/Q = 10$ M	$\theta_s = \delta s/\beta = 3.2 \times 10^{-7}$ rad
CORRECTION PER TURN	$\theta_c = g_0\ \theta_s : 1.7 \times 10^{-9}$ rad
LENGTH OF KICKER PLATE	$\ell = 200$ mm
PLATE SPACING	$d = \pm 30$ mm
KICK PER VOLTAGE U ON KICKER PLATES (TRANSMISSION LINE KICKER $1 + \beta$ BECAUSE OF E AND H DEFLECTION)	$\theta \simeq (1 + \beta)\ \frac{U}{2d}\ \frac{\ell}{p\beta}$ $\theta/U = 4.2 \times 10^{-9}$ rad/V
VOLTAGE FOR θ_c	$U_c = 0.41$ V rms
RMS VOLTAGE DUE TO NOISE	$U_n = g_0^{-1/2}$; $U_c = 5.6$ V rms
POWER ON 50 Ω	$P = (U_n^2 + U_c^2)\ /\ R \simeq 0.52$ W
AMPLIFICATION	$\alpha = P/I_n^2 R = 3.4 \times 10^{11}$ (115 dB)

The initial cooling rate measured on ICE at about 3.5×10^8 was $(4\ \text{min})^{-1}$ which agrees well with the results of table 5. It should however be mentioned that beam properties (N, σ_v) entering critically into the calculation are only known with limited accuracy.

Finally we mention the Fokker-Planck equation for betatron cooling. One has, neglecting for simplicity particle noise($\Gamma < x_x^2/x^2_{PU}$ as assumed above)

$$\Delta a_c / T_{rev} = \left(\frac{W}{N}\, g(a)\, \sin\theta\right) a$$

$$\Delta a^2_{ic} / T_{rev} = \frac{W}{N}\, g^2_{(a)}\, a^2_n$$

Hence, if we believe the recipe (4.1):

$$\frac{\partial\psi}{\partial t} = \frac{W}{N}\frac{\partial}{\partial a}\left[-(ag\,\sin\theta)\,\psi + \frac{1}{2}\, g^2 a^2_n\, \frac{\partial\psi}{\partial a}\right] \qquad (5.3)$$

For constant g the final equilibrium distribution $\left(\frac{\partial\psi}{\partial t} = 0\right)$ following from (5.3) is a Gaussian ψ (a) with rms width $A^2 = \frac{1}{2}\, g\, a^2_n / |\sin\theta|$ or $A^2_{final} = \frac{1}{2} A^2_{initial} / |\sin\theta|$ for $g = g_o \equiv a^2_{initial} / a^2_n$. This shows once again that the density increase is small if the cooling is fast.

5.2 Palmer Cooling

The single particle displacement at the PU is

$$x_i = \underbrace{x_{\beta i}}_{\text{due to betatran oscillation}} + \underbrace{\alpha_p \left(\frac{\Delta p}{p}\right)_i}_{\text{displacement due to momentum error}}$$

The single passage correction (referred back for the PU at a betatron phase θ upbeams)

$$\frac{\Delta p}{p} \to \frac{\Delta p}{p} - \frac{g}{\alpha_p} \langle x \rangle$$

$$x_\beta \to x_\beta + g \langle x \rangle \cos\theta$$

$$\tilde{x}'_\beta \to \tilde{x}'_\beta + g \langle x \rangle \sin\theta$$

Repeating Hereward's procedure we obtain the cooling rates for rms momentum error $\Delta = (\Delta p/p)_{rms}$ and rms betatron amplitude A in the case of perfect mixing:

$$\frac{1}{\Delta}\frac{d\Delta}{dt} = \frac{2Wg}{N}\left[1 - \frac{g}{2}\left(1 + \frac{A^2}{\alpha_p{}^2\Delta^2} + \frac{\Delta_n{}^2}{\Delta^2}\right)\right]$$

$$\frac{1}{A}\frac{dA}{dt} = \frac{Wg}{N}\left[\cos\theta - \frac{g}{2}\left(1 + \frac{\alpha_p{}^2\Delta^2}{A^2} + \frac{A_n{}^2}{A^2}\right)\right]$$

FULL APERTURE

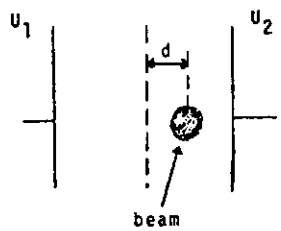

$U_2 - U_1 \approx \frac{d}{h}$

PARTIAL APERTURE
"1 COOLING REGION"

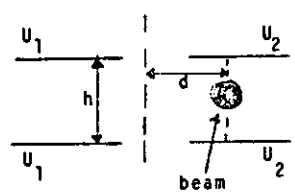

$U_2 - U_1$
$\approx \frac{2}{\pi}$ arctg exp $- \frac{\pi d}{h}$

PARTIAL APERTURE,
SEVERAL COOLING
REGIONS

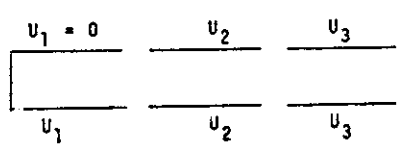

"superposition of expression
for 1 cooling region "

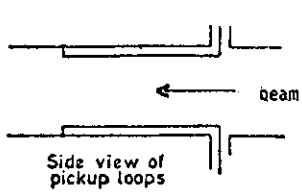

TABLE 6

DIFFERENCE PICK-UP DESIGNS

With partial aperture pick-ups (Table 6) and similar kickers, one can have several cooling regions with a position dependent gain. This behaviour can be emphasized by using filters producing a frequency , i.e. position dependent gain (via the relation between frequency and position). In this way small g can be produced at dense parts of the stack where heating by other particles is important and high gain at the low density and where fast cooling is required [29].

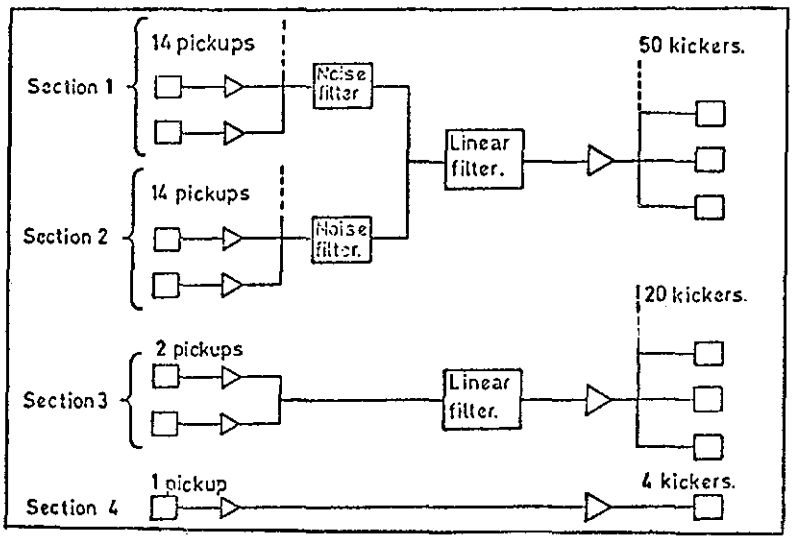

Fig. 5 :
Block diagram of the stack cooling system

The stack cooling in the AA ring [29] will in fact use a 3 or 4 stage system of Palmer type including filters to shape the gain versus position profile (Fig. 5-7).

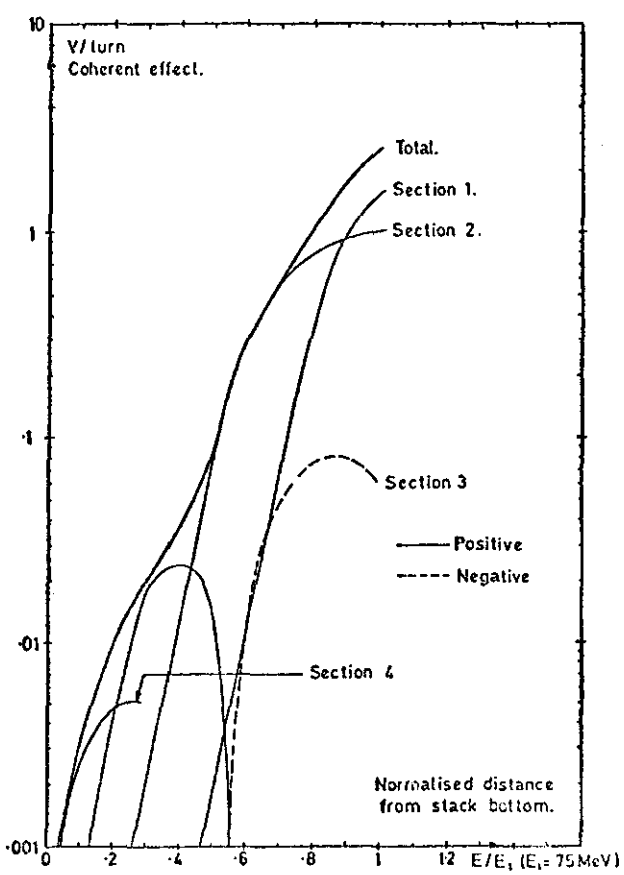

Fig. 6 : Gain curves for stack cooling system.

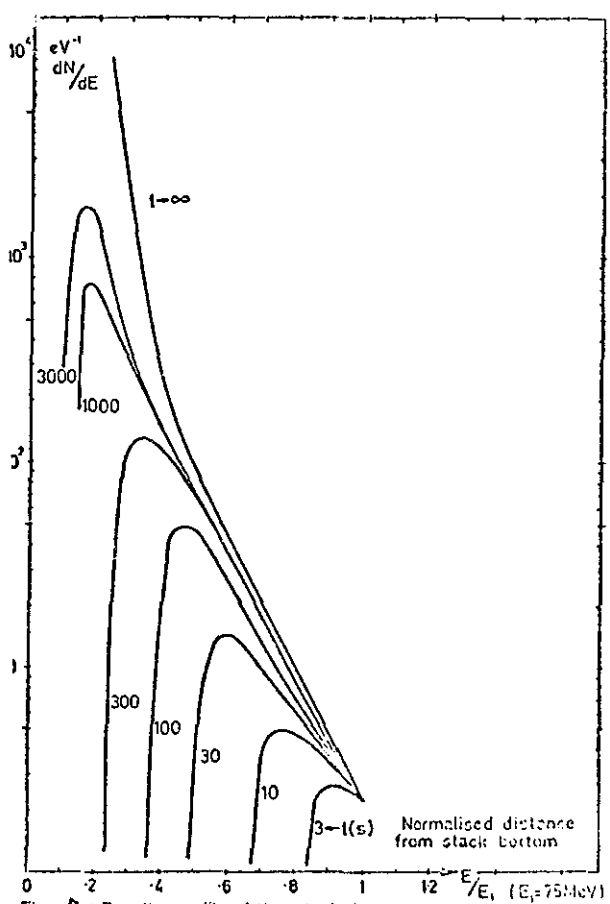

Fig. 7 : Density profile of the stack for a constant particle flux towards the stack bottom.

MOMENTUM COOLING, FILTER METHOD [22,24]

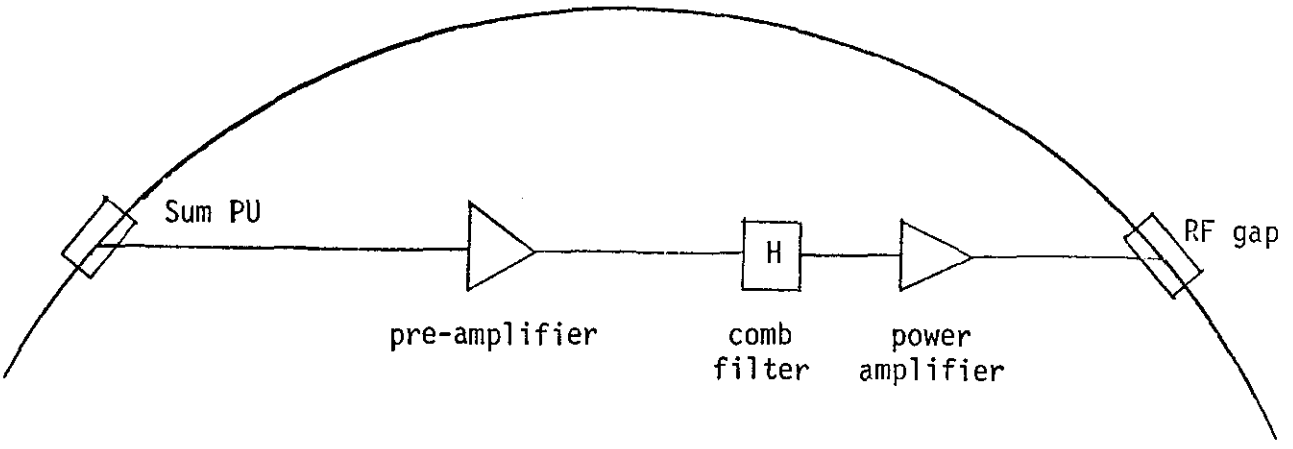

In the simplest case the filter is a transmission line shorted at the far end and with a length corresponding to half the circumference of the cooling ring. The notches at the harmonics of the revolution frequency are produced by $\lambda/2$ resonances where ideally the input impedance is zero and the phase changes sign. Due to this phase and amplitude characteristics, particles with a slightly too low momentum (to high frequency above transition) are accelerated and those with too high momentum decelerated until ideally all particles are "fallen into the notches".

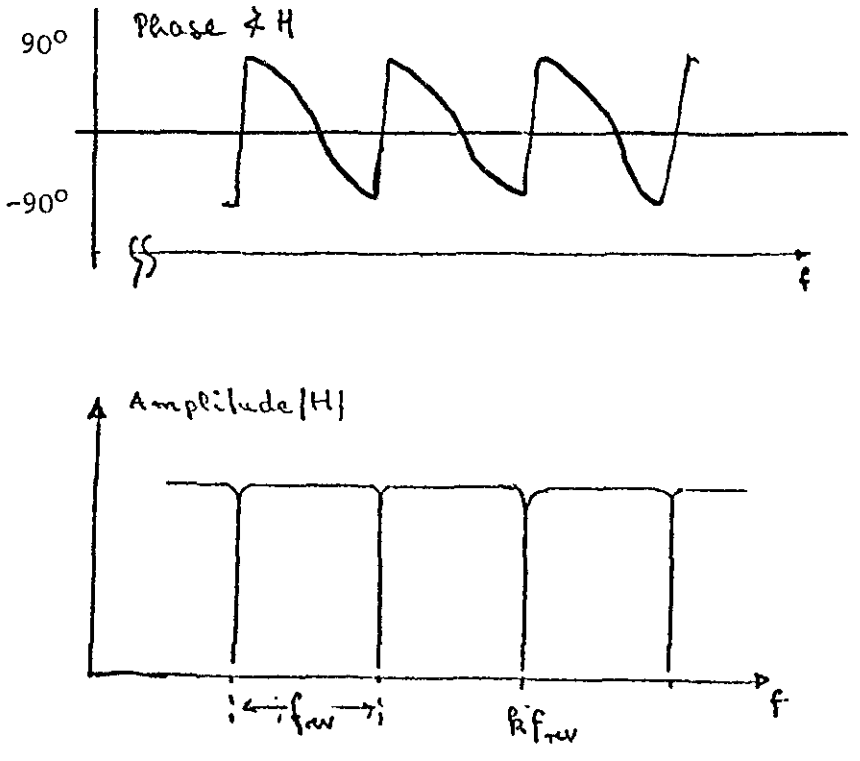

Fig. 8

Idealised characteristics of notch filter

If you prefer to look at the process in time domain: the pulse sent through the system by a particle of the nominal revolution frequency will be cancelled by its pulse from the previous turn reflected at the end of the line (T_{rev} changes slowly even for a strong RF). For too slow or too fast particles, the cancellation is imperfect and deceleration or acceleration will result.

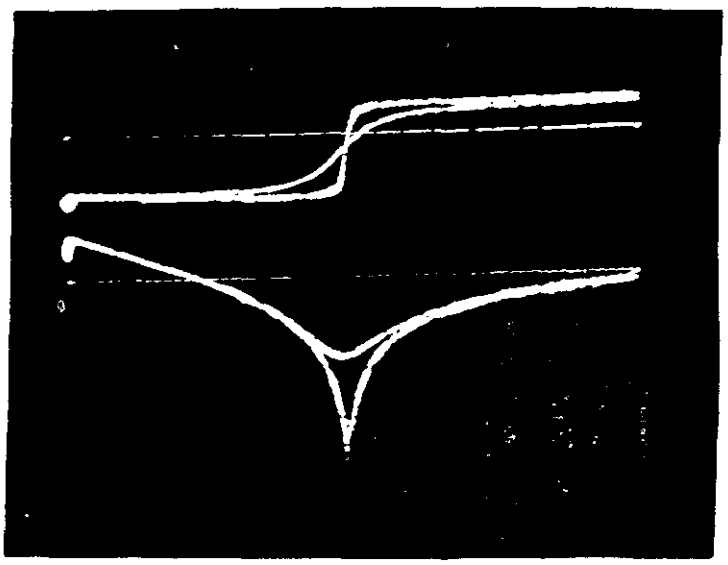

Fig. 9

Phase and amplitude at a notch of the ICE momentum cooling system. Steepening of the notch by a compensator circuit

Additional elements can be added to the filter to sharpen the notches and to reduce the gain between harmonics in order to filter out the preamplifier noise. The filter method is preferable for low intensity beams where high gain is needed and the amplifier noise becomes important. Moreover the sum pick-up produces as large a signal as can be obtained over the aperture and the use of ferrite rings gives sufficient wideband impedance even with a very short pick-up (Fig. 10).

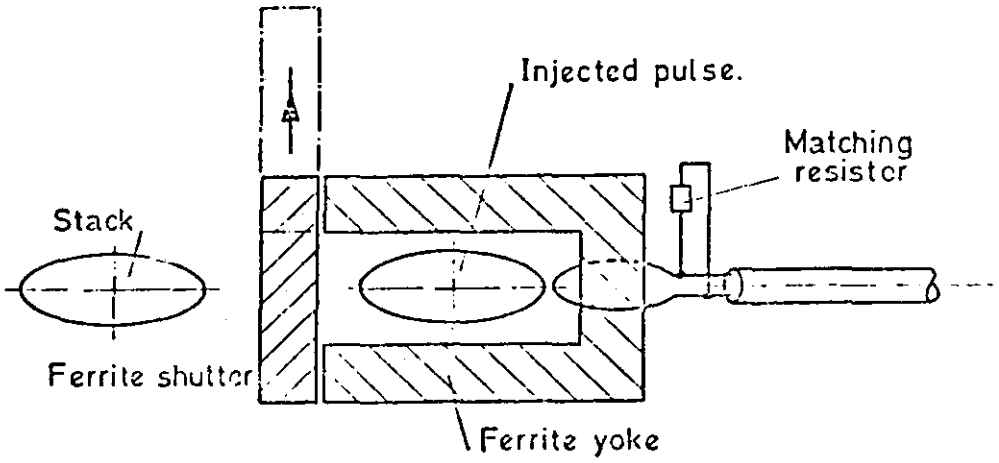

Fig. 10 : Schematic cross-section of sum Pick-up for momentum precooling in the Antiproton Accumulator

Following Sacherer[26] we use the F.P. equation (4.1) to analyze the Thorndahl cooling. Let E be the energy error and $G^2(E) = R_{gap} I^2_{gap} / R_{PU} I^2_{PU}$ the power transfer function from PU to the gap. The coherent energy correction of a single particle for one passage is

$$\left(\frac{1}{e}\right) \Delta E_c = 2\, e\, f_{rev}\, R \sum \mathrm{Re}\, G_n(E) \qquad \text{(Volts)}$$

i.e. the current per band multiplied by the mean of PU and gap impedance $R = \sqrt{R_{gap} R_p}$ (assumed to be purely resistive) and by the real part of the transfer function $G(E)$ taken at the revolution harmonics and summed over the Schottky bands involved.

Similarly, assuming white amplifier noise of $P'_n = e^{v/10} KT_n$ ($\approx 10^{-20}$ W/Hz) and Schottky noise due to other particles of $2\, e^2 f_o N R_{PU}$ Watts. in each band the mean square energy change per turn due to noise is

$$\left(\frac{1}{e}\right)^2 \Delta E^2_{ic} = P'_n\, f_{rev} R_{gap} \sum |G_n|^2 + e^2 f_{rev} R^2 \frac{dN}{df_o} \sum \frac{|G_n|^2}{n}$$

For a given system the filter characteristics

$$\sum R_e(G_n) = f_1(E), \quad \sum |G_n|^2 = f_2(E)$$

and

$$\sum \frac{|G_n|^2}{n} = f_3(E)$$

can be measured and inserted into the F.P. equation for numerical integration. This has been done for ICE and results agree with measurements.

For analytical calculations, it is useful to expand $G(E)$ near the notches assuming small losses. We use

$$G\left(\frac{\Delta f}{f_n}\right) \approx G_o \left[\frac{\Delta f}{f_n} + \frac{1}{2i\, q_n}\right] = G'\left[E + i\,\varepsilon\right]$$

where q_n is the quality factor ($\frac{f}{\delta f}$ with δf the distance of the $\pm 45^o$ degree phase points) of the n-th notch. One may write

$$\sum R_e(G_n) = \frac{W}{f_{rev}} G'E$$

$$\sum |G_n|^2 = \frac{W}{f_{rev}} G'^2(E^2 + \varepsilon_1^2)$$

$$\sum \frac{|G_n|^2}{n} = \frac{W}{f_{rev}} G'^2(E^2 + \varepsilon_2^2) \sum \frac{1}{n}$$

where ε_1 and ε_2 are related to the losses.

Further, following van der Meer, we normalize E and ψ to their initial values E_i and $\psi_i = N/E_i$ assuming an originally rectangular distribution, and we use a suitable normalization of time to reduce the number of variables.

Last but not least, we neglect the amplifier noise which turns out to be of no concern in the AA at $N \geq 10^7$ and in ICE at $N \geq 10^8$ (noise figure $v \not< 3$ dB at $T_n = 290^oK$). We can then write

$$\boxed{\frac{\partial \psi}{\partial t_n} = \alpha \frac{\partial}{\partial E}\left(E\psi + \alpha(E^2 + \chi^2)\ \psi \frac{\partial \psi}{\partial E}\right)} \qquad (5.5)$$

where ψ, E and t_n are now the normalized variables. The "gain parameter" is

$$\alpha = \frac{e^2\ R\ G'\ N \sum \frac{1}{n}}{2\ T_{rev}^2 |\eta| (\frac{\Delta p}{p})_i}$$

and the "loss parameter"

$$\chi = \frac{1}{q|\eta|(\frac{\Delta p}{p})_i}$$

with $$q = \left(\sum \frac{1}{n q_n^2} \Big/ \sum \frac{1}{n}\right)^{-1/2} ,$$

some sort of "average quality factor" of the filter line.

Finally, the normalization factor for time is

$$\frac{t}{t_n} = \frac{N \sum \frac{1}{n}}{4\, T_{rev}\, W^2 |\eta| \left(\frac{\Delta p}{p}\right)_i}$$

The advantage of (5.5) is that standard solutions can be calculated (numerically) as a function of the two parameters α and χ. Optimum conditions are found for $\alpha \approx 0.15 - 0.2$ provided that χ is small ($\chi < 0.05$).

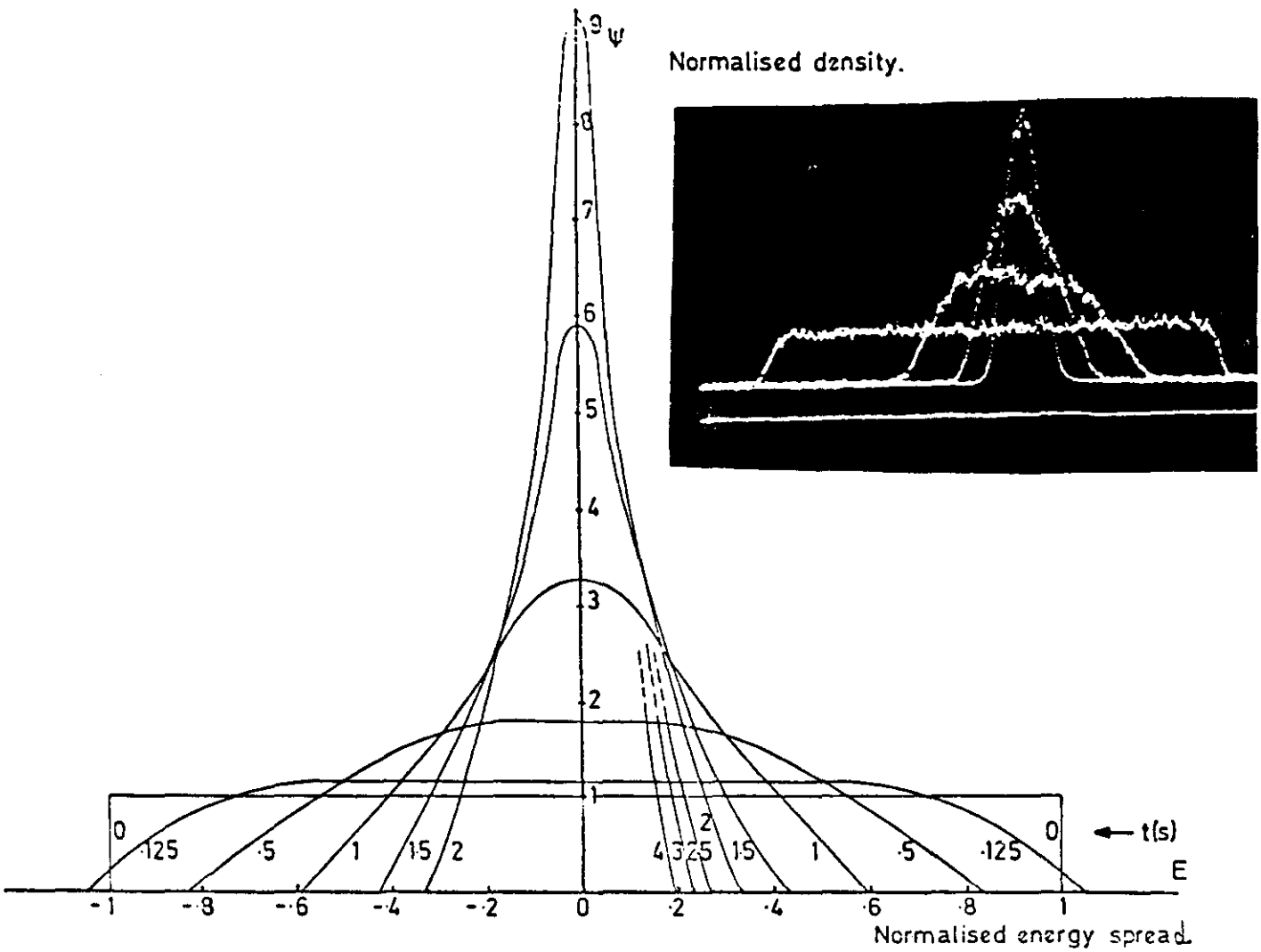

Fig. 11 : Precooling curves for the Antiproton Accumulator calculated from (5.5) for $\alpha = 0.15$, $\chi < 0.01$, and results from ICE (for a different set of parameters.)

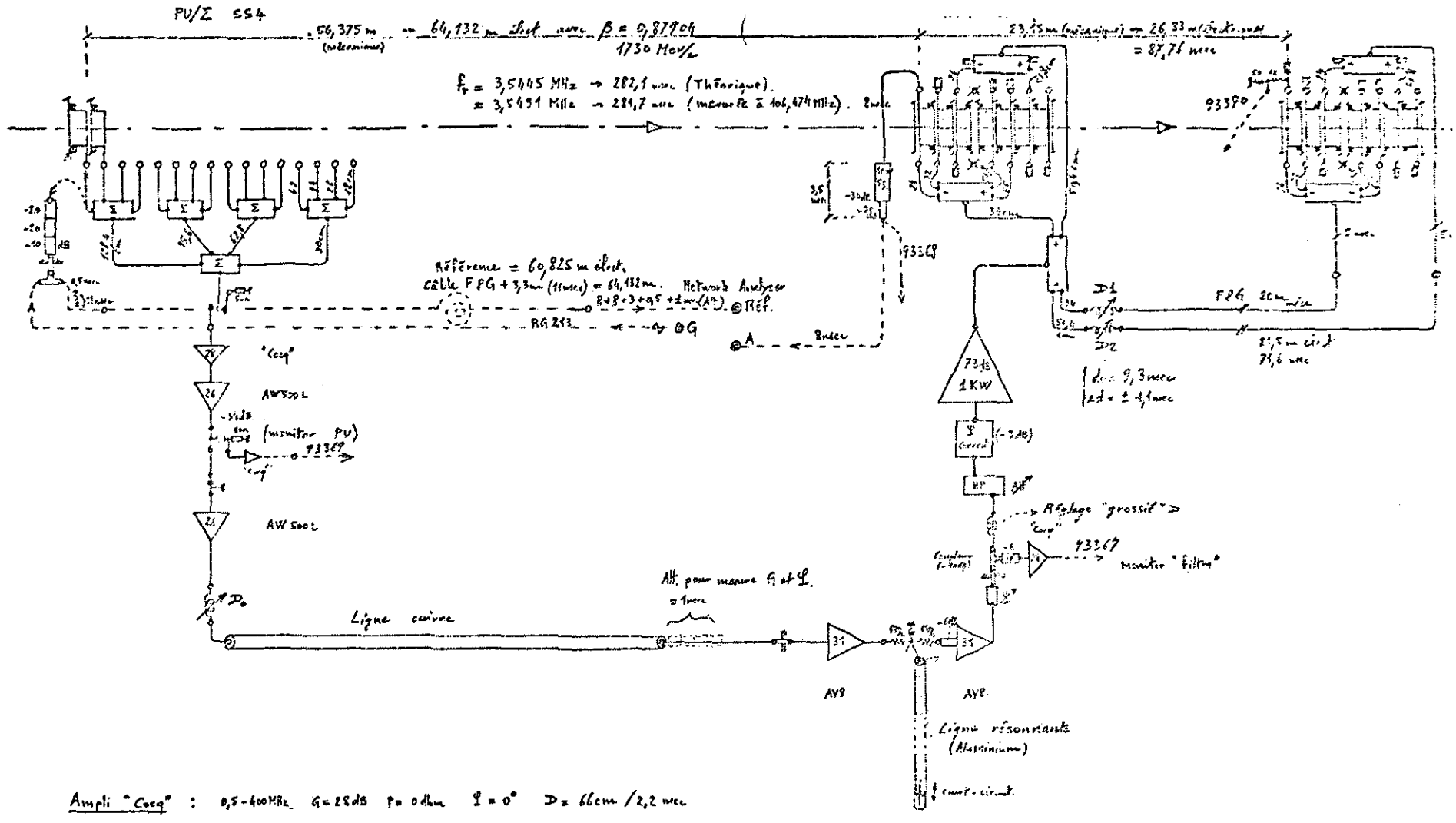

Fig. 12 :

ICE momentum cooling system

As a result of the losses, an asymptotic distribution will be reached

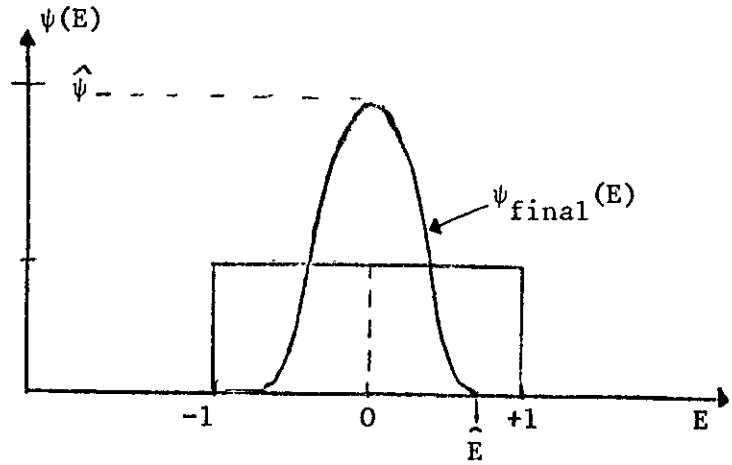

which can be obtained from (5.5) putting $\partial\psi/\partial t = 0$:

$$(5.6) \qquad \psi(E)_{final} = \begin{cases} \dfrac{1}{2\alpha} \ln \dfrac{\chi^2 + \hat{E}^2}{\chi^2 + E^2} & |E| < \hat{E} \\ 0 & |E| > \hat{E} \end{cases}$$

with $\hat{E}$ from $\hat{E} - \chi \arctan \hat{E}/\chi = \alpha$

PARAMETER	ICE	AA	
p	1.7	3.5	GeV/c
T_{rev}	280	540	ns
$\eta = \frac{1}{\gamma_t^2} - \frac{1}{\gamma^2}$	0.65	0.1	
$(\Delta p/p)_{initial}$	3×10^{-3}	1.5×10^{-2}	total
W	110	250	MHz
f_{max}	180	400	MHz
f_{min}	70	150	MHz
N	3.5×10^{8}	2.5×10^{7}	
ψ_i	75	0.49	eV^{-1}
t/t_n	12.5	0.12	
$t(t_n = 17)$	210	2	s
$qx = \frac{1}{\eta(\frac{\Delta p}{p})_i}$	512	667	
q for $x = 0.01$	5.1×10^{4}	6.7×10^{4}	

Table 7 :

ICE and AA parameters

Equation (5.6) has been used to compare the results obtained in ICE to the theory. In Fig. 13 we plot the inverse of the assymptotic width ($\hat{E}^{-1}$) as a function of the asymptotic height.

One concludes that in the early measurements the points follow a line with $\chi \simeq 0.3$ and in the later measurements after improvement of the filter with $\chi \simeq 0.05 - 0.1$. For very large density increase, the points seem to follow a curve of decreased losses. This is probably explained by the reduction of noise in the closed loop case which was mentioned above.

The Q values of the notches were measured and q was found to be about 7000 giving for ICE parameters $\chi \simeq 0.07$. With the optimum $\alpha = 0.15$ one expects an increase in peak density by about 8 for $\chi = 0.05$ or

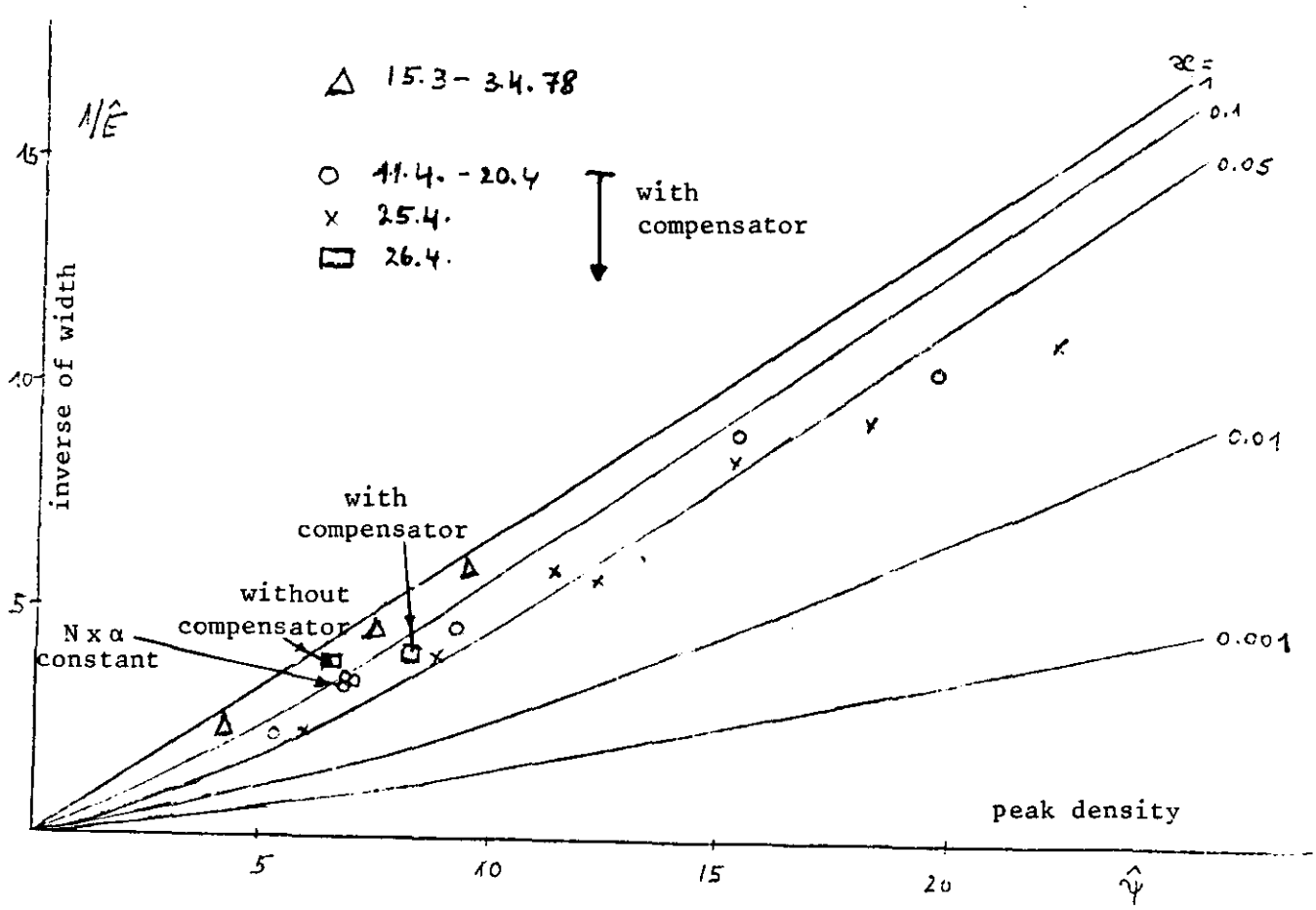

Fig. 13 : Asymptotic peak density and width
Theoretical curves and ICE results

by 6 for $\chi = 0.1$, both in a normalized time of $t_n = 17$, corresponding to 3.5 min in ICE at 3.5×10^8 p. The measured density increase under these circumstances was about 7. Scaled to precooling in the AA ring, this corresponds to the same density increase at the same χ or to the required increase by 9.5 in 2 s if $\chi \leq 0.01$ is ensured. Again some of the ICE parameters entering critically into the comparison could only be determined with limited accuracy at the time when these measurements were done. (A new run is presently under way).

With these reservations, we can conclude that the ICE results confirm the theory and the assumptions gone into the design of the AA precooling system where lower filter losses are foreseen.

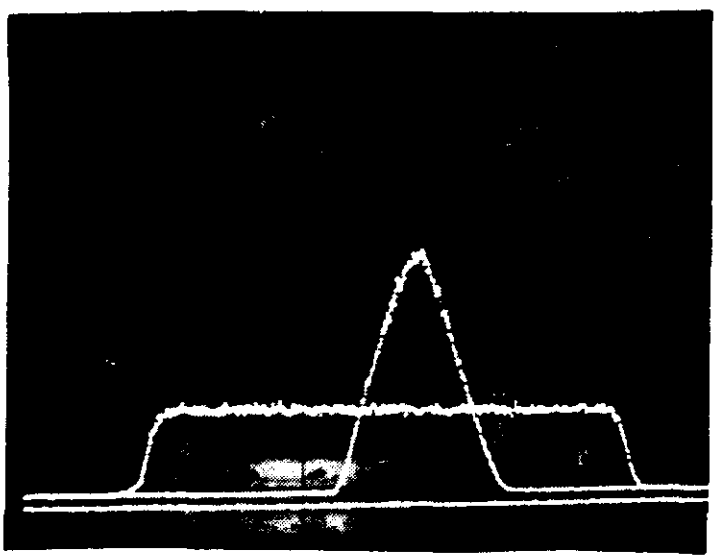

Fig. 14:
Schottky scan of momentum distribution initial and after 3.5 min of cooling. 3.5×10^8 p. The horizontal scale is momentum ($\Delta p/p = 0.5 \times 10^{-3}$/div) The vertical scale is proportional to the square root of particle density.

6. Applications of stochastic cooling

This is my (incomplete) list of applications:

1. Stacking of $\bar{p}$ and other rare particles.

2. Physics with highly monochromatic and sharply collimated beams.

3. High density heavy ion beams.

4. Increase of beam life time (compensation of multiple scattering effects, high order resonances, beam-beam interactions).

5. Non destructive observation of low intensity beams (50 circulating particles can be seen in ICE after cooling to $\Delta p/p = 10^{-5}$).

6. Bunched beam cooling at high energy (ICE results).

7. Stochastic trapping (i.e. cooling a coasting beam into a bucket).

7. Acknowledgements and credits

It is a pleasure to thank W. Hardt, L. Thorndahl and S. van der Meer for reading the manuscript of this talk and suggesting corrections and improvements.

Credit belongs to members of the Antiproton Accumulator Group, the ICE Team and the ISR-RF Group for developing the ideas and carrying out the work reported here. The role of F. Bonaudi, G. Petrucci, C. Rubbia, P. Strolin, L. Thorndahl and S. van der Meer in initiating and leading these studies, the experimental skill of G. Carron, H. Herr and L. Thorndahl as well as the advancement of the theroy by F. Sacherer, L. Thorndahl and S. van der Meer have been vital for the recent progress. The team work within the groups mentioned above was probably as decisive.

REFERENCES

1. S. van der Meer, Stochastic damping of betatron oscillations, CERN/ISR-PO/72-31.

2. W. Schnell, About the feasibility of stochastic damping in the ISR, CERN/ISR-RF/72-46.

3. R.B. Palmer, Stochastic cooling, BNL report BNL 18395, 1973.

4. J. Borer, P. Bramham, H.G. Hereward, K. Hübner, W. Schnell, L. Thorndahl, Non-destructive diagnostics of coasting beams with Schottky noise, IXth Int. Conf. on High Energy Accelerators, SLAC, MAY 2-7, 1974.

5. P. Bramham, G. Carron, H.G. Hereward, K. Hübner, W. Schnell, L. Thorndahl, Stochastic cooling of a stored proton beam, Nucl. Inst. Meth. 125 (1975), pp. 201, 202.

6. L. Thorndahl, Stochastic cooling of momentum spread and betatron oscillations for low intensity stacks, CERN/ISR-RF/75-55.

7. P. Strolin et al., Stochastic cooling of Antiprotons for ISR physics, CERN/EP Internal Report 76-05.

8. C. Rubbia, CERN/NP/Note 77-1.
D. Cline, P. Mc Intyre, F. Mills, C. Rubbia, FERMILAB TM 689 (1976).
C. Rubbia, P. Mc Intyre, D. Cline, in proc. of Aachen Neutrino Conf. (1976).

9. K. Hübner et al., Estimates of ISR luminosities with cooled beams, CERN/PS/DL Note 76-27 (1976).

10. H.G. Hereward, Statistical phenomena - Theory, Proc. 1st Course Intern. School of Particle Accelerators, Erice (1976), CERN 77-13, p. 281.

11. W. Schnell, Statistical phenomena, experimental results, Proc. 1st Course Intern. School of Particle Accelerators, Erice (1876), CERN 77-13, p. 302.

12. G. Carron, L. Faltin, W. Schnell, L. Thorndahl, Stochastic cooling of betatron oscillations and momentum spread, Vth All Union Particle Accel. Conf., Dubna, USSR (Oct. 1976).

13. G. Carron, L. Thorndahl, Stochastic cooling of vertical betatron oscillations in the frequency range 80 - 340 MHz, ISR Perf. Report, ISR-RF/LTS/ps (RUN 775), 22.11.1976.

14. L. Faltin, RF fields due to Schottky noise in a coasting particle beam, Nucl. Inst. Meth. 145 (1977), pp. 261-266.

15. L. Faltin, Slot - type pick-up and kicker for stochastic beam cooling, Nucl. Inst. Meth. 148 (1978), pp. 449-455.

16. W. Hardt, Augmentation of damping rate for stochastic cooling by the additional use of non linear elements, CERN/PS/DL 76-10 (1976).

17. G. Carron, L. Faltin, W. Schnell, L. Thorndahl, Experiments with stochastic cooling in the ISR, IEEE Transact. NS-24 No. 3 (June 1977), pp. 1402-1404.

18. G. Carron, L. Faltin, W. Schnell, L. Thorndahl, Recent results with stochastic cooling in the ISR, Int. Conf. High Energy Accelerators, Serpukhov, USSR, (July 1977).

19. E.D. Courant, Workshop on phase space cooling, in Proc. 1976 ISABELLE Workshop, BNL 50611

20. L. Thorndahl, Stochastic cooling of betatron oscillations in ICE, CERN/ISR Technical Note ISR/RF/LT/ps, March 1977.

21. ICE Team, Progress report No. 1 and 2 (CERN EP Division) (1978).

22. G. Carron, L. Thorndahl, Stochastic cooling of momentum spread with filter techniques, CERN/ISR-RF/78-12 and ISR-RF/Note LT/ps 6.1.1977.

23. S. van der Meer, Influence of bad mixing on stochastic acceleration, Internal note CERN/SPS/DI/pp 77-8, 5.5.1977.

24. L. Thorndahl, A differential equation for stochastic cooling of momentum spread with the filter method, Technical Note ISR-RF/LT/ps, 10.5.1977.

25. S. van der Meer, Normalized solution for linear momentum cooling of a square distribution, private communication, 27.10.1977

26. F. Sacherer, Stochastic cooling theory, CERN Internal Report ISR/TH 78-11

27. G. Carron et al., Stochastic cooling test in ICE, Phys. Lett. 77B, p. 353, (1978).

28. Design Study Team, Design study of a proton-antiproton colliding beam facility, CERN/PS/AA 78-3.
F Bonaudi et al., Antiproton in the SPS, CERN-DG 2, 1976.

29. S. van der Meer, Stochastic stacking in the Antiproton Accumulator, CERN/PS/AA 78-22.

Note on ep Collisions

T. Nishikawa* and E. Keil**

* KEK, Tsukuba, Ibaraki, Japan

** CERN, Geneva, Switzerland

I. Introduction

We consider a scheme for electron-proton colliding beams in which an electron beam of $E_e \approx 140$ GeV collides with a proton beam of $E_p \approx 20$ TeV. The parameters are chosen such as to achieve a luminosity of $L \approx 10^{32}\ cm^{-2}s^{-1}$. The center of mass energy of the proposed system is 3.3 TeV. A possible configuration of ep-system is also proposed as an option of a $p\bar{p}$ colliding-beam plan.

Most ring parameters for ep collisions will be determined similar to the studies on electron and proton accelerators at Group 1 and Group 2.[1)2)] The bending radius of the proton ring is 6.7 km assuming a bending field of 10 T. For the electron ring, we consider two specific examples where the bending radii are scaled as $\rho \propto E_e^2$ and $\rho \propto E_e^{3/2}$ from existing designs. The first example is suitable to the storage ring operation while the latter may be used for a synchrotron operation. If we take the $\rho \propto E_e^2$ rule, then the same bending radius as for the protons corresponds to an electron energy of 120 GeV with the field strength of 0.06 T.

2. Luminosity Optimization

Because of the asymmetric nature of the two beams, the choice of parameters to optimize the luminosity for ep collisions is a more complicated

problem than for e^+e^-, $p\bar{p}$ or pp collisions.

First we consider the case in which both the electron and proton beams are bunched, and then a burched electron beam colliding with a coasting proton beam. For simplicity, we assume a head-on collision and neglect the variation of beam radius along the longitudinal direction, z.

2-1. Case I (Bunched Proton Beam)

For bunched beam collisions, the luminosity is given by[3)]

$$L = f \frac{N_e N_p}{2\pi k_b} \frac{1}{\sqrt{\sigma_{ex}^2 + \sigma_{px}^2}\sqrt{\sigma_{ey}^2 + \sigma_{py}^2}} , \qquad (1)$$

where f is the revolution frequency, k_b the number of bunches in each beam, N the total number of particles, and σ the r.m.s. beam radius of each beam in each direction. Suffixes e and p denote electrons and protons respectively, and x and y the horizontal and vertical directions.

The linear tune shifts are given by

$$\Delta\nu_{ex} = \frac{N_p r_e \beta_{ex}}{2\pi k_b \gamma_e (\sigma_{px} + \sigma_{py})\sigma_{px}} \qquad (2)$$

$$\Delta\nu_{ey} = \frac{N_p r_e \beta_{ey}}{2\pi k_b \gamma_e (\sigma_{px} + \sigma_{py})\sigma_{py}} \qquad (2')$$

for electrons and

$$\Delta\nu_{px} = \frac{N_e r_p \beta_{px}}{2\pi k_b \gamma_p (\sigma_{ex} + \sigma_{ey})\sigma_{ex}} \qquad (3)$$

$$\Delta\nu_{py} = \frac{N_e r_p \beta_{py}}{2\pi k_b \gamma_p (\sigma_{ex} + \sigma_{ey})\sigma_{ey}} \tag{3'}$$

for protons, respectively. Here the β's are the β-functions at the crossing point, γ's the relativistic energy factors, and r's classical radii of particles. Again, the suffixes identify the kind of particles and the directions.

To simplify the following discussions, we assume that

$$\begin{aligned} &\sigma_{ex} = \sigma_{px} \equiv \sigma_x \quad , \quad \sigma_{ey} = \sigma_{py} \equiv \sigma_y, \\ &\Delta\nu_{ex} = \Delta\nu_{ey} = \Delta\nu_e = 0.06 \\ &\Delta\nu_{px} = \Delta\nu_{py} = \Delta\nu_p = 0.005 \ . \end{aligned} \tag{4}$$

These assumptions imply an appropriate choice of machine and beam parameters. For example, the β-functions for electrons and protons should satisfy the following relations;

$$\frac{\beta_{ex}}{\beta_{ey}} = \frac{\beta_{px}}{\beta_{py}} = \frac{\sigma_x}{\sigma_y} \tag{5}$$

and

$$\frac{\beta_{ex}}{\beta_{px}} = \frac{\beta_{ey}}{\beta_{py}} = \frac{r_p}{r_e}\frac{\gamma_e}{\gamma_p}\frac{\Delta\nu_e}{\Delta\nu_p}\frac{N_e}{N_p} \ . \tag{6}$$

We can rewrite eq.(6) as

$$\frac{\beta_{ex}}{\beta_{px}} = \frac{\beta_{ey}}{\beta_{py}} = 0.084\ a, \tag{6'}$$

where $a = N_e/N_p$.

With the additional assumption that $\sigma_y << \sigma_x$, we obtain the standard expressions for the luminosity

$$L = \frac{N_p f \gamma_p \Delta\nu_p}{2 r_p \beta_{py}} = \frac{N_e f \gamma_e \Delta\nu_e}{2 r_e \beta_{ey}} , \tag{7}$$

similar to those for symmetric collisions. Taking the proton parameters used for $p\bar{p}$ collisions[4] as

$$\frac{N_p}{k_b} = \frac{1}{4} \times 10^{12}$$

$$\beta_{py} = 6.2 \text{ m} \tag{8}$$

and $\quad f = 4.8$ kHz,

we obtain

$$L = 0.69 \times 10^{30} \, k_b \text{ cm}^{-2}\text{s}^{-1}.$$

For $L = 10^{32}$ cm^{-2}s^{-1}, this requires $k_b = 145$. If we take $a = 1$, i.e. $N_e = N_p = 3.6 \times 10^{13}$, then eq.(6') yields

$$\beta_{ey} = 0.52 \text{ m},$$

which is a reasonable value for the β-function of the electron ring.

It follows from eq.(4), (5) and (6), that the luminosity for $\sigma_x \approx \sigma_y$ becomes twice that for $\sigma_x >> \sigma_y$, if the other parameters remain the same.

2-2 Case II (Coasting Proton Beam)

From a technical point of view, a coasting proton beam system may be more practical. For this case, the luminosity is given by[3]

$$L = f \frac{N_e N_p}{\pi} \frac{\ell_{int}}{C} \frac{1}{\sqrt{\sigma_{ex}^2 + \sigma_{px}^2}\sqrt{\sigma_{ey}^2 + \sigma_{py}^2}} , \tag{9}$$

instead of eq.(1), where C is the total circumference and the beams are separated at $z = \pm\ell_{int}/2$.

The linear tune shifts for protons remain as given by eq.(3) and (3'), while the tune shifts for electrons are now given by

$$\Delta\nu_{ex} = \frac{N_p r_e}{\pi\gamma_e C(\sigma_{px} + \sigma_{py})\sigma_{px}} \int_{-\frac{\ell_{int}}{2}}^{\frac{\ell_{int}}{2}} \beta_{ex}(z)dz \tag{10}$$

$$\Delta\nu_{ey} = \frac{N_p r_e}{\pi\gamma_e C(\sigma_{px} + \sigma_{py})\sigma_{py}} \int_{-\frac{\ell_{int}}{2}}^{\frac{\ell_{int}}{2}} \beta_{ey}(z)dz. \tag{10'}$$

Here, we neglect the variation of the proton beam radius and the long-range interactions. The dispersion function is assumed to be zero in the interaction region. If we take that β_{ex} and β_{ey} vary as

$$\beta_{ex,y}(z) = \beta^*_{ex,y} + \frac{z^2}{\beta^*_{ex,y}} , \tag{11}$$

then we obtain

$$\Delta\nu_{ex} \approx \frac{N_p r_e \beta^*_{ex}}{\pi\gamma_e(\sigma_{px} + \sigma_{py})\sigma_{px}} \frac{\ell_{int}}{C} (1 + \frac{1}{12} \frac{\ell_{int}^2}{\beta^{*2}_{ex}}) \tag{12}$$

and

$$\Delta\nu_{ey} \approx \frac{N_p r_e \beta^*_{ey}}{\pi\gamma_e(\sigma_{px} + \sigma_{py})\sigma_{py}} \frac{\ell_{int}}{C} (1 + \frac{1}{12} \frac{\ell_{int}^2}{\beta^{*2}_{ey}}) , \tag{12'}$$

where β^*_{ex} and β^*_{ey} denote the values at the center of the interaction region. As a function of β^*_{ex} or β^*_{ey}, the tune shifts take a minimum[5] when the conditions

$$\frac{\ell^2_{int}}{\beta^{*2}_{ex}} = 12 \qquad \text{or} \qquad \ell_{int} = 2\sqrt{3}\beta^*_{ex} \tag{13}$$

and

$$\frac{\ell^2_{int}}{\beta^*_{ey}} = 12 \qquad \text{or} \qquad \ell_{int} = 2\sqrt{3}\beta^*_{ey} \tag{13'}$$

are satisfied.

Now, the assumptions (4) also require

$$\beta^*_{ex} = \beta^*_{ey} \equiv \beta^*_e$$

and

$$\sigma_{px} = \sigma_{py} = \sigma_x = \sigma_y \tag{14}$$

in addition to the condition (5).* Since we use a superconducting ring for protons, a circular cross section of the proton beam will be desirable. A strong coupling in horizontal and vertical oscillations of electrons is expected to result in $\beta_{ex} \approx \beta_{ey}$. Hence, the condition $\beta^*_{ex} = \beta^*_{ey}$ is also acceptable.[6][7]

Taking these considerations into account, we can rewrite the tune shifts for electrons as

$$\Delta\nu_{ex} = \Delta\nu_{ey} = \frac{N_p r_e \beta^*_e}{\pi\gamma_e\sigma_x\sigma_y}\frac{\ell_{int}}{C} . \tag{15}$$

Let this be equal to the tune limit, i.e. $\Delta\nu_e = 0.06$. Inserting eq.(15) into eq.(9), we get the maximum luminosity as

* For $\sigma_x >> \sigma_y$, instead of eq.(5), $\beta^*_{ex}/\beta^*_{ey} = 2\ \sigma_x/\sigma_y$ is required with the condition (13').

$$L = \frac{N_e f \gamma_e \Delta\nu_e}{2 r_e \beta_e^*} \tag{16}$$

Again, this is the standard expression as well as eq.(7). However, the value of the luminosity with the same choice of electron parameters will be halved compared to the bunched proton case since we assumed that $\sigma_x \approx \sigma_y$.

The condition (6), which is required from $\Delta\nu_e$ and $\Delta\nu_p$ limits, becomes

$$\frac{\beta_e^*}{\beta_p} = \frac{r_p}{r_e} \frac{\gamma_e}{\gamma_p} \frac{\Delta\nu_e}{\Delta\nu_p} \frac{N_e}{N_p} \frac{1}{4k_b} \frac{C}{\ell_{int}}$$

$$= 0.021 \; a \frac{C}{k_b \ell_{int}} , \tag{17}$$

where we also assumed that $\beta_{px} = \beta_{py} = \beta_p$. The number of electron bunches is k_b and a is the ratio N_e/N_p. For $\ell_{int} \simeq 2$ m, we obtain from eq.(13) that $\beta_e^* \approx 0.6$ m. For $k_b \approx 150$, a small ratio a or a large β_p is required. From considerations on the radiation effect, the beam radius of electrons should be $\sim$0.1 mm.[6] In order to make the beam radii of protons and electrons equal, β_p must be about 10m for a reasonable value of the proton beam emittance. Consequently, the ratio $a = N_e/N_p \lesssim 0.014$, i.e. the number of protons in the coasting beam should exceed that of electrons by a factor of 70. However, the longitudinal density of the protons is still smaller than in the bunched-beam case. A larger number of electron bunches, $k_b \gtrsim 1000$ is an alternative which raises the ratio a and therefore reduces the total number of protons required. However, such a electron beam might suffer from multi-bunch instability.

3. Additional Remarks

3-1 Radiation from Electron Beam

The average energy U_0 radiated in one revolution of a single electron is

$$U_0 \approx 4.8 \text{ GeV} ,$$

and the total radiation power from 3.6×10^{13} electrons is

$$P_b \approx 130 \text{ MW}.$$

The effect of the beam strahlung[1)] can be discussed in the same way as for electron-positron collisions. However, the effect is smaller since the proton bunches are much longer.

3-2 Other Comments

More careful studies on lattice design, beam dynamics and instability as well as technical feasibility studies are necessary. The assumptions (4) for luminosity optimization were made to reduce the complexity caused by the asymmetric nature of the beams. The beam radii anticipated from the above choice of parameters are 0.1 mm or less. This would require a new technical procedure to align the colliding beams on the same line in crossing region. The synchrotron radiation from the orbital motions may provide a signal useful to automatic beam controls. However, we may find it wiser to use a larger beam size of protons than electrons in order to make the beam alignment feasible.

Design of the experimental insertions is of course particularly important. A very strong forward peaking of the secondary particles is expected at such a very high energy ep interactions, necessiating an extensive study of detector systems.

3-3 A Possible Configuration of ep-System

As an option of an existing $p\bar{p}$ ring, we propose a possible configuration of e-p system as shown in Fig.1. This fancy sketch includes possibilities of all types of colliding beam experiments as $p\bar{p}$, pp, $e^{\pm}p$, $e^{\pm}\bar{p}$, and $e^{+}e^{-}$ as well as fixed target experiments!

Finally the authors have greatly profited from discussions in the Group 3 of this Workshop.

References

1) J.R. Rees et al: to appear in these Proceedings.

2) V. Yarba et al: ibid.

3) T. Suzuki: "General Formulae of Luminosity for Various Types of Colliding Beam Machines", KEK Report, KEK-76-3 (1976).

4) E. Keil et al: to appear in these Proceedings.

5) T. Nishikawa: "A Preliminary Design of Tri-Ring Intersecting Storage Accelerators in Nippon, TRISTAN", Proc. IXth Intern. Conf. on High Energy Accelerators, SLAC, p.584 (1974).

6) M. Sands: "The Physics of Electron Storage Rings", SLAC Report SLAC-121 (1970).

7) J.R.J. Bennett et al: "Design Concept for a 100 GeV $e^{+}e^{-}$ Storage Ring (LEP)", CERN Report CERN 77-14 (1977).

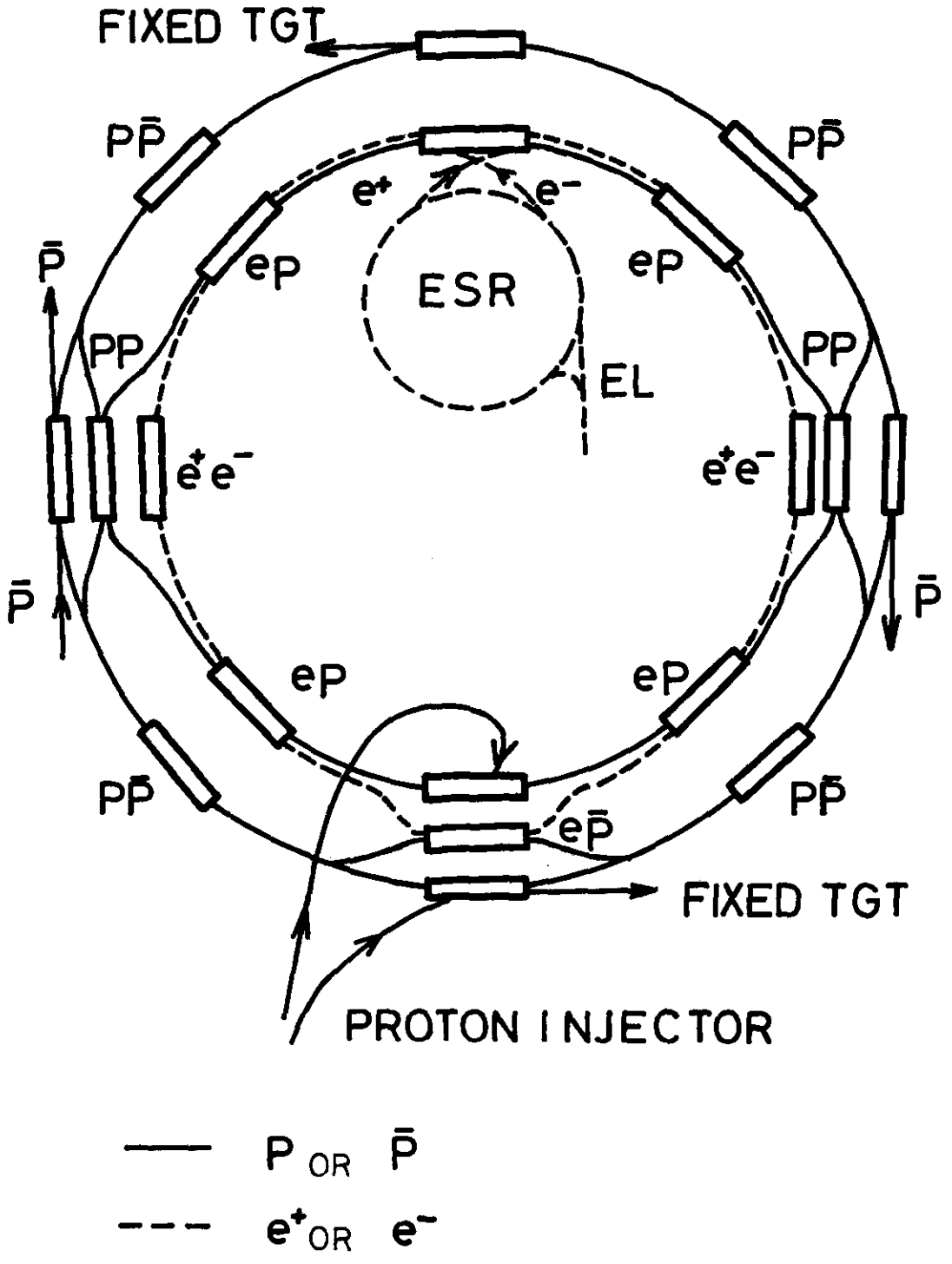

Fig. 1. A possible configuration of an ep system proposed as an option of a $p\bar{p}$ ring.

Experiments and Detectors

NEUTRINO EXPERIMENTS AT A 10-20 TeV PROTONSYNCHROTRON

U. Amaldi*, A. Diddens, C. Fisher and N. Samios

1. Introduction

This is the report of the group working on the extrapolation of neutrino physics to the 10-20 TeV energy range. Within the general framework fixed at the beginning of the workshop, we have been mainly looking at the possibilities and the limitations of the existing and the foreseeable techniques, devoting little time to the physics that will be tackled at that time. However, we would like to list here a few miscellaneous points that, on top of the physics we are now doing with neutrinos, we consider relevant to this field of physics.

(i) It is probable that at energies and momentum transfers much larger than those available today, the problem of the universal coupling of the leptons and their inner structure will be a central one. One can foresee that experiments that compare the behaviour of leptons will be very important, so that in the neutrino field one must devise ways of producing and using beams not only of ν_μ's, but also of ν_e's, ν_τ's and of the other yet undiscovered neutrinos.

(ii) If quarks are liberated at large energy and momentum transfers, neutrino (and charged lepton) production will give rise to quarks that are more energetic in the laboratory than the ones produced in e^+e^- collisions. The study of the interactions of high energy quarks with matter will be specific to neutrino physics and in general to collisions of leptons with matter.

(iii) Very probably leptons will still be used as probes of matter (nucleons, quarks, constituents of quarks, etc.). For these kinds of studies the flux and the quality of the beams will be essential, so that ν_μ-beams will be needed. According to present views, at increasingly large momentum transfers a proton at rest will be a reasonably unbiased source of quark-antiquark pairs of high mass flavours or, more precisely, of any pair of high mass fermion-

---

* Convener of Working Group 4, Neutrino Experiments

antifermion. Production of any new fermion through charged current interactions depends upon generalized Cabibbo angles that are not easily measured in high energy e^+e^- collisions. One can foresee that, while quark masses will be measured at e^+e^- beam machine, neutrino interactions will be important tools for determining the mixing angles.

(iv) Purely leptonic interactions of the type $\nu_\mu + e \rightarrow \nu_\mu + e$ will be studied at center-of-mass energies of the order of 4 GeV. These reactions, among the simplest ones, are inaccessible to e^+e^- colliding beam experiments and are unique for studying the effects of a possible lepton structure.

(v) Production of intermediate vector mesons and of new particles, will certainly be a large part of any physics program, together with the study of higher order effects in the electro-weak interaction. It is far too early to make any quantitative estimates of these effects, that will very probably be studied beforehand at e^+e^- colliding beam machines.

In summary there seems to be space for meaningful and unique experiments with neutrinos but one needs an assessment of the complementary roles of neutrino physics and of experiments performed with electron-proton colliding beams. If at these energies leptons still look pointlike and electron-muon universality holds true, neutrino experiments may become unnecessary. We are aware of the problem but have not tackled it for the moment. Our work has in fact concentrated on the technical problems connected with the scaling of the needed facilities from 0.5 TeV to the 10-20 TeV energy range.

2. Targets

At present targets of aluminium oxide are being bombarded with 10^{13} (30 GeV) protons per second and berylium oxide with 3×10^{13} (500 GeV) protons every eight seconds without any difficulty. These involve beam spills that are less than, or of the order of, 1 msec, which is also the characteristic time of heat transfer. It is anticipated that pure berylium targets and standard cooling methods are sufficient to handle 1 TeV protons with intensities of 5×10^{13} protons per pulse, again at the short spill (1 msec) domain. As such, one believes that there should be no difficulty in the viability of target at much higher energies, in that the multiplicity should rise logarithmically with energy and the intensities should be $\simeq$ few $\times 10^{13}$ per

pulse for short spills, $\lesssim$ 1 msec. For higher intensities of protons, one will have to improve the cooling, or use multiple targeting and multiple ejection, or increase the spill length appreciably, beyond 1 second. This problem has to be looked at in detail.

3. Horns and other focussing systems

Present horn focussing devices with currents of 100-300 KAmps work reliably, achieving almost perfect focussing of charged secondary particles in producing wide band neutrino beams. The combination of the more forward collimation of charged particles as the energy is increased as well as the greater interest in the higher end of the energy spectrum, appears to make the horn problem easier at higher energies than at lower energies for horn designs of the type used at Fermilab. The flexibility of the relative positioning of target and horn, as well as the geometry of the horn angle, should be sufficient to allow for adequately focussing the pertinent charged particle in forming neutrino beams at high energies. Horn currents do not have to be increased because the average transverse momentum of the secondaries remains the same and the horns have to give a p_T kick which is energy independent, as in the approach adopted by Fermilab for the 1 TeV neutrino beam. In this case the distance between the target and the horns would increase in proportion to the proton momentum P.

We now consider the scaling law for the focussing systems of a narrow band neutrino beam. Since the neutrino cross-sections increase with the neutrino momentum p_ν, one has the choice of scaling the beams at constant event rate or at constant neutrino flux. We feel the second choice is more reasonable, since high rates will certainly be needed for sophisticated experiments. We thus scale the focussing system by increasing the dimensions so that $\Delta p/p$ and $(p_T)_{max}$ remain constant. By keeping the topology of the focussing system fixed, one has

$$\frac{\Delta p}{p} \alpha \frac{Sp}{B\ell L} \; ; \quad (p_T)_{max} \alpha \lambda B, \tag{1}$$

where S is the source radius, ℓ the length of the system, L the length of the dipoles, and λ the length of the quadrupoles. Due to the heavy radiation fields we think normal temperature magnets will be used at these large energies also, and B has to remain constant. This implies that the length of the

quadrupoles may remain constant. Since we suppose that the source transverse dimensions remain the same, we may scale the length of the system and of the bending magnets proportionally to $\sqrt{p}$ and keep $\Delta p/p$ constant. Then the aperture of the quadrupoles, $R \alpha \ell\lambda B/p$, may even decrease proportionally to $1/\sqrt{p}$.

In conclusion, the focussing systems for neutrino beams do not limit the physics and their scaling laws are more favourable than the scaling laws of the accelerator itself.

4. Beams of ν_μ's and $\bar{\nu}_\mu$'s

The decay length d has to scale as the primary momentum P if one wishes to keep constant the fraction of pions decaying in muons. Certainly dichromatic beams will be used at these high energies and the next question has to be with the choice of the distance ℓ between the end of the main tunnel and the detector.

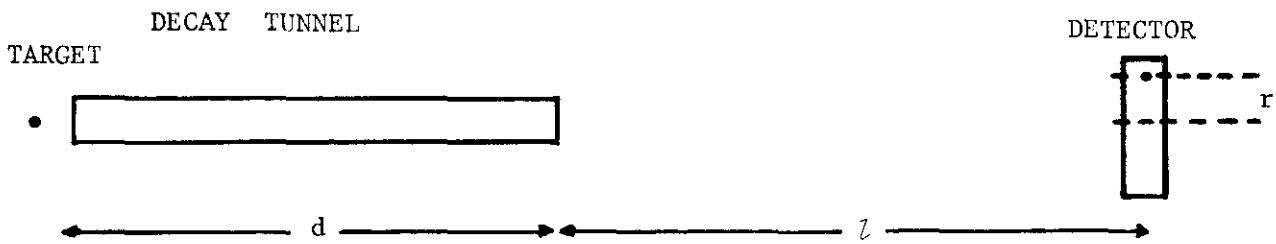

This length is determined by the fact that for events having vertex in the detector at a distance r from the center one likes to distinguish neutrinos produced by pions from neutrinos produced by kaons and compute the energy of the neutrinos from the measured value of r. The position uncertainty at the detector of a K-neutrino emitted at an angle θ_ν somewhere in the decay length d translates back to an angle uncertainty

$$\Delta\theta = \tfrac{1}{2}(\theta_{max} - \theta_{min}) = \tfrac{1}{2}\left(\frac{r}{\ell} - \frac{r}{\ell+d}\right)$$

which should be a small fraction η of the maximum θ_ν, thus

$$\Delta\theta = \eta \frac{p_{T\,max}}{P_\nu}$$

leading to a length ℓ

$$\ell = \frac{d}{2}\sqrt{1 + \frac{1}{\eta}\frac{2r}{d}\frac{P_\nu}{p_{T\,max}}} \qquad (2)$$

where P_ν is the neutrino momentum and $p_{T\ max}$ is the maximum transverse momentum in K-decay, i.e. 230 MeV/c.

We assume that the pion and kaon spectra are functions of $x = p/P$, where P is the proton momentum and p the secondary momentum, while their average p_T remains roughly constant. As shown in the previous section, one can scale the length of the focussing system proportionally to $\sqrt{p}$ and maintain the same neutrino fluxes. In fact we increase somewhat the neutrino flux because of the energy dependence of the secondary multiplicity. As in present neutrino experiments at CERN and Fermilab, we take d = 300 m for P_ν = 0.3 TeV. If the detector dimensions are kept constant with $r \lesssim 1$ m and one chooses $\eta \simeq 0.15$, Eq. 2 implies $\ell \simeq 3$ d. By taking for the narrow band beam $P_\nu^K \simeq 0.7$ P, we finally come to a target-detector distance:

$$(d+\ell)_{km} \simeq 3\ P_{TeV}\ ;\quad \frac{\ell}{d} \simeq 3\ . \tag{3}$$

At large energies muons radiate and the thickness of shielding material needed to range them out does not increase proportionally to the energy. The energy and the straggling of high energy muons have been computed by R.R. Wilson[1]. The <u>average</u> ranges in various materials have been calculated by D. Theriot and S. Mori by taking into account all the losses and appear in the Table together with the ratio of the bremsstrahlung and collision losses at the indicated energies.

E Muon energy (TeV)	Iron Av. Range $\bar{R}$ (km)	Iron $\left[\frac{(\Delta E\ brem)}{(\Delta E\ coll)}\right]$	Earth Av. Range $\bar{R}$ (km)	Earth $\left[\frac{(\Delta E\ brem)}{(\Delta E\ coll)}\right]$
1	0.25	1.5	1.6	0.6
5	0.50	8.3	3.0	3.3
10	0.60	17.3	3.8	6.5

Wilson has shown that (i) the fluctuations in the radiation process decrease by a factor $\ell n2$ the range and (ii) the fluctuations on the ranges of individual tracks (straggling) are smaller than might be

expected intuitively. Wilson computed the r.m.s. fractional straggling $S/\bar{R}$ and found that it is practically constant between 1 and 10 TeV and is of the order of 0.5. By taking as a safe value 4 r.m.s. value from the average range, one can then estimate the needed thickness of shielding:

$$\text{(shielding thickness)} \simeq \frac{\bar{R}}{\ell n 2}\left(1 + \frac{4S}{\bar{R}}\right) \simeq 2\bar{R} \ .$$

Comparing the entries of the table with eq. 3 we conclude that for proton momenta larger than $\simeq$ 2 TeV there is no need of iron shielding. If the path ℓ required to obtain a reasonable dichromatic beam is under earth, the muons would be ranged out by this natural shielding.

In conclusion a good narrow band neutrino beam of $P_\nu^K \simeq 10$ TeV could be obtained from a 15 TeV proton beam with $d \simeq 15$ km and $\ell \simeq 45$ km. These 45 km should not all be in earth since about 15 km of earth would be sufficient to shield the detectors from the muons: a hilly countryside is suitable for siting a 10 TeV neutrino beam. Since the muons in the shielding are in equilibrium with neutrinos, the increased muon range will produce a larger background than in present neutrino beams. The background flux scales as $\sigma_\nu \cdot \bar{R}$, i.e. roughly as $P_\nu \cdot \bar{R}$. Since in passing from 0.5 TeV to 10 TeV the flux increases by a factor $\sim$ 80, the background of muons may cause some problems to bubble chambers, but should be acceptable to electronics experiments.

5. Production of ν beams, other than ν_μ's

In the ν_μ beams presently in use the ν_e's are a small contamination. In order to enhance the ν_e content, pion decay should be suppressed, for instance by shortening the beams. Two ideas have been around, K_L beams and a muon storage ring, and at least one of them will presumably be implemented in the next years around the SPS or in FNAL.

In the first case[2)] all charged particles are swept out immediately after the production target (for a 15 TeV beam one needs 10^3 Tm). This is to be followed by a weaker sweeping magnet, to sweep away the pions produced in the decays of K_s and hyperons, thus reducing the ν_μ background (one needs $2 \cdot 10^3$ Tm). For an optimum ν_e flux the decay tunnel should

have a length similar to one for ν_μ's from π and K decay, since γct is similar. With the same decay path of the previous section one should obtain a ν_e-flux which is about two orders of magnitude less than the flux of ν_μ's from K decay. In case the detector is a bubble chamber, the K_L decay region probably has to be followed by a muon absorber. The beam consists of roughly equal amounts of ν_μ, $\bar{\nu}_\mu$, ν_e and $\bar{\nu}_e$, from $K_L^o \rightarrow \pi\mu(e)\nu$, in the form of a wide band spectrum. Also ν_μ and ν_e from charmed particle decay will be present in a comparable amount. To determine the ν energy and type, a tagging system would be needed, the size and complexity of which will probably defy attempts to make it feasible economically. At best one can hope that a detailed study will result in a design of a beam much shorter than optimum for intensity, that could be equipped with a tagging system and still have rates that are interesting. A tagged $K^\pm$ beam should then also be considered, since it might become competitive with a shortened K_L beam, despite the 5% branching ratio $K^\pm \rightarrow \nu_e$. A shortened decay tunnel also has the advantage of a smaller radius since the production angle of the particles goes as 1/P.

The second idea is to build a racetrack-like storage ring. Initially π and K decays would deliver ν_μ's and at a later time muon decay would give equal amounts of ν_e and ν_μ; finally (anti) protons would be left in the ring.[3] Tagging would not be useful. For 2 TeV muons the radius of curvature would be larger than 2 km.

The solution is certainly very expensive, but one could envisage using the same large acceptance ring for something else. For instance to collide pions and muons with the main ring or to produce $\mu^+\mu^-$ annihilations at large energies and very small luminosities. We think that the next workshop should devote some thoughts to these wild ideas.

Other neutrinos, like ν_τ from τ decay, will have to be produced in beam dumps, as the parents do not live long enough to make beams of them. In the dump the particles with decay distances $\gamma c\tau$ longer than their strong interaction absorption length λ will be prevented from decaying, but instead transfer their energy into a shower of which the last generation particles will finally be captured or decay and give low energy muons. Of the strongly interacting particles only charmed particles

and heavy flavours with lifetimes < 10^{-12} sec, will decay before interacting, for energies of 1 TeV and below. The charmed particles decay into $\mu\nu_\mu$ and $e\nu_e$, the heavy flavours also in $\tau\nu_\tau$. There is not enough known about production cross section in a new energy domain to guess something about the ν_τ fraction of events. Tagging will presumably be impossible but variations of target thickness might vary the relative neutrino mix. Also the p_t dependence of the various neutrino components is presumably different and might be helpful in enhancing a particular component.

6. A hybrid bubble chamber for neutrino physics in the TeV range

A large cryogenic bubble chamber equipped with external as well as internal hybridisation is well suited to many aspects of a future neutrino physics program. The technology is well developed and extrapolated performance features can be predicted with some confidence. A zeroth order approximation considered here is a cylindrical chamber about 5 metres long and 2 metres diameter equipped with a modest field of about 30 Kgauss. The volume ($\sim$ 15 m^3) is about one half of BEBC or the 15 ft FNAL chamber. The chamber would be equipped with a track sensitive target of approximately 3 x 1.5 x 1.5 m^3 (comparable in volume with that operated this year in BEBC). The chamber could then be used either as a pure hydrogen or deuterium chamber or as a pure heavy liquid neon or neon-hydrogen chamber or as an internal hybrid with two sections: a TST (hydrogen or deuterium) followed by heavy liquid (of variable radiation length 40-1000 cm). External hybridisation would include a hadron calorimeter and a muon identifier as minimal components.

We consider here only general features of the set up and clearly no detailed optimization has been included nor have alternative schemes such as the argon chamber proposed for the energy doubler been looked into.

The obvious advantages of the chamber based system are:

Excellent resolution and track measurement precision which allows together

1. Track counting before secondary interaction confuse the situation
2. Precise measurements of charged particle momenta including electrons in hydrogen and muons before they leave the chamber

3. Precise angle measurements
4. Excellent electron identification in neon hydrogen
5. Some visible gamma conversions to monitor the start of the hadron calorimetry
6. Strange particle detection and identification (K^0, Λ^0's) when they decay in the chamber

For a cross-section $\sigma \sim 0.8\ E_{GeV}\ 10^{-38}\ cm^2$ a 3 metre hydrogen filled TST will have $\sim$ 1 event per pulse for 10^{13} protons on the target ($10^{10}\nu$/pulse). The chamber could easily cycle at 1 per second taking 10 pictures, i.e. 10 events, per flat top.

Charged hadrons are measured within the TST (i.e. before secondary interactions become too serious) with precision

$$\left(\frac{\Delta p}{p}\right) \simeq 5\left(\frac{p}{100\ GeV}\right)\ \%$$

Muons are measured with improved accuracy

$$\left(\frac{\Delta p}{p}\right) \simeq 2\left(\frac{p}{100\ GeV}\right)\ \%$$

Electrons are identified by bremmstrahlung in the neon-hydrogen

100% efficiency. Electron measurements are made in hydrogen with an optimum length and precision which are only slowly varying with momentum ($\ell = 20\ p_{GeV}^{0.4}$cm) so that

$$\left(\frac{\Delta p}{p}\right) \simeq 7\ p_{GeV}^{0.2}\ \%$$

Angle errors for electrons are always in the range 0.1 - 0.4 mrad. Externally it would be useful to have a hadron calorimeter followed by a muon identifier. The muon identifier should be instrumented to give as good a momentum measurement as possible and help in correlating the tracks between the chamber and the EMI.

To allow photography of the full chamber depth of 2 metres the resolution is limited to 600 μm. The decay length of a particle of mass M is $\delta \sim \left(\frac{p}{M}\right)$ 30 n μm where $\tau = n \cdot 10^{-13}$ s. For $\frac{p}{M} \sim 100$ $\delta \sim 3$ n mm. Thus in a clean production situation, the normal resolution will allow clear longitudinal separation of vertices. Laterally the separation of

decay vertices from neighbouring tracks will be $\sim$ 30 n μm and is not feasible. However, in the "dirty" situation, i.e. many produced particles one of which is a new flavour, it should be possible to find the decay vertices by measurement and fitting. At a loss of rate of a factor less than 10 a slice of the chamber could be viewed with about 100 μm resolution.

In summary a first look indicates that reasonably conventional bubble chamber neutrino experiments will be viable and very interesting at high energies and could form a major part of the physics program at a multi TeV machine. More ambitious solutions such as the ARGONAUT system clearly also have attractions and should be considered alongside that considered here. Equally pure electronic experiments will certainly play a role. The short time available did not allow any serious consideration of the possible developments of these kinds of detectors.

7. Unconventional use of neutrino beams

The opening angle of the beam is so small that reasonable counting rates would be obtained at large distances from the decay tunnel. For instance, a detector of 20 x 20 x 25 m^3, containing 10^4 tons of material and placed at 3000 km from the target, would see one neutrino event for every 10^{13} protons on target. One can thus envisage directing the neutrino beam towards a far away detector. The possible uses of such a scheme have been listed by P. Koster et al. in a proposal recently presented to Fermilab.[4)] For the time being we leave this open as an interesting possibility.

8. Conclusions

In scaling up by a factor 10-20 of present day neutrino physics we have not found sharp limitations. However, we see many areas of potential problems. In particular the targets and the background flux of muons produced in the shielding have to be studied in more detail. Beams of unusual neutrinos call for new solutions, among which we consider the muon storage ring very attractive; especially if the same ring can find some other interesting utilization. It seems that bubble chambers will still be useful instruments, but the development of new devices, such as the argon time projection chamber, has to be followed in the next years.

A physics question dominates the whole development of neutrino physics: will electron-proton colliders make neutrino beams useless? The answer depends on what nature is still hiding from us, but still the problem is worth investigating on the basis of possible scenarios and we believe that this could be one of the main topics in the lepton working group of the next ICFA workshop.

We are grateful to S. Mori and D. Theriot for very informative discussions and for providing us with the data appearing in the Table.

References

1) R.R. Wilson, Evolution of particle physics, M. Conversi ed., Academic Press, 1970, p. 294.

2) Studies for a K_L beam have been made by Baltay et al., FNAL proposal 296 (1974). Mori, FNAL technical note 78 TM 769 (1978). See also Cline, Mori, Stefanski, FNAL technical note TM 802 (1978).

3) A muon storage ring has been considered by Koshkarev, CERN report ISR DI 74-62, 16 December 1974.
A comparison of various schemes has been made by Wojcicki, FNAL preprint (1978).

4) P. Koster, Some experiments with long terrestrial neutrino beam lines, 1978.

Report of the Hadron Experiments Group[+]

R. Diebold[*]

Argonne National Laboratory
Argonne, Illinois 60439
November, 1978

Summary

This group considered in a general way the scope and limitations of some specific strong-interaction experiments that might be performed in the early days of a 20-TeV proton accelerator, both fixed-target and $\bar{p}p$-colliding-beam experiments. The group was loose-knit with individual members working rather independently on various topics, including secondary beams. The general conclusion is that many of the present-day experiments can be easily extrapolated to higher energies. While these experiments will be somewhat more costly, the cost will not be linear with energy and will represent a smaller investment compared with the accelerator than at present laboratories.

[+] Talk presented at the workshop on "Accelerator and Detector Possibilities and Limitations" sponsored by the International Committee for Future Accelerators (ICFA) and held at Fermilab, October 15-21, 1978.

[*] Work done under the auspices of the U. S. Department of Energy.

The submitted manuscript has been authored by a contractor of the U. S. Government under contract No. W-31-109-ENG-38. Accordingly, the U. S. Government retains a nonexclusive, royalty-free license to publish or reproduce the published form of this contribution, or allow others to do so, for U. S. Government purposes.

Introductory Remarks

We first get a feeling for some of the angles likely to be encountered at the Very Big Accelerator (VBA) for a proton beam of 20 TeV. Typical angles for elastic scattering are:

$$\text{Coulomb interference} \qquad \theta \sim \frac{40\ \text{MeV/c}}{20\ \text{TeV}} = 2\ \mu\text{rad},$$

$$\text{Diffraction peak} \qquad \theta \sim \frac{300\ \text{MeV/c}}{20\ \text{TeV}} = 15\ \mu\text{rad}.$$

Instead of the more familiar mrad units, we are now in the realm of μrad,

$$1\ \mu\text{rad} = 1\text{mm/km},$$

and a Coulomb interference experiment might need a few kilometers of drift distance (relatively cheap vacuum pipe). Note that these are typical laboratory angles for both fixed target and colliding beams.

For fixed target operation at 20 TeV ($\sqrt{s}$ = 200 GeV), 90° in the center of mass corresponds to 10 mrad in the laboratory.

For 20 on 20 TeV colliding beams, $\sqrt{s} = 40$ TeV. This is a huge increase over present day energies and represents a total rapidity interval of

$$\Delta y \approx \ln s = 21 \text{ units of rapidity.}$$

This energy is equivalent to a fixed-target lab energy of $\sim 10^{18}$ eV, far beyond even most cosmic ray experiments. (With 8 Tesla magnets a fixed target machine of this energy would require a radius of 400,000 km, the distance from the earth to the moon!)

Five years ago Panofsky[1] made the compilation of machine energies versus time shown in Fig. 1. His straight line through the envelopes of the individual curves shows a factor of 10 increase in energy ($E_{lab} \propto s$) every

6 years. Such an exponential increase cannot continue forever, but if we can get the Very Big Accelerator (VBA) built by the year 2004, we will keep pace with the projection. This date certainly seems possible, and it would be fun to race the curve and beat it.

A compilation of multiplicities is shown in Fig. 2. An unimaginative extrapolation of the ISR fit would give $\langle N \rangle = 63$ charged particles per interaction at 20 on 20 TeV. The Centauro events with their high multiplicity of strongly-interacting secondaries, as well as the high multiplicities observed in extensive air showers (EAS), suggest a much steeper dependence, perhaps leading to some utterly spectacular interactions, radically different from those observed at present accelerators.

Beam Lines

As the beam energy increases and the particles become stiffer, beam lines get longer and require more magnetic field. In general, there is a tradeoff possible between the overall length of a beam and the length of the magnetic elements needed for focusing and momentum dispersion.

To study this in more detail we have taken a standard point-to-point beam stage shown in Fig. 3 with a parallel central region containing bending magnets (and possibly Cerenkov counters). The focal length ℓ of the quadrupole doublet has a dependence on momentum p

$$\ell \propto \frac{p}{B' L_Q}$$

where B' is the field gradient in the quadrupoles. If we fix B' and let all distances (both drift distances and magnet lengths) scale as $\sqrt{p}$, we

maintain the same focusing properties (in this case point-to-parallel-to-point). This scaling works to all orders and is not just a thin-lens approximation. If the length of bend magnet is also scaled as $\sqrt{p}$, then the dispersion, $D = \Delta x/\Delta p/p$, is also constant. For a fixed magnet aperture a, the angular acceptance in this scaling goes as

$$\Delta\theta \approx a/\ell \propto 1/\sqrt{p}.$$

Of more interest is the transverse momentum bite

$$\Delta p_x = p\Delta\theta \propto \sqrt{p}.$$

Using this scaling for a secondary beam, one eventually gets to a point of diminishing return when Δp_x becomes larger than the typical transverse momentum in the production processes of $\sim \pm 0.4$ GeV/c. One could then go to smaller magnets and/or longer drift distances.

As an example, we consider a 20-TeV beam stage of total length 2.3 km. Most of this distance would be in two 1-km drift lengths of buried vacuum pipe. The main cost of the beam would be in the $\sim$ 300 m of tunnel filled with quadrupoles and bending magnets. The focusing could be achieved with each element of the two quad doublets being 8 meters long (32 m for all four quadrupoles) with a strength that of the Fermilab Doubler quads, 80 T/m (we have taken a separation of 10 m between the quadrupole centers in each doublet).

The acceptance for an aperture of 2 cm radius would be

$$\Delta p_T = 20 \text{ TeV} \times \frac{\pm 2\text{cm}}{1000\text{ m}} = \pm 0.4 \text{ GeV/c}.$$

This would cover most of the forward peak at 20 TeV (but correspondingly less at lower momenta). While this has the obvious advantage of very high rates, it also means that unlike present-day machines which often have several beam lines looking at the same production target, at the VBA each secondary beam will need its own target and primary beam.

If we were to fill the central region with 200 meters of 8 Tesla bending magnets, the bend angle would be 24 mrad; with the focal length of 1100 m this becomes a displacement of 26 meters at the final focus. While 200 meters of 8 Tesla sounds like a lot of magnet, it is only 0.4% of that needed for the accelerator and can probably be obtained from the factory rejects - magnets not quite of accelerator quality, but adequate for beam lines. If we assume that multiple scattering effects are not important, and assume that we can make a ± 70 μm measurement at both the initial and final focus, we then get the spectacular resolution

$$\frac{\sigma_p}{p} = \frac{\pm\sqrt{2} \times 70\ \mu m}{26 m} = \pm 4 \times 10^{-6} ,$$

$$\sigma_p = 20\ \text{TeV} \times 4 \times 10^{-6} = \pm 80\ \text{MeV},$$

still better than one pion mass! For many purposes we could obviously get by with less bending.

At the energies being discussed here, charged hyperon beams should be relatively straightforward to construct. As an example of a relatively short beam stage, consider that sketched in Fig. 4; this example was kindly calculated by Jon Sauer (Argonne) using the program TRANSPORT. By using superconducting quadrupoles of ~ 28 kG/cm gradient, we can achieve a

suitable beam stage in only 232 m. At 15 TeV the mean free decay length for Ξ^- is 560 m, and about half of the Ξ^-'s would survive two such stages.

As shown, there is space for 60 m of sweeping magnet before the first quadrupole, enough to displace the 20-TeV proton beam by 5 cm at the first quadrupole, assuming a 15 kG sweeping field. If we used quads with an aperture of radius 1 cm, the acceptance would be

$$\Delta\theta = \pm 0.079 \text{ mrad} \qquad \Delta p_x = \pm 1.18 \text{ GeV/c}$$
$$\Delta\phi = \pm 0.130 \text{ mrad} \qquad \Delta p_y = \pm 1.96 \text{ GeV/c}$$

at 15 TeV (less at lower momenta)

The $\Delta p/p$ acceptance would be limited by the last quad to $\pm 3.2\%$ for a $\pm$ 1 cm aperture. The momentum resolution would be dominated by the primary-beam spot at the production target. Scaling the ± 0.5 mm spot at the Fermilab Meson Area target by $p^{-1/2}$ would give a spot of ± 70 μm. The dispersion at the focus is 0.89 cm/% and this leads to $\sigma_p/p = 0.0083\%$ or $\sigma_p = \pm 1.2$ GeV/c.

The physical layouts of the ZGS and Fermilab are compared with a highly conceptual layout for the VBA in Fig. 5. As the energy increases, the external beam lines occupy a smaller fraction of the site, as suggested by the square-root scaling. The exception to this may be the ν beam whose length tends to scale more linearly with energy, as discussed at this workshop by Amaldi. At the VBA a smaller fraction of the total cost of the accelerator complex will go to the external beams, and (assuming no major advance in accelerator technology), the machine itself will dominate both the costs and real estate.

Fixed Target Experiments

Sensitive Target

The use of a small rapid cycling hydrogen bubble chamber was considered by C. Fisher[2] as a track sensitive target for a hadron spectrometer. Such a system would allow the study of multiplicities, correlations, rapidity distributions, etc., in this new energy range, much as the 30-inch hybrid bubble chamber explored the Fermilab energies.

To minimize secondary interactions of the outgoing particles, the chamber would be kept fairly small, say a 20-cm diameter. Good separation of tracks would still be achieved by using two sets of cameras, one with high resolution and the other with a greater depth of field. With a cycle rate of 100 Hz, several thousand interactions per hour could be recorded, quickly filling up the world's analysis capability. Various beams could be used, including charged hyperons. Eventually, one might try to devise specific triggers in order to study particular classes of events. For example, triggers on K_s^o's and/or leptons might be used to enrich the sample with flavor cascades.

The high resolution system would also be useful in searches for particles with relatively short lifetimes. For example, a particle produced at rest in the center of mass and with a 10^{-13} sec lifetime would have a decay length of 3mm in the laboratory. This would allow studies of charm-producing events as well as searches for new, heavier particles produced at these high energies.

Exclusive and Inclusive π CEX and η Production

These processes have been studied at Fermilab by a Caltech-Berkeley collaboration using a segmented shower counter.[3] The resolution σ_E/E of such a counter improves with energy, and the counter would be moved back from the target, the drift length proportional to momentum to give the same separation of γ rays in the detector.

A sophisticated veto system would be used to suppress the inelastic background when studying the exclusive processes

$$\pi^- p \to \pi^0 n,$$
$$\to \eta n .$$

The cross sections for such exclusive processes fall with energy and are well described over the range from a few GeV to 200 GeV by the form

$$d\sigma/dt \propto s^{2\alpha(t)-2}$$

where $\alpha(t)$ is the $\rho(A_2)$ Regge trajectory for $\pi^0(\eta)$ production. Going from 200 GeV to 10 TeV is a factor of 50 increase in s, and at $t=0$ where $\alpha \approx 0.5$ we expect a loss in cross section of a factor of ~ 50; at $t \approx 0.6$ GeV^2 where $\alpha = 0$, this becomes a factor of 2500. Since the Fermilab experiment was able to collect 20,000 $\pi^0 n$ events at each of several energies, an experiment at 10 TeV will still be able to achieve reasonable statistics in the forward region, but it will be difficult to collect data at $t \gtrsim 0.6$ GeV^2 if the present energy dependence continues unabated - of course, this is the reason for doing the experiment, to see if some other more-slowly-varying mechanism eventually comes into play.

The same apparatus was used to measure the inclusive reactions

$$\pi^- p \to \pi^o X,$$
$$\to \eta X,$$

both for X = anything, the usual full-inclusive reaction, and for X = neutrals only (zero-prong events). The cross sections were well fit by the Triple Regge formulae

$$d^2\sigma/dtdx \;\; \alpha \; (1-x)^{1-2\alpha(t)} \quad \text{full inclusive,}$$
$$\alpha \; (1-x)^{1-2\alpha(t)}/s \quad \text{neutrals only.}$$

The trajectories are again expected to be those of the ρ and A_2 for π^o and η production, respectively, and qualitative agreement was in fact obtained between the trajectories from the exclusive and inclusive reactions. The full-inclusive experiment should, if anything, be easier at the higher energy (better σ_E/E), while the neutrals-only will suffer from the factor-of-50 reduction in cross section, but should still be feasible.

Scattering off Electrons

The elastic scattering of pions and kaons off electrons in liquid hydrogen targets has been studied at present machines to obtain information on the meson form factors. A 15-TeV beam incident on a stationary electron will develope a $\sqrt{s} = 4$ GeV, equivalent to an 8-GeV $e^- p$ interaction at SLAC. This is enough energy to not only improve considerably our knowledge of the meson elastic form factors, but to also begin studies of the "deep inelastic" characteristics of mesons for the first time.

Total and Elastic Cross Sections

These experiments should be straightforward extrapolations of present-day experiments, with drift distances proportional to energy. In addition to the standard set of particles ($\pi^{\pm}$, $K^{\pm}$ and $p^{\pm}$), we will have beams of hyperons ($\Sigma^{\pm}$, Ξ^{-}, Ω^{-}) and antihyperons available for these measurements.

Colliding Beam Experiments

Given the small angles characteristic of diffractive processes, measurements of small angle elastic scattering and even the total cross section will be difficult. Such experiments will require very parallel beams (high β) at the intersection point with some of the detectors embedded in the machine lattice at a position where the beam is focused down to a small spot. As an example we take the emittance $\epsilon = 13\,\pi/p$ mm mrad (p in GeV/c) found at Fermilab (basically, we assume that a machine such as that at Fermilab might be used as an injector for the VBA and that there is no dilution as the beam is accelerated). Then at 20 TeV and for $\beta = 1000$ m, the beam would have rms values of $\sigma_{p_x} = \pm 7$ MeV/c and $\sigma_x = 0.3$ mm. An elastic scatter of, say, $p_\perp = 100$ MeV/c will clearly take the particle outside the beam envelope, but it may prove difficult to devise a suitable detector which can be sensitive close enough to the beam to actually see such a scatter unless very long effective focal lengths can be used.

Observation of particles at large angles is certainly easier, and is presumably more interesting in that new heavy particles would likely give decay products with high $p_\perp$ in this region. Detectors could look much

like those presently planned for colliding beams at Fermilab and the SPS. A large magnet, either solenoid or dipole, would measure well the charged particles with $p_\perp \leq 50$ GeV/c, while higher energies would be measured in a hadron calorimeter. The electrons and γ-rays would be precisely measured in shower counters. Fig. 6 shows the resolutions for various particles calculated for a solenoid configuration at Fermilab.[4] The combination of magnetic field plus calorimetry works nicely for most particles over a broad range of energy. In particular, the measurement error on the energy of a jet is $\sigma_E/E = (2 \text{ to } 4)\%$ for all energies above a few GeV. At the higher energies the main limitation will likely come from the systematics in keeping a large calorimeter properly calibrated; with care and present technology one can probably do a factor of two better than the ±3% assumed in Fig. 6.

Present theoretical prejudices lead us to believe that the cross sections for particle and jet production at large $p_\perp$ will increase dramatically at these energies. Rick Field (Caltech) has kindly extended his QCD calculations[5] to $\sqrt{s} = 40$ TeV for this Workshop, with the results shown in Fig. 7. At $p_\perp = 200$ GeV/c the cross sections rise by 4 or 5 orders of magnitude in going from $\sqrt{s} = 1$ TeV to 40 TeV. Although the extrapolation is a long one, the calculations suggest that we should be able to see single particles with $p_\perp = 1000$ GeV/c even with modest luminosities. For example, consider a large-angle detector covering 15° to 165° ($\Delta y = 4$ rapidity units). Then

$$\frac{d\sigma}{dp_\perp} = 2\pi \, \Delta y \, p_\perp \left(E \frac{d\sigma}{d^3p} \right)$$

$$\approx 25\ p_\perp \left(E \frac{d\sigma}{d^3p} \right)$$

Taking a bin of width $\Delta p_\perp = 100$ GeV/c at $p_\perp = 1000$ GeV/c, the curves in Fig. 7 indicate a corresponding cross section of

$$\Delta\sigma = 1 \times 10^{-36}\ \text{cm}^2 \text{ for } \pi^o\text{'s},$$

$$= 0.5 \times 10^{-33}\ \text{cm}^2 \text{ for jets.}$$

A run of several months with an average luminosity of 10^{30} cm^{-2} sec^{-1} would give an integrated luminosity of 10^{37} cm^{-2} and thus 10 π^o's and 5000 jets in this bin. At 200 GeV/c, a bin with $\Delta p_\perp = 20$ GeV/c would have 8000 π^o's and 4×10^6 jets. Clearly we will need to suppress common garden-variety jets with such "low" $p_\perp$!

Limitations

Since the title of this Workshop includes the word "limitations," we have gone looking for them:

1) Particle identification. This has been discussed in detail by Willis.[6] Although transition radiation and synchrotron radiation are useful at very high energies, there are intermediate values of γ which are awkward. Already at present day energies it is quite difficult to identify particles over more than a very limited solid angle, so this is not really a new limitation for many types of experiments.

2) Beam splitting. As mentioned in an earlier section, each secondary beam will require its own target and thus its own primary beam. If more than one beam is to run simultaneously, the external beam must be split, presumably with electrostatic wire septa. This already poses problems at

Fermilab, and at 50 times the energy will be much more difficult at VBA.

3) Small-angle colliding beam experiments. Experiments to measure diffractive processes will need to be able to see down to $\leqslant 10$ μrad, and will require a long drift space, difficult to find in an accelerator. Even with a lens system with an effective focal length of 1 km a proton scattered by 10 μrad will still only be 1 cm from the beam. Coulomb interference with an angle of typically 2 μrad at 20 TeV will be especially challenging.

Conclusions

Many hadron experiments at the VBA will be straightforward extrapolations of experiments at present energies. In general, these experiments will be somewhat more costly, but scaling more slowly than linear with energy. The beam lines will also share this type of cost dependence. A simple scaling of beam line lengths is proportional to $\sqrt{p}$, but optimization and advances in magnet technology may well result in an even slower scaling of costs. Assuming no major advances in technology, it seems that beam lines and experiments will be a smaller fraction of the total cost of the accelerator complex than is true today.

Acknowledgments

In addition to the members of the Workshop with whom I discussed these ideas, I would like to thank D. Edwards (Fermilab) for help with beam-line calculations, J. Sauer (Argonne) for running the program TRANSPORT for the short hyperon beam, and R. Field (Caltech) for extending his QCD calculations to VBA energies.

References

1. W.K.H. Panofsky, Phys. Today, p. 24 (June 1973).
2. C. Fisher, these proceedings.
3. A. V. Barnes et al., Phys. Rev. Letters 37, 76 (1976); O. I. Dahl et al., Phys. Rev. Letters 37, 80 (1976); A. V. Barnes et al., CALT-68-664 and CALT-68-667 (1978).
4. C. Ankenbrandt et al., Fermilab Note CDF-11 (1978).
5. R. D. Field, Plenary talk at the Tokyo Conf., CALT-68-683 (1978).
6. W. Willis, these proceedings.

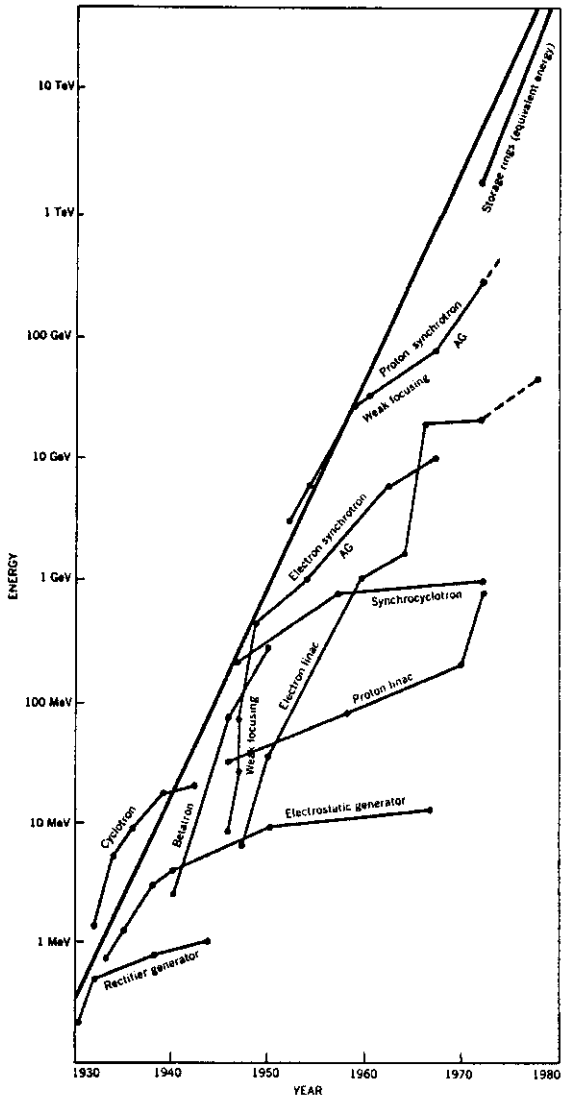

Fig. 1. Energy growth of accelerators compiled by Panofsky in 1973 (Ref. 1).

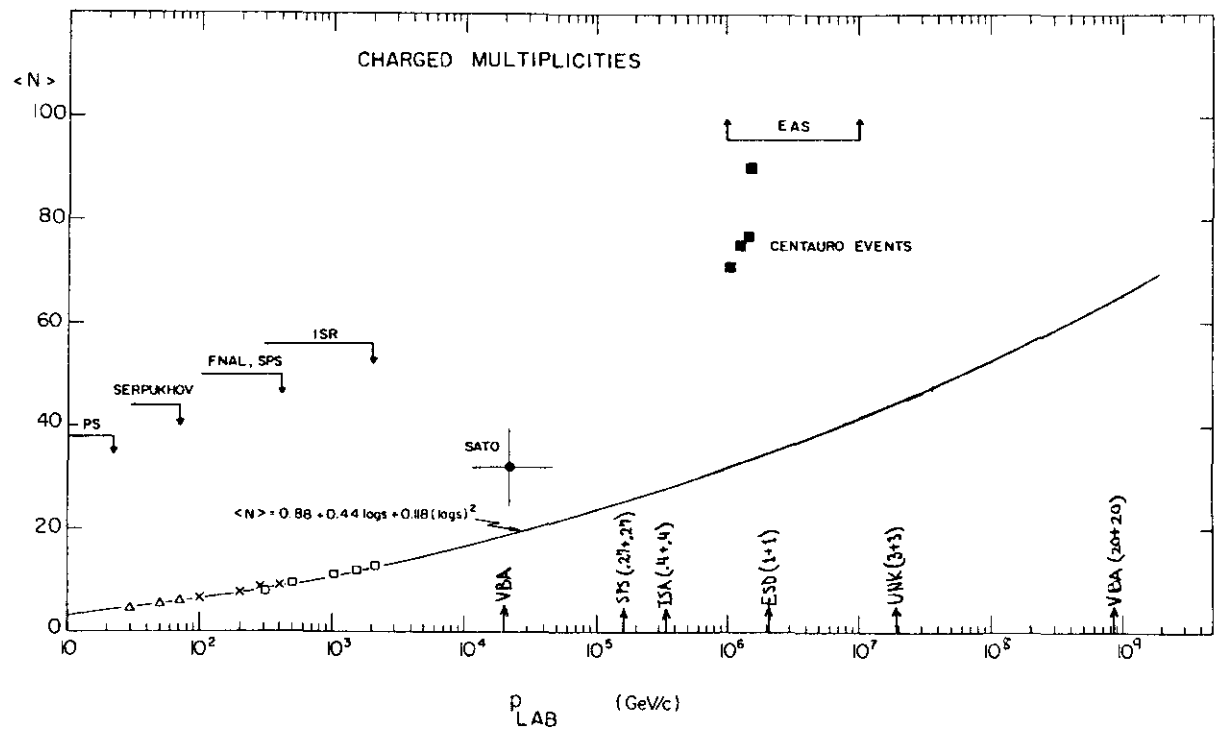

Fig. 2. Charged particle multiplicities plotted as a function of laboratory energy. The Centauro points show strongly interacting particles per event and are taken from Paper 434 submitted to the Tokyo Conference. The quadratic fit found at the ISR has been extrapolated to higher energies.

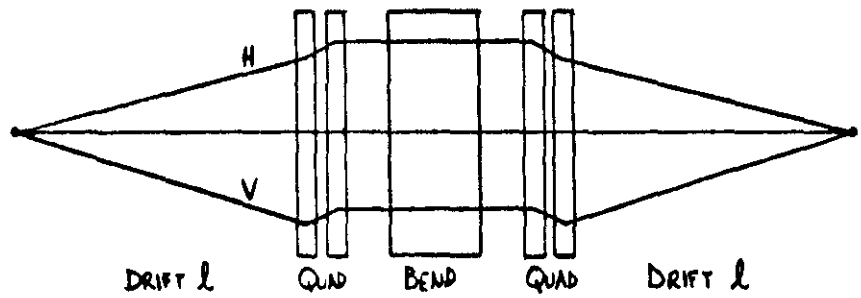

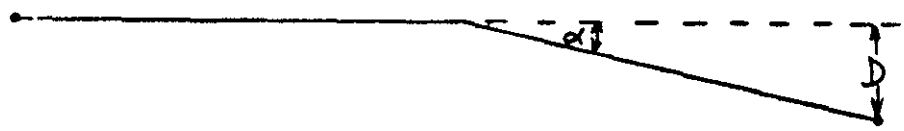

Fig. 3. Point-to-point beam stage.

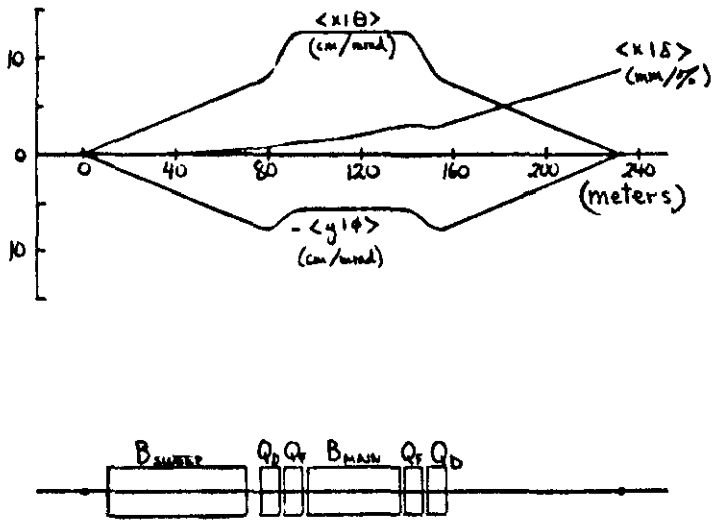

B_{SWEEP}	15 kG × 60 m	⇒ 1.8 mrad bend
B_{MAIN}	80 kG × 40 m	⇒ 6.4 mrad bend
Q_D	$-27.8\ \frac{kG}{cm} \times 8$ m	
Q_F	$24.8\ \frac{kG}{cm} \times 8$ m	

Fig. 4. 15-TeV hyperon beam.

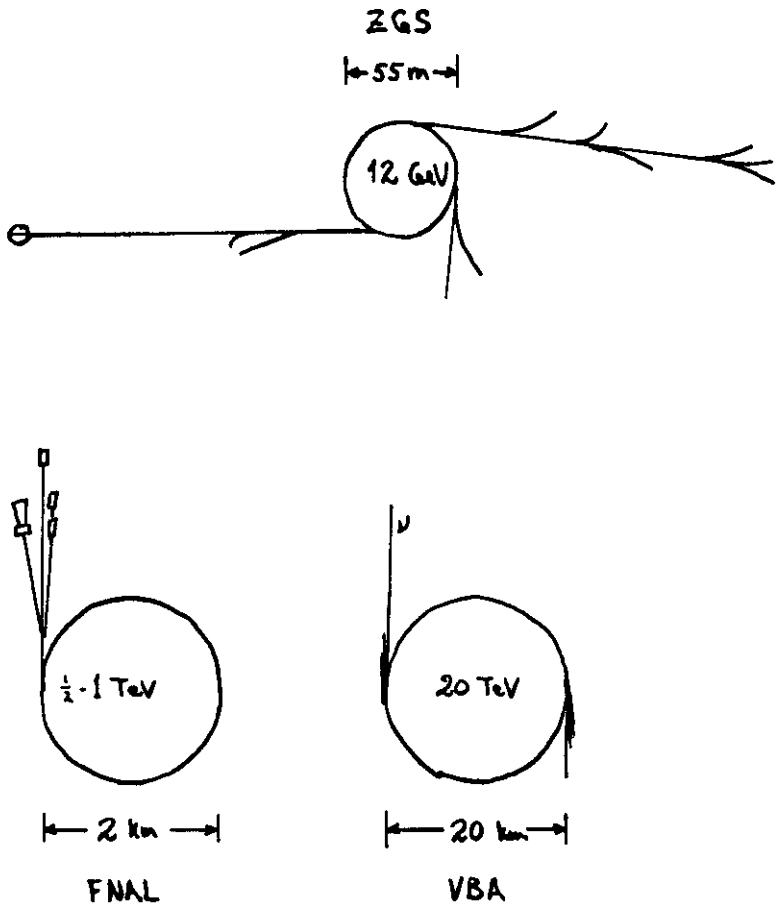

Fig. 5. Site plans for three laboratories, showing that the external beam lines become a relatively smaller part of the laboratory as the energy increases.

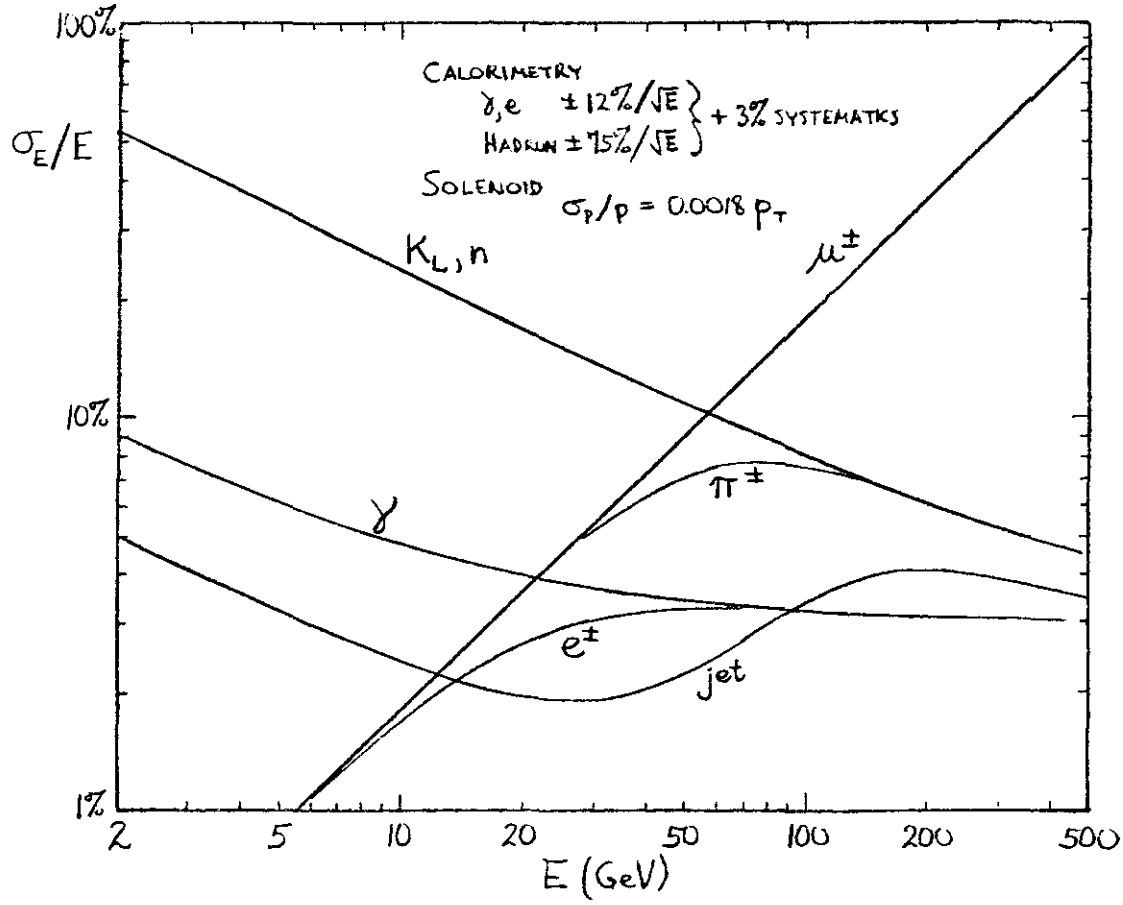

Fig. 6. Energy resolution calculated for various types of particles to be detected in a large solenoid detector system (Ref. 4).

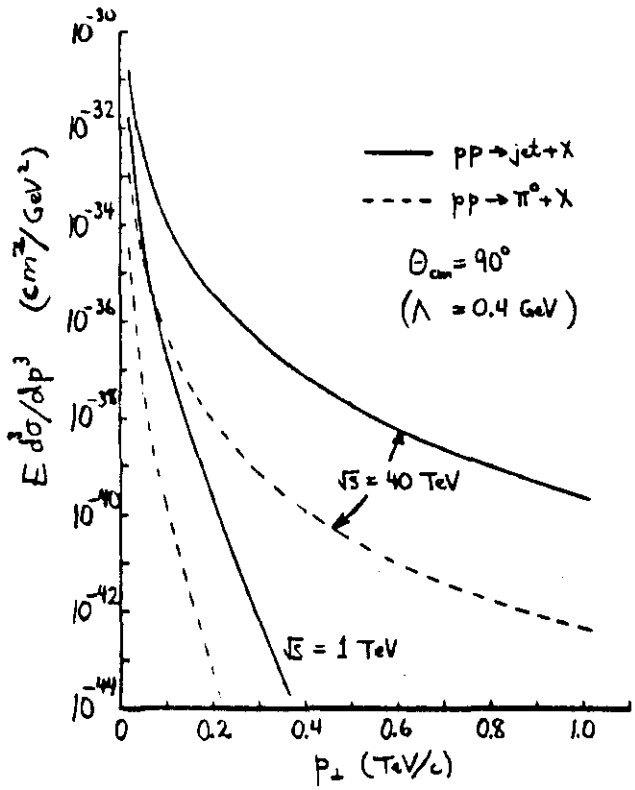

Fig. 7. QCD calculations by R. D. Field

FEATURES OF EXPERIMENTS AT ENERGIES ABOVE 1 TeV

V. I. Kryshkin, Yu. D. Prokoshkin, A. S. Vovenko,
V. A. Yarba, and A. M. Zaitsev
Institute for High Energy Physics, Serpukhov, USSR

1. INTRODUCTION

One can hope that, in the not very distant future, physicists will have the opportunity to work at accelerators in the TeV energy range. Striving for still higher energies is natural, but in this case one should meditate on how much the energy growth corresponds to potentialities of the experimental technique. The present paper is aimed to the discussion of the problem of particle detection at 2 to 5 TeV proton accelerators.

Before taking up this subject, it is useful to formulate briefly the main trends of experimental research for the TeV energy range. Recent years are remarkable for tremendous progress in high energy physics. Among the most important discoveries, we should note the growth of the total cross sections, the scale invariance phenomenon, and discovery of neutral currents, of a heavy lepton and of a family of particles with new quantum numbers. The bulk of the experimental data at present and the efforts of theoreticians have made more profound our understanding of elementary particle structure and their interactions. Realistic renormalizable models of weak interactions have been put forward, and they unified weak interactions with electro-magnetic ones thus stating a fundamental fact on the unity of these forces of nature. Great progress in the development of quark models brought us to a new level of understanding of the nature of strong interactions.

Future experiments at even higher energies will allow us to check the modern notions, to develop them further, and to clarify the details.

Elementary particle theory is based on quantum field theory, whose fundamental principles are causality, relativistic invariance, and unitarity. Just from these principles there follow dispersion relations, as well as a number of asymptotic theorems that put limitations on the behavior of both elastic and inclusive processes at high energies. Consequently, the higher the energies the more possibilities we have to check the basic principles of the theory. For instance, deviations from the predictions would be evidence of the existence of an elementary length, which might crucially change the principles of the theory. Hence the modern level of elementary particle physics raises a number of long-term physical problems that demand experimental study and determine our choice of the main trends in investigations to be carried out at a proton accelerator with the energy of about some TeV. These are as follows:

a) search for and detailed study of hadrons containing heavy quarks (in this case both the study of states with the known quarks (c, b) and with the suspected ones (for example, t-quarks) is implied. An important circumstance in the transition to high energies is not only an increase of the mass range accessible but an increase in the particle production cross sections, as well as the relativistic growth of their life-time in the lab system;

b) search for heavy leptons, the study of their decays and production mechanisms;

c) at TeV energies, there exists an essentially extended

opportunity to search for objects of a new type, such as free quarks and color states, Higgs bosons, intermediate vector bosons, exotic (from the viewpoint of the quark model) systems, for example, bound states of a few gluons (glueballs), multi-quark bound states, etc.;

d) the high energy neutrino interaction will make it possible to study the structure of weak currents and may become a source of intermediate bosons. A detailed study of neutrino interactions will enable us to judge on the presence of intermediate bosons even in the case of their mass exceeding 50 GeV. Intense beams of polarized muons will also assist the study of high energy weak interaction effects;

e) to define more accurately the structure of hadrons, and the dynamics of quark-gluon interaction at small and large distances, a wide scope of research is necessary to be carried out. This includes:

- the study of multiparticle processes with a large momentum transfer in hadron-hadron collisions, the study of the composition of hadron jets;

- the study of two-particle and quasi two-particle processes with a large transverse momentum, those in charge exchange reactions included;

- the study of the phenomenon of the total cross section growth; the study of the characteristics of inclusive processes;

f) the study of lepton-hadron deep inelastic interactions in a wide energy range; the study of leptonic pair production in hadron collisions.

The experiments which are necessary to be carried out in

the energy range exceeding 1 TeV in order to solve these problems require complicated facilities to be created, and the development and perfection of particle detection methods. Below we shall discuss the features of the superhigh energy experimental technique. Neutrino experiments requiring complex facilities will be considered separately.

2. EXPERIMENTAL TECHNIQUE

a) Particle Identification

The problem of selecting particles of different masses is often faced both in identifying the components of beams and in identifying secondaries produced in the setup target.

The former problem is solved more easily despite the fact that the beam particles have far larger momenta than the secondaries. That this is so is related to the fact that in the former case single particles having small angular divergence and momentum spread are identified. The presently existing technique of Cherenkov counters allows us to select beam particles of a given sort in the energy range up to a few TeV. On the other hand, the difficulties in identifying the secondaries with their high multiplicity, large angular divergence and wide momentum spectrum will be rather great and will call for an essential development of the experimental methods, at least in quantitative respect.

Cherenkov Counters

A gas threshold Cherenkov counter is the simplest Cherenkov detector to identify superhigh energy particles. The Cherenkov counter length necessary to separate the beam particles grows

proportionally to E^2. At $E \simeq 1$ TeV, it reaches 1-2 km if pions and kaons are to be separated.

To select particles in a differential Cherenkov counter the dependence of Cherenkov radiation angle on the velocity is used. The resolution of a differential Cherenkov counter is improved with a decrease in the angle of Cherenkov radiation and optic system, angular spread of beam particles, and multiple scattering in the counter matter. To achieve a good velocity resolution, the radiation angle has to be reduced, yet the number of photoelectrons must be sufficiently large to gain the detection efficiency required. Under the condition that the main contribution to the resolution is determined by the dispersion of the refractive index in gas (i.e., in well collimated beams with angular spread less than 10^{-6}) a counter about 200 m long with dispersion compensating optics is sufficient to separate $E = 3$ TeV kaons and pions.

Recently, the application of Cherenkov counters for measurement of the velocities and angles of a few particles at a time has started. As to their principle of operation, they are similar to differential ones, yet with a significant difference in that instead of a diaphragm selecting light emitted in a definite angular interval, they employ a system of PMs to measure the Cherenkov radiation angle. The Cherenkov light is detected by a large number of small-scale PMs or special PMs that permit the identification of the point at which light strikes the photocathode. The velocity resolution of 10 m long counters of this type is $3 \cdot 10^{-6}$; this makes it possible to separate pions and kaons of an energy up to 150 GeV. The basic novel feature of this

counter is an option of simultaneous detection of a few particles.

Transition Radiation Detectors

The velocity of ultrarelativistic particles can be measured with the help of the transition radiation at the interface between two media. This radiation has a strong directivity, $1/\gamma$, its intensity grows linearly with γ, and the characteristic energy of γ-quanta used for detection is about 1 KeV. Since about 10^{-2} photons are emitted at one interface, this makes it imperative to employ a radiator consisting of about 10^3 foils. To form transition radiation each foil has to be sufficiently thick ($\simeq$ 0.03 mm), in which case the total thickness of the radiator matter will amount to $\simeq$ 3 cm. Materials with the minimal Z are to be used to avoid photon absorption. To detect γ-quanta xenon-filled proportional chambers or other detectors of X-ray radiation are used.

A detector of this type is actually a threshold device because the cross section for photon absorption shows a sharp increase with a decrease in their energy (for example, if a lithium foil radiator is used, only particles with $\gamma > 2 \cdot 10^3$ are detected). To achieve spatial separation of the transition energy photons and the particle itself, use is made of the natural divergence of transition radiation or of particle deflection in the magnetic field. This technique is gradually becoming available in practical form in physics experiments.

Detectors of Synchrotron Radiation

An electron passing through a magnetic field emits energy $\propto E^2B^2$. Thus, an $E = 0.1$ TeV electron which has transversed 5 m of 20 kG magnetic field will emit 20 photons of 10 MeV energy. This radiation can be detected in a fairly simple way by means of

conventional counters. Application of synchrotron radiation has prospects for future electron beams in proton accelerators.

Ionization Measurements

The measurement of ionization losses in the region of relativistic rise enables us to identify charged particles (pions, kaons, protons) in the 5-100 GeV/c momentum range. Above this energy ionization losses reach a plateau due to the density effect. The difference in losses for particles of various masses is small, $\simeq$ 10%, therefore the detector should have a high energy resolution. Besides, due to large fluctuations of ionization loss, multiple measurements are necessary to determine the primary ionization. Gas gaps of each sampling should be at least 5 cm thick so that the measurement at each point on the track can have a low statistical fluctuation and the number of samples should be about 150. Early detectors of this type have recently been tested successfully.

Time-of-Flight Measurements

The difference in time-of-flight on the base L of particles with masses M_1 and M_2 equals $(M_1^2 - M_2^2) \cdot L/2E^2c$ (note that for this technique $L \sim E^2$). For antiprotons and antideuterons the difference is, for instance, $2\ 10^{-11}$ sec on a 1 km long base with E = 0.5 TeV. Presently existing scintillation counters have a time resolution down to 10^{-10} sec, which is an actual limit for a scintillator-PM system. In parallel-plane spark counters comprising one semiconductor, time resolution less than 10^{-10} sec can be achieved. Such detectors can be applied for detection of comparatively slow secondaries.

b) The Measurements of Charged Particle Coordinates and Momenta.

To determine the momentum of a particle above 1 TeV an improvement in the accuracy of measuring its trajectory upon deflection in a magnetic field is necessary. In this case the limited possibilities to increase both the value of the magnetic field and the path length of the particle traversing it are to be considered. Below we shall discuss the capabilities of two types of track detectors mostly used nowadays.

Drift Chambers

The basic advantage of these detectors is a small number of signal channels per unit of area and their high spatial resolution (better than 0.1 mm). The counting rate for short lengths of signal wires is constrained by space charge and for large lengths by the signal duration at the amplifier input, and, as a result, by a flux of up to 10^6 part/sec per wire (a typical wire spacing in drift chambers is 10 cm). With large drift spacings one should also take into account the drift time imposing additional limitations on the admissible count. The presently achieved accuracy of measuring the coordinates in drift chambers can be improved to $\simeq$ 0.05 mm.

At present these chambers are an optimal detector in cases when large areas (tens of square meters) are necessary to be covered and particle fluxes do not exceed 10^5 part/sec per wire.

Proportional Chambers

A typical spacing of signal wires in a proportional chamber is 2 mm. Therefore 50 times as much particle flux can enter a proportional chamber as compared to a drift chamber. There are

possible further improvements of wire chambers, which will probably make their counting rate still higher.

The accuracy of particle track localization in proportional chambers is $\simeq$ 0.3 mm in a conventional operating mode. With read-out of an induced signal, accuracies better than 0.1 mm are achieved. However, in this case there appear difficulties in making big chambers.

The space resolution of gas coordinate detectors is limitted by appearance of delta-electrons resulting in the center of gravity of an electric pulse biased with respect to the particle trajectory. This value lies in the range of 0.01 mm, which seems to be the limit for gas detectors.

The aforementioned accuracies of coordinate measurements are sufficient for comparatively precise measurements of particle momenta with the help of a standard method of magnetic analysis. This method will still be basic at a 2-5 TeV energy accelerator as well. With reasonable lengths of magnetic path (tens of meters) and a 100 m deflection basis, the momenta of the highest energy particles will be measured with an accuracy better than 1% (yet, one should keep in mind that 1% of 5 TeV is 50 GeV).

c) <u>γ-Quantum Detectors. Calorimeters</u>.

For measuring particle energies and coordinates, particular importance will be attached to calorimeters. With an increase in the collision energy the multiplicity of secondaries is rising, the final states contain tens of particles, and π^0 mesons and other particles decaying into γ-quanta make up one-third of them. Therefore a systematic study of interactions in this energy range is impossible without devices simultaneously detecting a great

number of γ-quanta. A promising technique using a Cherenkov counter hodoscope has recently been developed, which provides an opportunity to carry out highly accurate simultaneous measurements of the coordinates and energies of a large number of γ-quanta and reconstruct masses and coordinates of the decay particles. The accuracy of these detectors is improved with energy, $\sim 1/\sqrt{E}$, and at 2 TeV it will be: $\Delta E/E < 1\%$, $\Delta X < 1$ mm, $\Delta M/M < 1\%$.

The calorimeter dimensions are determined by the shower length and have only a logarithmic growth with energy. This is a most important advantage of calorimeters, which makes them the basic instruments at energies above 1 TeV. They will play an important role also in detection of hadrons. In this case, a conventional device will be a sandwich comprising an array of heavy plates, whose total thickness will be about 10 collision lengths. A scintillator, liquid argon, or a high pressure inert gas can be used as an ionization detecting medium. If uranium plates are employed, this detector will be 1-2 m long, the energy resolution for 2 TeV hadrons will be a few percent, and the space resolution (providing a detector of a hodoscope type is used) will be better than 1 cm.

The counting rate limit of a calorimeter utilizing a sufficiently fast-operating scintillator is determined by delayed radiation (neutrons from nuclei) and is dependent on the detection threshold. If the threshold is a few GeV, such a detector will be able to operate in a flux of 10^7 pps.

d) Detectors of Short-Living States.

In recent years search for particles with a life-time of

10^{-13}-10^{-14} sec has resulted in an acute necessity for detectors to examine particles with a range of 0.01-0.1 mm prior to decay. For these purposes, photoemulsions are being used, in conjunction with electronic methods which identify particles and localize the interaction point in order to reduce the volume of scanning. This technique will also be improved in the future, but decisive progress in this direction is connected with the development of methods of electronic detection of short-lived states.

To solve this problem a great number of detectors is being developed at the moment. These include:

- high pressure streamer chambers;
- streamer chambers with detection of laser light scattered on the ionization centers;
- liquid argon ionization chambers with very narrow ($\simeq$0.01 mm) strip electrodes;
- liquid chambers with ionization transfer into gas for further amplification and detection;
- electroluminescent detectors;
- solid detectors with high space resolution.

The development of techniques in this direction may prove to be useful in solving other experimental problems.

3. NEUTRINO EXPERIMENTS

a) Neutrino Beams

The two types of neutrino beams used in the presently existing accelerators (wide band and narrow band beams) will also be used in superhigh energy accelerators. Though the highest

energy region will become most interesting for neutrino research, the low energy one, where the maximal neutrino flùxes are achieved, will also be important for a long period of time. At superhigh energies the idea of tagging neutrinos in specialized neutrino beams (dichromatic beams of muonic neutrinos) will probably become possible. Tagging will allow a more precise measurement of neutrino energy and will avoid ambiguity (pion or kaon neutrinos). However, the problem of tagging is rather complicated due to a high level of detector loading (more than 10^8 muons per cycle).

Beams of electron neutrinos will also be of great interest. Electron neutrinos (less than 1%) present in usual beams of muonic neutrinos are scarcely suitable for a detailed study of their interaction. A sufficiently pure beam of ν_e from K decay ($\nu_e/\nu_M = 1.4 : 1$) can be obtained by forming a neutrino beam from a neutral one.

b) Neutrino Detectors

Bubble Chambers

With an increase in the energy and intensity of neutrino beams a "pure" bubble chamber looses its capabilities as an efficient instrument. At the already achieved neutrino energies there arose a necessity to equip the big existing chambers with peripheral identifiers of particles. With further increase of the accelerator energy by an order of magnitude, the momenta of highest energy particles will be practically unmeasurable. Particles produced in neutrino-nucleon interactions lies within a very narrow cone; this does not allow one to identify and to separate them spatially. However, bubble chambers will remain as long-term instruments for vertex detection in combined systems

(see below).

Detectors of Calorimeter Type

Neutrino detectors based on a hadron calorimeter and a muon spectrometer made of magnetized iron are rather promising at superhigh energies. In such detectors, separate hadrons cannot be detected, but the energy of the hadron system is measured with a good accuracy ($\sim 1/\sqrt{E}$ (see above), i.e., a few percent). With a calorimeter containing track detectors there is the possibility of determining the neutrino interaction vertex, the muon angle, and the direction of the total momentum of hadrons (with an accuracy $\simeq 1/E$ (TeV), mrad).

Identification of muons and measurement of their energies in the 1-10 TeV range remains possible by using conventional (for neutrino experiments) magnets made of magnetized steel (about 20 m long). In this magnet, the sagitta of a 2 TeV muon will amount to 15 mm, and the measuring accuracy of a muon is basically determined by multiple scattering.

A possible version of the experimental setup to study neutrino interactions in the TeV energy range is a $\simeq$ 20 m long iron-filled calorimeter (about 1,000 tons) followed by a muon spectrometer. The research quality of high energy neutrino interactions will be noticeably higher owing to an improvement of the energy resolution for hadrons and muons. While studying deep inelastic neutrino scattering, it will be possible to ensure an appreciably better accuracy in measuring the variables X and Y. The study of processes with production of a few muons at superhigh energies is more promising because backgrounds from pion and kaon decays will decrease with energy. In a detector of this type one

can find an intermediate W-boson (from $\mu^+\mu^-$ events in a neutrino beam without energy release into hadrons).

To carry out experiments with electron neutrinos at superhigh energies a calorimeter detector is necessary, which can efficiently separate electromagnetic showers from hadronic ones and is also sensitive to the muonic component from muon neutrino interactions in the detector. Such a detector can, for example, consist of sections of a scintillator alternated with those of heavy shower detectors.

Hybrid Detectors

A hybrid detector which is a combination of nuclear emulsion target and a magnetic spectrometer can be used in wide band neutrino beams. Particle momenta are measured and coordinates inside the nuclear stacks predicted with the help of track detectors, which are a part of the spectrometer. Usage of additional detectors, i.e., hadron calorimeter, shower detectors and muon identifier, will allow the identification of secondary particles. Such a combined facility will enable, for example, a search for new short-lived particles.

Finally, a hybrid detector with a bubble chamber as a target and external electron detectors is a promising facility to study neutrino interactions at superhigh energies. Such a detector is capable of providing complete information on each neutrino event. However, the existing big bubble chambers having too much matter in the path of secondaries (chamber walls, magnet windings) will have to be modified, otherwise particle identification is difficult.

4. CONCLUSION

Above we have attempted to analyse briefly the features of experimental setups in the TeV energy range. We were interested mainly in whether this great step in the energy range, as opposed to that already handled by physicists, will lead to the necessity of a new approach in experimental methods and will require particle detectors of a new type. As shown in this survey, present day methods permit successful detection and identification of particles in the TeV range. The main difficulty lies in a new level of requirements imposed on physics research rather than in high energy itself.

A successful solution of the experimental problems will require the creation of very big facilities. Their information collection capability will become far larger at the cost of increase in the number of detecting elements (the number of wires in the chambers, counters, amplifier channels, etc.) as well as due to detectors of different types applied in one installation. Within the decade separating us from constructing accelerators of the next generation, experimental techniques will be developed significantly and undoubtedly they will not slow down experimental advance in high energy physics.

Table 1.

a) Particle Identification Methods

Type of Detector	Energy Range for π and K Identification	Principle Formulas	Notes
Threshold Cerenkov counter	$P < 1$ TeV	$\ell \sim E^2$	$\ell = 1$ km
Differential Cerenkov counter	$P < 3$ TeV	$\ell \sim E^2$	$\ell = 200$ m $\Delta\theta < 10^{-6}$
Multicell Cerenkov counter	$P < 0.2$ TeV	$\ell \sim E^2$	$\ell \simeq 20$ m can measure the velocity of several particles.
Transition radiation	$P > 0.2$ TeV	$n_\gamma \sim \gamma$	The required path is $\simeq 10$ m, 2g of material on particle trajectory.
Ionization measurements	0.005 TeV $< P < 0.2$ TeV	$I \sim \ell n_\gamma$	$\ell \simeq 10$ m
Synchrotron radiation	$P > 10$ eV	$E_\gamma \sim E^2B^2$	Only for electrons.

b) Particle Energy Measurements

Device	Parameters	ΔX	$\Delta\theta$	ΔP for 1 TeV
Magnetic Spectrometer	B x L = 10T x m path $\simeq$ 20 m	0.1 mm	10^{-5}	$\frac{\Delta P}{P} \sim P$ $\frac{\Delta P}{P} \simeq 0.5\%$
Lead-Glass detector	$\ell \simeq 1$ m path $\simeq$ 100 m	1 mm	10^{-5}	$\frac{\Delta P}{P} \sim 1/\sqrt{P}$ $\frac{\Delta P}{P} \simeq 0.5\%$
Hadronic calorimeter	$\ell \simeq 2$ m path $\simeq$ 100 m	10 mm	10^{-4}	$\frac{\Delta P}{P} \sim 1/\sqrt{P}$ $\frac{\Delta P}{P} \simeq 2\%$

PARTICLE DETECTORS AND THEIR LIMITATIONS

George Charpak
CERN, Geneva, Switzerland

Introduction

The scaling up of experiments from a few hundred GeV to energies one or two orders of magnitude higher leads to problems very dependent on the type of accelerators foreseen, colliding beams or fixed targets, and on the type of experiments envisaged.

Some of the questions which can be raised in the field of particle detectors are the following:

- Limits in detection accuracy. Can we locate the particles with enough precision to make momentum measurements by magnetic deflection feasible over reasonable lengths?

- Limits in particle separation. Can we separate particles often bunched into narrow cones ?

- Particle identification. With rising γ's can we utilize the old arsenal or are new methods available?

- Calorimetry. Can we still measure the total energy of particles with enough accuracy to single out accurately different processes?

- Data handling. The considerable extension of the scale of the experiments, both in space and in complexity, may force us to new conceptions in the data treatment. Can we already elaborate possible new approaches from the latest available components of the electronics industry?

In addressing ourselves to these questions our working group composed of W. Willis, W. Lippach, B. Knaff, L. Lederman, J. Sandweiss, P. Lehmann.

K. Lanius, and G. Charpak, decided that while it is impossible with our limit of focus to exhaust these questions, a few reports on the state of the art and the foreseen developments on some selected topics may be useful to a formulation of ideas exchanged in these fields.

The following reports will be made:

- Limitations in spatial resolutions and rates in some particle detectors, by G. Charpak.

- Particle identification and energy measurements at growing energies. by W. Willis.

- High accuracy vertex detectors for the measurement of short-lived states, by K. Lanius.

SOME LIMITS IN THE LOCALIZATION OF CHARGED PARTICLES

G. Charpak
CERN, Geneva, Switzerland

I. Multiwire Chambers

Localization accuracy

Each gap has intrinsically a two dimensional capability with quite different properties.

(a) For large chambers the closest practical wire distance is 2 mm. For 20 × 20 cm it is about 1 mm. At atmospheric pressure we have an example of 12 × 12 cm^2 with 0.5 mm spacing. It is very difficult to operate it and the reduction in gaseous gain and use of low noise amplifiers has led to the necessity of 50 nsec resolution, instead of 30 nsec for 1 mm wire spacing. It is excellent indeed for particle separation.

At high pressures the situation is different (J. Sandweiss) and 4 wires/mm can be operated, with very small surfaces, so far.

The recent progress in the reflection of the pulses induced on the cathodes and neighboring wires (CERN and Brookhaven) leads to a lifting of the right-left ambiguity and a subsequent gain in accuracy by a factor of 2. Thus 1 mm wire spacing leads to $\sigma \sim 150$ μm!

(b) The measurement of the coordinate along the wire permits accuracies of $\sigma \sim 50$ μm with time resolutions of 30 to 50 nsec.

It seems realistic to foresee the utilization of square meter chambers with this readout, thus competing directly with the drift chambers. The advantage is in the much better occupation time, in the two-dimension character of every chamber with a good accuracy in all directions. The

disadvantage is in a poorer separation, however. It is of the order of the anode-cathode gap ~ 6 mm for large chambers.

A combination of drift time and centroid readout would permit the construction of large planes within two-D 100 μm accuracy. This fulfills precisely the needs that can be forseen in scaling up some types of experiments for 400 GeV to 20,000 GeV, as illustrated by the example given by L. Lederman about the dilepton experiment. In this particular case the reduction in magnet volume (due to the contraction of the lateral dimensions), combined with 50 μm to 100 μm detectors leads to a reduction in the cost of the spectrometer.

Rate limitations

They come from two factors:

- The anode-cathode gap of about 6 mm leads to occupation times of about 150 nsec which are the main source of accidentals for large chambers.

- The space charge limitations due to the slow motion of positive ions is about 10^4/sec mm of wire. This is the dominant factor for small surface detectors with high rates and high multiplicities in narrow cones. We will see that this is precisely the effect eliminated by present development of multistep chambers.

Particle separation

It is a function of wire separation and can be estimated to two or three wires. For the coordinate along the wire it is of the order of anode-cathode gap, i. e. ~ 6 mm for large chambers.

II. Drift Chambers

An accuracy of ~ 50 μm is claimed at atmospheric pressure. The work of Heintz et al. and Dolgoshein et al. show that at high pressures accuracies of about 15 μm can be reached. This is due to the reduction in range of the δ-electrons. This improvement can also possibly be exploited in the charge centroid method. More research is indeed required to investigate the practical difficulties in exploiting this intrinsic accuracy but it seems a safe path if such accuracies are requested.

The track separation in drift chambers is 2 mm. It is probably by far the best that can be obtained in large surface detectors, since with MWPC the wire spacing has to be > 2 mm. It may appear as the most important property justifying the drift chambers. It will also scale down at higher pressures (with thinner anode wires). This particle separation power is the main advantage over centroid readout chambers which have the serious advantage of better resolution times.

III. Multistep Gaseous Detectors

Recent developments at CERN have shown that it is possible to pre-amplify by a factor of ~ 1000 the initial ionization in a parallel grid gap and to transfer around 20 % of the electrons to various proportional detectors: wire chambers or parallel grid gaps, without any amplifying wires. The first advantage of this scheme is that it permits amplifying in the final stage only selected events thus eliminating the space charge limitation introduced by the more intense primary beam.

In the case of two parallel grid gaps the intrinsic jitter due to wire spacing in MWPC is eliminated. The presently attained time resolution of

10 nsec (FWHM) is probably preliminary to the final stage that can be reached by further research. The fantastic time resolution reached by parallel plate counters of various kinds (~ 100 psec for the parallel plate spark counter developed at Novosibirsk, ~ 200 psec for low pressure counters and with heavily ionizing particles) is in this respect very stimulating.

The possibility to drift the final electrons through successive readout wire grids external to the amplification region opens the way for convenient 2-D read out in non-planar structures since the exact parallelism of the readout surfaces is not a must anymore.

The spatial accuracy with the multistep detector has been measured to be 100 microns FWHM for charged particles. The separation power is degraded by the lateral propagation specific to the amplification process (~ 2 mm).

Single electrons are easily detected and localized and this offers promising features for the detection of the Cerenkov rings.

IV. Exotic Developments

Although the above mentioned developments in gaseous detectors offer promising perspectives in fulfilling some needs foreseen with higher energy machines in terms of spatial resolution or rate limitations they differ from severe drawbacks when very complex configurations with huge multiplicities are contemplated. The need to multiply the number of wires poses serious problems of reliability for large size systems. It is worth mentioning at this stage the project at Brookhaven of a 250,000 wire system. Each wire is inbedded in an independent thin aluminum tube, thus improving

considerably the reliability by making the breaking of individual wires insignificant. The high accuracy in localization is obtained from drift time measurement and the mass integration of electronic circuits permits a full exploitation of all the information at a reasonable cost: time measurements and pulse height measurements whose importance is great as can be seen from Willis's report. However, different solutions are under investigation and may prove most important 10 years from now.

Solid state avalanche detectors of the type developed by Ch. Gruhn (Los Alamos) aim at 20 μm resolution with time resolution well below 1 nsec. The particle separation will be < 100 μm.

Scintillator filaments of 100 μm, with large attenuation lengths, coupled to silicon photodiodes (Willis) should permit an enormous gain in resolution, separation, complexity. Various other daring undertakings are listed in the reports of K. Lanius and W. Willis showing that by the time the machines are built the landscape may have changed in particle detectors since the changes there can be more rapid than in machine construction!

Particle Identification and Energy Measurement at High Energies

W. Willis

CERN, Geneva, Switzerland

1. Electromagnetic Radiation

We consider the case where

$$\beta \to 1 \quad , \quad \text{e.g.} = \beta = 0.9999999.$$

Therefore, we need an interferometric method to compare βc with c. When we think of interferometers, we think of gratings. So did Purcell (Smith and Purcell, Phys. Rev. 1953, p. 1069). The sketch shows a particle travelling parallel to the surface of a grating in a medium with index of refraction n.

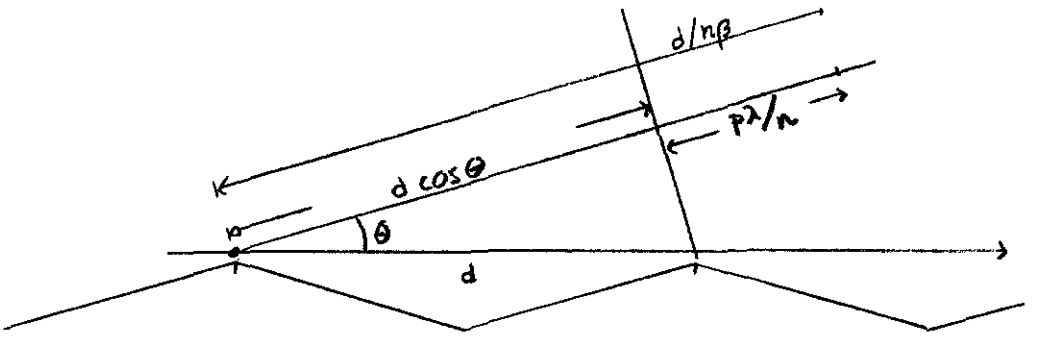

The condition for constructive interference of order p is

$$p\frac{\lambda}{n} = \frac{d}{n\beta} - d\cos\theta .$$

For p = n = 1

$$\cos\theta = \frac{1}{\beta} - \frac{\lambda}{d}$$

or

$$\theta^2 \simeq \frac{2\lambda}{d} - \frac{1}{\gamma^2} \qquad (1-\beta \simeq \frac{1}{2\gamma^2}).$$

A dipole e oscillates $1/\alpha$ times to make one photon per octave.

To have θ sensitive to γ, we need $\gamma^2 \sim \lambda/d$. Then, we get a yield of photons

$$\frac{dN}{dx} = \frac{\alpha}{d} \cong \frac{\alpha}{\gamma^2\lambda} \qquad \text{per octave per cm.}$$

Compare the above with the case for which p = 0 and n>1, Cerenkov radiation

$$\cos\theta = \frac{1}{n\beta}$$

$$\frac{dN}{dx} = \frac{d}{\gamma^2\lambda} .$$

This is the same result. In this way, Purcell (1961) concluded that a grating interferometer has no advantage over a Cerenkov interferometer. But this is not quite right; Garibian (1961) pointed out that a grating also works with x-rays, where n<1, even if the particle passes through the grating material

For a Cerenkov radiator with $\lambda \approx 10^{-5}$ cm, we need ~50 photons. For an x-ray radiator with $\lambda \approx 10^{-8}$ cm, we only need ~10 photons. Overall the x-ray radiator is shorter by a factor of 5000.

A practical grating is made of foils ("transition radiation"). We want $Z \sim 1$, since absorbtion goes as $Z^{3.5}$. We have to consider the effect of n:

$$n = 1-\frac{\omega_o^2}{\omega^2} \qquad (\omega_o \sim 10 \text{ eV}).$$

In order that the interferometer be sensitive to $1/\gamma^2$, we need $1-n \sim 1/\gamma^2$; therefore

$$\omega \sim \gamma\omega_o .$$

For $\gamma = 10^3$, $\omega \sim 10$ keV, which is all right. But $\gamma = 10^2$ implies $\omega \sim 1$ keV - a bad region in which to work.

The formula we have given is for a threshold detector, Cerenkov or TR. A differential detector measures θ - "ring imaging".

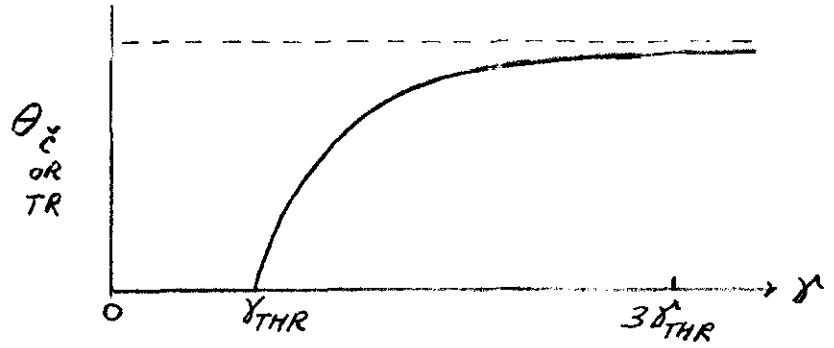

If we measure θ to 1%, we can distinguish $3\gamma_{THR}$ from ∞. The <u>effective</u> threshold is 3 times higher, but the $\frac{dN}{dx}$ is 3^2 times greater than a detector with γ_{THR} raised by 3. However, we need more photons to define the ring, and the length required is perhaps reduced by a factor of 3. If the radius can be determined with higher precision as in the DISC counters, the length required is reduced still more. In TR, the ring is fuzzy because of broad bandwidth used, and strong variation of n:

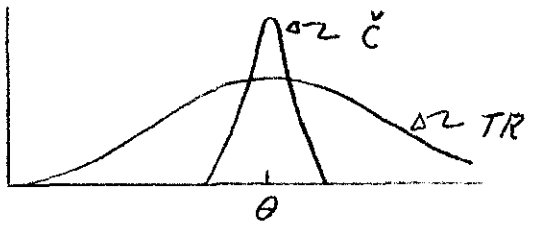

The θ measurement requires no more photons, rather fewer, because of the <u>elimination</u> of the signals due to the <u>track</u> <u>itself</u>, and the advantage in length is again ~3.

Note also that π-e separation requires radiation from the e be detected efficiently, but K-π etc. separation over an appreciable momentum band requires dealing with π near threshold giving fewer photons and K's just above threshold, giving a few photons. This requires more length for a threshold detector.

The Cerenkov picture is summarized in Figure 1 by giving the length L required for identification of particles with a given γ. We include a line for the DISC type which determines $\Delta R/R$ with high precision, but requires a highly collimated particle beam. Devices with moderate solid angle, such as spot focusing detectors, can be built with lengths in between DISC and ring imaging detectors.

Similar details affect TR detectors. Here one has a choice of keeping the photon bandwidth at ~10 keV, convenient for PWC Detection, or allowing it to grow with γ. The latter is more natural from the radiator design aspect, and leads to an L which grows only $\propto\gamma$. The former requires special foil fabrication to lower the foil density, and thus ω_o, and gives $L\propto\gamma^2$.

As γ is lowered below 1000, severe problems are encountered:

The photon energy falls and self absorption in the radiator becomes important.

The foil thickness becomes just a few microns, but it is more important than ever to use a low Z material.

A very practical radiator can be made with 30 μm lithium foils, 20-40 cm thick, giving ~10 photons for γ = 3000. These have been used for electron detection at the ISR, the SPS Y-beam, and the BNL-MPS. An Aachen-BNL-CERN-Moscow collaboration is now attempting to make a γ = 600 radiator based on 50 cm of 3 μm Li-H dust, with a volume fraction 10%. Calculated performance is shown in Figure 2.

For $\gamma \gtrsim 10^4$, the TR radiator may not be the optimum choice. Consider synchrotron radiation:

$$\frac{dN}{dx} = 1.2H \frac{d\lambda}{\lambda} F(\omega) \quad \text{per meter}$$

where H is in Tesla and $F(\omega)$ is of order unity below a cutoff.

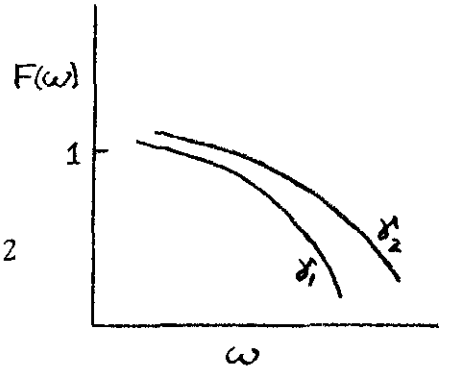

$$R \equiv \frac{\text{synchrotron radiation}}{\text{transition radiation}} = \frac{1.2}{\alpha} H\lambda\!\!\!^{-}\gamma^2$$

$$= 1 \text{ at } \gamma_s = \sqrt{\frac{\alpha}{1.2}\frac{1}{\lambda\!\!\!^{-}}} \quad .$$

For $\omega_{T.R.}$ = 10 keV and H = 1 Tesla, γ_s = 20,000. Most important - note that dN/dx does not depend on γ! If we take H = 3T, then L - 3m produces 10 photons for $\gamma = 10^4$ up to ∞.

The other detectors depend on γ <u>only</u>, but for synchrotron radiation, we must consider the mass as well, to make sure that $E_{crit}(\text{eV}) = .9\text{x}10^{-4}\ \frac{\gamma^2 H}{m}$ (T, MeV) is in a detectable range, say >1 keV. π's at γ_s are ok (x-rays), k's at $\gamma = 10^4$ give radiation which is too soft, unless H is $\gtrsim$ 6T. (The optical region is not attractive with present technology.)

A detector would look like this:

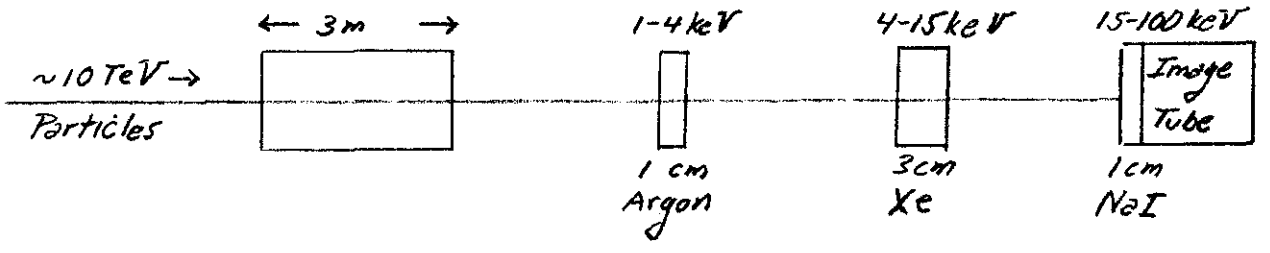

The combination of the three spectral detectors will allow k/π/p separation above 3 TeV, up to ~50 TeV!

It will be noted that there is a <u>gap</u> in the γ coverage of the detectors described so far $200 \lesssim \gamma \lesssim 600$, at least for large

solid angle coverage (a DISC can go to $\gamma = 600$). If we want to do the job in ~1 m, our general dimensional scaling laws developed at the beginning of this paper suggest we should use photons $\omega \gtrsim \gamma\omega_0$ ~few hundred eV. But in this energy region,

(1) n varies wildly,

(2) there is very strong absorbtion.

It is therefore impossible to make an interferometer with transmission through matter in this region.

Gratings in vacuum could be used. No practical method has been suggested. Something cruder must be done. The "production" of virtual photons in this (100 eV) energy range is increasing linearly with energy; this interacting with an exponential tail of the atomic wave function, produces a $\ln \gamma$ rise in ionization. This is weak compared to the threshold shapes $(\sqrt{\gamma^2-\gamma_0^2})$ of our interferometers, but this is to be expected.

Furthermore, the ionization distribution is fluctuating in a strongly non-gaussian manner. Many (~200) samples are required, to achieve sufficient measurement accuracy. To carry that out in a small L, allowing 10-20 primary ionizations/sample, one pressurizes the gas. But polarization in a dense gas shields the field and cuts off the increase at large distance, i.e. large γ. The L required goes as

$$L \propto (\gamma_{max})^2.$$

We now summarize all this in Figure 3.

2. Calorimeters

The length of a calorimeter scales as $\ln E$, leading to the following table

length (m)		E	
		10 GeV	10 TeV
material	F_e	2	4
	U	1	2

Regarding hadron energy resolution, three contributions should be noted:

(a) Sampling: if $\sigma \propto E^{-\frac{1}{2}}$, then for Fe with 1.5 mm plates, $\sigma \sim 8\%/\sqrt{E_{GeV}}$. At 10 TeV, the energy resolution would be ~0.08%!

(b) Binding Energy Fluctuations: (see Figure 4)
This effect probably leads to resolution scaling according to

$$\sigma \propto \frac{1}{E^{\frac{1}{2}} \ln E}$$

and may be important.

(c) Technical limits:

(i) Photomultiplier tubes ~1-2%
drift
rate effect
uniformity

(ii) Ion chambers - 0.1-0.2%
liquid argon
gas
other

(iii) Radiation damage
scintillator dies after $\sim 10^6$ rads.

Outlook: The $\ln E$ term may be important in Fe; in U_{238}, the binding energy is already down to $25\%/\sqrt{E}$. It could be that $\sigma_{Hadron} \sim \sigma_{sampling}$ at 10 TeV, even in Fe. We need measurements at 400 GeV. In any case, the "technical limits" probably dominate.

Consider the rate limitations. It's hard to get below 20-30 ns with the scintillator - photomultiplier combination. In ion chambers, either gas or liquid argon, the collection time is ~100 ns. But, as a new idea, how about the use of highly poisoned liquids? Typical current signals might appear as sketched below.

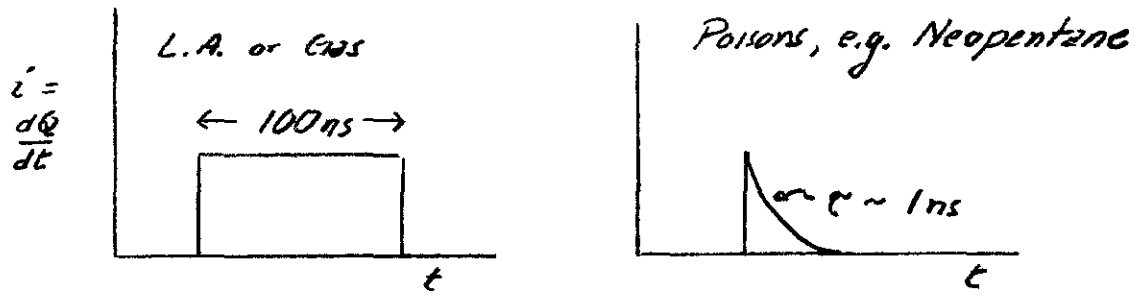

In the poisoned case, Q is down by ~100, but that is ok for the TeV range.

Can calorimeters work with pile-up? (See "Impactometer" 1971). We are measuring power laws; pile-up produces Gaussians.

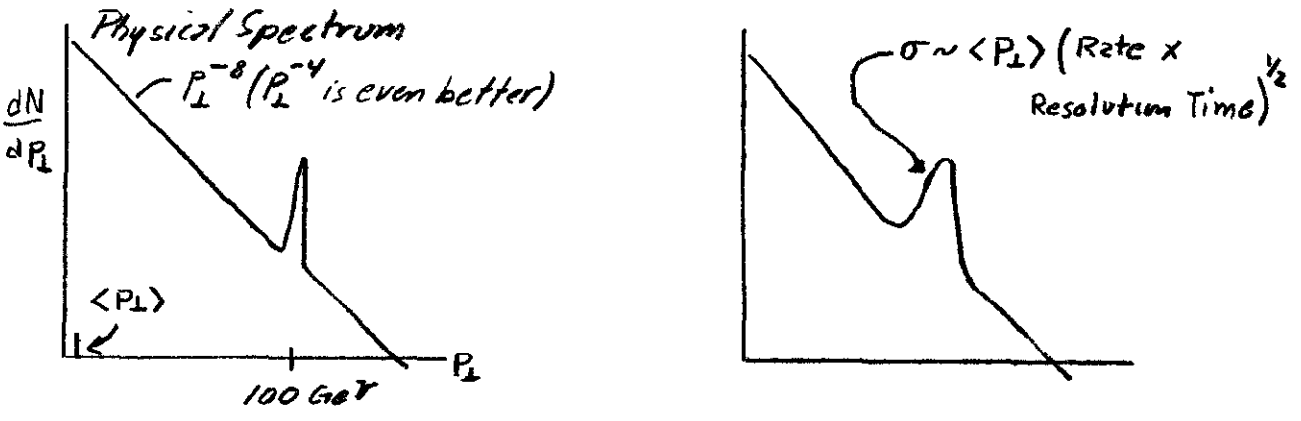

If the rate is $\sim 10^{10}$ Hz and $\tau \sim 10$ ns, then $\sigma \sim 3$ GeV, which is ok.

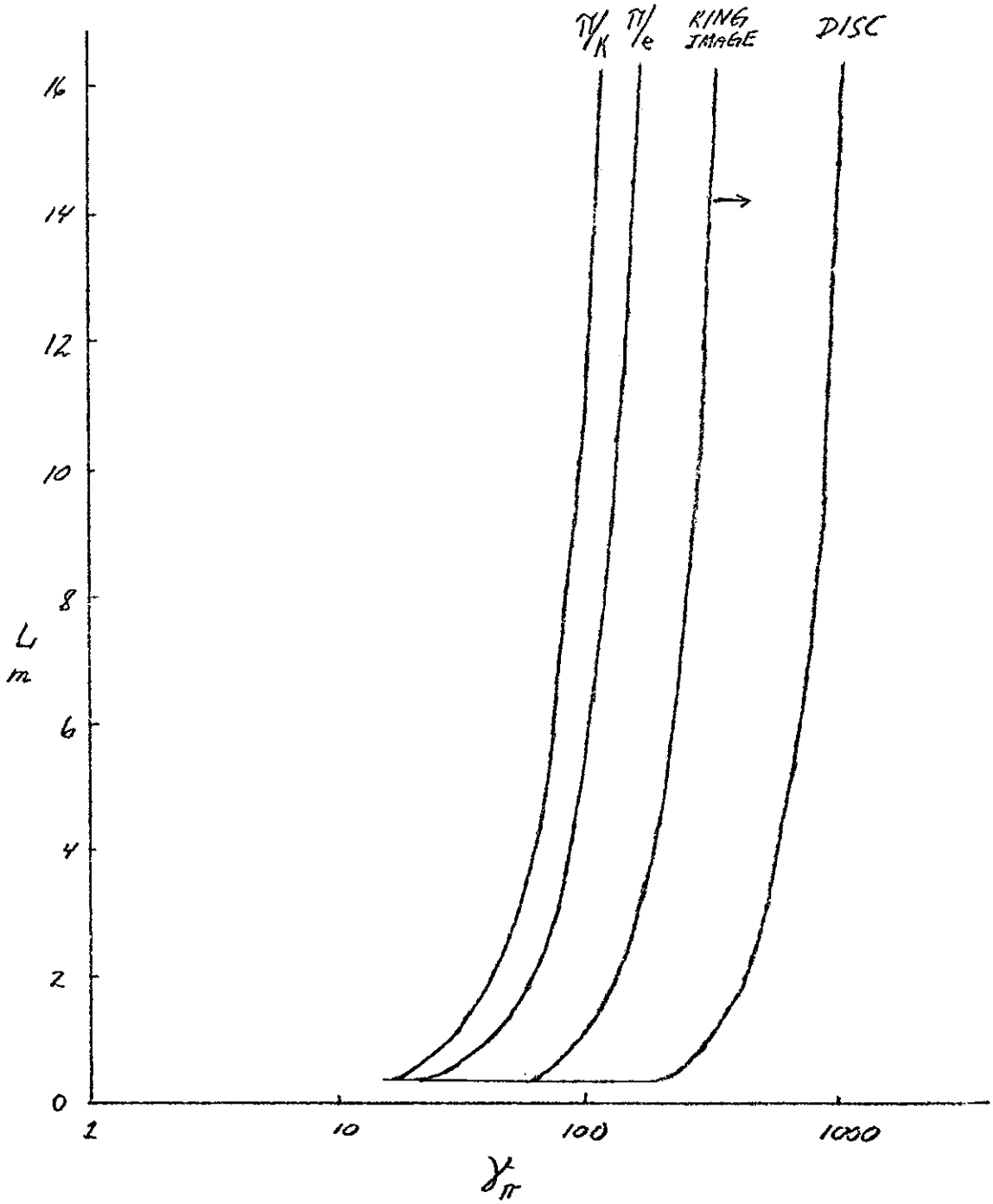

Fig. 1

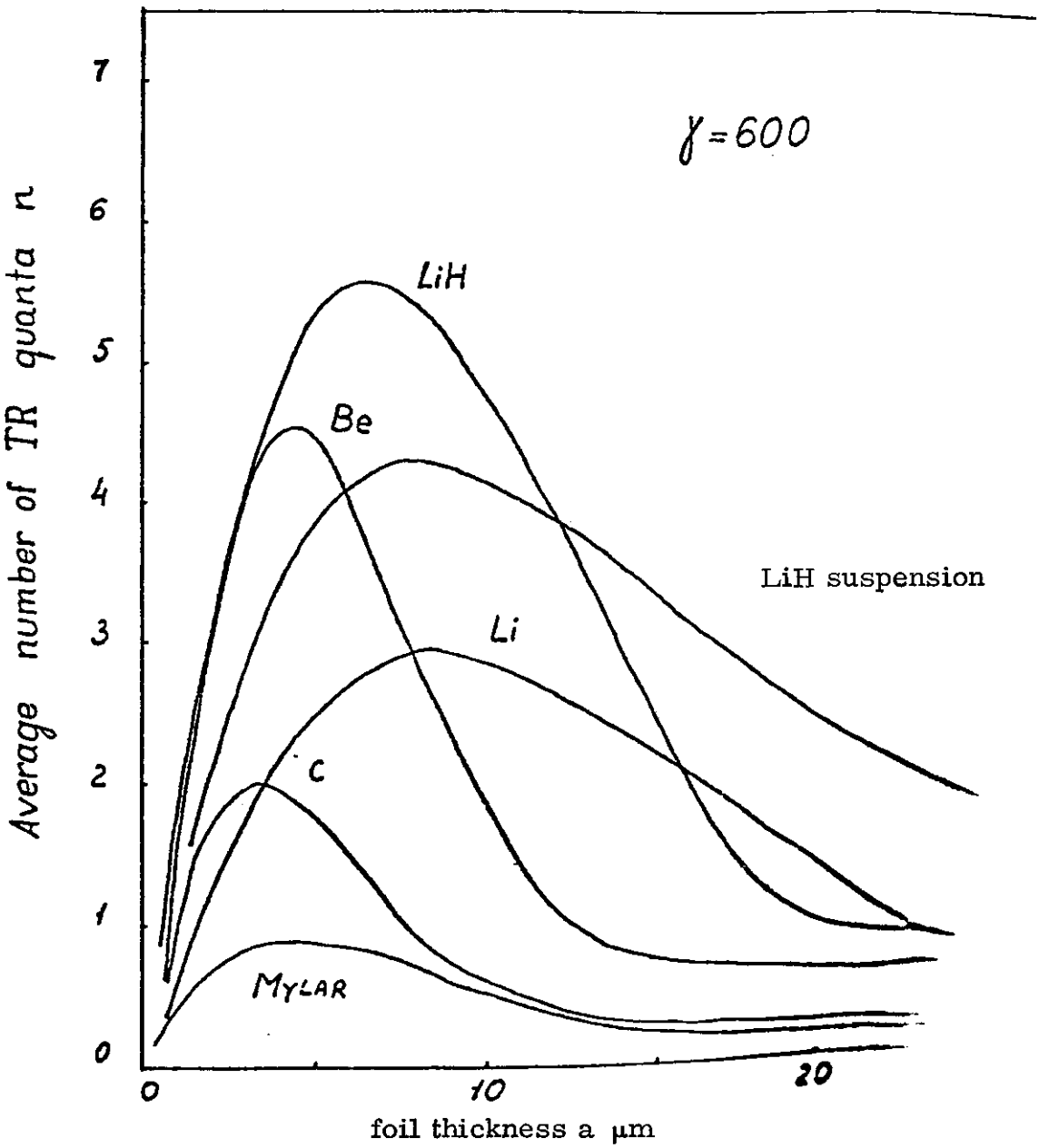
γ=600
LiH
Be
Li
C
MYLAR
LiH suspension
Average number of TR quanta n
foil thickness a μm
0
1
2
3
4
5
6
7
0
10
20

Fig. 2

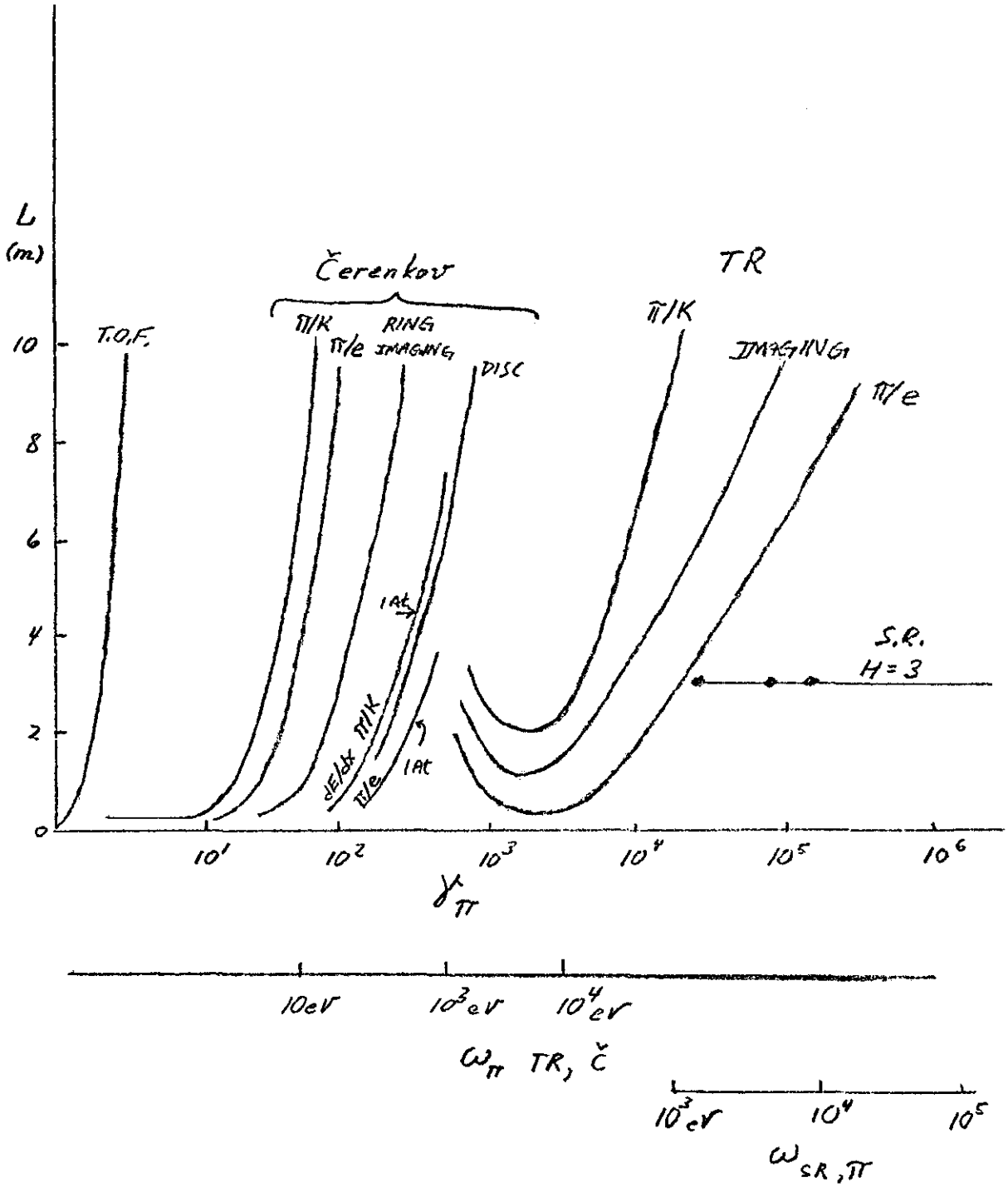
L
(m)
10
8
6
4
2
0
T.O.F.
Čerenkov
π/K
π/e
RING
IMAGING
DISC
TR
π/K
IMAGING
π/e
1At
dE/dx π/K
π/e
1At
S.R.
H = 3
10¹
10²
10³
10⁴
10⁵
10⁶
γπ
10eV
10³eV
10⁴eV
ωπ TR, Č
10³eV
10⁴
10⁵
ωSR,π

Fig. 3

High accuracy vertex detectors for the measurement of short living states, by K. Lanius

After the discovery of the charmed particles and the τ-lepton, there was a strong motivation to improve the spatial resolution of vertex detectors, to the point where the tracks of all particles could be observed and the decay vertex spatially separated from the production vertex for each event.

The problem of vertex identification and the correct association of final state particles to the decay vertices is dominated by transverse separation tracks rather than the longitudinal separation of the vertices. To a first approximation the problem becomes independent of the particle momentum since the transverse separation is:

$$\langle \Delta y \rangle \simeq \theta \cdot \ell_{decay} = \frac{p_\perp}{p} \cdot \ell_{decay} = \frac{p_\perp}{mc}(c \cdot \tau) \simeq c \cdot \tau$$

1) Nuclear emulsion

The only well established technique providing spatial resolution in the micron range is nuclear emulsion.

Emulsion, with a position resolution of better than one micron, permits direct observation of particle decays with lifetimes as short as $2 \cdot 10^{-15}$ seconds. In order to localize the events in some extent the emulsions are tagged with electronic spectrometers.

One event which could be interpreted as a charmed particle production in neutrino-nucleus interaction has been observed in an experiment utilizing nuclear emulsions and an electronic tagging system [1].

The advantage of emulsion is clearly resolution but the limitations are considerable:

a) No time resolution. Events cannot be selected using the precise timing information.

b) High event density. All events are recorded in the emulsion because of (a). Therefore in one experiment only a small number of events can be analysed (about 100 - 1000 events).

c) Very time consuming scanning and measuring work.

2) High resolution bubble chambers

As was shown by Fisher et al. [2] a spectrometer containing as its vertex detector a small rapid cycling hydrogen bubble chamber could be used for studying short living particles.

Bubbles begin small (diameter $d < 1\,\mu m$) grow at least until recompression sets in, with $d \sim \sqrt{t}$, where t is the time. Thus by triggering the flash after 10 - 50 μsec bubbles of size $\sim 10\,\mu m$ are produced. The depth of field for an optical system with resolving power of $10\,\mu m$ is $\lesssim 1$ mm. Such a system can in principle be constructed without too much difficulty, provided that the area of the beam plane

over which it is required that interactions be seen is about 10 cm.

In order to allow high resolution with reasonable depth of field a possible way could be the use of holography.

In order to achieve a reasonable number of triggered events the cycling rate has to be sufficient. Bubble chambers which cycle at frequencies up to $\sim$ 50 Hz are currently used or under construction. In the case of a small bubble chamber the extension of the technique by using ultrasonic expansion systems could allow cycling rates in the kilohertz region. The limitation of the cycling rate would be probably the thermal diffusion for recompressed bubbles in liquid hydrogen.

A small heavy liquid bubble chamber was recently tested by Hahn et al. [3]. The chamber operated at a bubble density of 300 bubbles/cm and an apparent bubble size of 30 μm in real space.

3) High resolution streamer chamber

Typical spatial resolution for atmospheric pressure streamer chambers is $\sim$300 μm. The principle used by Sandweiss et al. [4] in designing the high resolution chamber is a scaling rule for avalanche formation in gases. If the gas pressure and the electric field are scaled by a factor s the streamer diameter is reduced by about the same factor s.

At Yale a small high pressure streamer chamber (Ne/He 90/10) at 20 atmospheres was constructed. The streamer diameter is ~50 μm and the width of a track is 150 μm because of diffusion of the seed electron during the time delay between the passage of a particle and the application of the high voltage pulse.

The depth of field for an optical system with resolving power of 50 μm is ~2 mm. In order to reduce flares the chamber was operated at slow avalanche and streamer growth rates. Therefore image intensifier have been used.

Work is in progress in order to get track width ~50 μm by depth of field ~ 2,5 mm with higher pressure (~100 at) and laser firing.

A possible way for future development is the use of laser induced liquid streamer chambers with track width as small as 2 μm. The depth of field for an optical system for a real image of ~2 μm is ~100 μm. Larger depth of focus may be obtained with holographic methods.

4) Liquid argon ionization chamber

An alternative approach which leads to high spatial resolution and which possess all the advantages of electronic detectors is the use of liquid filled chamber. The advantage of the liquid arises from the ~ 800-fold increase in density over that of gas, permitting the use of much smaller thickness, larger ionization statistics, and redu-

ced effect of electron diffusion.

A measurement of the spatial resolution of a small gap liquid argon filled chamber was performed with minimum ionizing particles by Derenzo et al. [5]. Two multistrip chambers with 20 μm strip spacing operating in the ionization mode were used. The anode metallic pattern was done using standard integrated circuit techniques.
Under the best conditions, the spatial resolution for a single strip was measured to be better than 20 μm rms with an efficiency of nearly 100 %.

At present a system of small-gap (2 mm) and wide-gap (up to 35 mm) liquid argon chambers is tested by a Berlin-CERN Collaboration [6].

5) Solid state micro-detector

Solid state detectors have been used mainly in high resolution nuclear experiments. Kanofsky [7] proposed a solid state detector in which the strips along the crystal are built using the standard integrated circuit techniques. The electrodes would be doped in columns along the crystal length so as to make conducting and nonconducting regions. These columns could be $\lesssim 100$ μm in width, and electrodes would be attached at the crystal surface.

A system of very thin micro-detector planes is proposed for the detection of short living particles.

6) Liquid xenon drift chamber

A liquid xenon drift chamber with an electron drift space of 13 mm was constructed and tested by Doke and Kubota [8]. A spatial resolution of about 20 μm was achieved using an alpha particle source.

In liquid xenon the electron drift velocity is almost constant if the electric field is > 3 kV/cm. For measuring the electron drift time, the scintillation pulse directly produced by an alpha particle was used as a trigger signal and the proportional scintillation pulse was used as an arrival signal of the drifting electrons.

For minimum ionizing particles it is expected that the spatial resolution is in the order of several microns except multiple scattering effects. Therefore the authors are testing now a multi-wire liquid xenon drift chamber.

References

[1] E.H.S. Burhop et al., Phys. Letters 65B (1976) 299

[2] D. Crennel et al., The possibility to study the production and decay systematics of short-lived ($\tau \gtrsim 10^{-13}$ sec) new particles in hadronic reactions using the bubble chamber technique. Preprint, Rutherford Laboratory, Oct. 1977

[3] B. Hahn et al., Search for short lived particles using a high precision mini-bubble-chamber, University of Berne, May 1978, Fermilab proposal No. 606

[4] M. Dine et al., Search for short lived particles using a high resolution streamer chamber, Yale University and Fermilab, Fermilab proposal No. 490

[5] Derenzo et al., Nuclear Instr. and Meth. 122 (1974) 319

[6] R. Leiste et al., Berlin-Zeuthen Internal report

[7] A. Kanofsky, Nuclear Instr. and Meth. 140 (1977) 429

[8] T. Doke and S. Kubota, Liquid xenon drift chamber, Waseda University, Tokyo, 1978

VERTEX DETECTORS FOR ULTRA HIGH ENERGY HADRON SPECTROMETERS

C. Fisher
Rutherford Laboratory, Chilton, England

and

J. Sandweiss
Yale University, New Haven, Connecticut USA

The importance of detailed high resolution studies of the vertex region in hadron processes arises principally from the need to detect and study the production of new flavor particles such as Charm, Bottom, . . . etc. This can either be regarded as part of the particle-identification problem at the VBA in the same way as we need to identify strangeness, leptons, etc., or if the physics is still interesting, as a means to search for new flavors and their associated spectroscopies. The ground state particles are expected to have lifetimes in the range 10^{-14}-10^{-12} sec and masses ~ 5 GeV for bottom etc. with associated decay lengths ranging from ~ 150 μm (P/M = 50, $\tau = 10^{-14}$ sec) to ~ 15 cm (P/M = 500, $\tau = 10^{-12}$ sec).

The production vertex is expected to be very complex due to

(a) Many associated pions, kaons, etc. in addition to new flavor particles.

(b) Pair production of new flavors followed by high multiplicity decay

or:

(c) Cascade decays down the flavor chain, i. e.,

Bottom → Charm → Strangeness, etc.

In general there will be the problem of selecting those events containing new flavor particles from the background and subsequently to correctly assign the downstream particles to their vertex or origin (at least three possibilities!). To achieve this selection and association in a situation where the background of multiparticle production is very high requires the direct observation of the new flavor decay vertices.

At the VBA, we should not ignore the more esoteric possibility of observing free quarks which could either be unit charged and decay with lifetimes $\sim 10^{-13}$ sec (Pati and Salam) or fractionally charged and stable. There is also the chance to observe completely unexpected phenomena and the general approach must be to maximize the information available on all events.

Properties Required for a Vertex Detector

(a) Spacial resolution. Studies have been made of the problem of optically resolving the decay vertices from each other and from neighboring tracks. In general, the problem is independent of the momentum of the incident particle since the detection efficiency is governed by the transverse separation of the vertices from the other tracks in the event rather than the longitudinal separation. In simple terms the transverse separation is given by

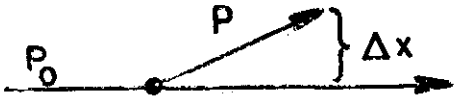

$$\Delta x \simeq \frac{p_\perp}{M} \cdot \tau c$$

and for $(p_\perp/M) \simeq \frac{1}{2}$, $\Delta x \simeq 15\ \mu m$ for $\tau \sim 10^{-13}$ sec.

One could argue that the event be detected (rather than have separately resolved vertices) if one large angle track from the decay does not project back to the main vertex, i. e.,

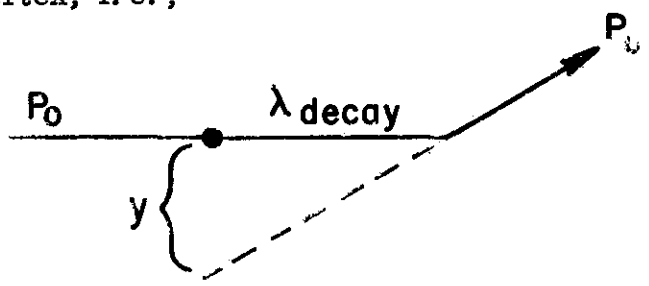

$$y \sim \frac{p_{\perp i}}{M_i}\,\tau \quad \text{i.e.,} \sim (3-10)\,\tau$$

or ~ 100 μm for $\tau \sim 10^{-13}$ sec.

We should clearly aim for the first situation, i. e., to have a detector able to resolve the decay vertices from the surrounding tracks. To a first approximation the resolution required is ~ 1 μm for $\tau \sim 10^{-14}$ sec, 10 μm for $\tau \sim 10^{-13}$ sec, etc., and is independent of the beam momentum. Of course, because of the variable nature of the background associated tracks, the production and kinematics, the exponential decay distribution there remains some efficiency for the detection of particles with $\tau \sim 10^{-14}$ sec using a detector with resolution 10 μm, etc.; however, these simple pictures give a guide to the resolutions required.

(b) New flavor cross sections and lifetimes; rates and trigger considerations. The current estimates for Charm lifetimes are ~ 5×10^{-13} sec and for Bottom ≥ 10^{-13} sec corresponding to resolution in the region $\lesssim$ 50 μm and ≃ 10 μm. Cross-section estimates at 20 TeV ($\sqrt{s}$ = 200) taken from Babcock et al. are ~ 100 μb for charm and ~ 1 μb for pp→bb+x; m_b = 5 GeV. If we accept the charm interpretation of the beam dump experiments indicating σ Charm ~ 40 - 100 μb

at 400 GeV ($\sqrt{s}$ = 27.4) we might expect somewhat larger cross sections than currently predicted for new flavor production at the VBA. An apparent rule is that each new flavor is produced at a few per cent of the previous new flavor

$$\frac{\sigma_s}{\sigma_{ns}} \simeq \frac{\sigma_{ch}}{\sigma_{st}} \simeq \frac{\sigma_b}{\sigma_{ch}} = \ldots \text{ few } \%.$$

The small cross sections expected for heavy new flavor particle production coupled with the complex nature of the events has serious consequences for the design of the detection system. All detectors searching the microbarn and sub-microbarn level require some form of triggering either on-line or off-line. Several trigger possibilities exist, e.g.,

(1) To trigger on strange particle production in a particular kinematic situation. This will usually represent a trigger cross section of order 1 mb.

(2) To trigger on direct lepton production, i.e., a muon or an electron directly produced. The trigger cross section will be $\simeq 10^{-14}\sigma(\pi) \simeq 50\ \mu b$ + background.

(3) To trigger on some characteristic correlation, e.g., a "jet" trigger using a hadron calorimeter downstream. The trigger cross sec ion will depend on the jet definition and the jet $p_\perp$ etc.

Various trigger cross sections can be chosen; however, clearly the choice of trigger determines the kind of physics under study. We do not consider this in any detail but merely note that one can conceive of (a) very

loose triggers where a large quantity of data is stored for off-line analysis, or (b) rather selective tight triggers, such as high $p_\perp$ jets for example, where the trigger cross section is small and the physics selection is on-line. The choice of trigger in addition to the physics aims will influence the choice of vertex detection technique. Important parameters for the detector which determine the triggering possibilities and hence the range of physics available are clearly:

(a) Overall data rate. How many interactions per second can one tolerate in the detector.

(b) Memory time. Which essentially determines the overall rate and the sophistication possible in the trigger.

(c) Dead time. For how long is the detector dead following a trigger.

A high overall data rate is necessary to study processes with very small cross sections; however, we also require either a very short dead time for data acquisition followed by off-line selection or a very small trigger cross section if the dead time is significant.

Clearly the memory time must be such as to allow the trigger condition to be applied.

Finally, as a requirement for any vertex detector at TeV energies, it is clear that multitrack efficiency is essential.

We now consider the performance of detectors currently in use or under development.

Current Technology and Its Use

(a) Nuclear Emulsion. Emulsions have been around for a long time and the properties are well known. The search for Charm has recently revived interest in the technique since it is the highest resolution detector available. Resolution is in the submicron range (grain size ~0.5-1.0 μm) with grain densities on minimum ionizing particle tracks ~200/mm. Very useful as an exploratory technique but not suitable for studies of low cross-section phenomena. Disadvantages arise from the complete absence of time resolution and consequent difficulties in associating events with downstream spectrometer information

(b) High resolution bubble chambers. A high resolution hydrogen bubble chamber will be used next year to search for charmed particle tracks at the SPS. The properties of the chamber are given in Table I.

The spacial resolution is only limited by optical considerations which represents a fundamental limitation for all dynamic visual detectors. Thus bubbles grow according to diameter $d \propto \sqrt{t}$ from a critical radius $\lesssim 1$ μm. The delay between the event and the flash is chosen to allow the bubbles to grow sufficiently to be optically resolved. The optical resolution is related to the depth of field D (in the chamber) through $\text{Res} = 0.61\sqrt{\lambda D}$ where λ is the wavelength. The resolution chosen for the CERN high resolution chamber is 20 μm corresponding to D a depth of field of 2 mm. This depth has to contain the beam and secondary particles leaving this band go quickly out of focus. The bubble chamber has the positive feature that the bubbles continue to grow and if necessary a second picture can be taken of the same event with

worse resolution but a larger depth of field, e.g., 100 μm and 5 cm. If we wish to achieve resolutions in the 1 μm region then the field is ~5 μm, i.e., we have "microscope" optics. The problem is to contain the beam within a 5 μm region of the chamber. This is probably impractical and it would seem not possible to design a chamber using classical optics which will have resolution better than ~10 μm. Higher optical resolution can be obtained if holographic techniques can be exploited.

If we consider now the accuracy with which we can find the center of a bubble (bubble centers should be on the particle trajectory to better than 1 μm) then this is typically 10-20% of the diameter which is in the region of 1 μm. Thus measured reconstructed events could (we should call this precision to avoid confusion with optical resolution defined above) have effective resolution ~1 μm.

There is also a limit on the bubble density arising from the density of δ-rays in hydrogen (or the medium) having energy greater than the minimum energy required for bubble nucleation. In hydrogen this appears in the region of 300-1000 bubbles/cm.

In the existing conventional chamber the rate is expected to be 30-100 Hz with chamber diameter ~20 cm. The maximum visible track length in hydrogen is therefore ~30 meters/sec corresponding to a maximum rate ~1 event/mb/sec. (The present chamber is only expected to run at ~30 meters/sec.)

(c) The high pressure streamer chamber. The high pressure streamer chamber operated this year at Fermilab contains 90% Ne/10%

hydrogen at ~25 atmospheres. Successful operation was achieved with track widths ~150-200 μm/(effective resolution) limited by the diffusion of the seed electrons away from the particle trajectory before the application of the high voltage pulse. A program to improve the resolution by using ~100 atmospheres argon and a CO_2 laser to induce streamer formation is underway and should reach $\lesssim$ 50 μm. The resolution is ultimately limited by purely optical considerations as for the bubble chamber; i. e., the depth of field to contain the beam and the detected secondary particles is related directly to the resolution.

The advantage of the technique is clearly in terms of rate. The existing chamber is ~4 cm long, so that 10^6 particles per second (memory ~1 μsec) will yield a basic event rate of ~10 events/mb/sec, i. e., about two orders of magnitude greater than the current bubble chamber experiment. The disadvantages of having a heavy nucleus target are the presence of nuclear fragments which can cause obscuration of the production vertex and the possibility of secondary interactions simulating decays, although the latter will be a negligible background to those events where a pair of decays are detected.

The advantages of a high data rate can only be realized if a suitably selective trigger can be found. Thus for the streamer chamber experiment the use of a direct muon trigger improves the signal-to-noise by a factor ~30, but this is offset by the fact that ~90% of the triggers are in the walls of the pressure vessel. The problems of the trigger are essentially related to the use of film as a recording medium so that the dead time of the system is determined by the camera wind-on dead time. Film has the advantage of good resolution so that images down to ~5 μm can be recorded. In principle

one can use large arrays of C. C. D.'s to achieve the same resolution (by adjusting the optical demagnification factor) and hence reduce the dead time of the system.

A development which significantly improves the resolution of the streamer chamber is the Laser Induced Streamer Chamber (LISC). In this development (Los Alamos-Yale collaboration), a chamber will be constructed using up to ~ 100 atmospheres of argon gas (much less thermal diffusion of the "seed" electrons) and to grow the streamers by laser illumination of the chamber. With such a chamber a resolution (track width) should be achievable in the region of 20-50 μm.

(d) High Resolution Drift Chambers. The question naturally arises what is the ultimate resolution achievable with a mini-TCP drift chamber system. Lanius et al. are constructing (have constructed ?) a target chamber assembly for use at CERN consisting of an argon drift chamber with 20 μm wires at 20 μm spacing. The resolution is limited by the diffusion of the electrons during the drift distance to the wires. Of course, the resolution is in one dimension only--normal to the wire direction. No depth of field problems exist and presumably very high rates can be achieved. This development looks extremely promising.

Future Possibilities and Developments

A future development which would remove the depth of field limitation would be the application of holography to both the bubble chamber and the streamer chamber. We are not aware if any fundamental reasons why such systems should not substantially improve the resolution and extend the depth of field.

Possible future developments of specific techniques are:

(a) The development of single shot standing wave ultrasonic helium bubble chambers. In principle this is possible and allows the construction of a bubble chamber of sensitive depth $\sim \frac{1}{4}\lambda$ where λ is the wavelength of the sound in helium ($\lambda \sim 2$ cm for $\sim 10^4$ Hz). Hydrogen would be much more difficult because of the large pressure swings required and the consequent mechanical problems of the piezo electric transducer design. The difficulty with such high rates will be the bubble recompression (although this would probably be achievable for the extremely small bubbles ($\lesssim 10$ μm) required for high resolution work) and the diffusion of heat away from the site of a recompressed bubble. The latter have time constants of ~ milliseconds so that to prevent the renucleation of bubbles on old tracks it would be necessary for rates above ~ 1 kilohertz to have a liquid flow sufficient to move the bubbles away from the pressure antinodes between cycles to a reasonable fraction of the sound velocity! Clearly a development program is needed to establish this technique. If successful however we might have very high rate, high resolution helium chambers as possible vertex detectors for the future.

(b) The development of the Laser Induced Streamer Chamber could proceed in several interesting directions. Modern laser technology might allow operation of a streamer chamber with liquid densities. Based on our present incomplete knowledge, such a chamber would require energy densities of some tens of joules per cm^2 and pulse widths of some tens of picoseconds. If the technical problems of such a device could be solved, the expected resolution would be of the order of 1 micron.

Another direction in the development of the streamer chamber would be to attempt to record the data by the illumination of the chamber by a second laser beam and photographing the light scattered from the streamers. Such a development would allow holographic recording and thus much larger sensitive depths at high resolution than would be possible with direct imaging.

Table I. CERN High Resolution Bubble Chamber 1979.

Diameter	20 cm	
Depth	3.5 cm	
Rate	≥ 30 Hz	
Resolution (aimed at)	~20 μm;	precision ~2.3 μm
Liquid	Hydrogen	
Walls out of Lexan		
Trigger	Interaction trigger ≥ 50% events in H_2	

ICFA WORKSHOP ATTENDEES

U. Amaldi, CERN
J. Augustin, University of Paris
B. Barish, Caltech
G. Charpak, CERN
S. Y. Chen, IHEP, Peking
C. K. Chou, IHEP, Peking
F. C. Chu, IHEP, Peking
E. Courant, BNL
Y. Derbenev, INP, Serpukhov
A. Diddens, University of Amsterdam
R. Diebold, ANL
N. Dikansky, INP, Novosibirsk
J. Dowell, University of Birmingham, Great Britain
Y. Fedotov, IHEP, Serpukhov
C. Fisher, Rutherford
E. Goldwasser, University of Illinois
V. Gridasov, IHEP, Serpukhov
E. Keil, CERN
N. King, Rutherford
K. Lanius, Akademie der Wissenschaften der DDR, Berlin
L. Lederman, Fermilab and Columbia University
P. Lehmann, Saclay
B. McDaniel, Cornell University
A. McInturff, BNL
P. McIntyre, Fermilab
D. Möhl, CERN
K. Myznikov, IHEP, Serpukhov
K. O. Nielsen, University of Aarhus, Denmark
T. Nishikawa, KEK, Japan
J. Rees, SLAC
B. Richter, SLAC
C. Rubbia, CERN and Harvard
N. Samios, BNL
W. Sampson, BNL
J. Sandweiss, Yale University
J. Sanford, BNL
W. Sippach, Columbia University
N. Skrinsky, INP, Novosibirsk
R. Stiening, SLAC
L. Teng, Fermilab
M. Tigner, Cornell University
V. Titov, INP, Serpukhov
A. Tollestrup, Fermilab
G. Trilling, LBL
M. Vivargent, LAPP, Annecy-Le-Vieux
G. Weber, DESY
H. Wiedemann, SLAC
W. Willis, BNL/CERN
R. Wilson, University of Chicago
Y. Yamaguchi, University of Tokyo
V. Yarba, IHEP, Serpukhov

☆ U.S. GOVERNMENT PRINTING OFFICE: 1979—651-554